FIRE BEHAVIOR IN MODERN BUILDINGS CONSIDERING WINDOW GLASS FALLOUT AND ACTIVE VENTILATION

TIANWEI CHU

PhD

The Hong Kong Polytechnic University

2025

The Hong Kong Polytechnic University

Department of Building Environment and Energy Engineering

Fire Behavior in Modern Buildings Considering Window Glass Fallout and Active Ventilation

Tianwei Chu

A thesis submitted in partial fulfilment of the requirements for
the degree of Doctor of Philosophy

August 2024

CERTIFICATE OF ORIGINALITY

I hereby declare that this thesis is my own work and that, to the best of my knowledge and belief, it reproduces no material previously published or written, nor material that has been accepted for the award of any other degree or diploma, except where due acknowledgement has been made in the text.

_____(Signed)

Tianwei Chu (Name of Student)

Abstract

Modern architectural designs increasingly preferred larger open-plan layouts to enhance spatial flexibility and larger glass windows for more natural lighting as well as better inhabiting experiences. However, such designs fundamentally change fire safety design practices, as the fire behavior in these compartments exhibiting time-variant localized burning is different from the traditional paradigm that focuses on ventilation-controlled fires in small compartments. In this thesis, the first main objective is to better understand fire behavior in modern designed compartments, and the interaction between window glass failure and fire development has been identified as a crucial factor. This inspires the second objective of this thesis, which is to develop an innovative solution of 'active opening' windows to mitigate fire development in modern large open plan compartments.

In this thesis, **Chapter 1** presents a comprehensive review of the literature on glass behavior and compartment fire research, which illustrates the complexities of considering glass fire behavior in compartment fires. Particularly, the localized burning in large compartments would impose complex fire action on glass panels and complete failure of glass to ensure the commonly assumed initial window openings cannot be achieved within a few minutes. Hence, it is of vital importance to re-assess the role of window glass in providing crucial ventilation to speed up or to slow down the fire development. To address these needs, **Chapter 2** establishes a 'criterion-controlled' approach to bring glass fallout effect to the CFD fire simulation. This modelling approach subdivides the glass panel into multiple glass sub-modules, and the removals of these sub-modules are controlled by the fallout criteria derived from Shields Tests. After validation against fire test data, this approach is applied to the simulation of modern large open-plan compartment fires, which surprisingly shows that the fire development path has been fundamentally altered. The fire spread becomes much faster due to the later window glass fallout, whereas the presumed sufficient ventilation conditions become invalid. In view of the uncertainties of glass fallout in fire, **Chapter 3** introduces a Weibull probability distribution model into the Shields fallout criteria governed by the glass surface temperatures. Implementing this probabilistic approach with 200 large-scale fire simulation cases, diverse fire development patterns are found as influenced by the stochastic nature of glass fallout and varying thermal conditions. These results clearly demonstrate the complexity introduced by glass fallout to fire behaviors in open-plan compartments and the necessity of considering glass-fire interaction.

Inspired by the slower fire development observed in Chapter 3 with virtually very early glass removal, **Chapter 4** introduces an innovative 'active opening' strategy. In contrast with the common intuition of enhancing glass fire resistance, this thesis proposes to actively open windows at an early stage of a fire to mitigate fast fire development in modern compartments. This concept has been verified with CFD simulations, in which fast fire spread is avoided, benefiting from a thin smoke layer after

active window opening. Through various modelling attempts, the factors including the upper edge of windows and the activation temperatures are found to be important in achieving effective mitigation of fire spread. Subsequently, **Chapter 5** validates the 'active opening' strategy for the first time using real fire tests and demonstrates the fast fire spread in the same scaled compartment with window glass. The mechanisms of 'active opening' have been analyzed with the test data and the corresponding simulation. The benefit of reduced smoke radiation is found dominant compared to the introduction of fresh air, which prevents fast pre-heating of floor fuel and avoids rapid progression of flame front. **Chapter 6** further examines the effectiveness of using 'active opening' in more realistic applications, which numerically investigates a tall building model of non-uniform fuel load and opening configurations. It is shown that the implementation of 'active opening' effectively reduces smoke and mitigates flame spread, as well as reducing the heating impact on building façades, avoiding the risk of vertical fire spread. The effects of window opening setups, the number of windows opened, and detector designs are investigated. In **Chapter 7,** the overall conclusions of this thesis are drawn**,** followed by the discussion of future tasks of implementing active opening towards real applications in modern buildings.

Acknowledgments

This research received financial support from the State Key Laboratory of Disaster Reduction in Civil Engineering (No. SLDRCE20-02), the Hong Kong RGC General Research Fund (No.15220223) and the BEEE Strategic Fund (No. P0052458), which was crucial to the completion of this project. I am deeply thankful to everyone who has supported me on this research journey.

First and foremost, I extend my deepest gratitude to my supervisor, Prof. Liming Jiang, whose invaluable guidance and unwavering support have been fundamental to the success of this research. His profound insights and commitment to high academic standards have not only shaped this chapter but also inspired my professional development. His willingness to give his time so generously has been very much appreciated. His encouragement in pursuing novel research avenues and his commitment to maintaining high academic standards have been a constant source of motivation.

I am also deeply grateful to my co-supervisor, Prof. Asif Usmani, for his expert advice and invaluable contributions to the framework of my thesis. His mentorship has been a vital source of inspiration and motivation in my research journey. His detailed feedback and engaging discussions were crucial in refining my work. I also wish to express my heartfelt thanks to all my academic colleagues for their assistance and care in both professional and personal spheres. The three years spent with everyone at ZN808 were some of the most enjoyable and fulfilling of my life, filled with collaborative spirit and mutual support.

Special thanks are extended to Prof. Diping Yuan and Prof. Guowei Zhang from the Shenzhen Research Institute of China University of Mining and Technology. Their provision of the experimental platform was crucial to my experimental studies, and their collaboration was immensely helpful in the success of this project.

I would like to express my gratitude to Prof. Ruben Van Coile for his guidance and care during my six-month exchange at Ghent University. His mentorship was invaluable, and his concern for my well-being made my time in Europe both productive and enjoyable. Additionally, I am thankful for the companionship of my colleagues at the Magnel Laboratory during the exchange. Meeting them and sharing daily experiences enriched my life in Europe immensely and made my stay there memorable.

I am immensely grateful to my family and my wife (Ms. Jie Ruan) for their endless love and support. Their unwavering belief in my capabilities and their constant encouragement have been crucial in sustaining my drive and passion for my research.

Tianwei Chu

Hong Kong

August 2024

Table of Contents

Publications

Refereed Journal Papers

1. T. Chu, L. Jiang, A. Usmani (2023). *Introducing an active opening strategy to mitigate large open-plan compartment fire development*. **Fire Safety Journal**, 141, 103981.
2. T. Chu, L. Jiang, G. Zhu, A. Usmani (2024). *Integrating glass breakage models into CFD simulation to investigate realistic compartment fire behavior*, **Journal of Building Engineering**, 82, 108314.
3. T. Chu, W. Zeng, G. Wang, C. Chen, G. Zhang. D. Yuan, J. Wang, A. Usmani, L. Jiang. *Explain why active opening of windows can mitigate fire spread in modern building compartments*, **Journal of Building Engineering**, 99, 111615.
4. T. Chu, R. Van Coile, L. Jiang. *Effects of uncertainty in glass fallout criteria on fire behavior*. (Submitted)
5. T. Chu, W. Zeng, L. Jiang. *Using 'active opening' of windows for fire safety of modern buildings considering more realistic setup*. (Submitted)

List of Papers not included in the Thesis

1. T. Chu, L. Jiang, G. Zhu, A. Usmani. (2023). *Fire impact on vertical components subjected to a localized fire estimated using a line source model*. **Fire Technology**, 59, 2299-2331.
2. X. Zhang[1], T. Chu[1], Liming Jiang, G. Zhu, X. Liu, X. Xu, Z. Wu. (2023). *On the orientation effect on the flame spread over discrete fuel using a mass-transfer number*. **Fire Safety Journal**. 135, 103730.

Conference Presentations

1. T. Chu; L. Jiang; A. Usmani. *Estimation of thermal impact on vertical components due to localized burning in large compartment fires*, **12th International Conference on Structures in Fire** (SiF2022), Hong Kong, China, 30 Nov. - 2 Dec. 2022.
2. T. Chu; L. Jiang; A. Usmani. *Introducing an active opening strategy to mitigate large open-plan compartment fire development*, **14th International Symposium on Fire Safety Science** (IAFSS2023), Tsukuba, Japan, 22 - 27 Oct 2023 (received Sheldon Tieszen Student Award).
3. C. Chen, T. Chu, G. Rein, A. Usmani, L. Jiang. *Fire development in large compartments with mixed-timber-section ceiling*, **13th International Conference on Structures in Fire** (SiF2024), Coimbra, Portugal, 19 - 21 Jun. 2024.
4. T. Chu; L. Jiang; A. Usmani. *Insights into Mitigating Effects of Active Opening Strategy to Compartment Fires: Evidence from Medium-scale Experiments*, **4th International Conference on Structural Safety Under Fire & Blast Loading** (CONFAB 2024), London, United Kingdom, 9-10 Sep. 2024.

Chapter 1: Introduction

1.1 Background and motivation

Modern architectural designs are increasingly adopting large open-plan layouts [1] and large glass windows. Such designs not only offer greater flexibility for various functional needs, but also favorably improve living comfort of end-users. For example, modern office buildings, shopping centers, exhibition halls, and residential apartments often adopt large open-plan layout and large façade windows, as shown in Fig. 1.1. Consequently, these designs have introduced new challenges to the modern fire safety designs, as the compartmentation approach relying on limiting ventilation becomes invalid. In recent years, there has been a notable rise in the frequency of fires in modern designed buildings. One of the tragic accidents was the World Trade Centre tower fires, where massive fires induced by the hijacked airplanes led to approximately 2 977 deaths and the eventual collapse of the towers [2].

Fig. 1.1 Fire accidents in modern tall buildings [2–7].

The unbearable losses of these events have drawn global attention and prompted a re-evaluation of the fire safety approaches associated with modern designs. Real fire accidents and analyses demonstrated that once a fire breaks out in an open-plan building with large façade windows, the lack of walls or other barriers to restrict the spread of flames, together with the significant fuel load in a compartment, can lead to a massive fire of large scope and high intensity compared to those in traditionally compartmentalized spaces. Such high-intensity fires pose a severe threat to the structural integrity of the buildings, potentially causing further spread of fires and even structural collapse. Furthermore, fires in modern buildings impose greater challenges to timely evacuation and firefighting efforts. Generated smoke and toxic gases permeate the entire space without obstruction and largely reduce the visibility of the inner environment. In that case, the large space affected by fire and smoke

can increase the time required for individuals to reach safe exits and complicate the tasks of firefighters in pinpointing the origin of fire and carrying out extinguishing operations.

In view of these emerging challenges attributed to modern building designs, understanding the fire dynamics in large open-plan spaces has become a frontier research topic. To this date, various researchers have conducted extensive experiments [8–14] to investigate the fire behavior in contemporary building designs, which identified the generic 'travelling' fire behavior in large open plan compartments. Despite providing valuable insights, these real-scale fire tests typically simplify the consideration of glass windows, adhering to the 'no glass' assumption adopted in typical small compartment fire tests [15–19]. This prevailing assumption is based on the observation that glass completely falls off before flashover in most of small compartment fires, and the breakage and falloff complete within in a very short period after the ignition (2-5 minutes). In the perspective of detailed responses, the state of glass windows directly controls the ventilation conditions to fire development and leads to rapid smoke accumulation prior to glass fallout, while the fire impact owing to hot smoke in turn influences the state of the glass windows including glass breakage and fallout.

Particularly, large areas of glazing windows have often been adopted in modern buildings [20] for the purpose of natural lighting and expansive views. These large windows after glass fallout would bring in excessive fresh air to the fire development, which might cause a massive fire since limiting ventilation to control fire intensity becomes ineffective. Moreover, the failure patterns of these glass windows could be further complicated by the fire behavior in large compartments, as the expected 'travelling fire' behavior exhibits a moving localized fire along the floor plan. Hence, considering glass windows as initial openings would be oversimplified, which substantially restricts the understanding of fire dynamics interacting with glass fallout. Furthermore, this oversimplification might miss the opportunity of discovering novel solutions to both mitigating fire development and preserving the modern design features.

In light of this need, the research conducted in this thesis begins with incorporating glass windows into CFD fire simulation to investigate the effect of 'criteria-controlled' glass fallout to the fire development in large compartments. While understanding the importance of providing early ventilation through glass windows in mitigating fire development, a novel 'active opening' strategy is proposed. This solution tends to actively open glass windows at a very early stage, triggered by early fire detection, which could prevent smoke accumulation and mitigate fast fire spread. Numerical and experimental studies will be conducted to investigate the feasibility of such a counter-intuitive approach, and the results as reported in the thesis have shown great potential of this solution. The appropriate use of active opening could enhance the overall safety of buildings and better protect life safety.

1.2 Literature review

1.2.1 Research on compartment fires

1.2.1.1 Traditional compartment fire framework

The concept of compartmentation, originating from traditional fire safety strategies in the early 20th-century, relies on using physical barriers such as walls, floors, and ceilings to divide a building into several small fire-resistant compartments. This approach aims to confine fire damage within limited space and facilitate manageable evacuation routes for occupants, thereby preserving the overall integrity of the building and ensuring the safety of individuals. While adopting a compartmentation approach, characterizing the fire behavior and fire impact in compartments was a major task of fire safety engineering. A milestone effort was carried out by Ingberg [21] with a series of full-scale compartment fire experiments, which quantified fire severity through the intensity and duration of fully developed fires. His methodology fostered the development of temperature-time curves, which were thereafter integrated into many fire-resistance assessment standards, including BS 476-20 [22], ASTM E119 [23], ISO 834 [24] and Eurocode 1 [25]. It should be acknowledged that Ingberg's experiments established a widely adopted description of compartment fire development, as illustrated by the red solid line in Fig. 1.2.

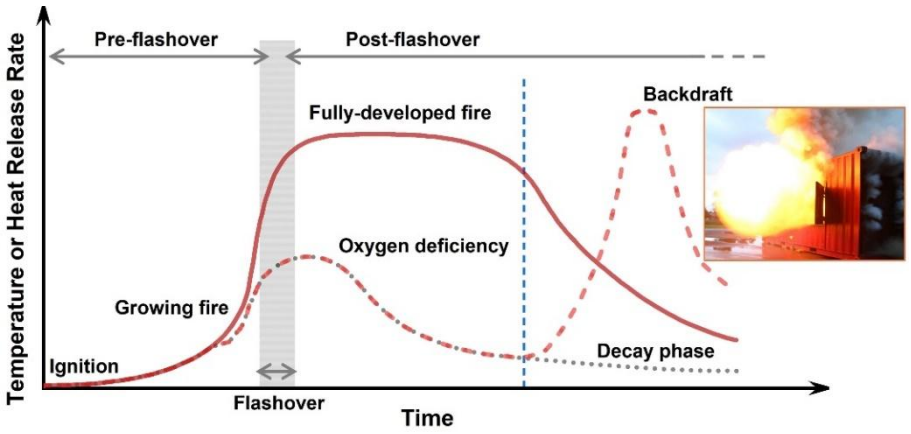

Fig. 1.2 Typical stages of compartment fires.

Under the premise of sufficient fuel and relatively small sizes, the development of compartment fires after ignition typically undergoes four main stages:

- **Ignition stage:** The initial phase after the fire is ignited, usually represented by low heat release and localized burning.

- **Growth stage:** The fire size grows while flame front spreads, and the average room temperature remains relatively low.

- **Fully developed stage:** Nearly all combustible items are ignited after flashover (spontaneous ignition and rapid fire growth), and the fire reaches its peak intensity.

• **Decay stage:** The fire begins to weaken as the available fuel is exhausted. During this stage, the average temperature of the compartment gradually decreases.

The transition from a growing fire to a fully-developed fire is commonly termed flashover [26]. This short-duration event refers to the phenomenon where the heat in a confined space accumulates to such an extent that almost all combustible materials are ignited simultaneously. Flashover is therefore regarded as a critical consideration in fire safety design due to its indication of potentially severe fires, which has prompted a series of follow-up studies [27–32] aimed at understanding and predicting the occurrence of flashover. Moreover, experimental observations have highlighted that fire development in oxygen-starved scenarios differ significantly from post-flashover fires, which typically occur in well-sealed small compartments with closed doors and windows. In such scenarios, the fuel tends to burn slowly and inefficiently, potentially leading to self-extinguishment, as represented by the gray dashed line in Fig. 1.2. If a door is opened (or a window breaks) at this fire state, fresh air rushes in while hot combustion products flow out. The accumulated flammable gases in the compartment are immediately ignited upon mixing with the incoming air, as indicated by the red dashed line. The burning gases can erupt through openings, forming explosive fireballs [33] that may cause severe injuries to people, e.g., firefighters. This phenomenon is known as 'backdraft' [34], and its visual representation can be seen in Fig. 1.2.

Regardless of feeding air at growth stage or backdraft stage, the mechanisms of glass-fire interaction were not yet thoroughly examined due to the prevalent 'no-glass' assumption in fire research during the mid-20th century. This is originated mainly from two considerations: a) fully-developed fires (indicated as red solid line in Fig. 1.2) are considered crucial design scenarios for fire safety of building structures; b) due to the poor fire-resistance of window glass in earlier times, the heat and pressure generated by a well-developed fire could easily cause glass breakage and fallout forming ventilation. This failure of the glass commonly occurred in the pre-flashover stage and was therefore assumed to have no significant impact on the subsequent fully developed fire stage. Given the 'no-glass' assumption simplified the experimental design of compartment fires, extensive research on fully-developed fires were conducted during 1950 s to 1970 s, such as the works led by Kawagoe [35,36], Thomas [15,37–39], and Harmathy [40–42].

Kawagoe [35] summarized a decade of work on multi-scale room fire experiments, initially establishing the empirical link between the combustion rate (or temperature rise) and ventilation flow rate of compartments. His subsequent [36] work further elucidated the energy balance within compartments, indicating that energy production and convective losses are proportional to $A_o\sqrt{H_o}$ (A_o and H_o are the area and height of openings), while heat conduction losses are proportional to the total internal surface area A_T (the compartment area excluding the floor and openings). The ratio of these two items, $(A_o\sqrt{H_o})/A_T$, commonly referred to as an 'opening factor', is crucial in assessing fully

developed compartment fires. From the perspective of buoyancy-driven flows caused by fire-induced pressure, Babrauskas [43,44] theoretically derived the relationship between the combustion rate and 'opening factor' observed by Kawagoe. Concurrently, Thomas et al. [15,37] experimentally validated the impact of ventilation on the maximum combustion rate of compartment fires, and later proposed a similar concept, called 'inverse opening factor' [38], to quantify the maximum temperature of fully-developed fires. Fig. 1.3 presents the correlation between the 'inverse opening factor' and the peak compartment temperatures measured in their fire tests. A vertical dashed line divides the experimental data points into two regimes: Regime I (ventilation-controlled) and Regime II (fuel-controlled). In Regime I, the compartment openings are relatively small compared to the size of the compartment, and the air supply through openings is insufficient to support the combustion of the available fuel, which is often accompanied by flames ejecting from the openings. In other words, the mass burning rate or fire severity is primarily governed by the opening size. As shown in Fig. 1.3, there is an approximately linear trend derived from the data points in the blue-shaded region, where the room temperature increases with a decrease of the inverse opening factor (or an increase in the venting area).

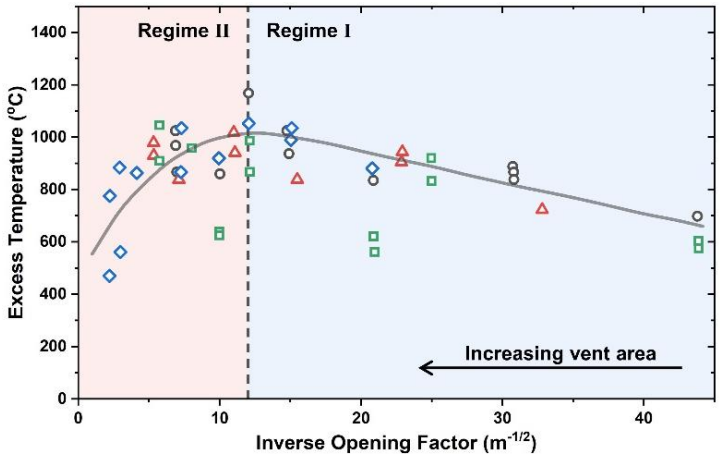

Fig. 1.3 Two fire regimes from Thomas' tests [15] (symbols represent compartments and openings of different geometries).

This linear trend continues until the 'inverse opening factor' decreases to about 12, beyond which the fully developed fire falls within Regime II. This regime is characterized by well-ventilated compartments, where the sizes of both the compartment and openings are sufficiently large, making combustion primarily dependent on the amount of available fuel. Moreover, the intake of oxygen is governed by the fire-induced pressure differences, and this momentum-driven flow pattern adds complexity to resolve fire behaviors [45]. For this reason, the peak room temperature of Regime II cannot be solely defined by $A_T/(A_o\sqrt{H_o})$. In contrast, Regime I fire is almost independent of the fuel quantity and is primarily proportional to the amount of air supplied through the openings. This characteristic significantly simplifies the complexity of the issue, making it more suitable for engineering applications. Hence, prescriptive codes prefer to maintain the traditional compartment designs within Regime I to achieve predictable fire behavior.

During the same period, Harmathy [40,41] also developed a theoretical framework that described the combustion rates for fuel-controlled fires (Regime II) and ventilation-controlled (Regime I) fires, and attempted to translate these findings into design methods focused on structural performance. His subsequent work [46,47] endorsed the advantages of Regime I fires promoted by Thomas et al., and further explored the feasibility of utilizing fire characteristics of Regime II for compartment design. He emphasized that the peak temperatures produced by Regime II fires are typically lower than those in Regime I, unless the ventilation is extremely inadequate, as illustrated in Fig. 1.3. From this perspective, if the vent area is sufficiently large, the excessive air entering the compartment can have a cooling effect, thereby reducing the overall burning rate. These discussions fostered two distinctly different compartment design approaches, as shown in Fig. 1.4, featuring compartments with fire-rated boundaries but small openings versus those with large openings but general fire resistance.

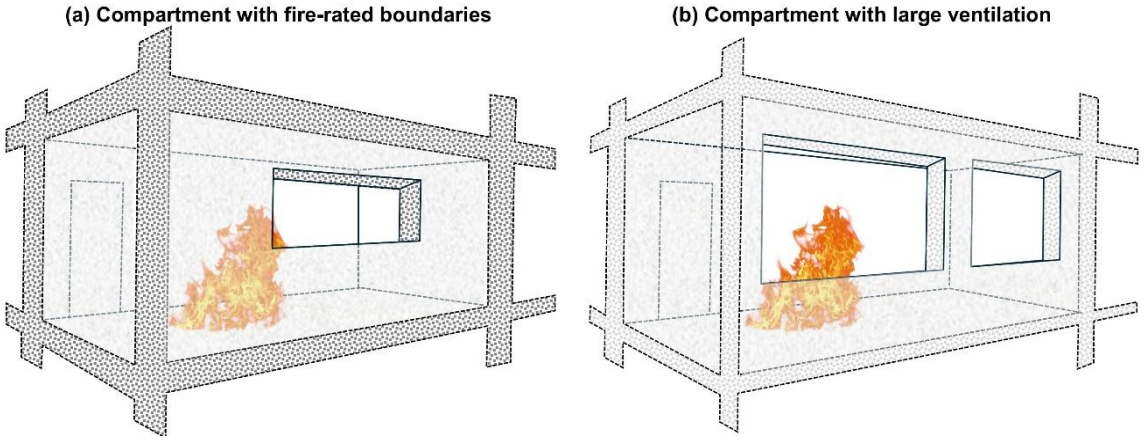

Fig. 1.4 Choices in providing fire safety: (a) by fire-rated boundaries and (b) by large ventilation (adapted from Ref. [47]).

Harmathy's viewpoint sparked extensive debate within the fire safety community and the ventilation-limiting approach eventually gained widespread acceptance due to its provision of convenient and manageable designs. Various contemporary studies, such as the work reported by Law [48], Emmons [49–51] and Quintiere et al. [52,53], provided significant contributions to the knowledge of compartment fires. These contributions led to the development of the Compartment Fire Framework, becoming the foundation of current fire safety engineering for buildings. Furthermore, research on traditional compartment fires also focused on the study of fire spread behavior [54–59], particularly the phenomena of spilled fires observed by Yokoi [60] and its induced façade fires. Lee [61,62], Delichatsios [63,64], Chow [65,66], and Hu et al. [67,68] have made significant contributions to this area, and these research efforts have been comprehensively reviewed by Sun et al. [69]. Nevertheless, it should be emphasized that most of these studies have predominantly concentrated on fully developed fires under ventilation-controlled conditions, as depicted in Fig. 1.3, often neglecting the early-stage fire growth processes. Consequently, the results from these studies may not be directly applicable to localized fire stages, nor suitable for addressing fire scenarios in large open-plan compartments. The

advance of Computational Fluid Dynamics (CFD) technology, notably the widely adopted Fire Dynamics Simulator (FDS) [70], has provided researchers with a robust and powerful simulation tool to capture the dynamic changes during fire development. It has been proven valuable for investigating fire spread [71], smoke movement [72,73], temperature distribution [74], and changes in gas composition [75,76]. The history concerning fire simulation has been reviewed by Novozhilov [77].

1.2.1.2 Fire behaviors in large open-plan compartments

In the 21st century, compartment fires in large open plan rooms have been of increasing interests from the fire safety engineering community. The concept of open-plan layouts traces back to the 1920s, championed by the architects trained in Bauhaus School [78] in Germany. This design philosophy, characterized by reducing or eliminating interior walls to create more expansive and multifunctional spaces, began to gain popularity in the mid-20th century. Nevertheless, pursuing large open plan space has raised a contradicting question on fire safety, as the compartmentation concept and ventilation-limiting approach prefer relatively small rooms. It should be admitted though that such design philosophy did not initially raised concerns of fire safety engineers until the catastrophic fires occurred in World Trade Center buildings [2], and the investigations revealed different fire behavior challenging the traditional understanding. Investigations led by the National Institute of Standards and Technology (NIST) into the World Trade Center fires [79] found that the flames predominantly spread around the lift core rather than burning uniformly across the floors (see Fig. 1.5).

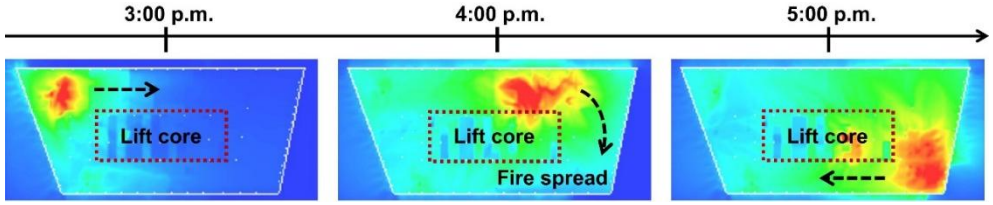

Fig. 1.5 Travelling fire in WTC 7 (adapted from Ref. [79]).

Similar fire behavior has been identified in other fire incidents, including the One Meridian Plaza fire in 1991 [3], the Windsor Tower fire in 2005 [80], and the TU Delft Faculty of Architecture Building fire in 2008 [81]. These fire incidents exhibited a localized burning zone moving across the floor plan, and this fire phenomenon was termed ‘travelling fire’ by Rein et al. [82]. Such fires can generate very high temperatures in one area (near field) while leaving other parts comparatively cooler (far field). This uneven thermal exposure poses complex non-uniformity on structural members than the assumed traditional fire models adopting uniform heating assumption. Stern-Gottfried et al. [83] reviewed experimental studies on fires in larger compartments, highlighting the findings from the Cardington series of fire tests [8,84–86] led by the Building Research Establishment (BRE) in the UK, as well as scaled fire tests of open-plan compartments conducted by Thomas et al. [87]. These studies consistently reported that fires did not burn simultaneously throughout an entire enclosed space. Typically, fires start in areas distant from ventilation and rapidly spread to oxygen-rich zones near vents, consuming fuel

around these points. Subsequently, the flames slowly move towards areas farther from the vents, thus depleting most of the available fuel. This fire behavior results in temporally and spatially varying temperatures and thermal loads across different areas. This renders the potential inadequacy of traditional fire design methodologies for large compartment fires, as the assumption of uniform combustion and homogeneous temperature conditions within compartments (represented by standard fire [24] and parametric fire [25] curves) does not exist.

To describe the non-uniform fire behavior in large compartments, Clifton [88] was among the first to propose a solution that subdivides large spaces into smaller regions and utilizes a time-lagged parametric fire model to represent the uneven temperature distributions within these areas. As a milestone work, Stern-Gottfried and Rein [89] developed the 'Travelling Fire Methodology' (TFM), which represents localized burning areas with uniform temperature zones ranging from 800 to 1200 ^{o}C and employs Alpert's ceiling jet correlations [90] to consider far-field smoke temperatures. Experimentally, full-scale travelling fire tests conducted in Veselí [91], and later in Tisova [92], further assessed the performance of TFM. Inspired by these tests, researchers at Edinburgh University [93] proposed the Extended Travelling Fire Methodology (ETFM), which introduced a localized fire model to represent the fire action at near field. Later, the 'Improved Travelling Fire Methodology' (iTFM) [94] was proposed to account for flame flapping, which was followed by the Travelling Fire Methodology considering flame extension (fTFM) [95]. Regarding application of travelling fire models, Jiang et al. [96] incorporated the ETFM into computational tool OpenSees for fire [97], enabling detailed thermal and structural analyses in complex fire scenarios. It should be noted that these simplified methods for simulating moving fires rely on an overly idealistic assumption that the localized fire zone remains a constant size as it spreads across the open-plan compartment. However, earlier Cardington series of fire tests [84] observed that large compartment fires could exhibit multiple spreading patterns, and real fires in large compartments could be more complex due to real fuel load and geometries.

Explorations of these fire dynamic patterns in large open-plan compartments were initiated following Torero's re-assessment of compartment fires at the 11th International Symposium on Fire Safety Science (IAFSS) [45]. The work pointed out that the data supporting the Compartment Fire Framework were predominantly derived from small-scale cubic-shaped compartment fire tests, as presented in Fig. 1.6a. The spatial geometries of modern architecture (as seen in Fig. 1.6b) have increasingly diverged from these traditional compartment settings, with one dimension typically exceeding 20 m.

Recent experimental efforts in large compartments demonstrated the inability to describe complex fire behavior via the traditional framework. For instance, in the Dalmarnock fire tests [100] (in a real apartment with dimensions of 4.75 m × 3.50 m × 2.45 m), the temperature distributions showed variability in both space and time and exhibited lower magnitudes than the predicted values given by the Thomas' curve [15].

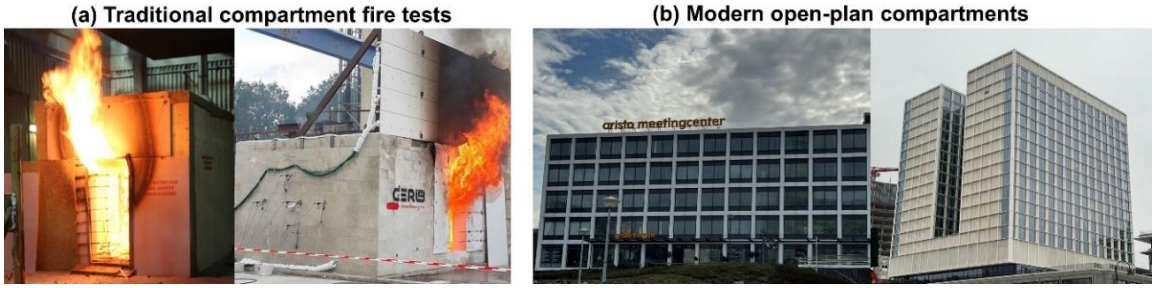

Fig. 1.6 Deviation of modern open-plan designs from traditional compartment fire test settings [98,99].

To investigate the realistic fire behavior in tall buildings of evolving architectural design, Torero led the Real Fires for the Safe Design of Tall Buildings project and conducted a variety of real-scale fire tests [9]. A compartment measuring 5 m × 18 m × 2 m was constructed for fire tests, with fifteen openings on its front wall (each opening was 1.5 m high and about 1 m wide, as illustrated in Fig. 1.7a). These openings could be opened or closed to vary the 'opening factor', which systematically facilitated exploring the impact of ventilation conditions on fire behavior.

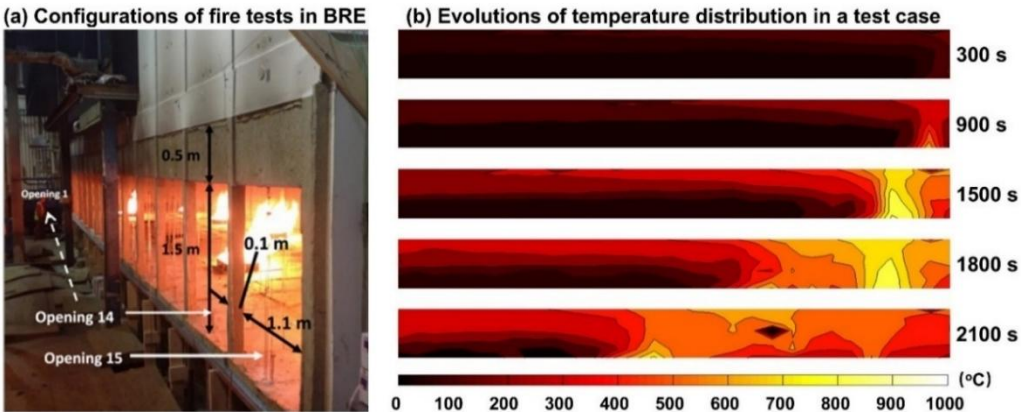

Fig. 1.7 High-fidelity fire tests showing travelling fire behavior in open-plan compartments (adapted from Ref. [9,45]).

The outcomes of these tests indicated that the large dimensions of the compartment allowed for the formation of temperature gradients both vertically and horizontally. This can be seen from the illustration shown in Fig. 1.7b, where the used wood cribs covered the entire floor and were ignited at one end, with the openings fully open. The flames were initiated at the right-hand corner of the long compartment, and the flame spread was significantly slower than the smoke propagation under the ceiling. At about 1500 s, smoke temperatures exceeded 500 ᶻC, and rapid fire spread (similar to flashover) was observed in the right-hand half of the compartment. Subsequently, the flames continued to spread to the left side of the compartment, but global flashover was not observed.

Based on the analysis of the ratio between fire spread rate V_s and burnout rate V_{BO} from this test series, Hidalgo et al. [9] identified four different fire behavior modes in modern open-plan compartments:

- **Mode 1:** Fully developed fire. This mode is characterized by an extremely high V_s/V_{BO} ratio,

indicating rapid fire spread covering the entire compartment almost simultaneously, which is equivalent to the classical definition of Regime II fires [15].

• **Mode 2:** Growing fire. In this mode, V_s/V_{BO} is greater than 1 but not infinite, indicating noticeable fire spread but not instant involvement of the entire space.

• **Mode 3:** Travelling fire. The V_s/V_{BO} of this mode is approximately 1, indicating that the fire moves through the compartment at a rate similar to its consumption and depletion of available fuel, which equates to the idealized concept of 'travelling fires' [82].

• **Mode 4:** Self-extinguished fire. This mode shows similar behavior to the burnout of fires where the consumption of the fuel occurs far faster than virgin fuel becomes available, i.e., $V_s/V_{BO} \ll 1$.

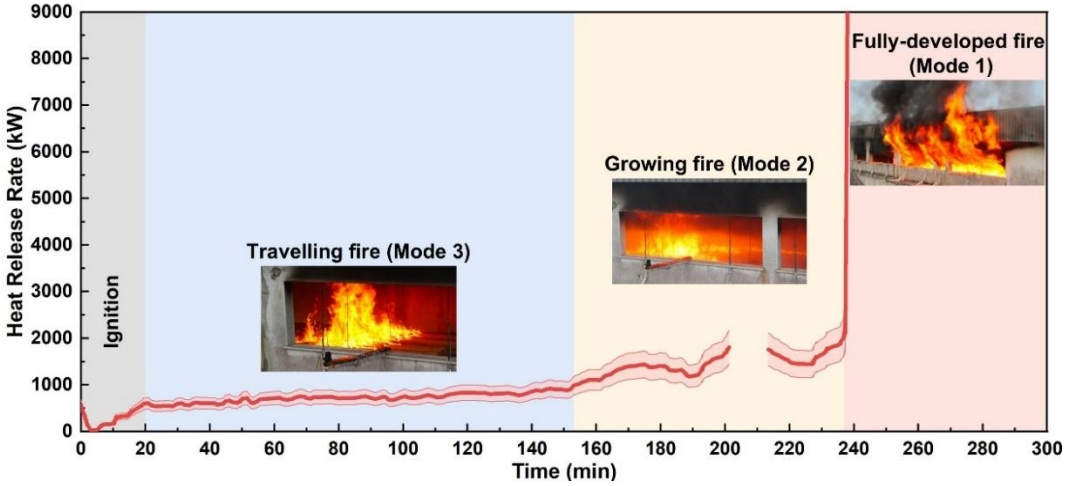

Fig. 1.8 Observations of fire modes 1-3 in Malveira fire test (adapted from Ref. [10]).

The first three fire modes were observed in the subsequent large-scale Malveira fire tests [10]. Fig. 1.8 clearly demonstrates the HRR development of each mode in the test, along with the progression and intensity of the flames over time. Notably, the rapid ignition of the cork layer in the right part of the compartment quickly led to the rapid spread of flames, resulting in the formation of a fully developed fire. This phenomenon suggests the enhanced thermal feedback to the fuel bed (i.e., strengthening the spread rate V_s) potentially acts as a mechanism facilitating the transition from a travelling fire (Mode III) to a growing fire (Mode II) or a fully developed fire (Mode I). Harnessing this knowledge could potentially prevent such detrimental transitions. Nevertheless, these findings substantially challenge the simplified assumptions commonly adopted in fire safety engineering, providing a specific scheme to describe the large open-plan compartment fires.

Later in 2019, the European TRAFIR (Characterization of Travelling Fires in large compartments) project conducted three large-scale fire tests [14,101,102] in a compartment measuring 15.0 m by 9.0 m by 2.9 m, with a designed fuel load density of 511 MJ/m^2. The opening areas of these three tests were respectively altered to 85.2 m^2, 30.0 m^2 and 10.0 m^2, aiming to further explore the impact of ventilation conditions on fire development. It was found that the reduction in opening size increased the smoke

layer thickness in the far-field area and thus led to more heat transfer to the structural components. Moreover, the experimental observations further confirmed the inferences from the Malveira fire tests [10]: due to significantly varying heating effects from the smoke layer on the fuel beds in these three tests, travelling fires were observed in the two tests with opening areas of 85.2 m^2 and 30.0 m^2, while a transition to a fully-developed fire was noted in the test with 10.0 m^2.

In 2021, Rein and Wegrzynski [11,13] led the 'X' series of travelling fire tests in a large compartment in Poland. The compartment model was configured to be 35.5 m long, 10.8 m wide and 3.19 m high, with venting area maintained at 56 m^2. These tests primarily explored the impact of fuel load density on compartment fire modes, showing that higher fuel load density resulted in a faster spread rate and a larger scale of the travelling fire region but shortened the fire duration.

Following the design of the X' series tests, the more recent full-scale fire tests, CodeRed series led by Kotsovino et al. [103–105], incorporated timber ceilings into the experimental design. These experiments further enhanced the understanding of the dynamics of fires in open-plan compartments with much higher ceiling heating due to ignited timber slabs. Several aspects have been addressed for assessing the fire safety performance of timber structures, such as increased heat release rates by wood combustion [106], smoldering [107], and external flaming [108].

As briefly reviewed, the past research efforts revisiting the compartment fires have found that ventilation conditions and fuel loads are crucial to fire development. Particularly, the fire dynamics in large open-plan compartments are more complex due to their non-uniformity of heating impact, unlike the relatively uniform fire action assumed and observed in traditional small compartment fires. While glass windows were often assumed as initial openings, the uneven thermal heating owing to a localized fire in large compartments can significantly reduce the fire damage on window glass, lowering the likelihood of glass breakage and delaying the formation of façade ventilation. This contradicts the presumption of 'travelling fire' framework, as it requires sufficient ventilation through the assumed opening of large windows.

Given that ventilation changes caused by window glass fallout can significantly alter fire behavior patterns in large compartments, it is imperative to integrate the role of window glass into future studies on large compartment fires, rather than excluding window glass setting as in traditional small compartment fire tests.

1.2.2 Research related to glass fracture

The behavior of glass breakage and fallout under fire conditions is extremely complex, involving many uncertainties, which vary in glass window setup and different fire exposure conditions. These aspects will be briefly reviewed and discussed. Fig. 1.9 provides an overview of the connection between glass fracture and compartment fires. The term 'glass fracture' describes the sudden rupture of glass materials when subjected to internal stress (induced by mechanical pressure, temperature changes, or

similar factors) exceeding their load-bearing strengths. This concept originated from systematic studies in the field of solid materials mechanics since the 1920s. During that period, the primary focus was on understanding the fundamental properties of materials under various stress conditions.

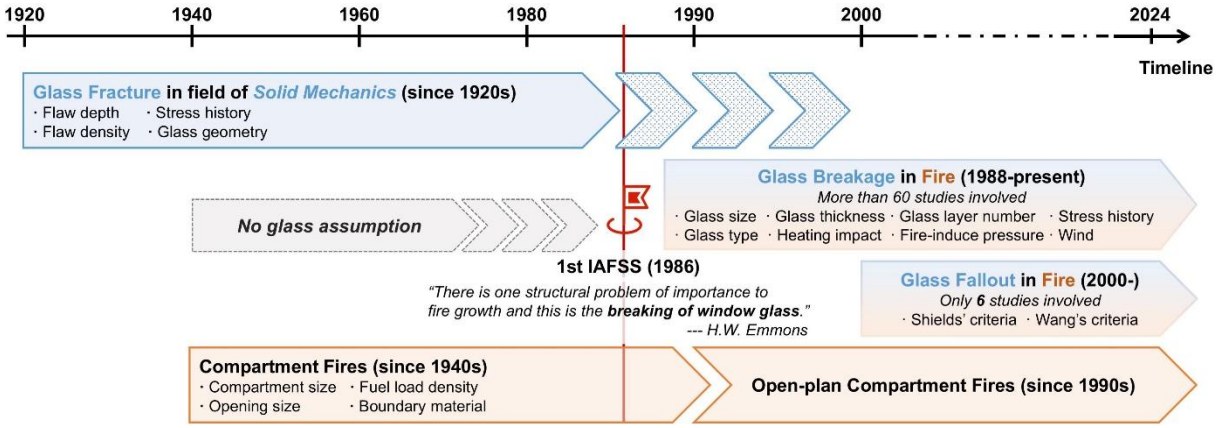

Fig. 1.9 The connection between glass fracture and compartment fires.

In the field of fire safety science, the term 'glass fracture' is often referred to as 'glass breakage'. This terminological distinction reflects that earlier research on glass fracture once stood apart from the field of fire safety science, primarily due to the assumption of 'no glass presence' in traditional compartment fire scenarios. This assumption was unquestioned until 1986, when Emmons [109] explicitly pointed out the potential impact of breaking window glass to fire development at the first International Symposium on Fire Safety Science (IAFSS), sparking widespread academic interest. Subsequently, researchers in the fire science community devoted themselves to studying glass breakage under fire (heating) conditions, which revealed that post-crack glass fallout is a critical event affecting the dynamics of compartment fires. The phenomenon of 'glass fallout' thereafter received further research attention in the context of fire development in compartments.

It is worthwhile to clarify that 'glass breakage' and 'glass fallout' have distinctly different meanings. Specifically, 'glass breakage' refers to the phenomenon where glass cracks or shatters due to conflicts with rigid frame materials, whereas 'glass fallout' describes the situation in which glass falls out of its installation position. This event implies the formation of new ventilation pathways that facilitate the influx of fresh air, potentially fueling the fire within an enclosed space. This section aims for a relatively comprehensive review of past research on glass fracture, as well as subsequent advancements in the study of fire-induced glass breakage and fallout.

1.2.2.1 Earlier studies on glass fracture

The investigation of glass fracture dates back to the early 20th century and falls within the domain of solid mechanics. During this period, scientists and engineers began to systematically study the mechanical properties of materials, with particular emphasis on the breakage behavior and crack propagation in brittle materials such as glass.

In the 1920s, Griffith [110], based on experimental observations, discovered that fractures of solid materials originated from pre-existing surface flaws introduced during the manufacturing process. To describe the onset of fracture induced by the surface flaw, the work proposed a principle stating that the released strain energy must at least have the energy necessary for generating two newly formed crack surfaces. This theoretical framework, known as the Griffith Fracture Theory, is utilized to determine the critical conditions at which instantaneous fracture occurs:

$$\sigma_f = \sqrt{2E\gamma/\pi a_c} \tag{1.1}$$

where σ_f is the fracture stress, E is Young's modulus, γ is the fracture surface energy (nearly 3 J [111]), and a_c is the critical crack (flaw) length.

Subsequent microscopic observations of crack propagation behavior in brittle materials help to identify three distinct crack opening modes (as shown in Fig. 1.10): Mode I, which involves crack opening due to tensile stress perpendicular to the crack plane; Mode II, which involves crack shearing due to shear stress acting parallel to the crack plane and perpendicular to the crack front; and Mode III, which involves crack tearing due to shear stress acting parallel to both the crack plane and the crack front. These modes became the basis of modern Linear Elastic Fracture Mechanics (LEFM) framework [112].

Among them, Mode I is considered the primary crack propagation mode in glass materials. The shear effects involved in Mode II and Mode III can often be equivalently transformed into the tensile effects of Mode I.

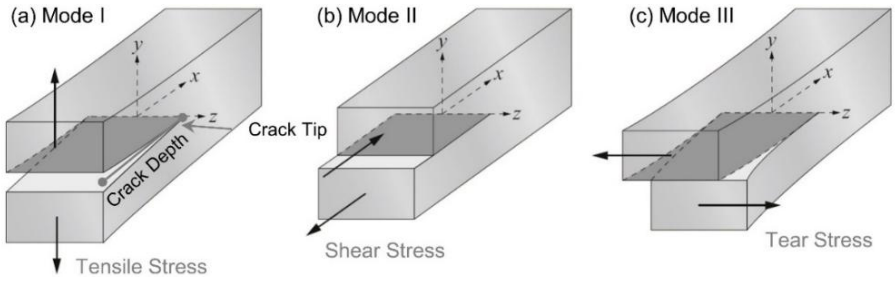

Fig. 1.10 Crack opening modes in fracture mechanics (adapted from [112]).

Based on this assumption, Irwin [113] introduced the stress intensity factor for Mode I, denoted as K_I, to quantify the stress intensity at the crack tip:

$$K_I = Y\sigma_n\sqrt{\pi a} \tag{1.2}$$

where σ_n is the tensile stress normal to the plane of the crack, and a represents the crack (flaw) depth, as depicted in Fig. 1.10a). Y is a correction factor that accounts for the geometry of the crack and the specimen, and its typical values based on analytical solutions are summarized in Table 1.1. Among these types, Type I is commonly used for surface crack analysis.

Table 1.1 Typical values of geometric factor Y for flaws [114–116].

Type No.	Type of flaw	Geometry factor Y
Type 1	Long, straight-fronted plane edge crack in a semi-infinite specimen	1.12
Type 2	Straight double-ended crack in an infinite solid	1
Type 3	Quarter-circle crack on glass edges	0.722
Type 4	Half-penny shaped cracks within a semi-infinite specimen	0.637 - 0.713

In the same work, a new glass fracture criterion was proposed, indicating that the immediate fracture of glass material occurs when the stress intensity at the crack tip K_I exceeds a threshold value known as the fracture toughness, K_{Ic}. The fracture toughness K_{Ic} is generally regarded as an intrinsic constant of the material. For modern soda-lime silicate glass, the applicable value is usually 0.75 MPa·m$^{0.5}$. Although subsequent studies [117–120] have reported varying values ranging from 0.72 to 0.82 MPa·m$^{0.5}$, these minor differences were attributed to the high sensitivity of the fracture toughness K_{Ic} to the moisture content in the air (ambient humidity). Thus, the tensile stress required for a single crack to cause fracture can be determined as follows:

$$\sigma_f = \frac{K_{Ic}}{Y\sqrt{\pi a_c}} \tag{1.3}$$

In spite of different forms, equations (1.1) and (1.3) both indicate that the fracture caused by a single crack on the glass surface is highly dependent on the size of pre-existing surface flaws. Considering that the surface of glass components in real-world typically contains a large number of flaws of various sizes, it seems overly simplistic to use the strength of a single crack (flaw) to represent that of the entire glass component.

To address this, Weibull [121] pioneered the use of statistical tools to extrapolate the strength of a single crack to the entire glass component, leading to the development of the well-known Weibull distribution. This approach later became known as the Random Surface Flaw Population (RSFP) method, which is generally based on the following assumptions: (a) the flaw size on the material surface can be described as a random variable with a statistical distribution; (b) individual flaws do not influence each other; (c) the fracture of the glass element occurs upon the failure of the first flaw; (d) sub-critical crack growth is disregarded. Thus, the failure probability P_f of a single crack (flaw) is simply determined by the probability that its random flaw size a exceeds the critical flaw size a_c:

$$P_f(a \geq a_c) = \int_{a_c}^{\infty} f_a(a)\,\mathrm{d}a = 1 - F_a(a_c) \tag{1.4}$$

where f_a and F_a represent the probability density function (PDF) and cumulative distribution function (CDF) of the flaw size, respectively. In this context, the power law is employed to describe the PDF of flaw sizes:

$$f_a(a) \propto a^{-r} \tag{1.5}$$

and the corresponding CDF thus following a Pareto distribution [122]:

$$F_a(a) = \begin{cases} 0 & for\ a \le a_0 \\ 1 - (a_0/a)^{r-1} & for\ a > a_0 \end{cases} \tag{1.6}$$

where a_0 is the minimum effective flaw size, beyond which the occurrence of fracture becomes possible. Through substantial rearrangement without introducing additional simplifying assumptions, the inert failure probability of a glass element can be reorganized to adopt the form of a two-parameter Weibull distribution with a scale parameter θ_A and a shape parameter β, which is given by:

$$P_f(\sigma) = 1 - \exp\left(-\left(\frac{\sigma}{\theta_A}\right)^{\beta}\right) \tag{1.7}$$

Here, θ_A and β are defined as:

$$\theta_A = \left(M_0 \frac{A}{A_0}\right)^{-1/\beta} \frac{K_{Ic}}{Y\sqrt{\pi a_0}} \tag{1.8}$$

$$\beta = 2(r-1) \tag{1.9}$$

where M_0 is the mean number of flaws. Given that a_0 and M_0 are difficult to directly measure, the empirical estimation of θ_A and β through experimental data typically serves as alternative solutions. This Weibull distribution has been widely implemented in reliability analysis. European standard (EN 572-1) [123] has also adopted this approach, and provides recommended values, θ_A= 74 MPa and β = 6, for float soda-lime-silica glass. Blank [124] used 11.4 kg/m^2 of sand dropped from a height of 1.5 m to impact the glass, artificially inducing homogeneous surface damage. These treated glass specimens were employed to represent the long-used glass, and then R400 tests [125] on these specimens facilitated the determination of Weibull distribution for the strength of aged glass, θ_A= 32 MPa and β = 25. These two distributions are plotted in Fig. 1.11 to illustrate the uncertainties in glass fracture. It is noted that when applying these distributions to practical design considerations, the size effect should also be taken into account to correct the scale parameter θ_A. This relationship is commonly expressed as follows [123]:

$$\frac{\theta_{A_1}}{\theta_{A_2}} = \left(\frac{A_2}{A_1}\right)^{1/\beta} \tag{1.10}$$

where A_1 and A_2 are the surface areas of different glass specimens. Based on the similar methodology to Weibull, subsequent glass strength models [126–129] were developed by utilizing various types of

distributions to describe the flaw conditions on the glass surface, which were integrated in the assessment of glass strength.

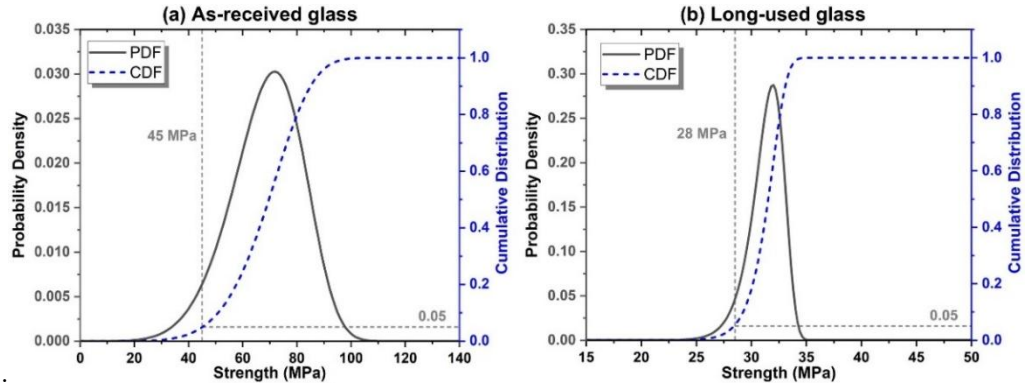

Fig. 1.11 Weibull distribution for the strength of float glass: (a) as-received glass and (b) long-used glass.

This section briefly reviews the major research advancements in glass fracture from the perspective of solid mechanics. It can be concluded that the flaw size is the primary factor determining the glass fracture. Additionally, the duration of glass usage also affects the overall strength. For glass products using more advanced manufacturing technologies, such as tempered glass, the strength of the glass samples largely depends on the residual stress added to the glass surface (typically ranging from 69 to 100 MPa) during the tempering process. The influence of aforementioned key factors is clearly summarized illustrated in Fig. 1.12.

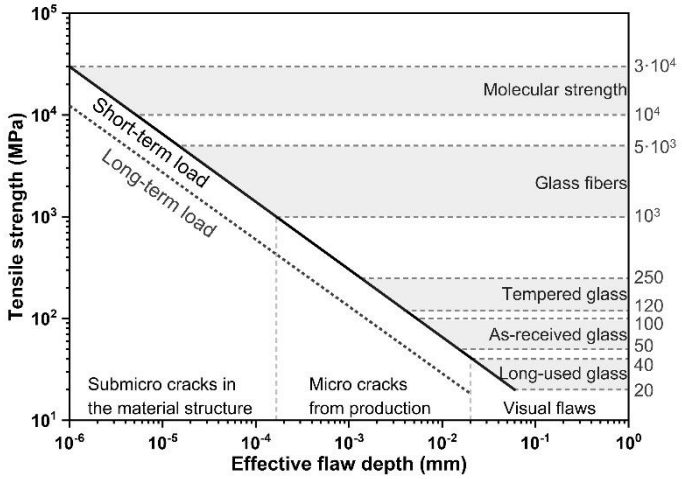

Fig. 1.12 Key factors influencing the tensile strength of glass products (adapted from [130]).

1.2.2.2 Glass breakage in fire tests

In 1998, Keski-Rahkonen [131] proposed a theoretical criterion for glass breakage induced by uniform incident heat flux:

$$\sigma_f = \alpha E(T_n - T_\infty) \tag{1.11}$$

where α is the thermal expansion coefficient, and T_n and T_∞ represent the temperature of the glass pane and the ambient temperature. This criterion indicates a threshold temperature difference of

approximately 80°C for ordinary float glass (using σ_f=50 MPa, α=8.1×10^{-6} K^{-1} and E= 80 GPa), while this theoretical analysis is somewhat limited due to the following assumptions: (a) no temperature gradient across the glass thickness; and (b) the temperature of the shaded edge remains at room temperature. Pagni and Joshi [132,133] addressed these limitations by introducing Beer's law to describe the temperature gradient within the glass thickness and theoretically calculated the temperature in the shaded area for varying shading lengths. Their results indicated that when the shading length exceeds twice the thickness of the glass, the temperature of the shaded edge is nearly at ambient temperature, which suggested the second assumption could be acceptable under this condition.

Subsequent work has been conducted as experimental studies. Two common methods were used in these tests to provide thermal boundary conditions for glass specimens: one involves realistic fire sources, and the other utilizes radiant heating panels. Skelly et al. [134] conducted fire experiments in a reduced-scale two-story compartment to test the fire performance of glass panes with and without shaded edges, aiming to validate the aforementioned theoretical solutions. The experimental outcomes showed that the breakage of shaded glass pane occurred when the critical temperature difference between the heated central part of the glass pane and the edge was approximately 90°C, which is close to the theoretical value. Nevertheless, for glass panes without shaded edges, fewer cracks were observed, with almost no crack propagation, and the glass temperature at the time of breakage was around 197°C, much higher than the previous cases. This discovery experimentally confirmed the influence of shaded width on the glass breakage and sparked the following related research [135,136].

Chen et al. [135] conducted a series of compartment fire tests using float glass with dimensions of 600 mm × 600 mm × 6 mm, aiming to investigate the effect of shaded width (ranging from 10 to 50 mm) on the time of oberving first glass crack. The test results indicated that the average time to first crack initially decreased and then increased with the shaded width, where the turning point is 20 mm. However, a recent study by Jørgensen et al. [136], using radiant panels to heat float glass with dimensions of 400 mm × 400 mm × 4 mm, reported that the increase of shaded width (10-25 mm) should monotonically shortened the time to crack. This slight deviation may be attributed to the difference in glass geometry (i.e., exposed area [137] and thickness [138–140]), and these two factors have been identified as factors influencing the behavior of glass breakage. Wang et al. [137] conducted experiments on glass panels of different sizes with pool fires and found that the fire performance of glass panels decreased with its size (exposed area). They attributed this finding to the presence of more surface flaws on a larger glass panel, which might weaken the strength of the glass. This inference establishes the connection with the studies in solid mechanics mentioned in the previous section.

As per the effect of glass thickness, the full-scale fire experiments conducted by Xie et al. [138] reported that a larger temperature difference was required to lead to the breakage of thicker glass panels. Following this, Li et al. [139] provided further evidence that thicker glass maintains a lower surface

temperature during heating, resulting in a longer time to the first crack. The subsequent studies by Yang and Chow [140], along with simulations by Wang et al. [141], reaffirmed these findings, reinforcing the understanding of thickness effects on glass breakage. Additionally, Dembele et al. [142] found that subtle differences in glass edge conditions can lead to significant variations in glass breakage time. Through numerical simulations, they discovered that glass with 'as-cut' edge conditions broke later than glass with ground or polished edges.

Another notable experiment [143] that has significantly inspired the study of fire-induced glass breakage was led by Mowrer from National Institute of Standards and Technology (NIST). A series of experiments utilizing radiant panels to heat glass panels helped identify a range of factors influencing the time to glass breakage. These factors primarily include: (a) the external heating conditions; (b) the type of glass (such as float or tempered glass); (c) the configuration of window assembly (such as single or double panels); and (d) the material of the window frame. Building on these foundational findings, subsequent work further expanded on the understanding of these factors. Regarding the first factor, Shields et al. investigated the performance of single-pane float glass under fires of different HRRs at the center [144] and corner [145] of an ISO 9705 room, as well as the double-pane float glass under the corner fire condition [146]. These experiments provided well-documented data records, including HRR history, compartment gas temperature, heat flux distribution, glass surface temperature, shaded edge temperature, thermally induced strain, and the time of first crack. Through statistical analysis, the experiments revealed the variation of the time to first crack with HRR, room temperature, and the heat flux received by the glass surface. Similarly, Wang et al. [147] and Choi et al. [148] conducted separate studies on the impact of fire source location and HRR on the time to glass breakage. These studies indicated that altering the location and HRR of the fire source fundamentally influenced the initial breakage time in the same manner, i.e., altering the heat flux applied to the fire-exposed surface of the glass, which in turn changed the rate of temperature rise on the glass surface.

Additionally, Wang et al. [149,150] conducted a series of pool fire experiments in open space to investigate the fire performance of coated glass, insulated glass, and laminated glass, determining the critical conditions for the breakage of each type. The results showed that insulated and laminated glass could survive longer than coated glass. This increased resilience of insulated glass is attributed to the air gap and the fire-side pane, which provide thermal resistance to the ambient-side pane. The fire performance of three-layer and four-layer laminated glass were also investigated in his subsequent work [151], and it is reported that the interlayer keeps the glass intact although all panes of laminated glass cracked, effectively preventing the formation of new ventilation openings. However, it is important to note that Ni et al. [152] raised additional concerns from their full-scale fire tests. These tests examined the fire performance of double-skin facades made of double-pane glass, where the internal glass layer consisted of 6 mm thick double-pane glass, and the external glass layer was 12 mm thick double-pane glass, with an interlayer of adhesive material. The observations revealed that after the inner glass layer

broke, the ignition of the interlayer could lead to the failure of the external glass layer. In response to these concerns, some efforts have been made to examine the HRR of interlayer materials [153] and conduct case studies [154] on their potential hazards. Furthermore, Wang et al. provided a systematic study [155,156] on the installation methods of window assembly, including exposed frames, horizontally hidden frames, and vertically hidden frames. The test results indicated that glass in exposed frames is more prone to breakage than that in semi-exposed frames, but glass in semi-exposed frames is more likely to fall out. Nevertheless, further quantitative analysis regarding the effects of installation methods remains necessary to be addressed.

Besides, current understanding remains limited as the effects of combustion products such as water vapor, carbon dioxide, and particularly soot have not been studied regarding the glass behavior in compartment fires. The presence of water vapor and carbon dioxide may alter the spectral radiation characteristics within compartments, potentially affecting the radiative heat flux distribution on glass panes. Even more notably, soot deposition on glass surfaces could substantially change their optical properties, including absorptivity and emissivity. Given the glass breakage mechanisms are not the main interest of this thesis, future research may be proposed to investigate the mechanisms of fire products affecting glass behavior in fire.

1.2.2.3 Investigations on post-crack glass fallout

Glass breakage plays a crucial role in compartment fire dynamics, primarily because windows serve as enclosure boundaries before breakage and as ventilation openings afterward [157]. If a sufficient accumulation of pyrolysis products exists in the hot layer of compartment, this sudden change in ventilation conditions can potentially lead to dangerous flashover and backdraft events. However, researchers have incrementally realized that this statement is not entirely accurate. Glass breakage does not guarantee the formation of a ventilation opening. Instead, post-crack glass fallout is the key event that led to the formation of openings for ventilation. In reality, glass fallout usually occurs a few minutes after the initial glass breakage.

In 2000, Harada et al. [158] conducted early attempts in characterizing the process of glass fallout. Through 50 radiant panel heating tests on float glass, they documented the first crack of glass and the fallout procedure, as illustrated in Fig. 1.13. Their results highlighted that glass fallout was considerably later than the occurrence of glass breakage, and this time delay was primarily related to the applied heat flux with less dependency on the restraint conditions of glass panels. Shields et al. [144,145] conducted a series of 33 full-scale compartment fire tests to investigate the fire performance of 6mm thick (tempered) float glass, meticulously recording instances of glass fallout. Through statistical analysis, the criteria for glass fallout in real fire scenarios were proposed as one of the earliest attempts: (a) the glass surface temperature exceeds 447°C or (b) the average incident heat flux on glass surface exceeds 35 kW/m². Using a similar compartment model, Manzello et al. [159] conducted one full-scale test

where a window glass assembly was exposed to a realistic fire. The window assembly comprised four glass sections, with two sections fitted with 6 mm thick single-pane tempered glass and the other two with double-pane tempered glass. The results found that the fallout of single-pane glass occurred when the surface temperature of was approximately 400°C with the incident heat flux of about 50 kW/m², which supported the Shields' glass fallout criteria.

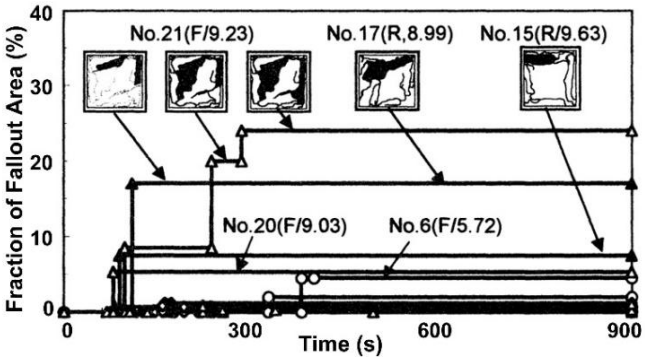

Fig. 1.13 Observations of gradual fallout of glass panes (extracted from [158]).

Following the above-mentioned studies, most of the research efforts remained on investigating glass breakage in fires and a few studies were on glass fallout. In 2018, Wang et al. [160,161] conducted two series (a total of 19) reduced-scale compartment fire tests using pool fires to heat 6 mm-thick tempered glass. The temperature difference between the glass surface and frame was chosen as the criterion for glass fallout, rather than the glass surface temperature as Shields et al. [144,145] adopted. The temperature differences at a 5% fallout probability for the two series of experiments were reported as approximately 301 ºC and 340 ºC, with corresponding incident heat fluxes of 36 kW/m² and 46 kW/m², respectively. Xie et al. [162] then performed statistical analyses on the results of Wang et al.'s tests using seven different statistical functions, including normal, log-normal, two-parameter Weibull, three-parameter Weibull, exponential, gamma, and logistic distribution. The key parameters analyzed included the temperatures of the glass surface and edges, along with their temperature difference, and the incident heat flux on the glass surface. The results indicated that the three-parameter Weibull distribution was the most suitable for the statistical analysis of tempered glass fallout behavior in fires, and the suggested temperature and incident heat flux should be controlled below 319 ºC and 38.5 kW/m², to prevent the fallout of 6 mm-thick tempered glass. Furthermore, they found that surface temperature is a more reliable predictor of tempered glass detachment than other factors based on a comprehensive correlation analysis. Nevertheless, these studies primarily focused on analyzing the glass fallout behavior in isolation, while the interaction between glass and compartment fire dynamics was not fully reflected.

1.2.2.4 Investigations on fire-glass interaction

Recently, the Lai'an fire tests conducted by Wang et al. [163] highlighted the significance of this fire-glass interaction. These full-scale experiments were carried out in a real residential building

measuring 4.4 m × 3.3 m × 2.8 m, with a fuel load of 407 MJ/m². The windows and doors of the room were kept open in the first test while closed in the second test. The results showed that opening conditions significantly affected the occurrence of flashover, smoke movement, and temperature distribution. Particularly, in conditions where both windows and doors were closed, the fire initially showed a decay tendency, whereas the subsequent fallout of glass panels significantly altered the fire dynamics, transforming the fire from smoldering combustion to a post-flashover fire, as presented in Fig. 1.14.

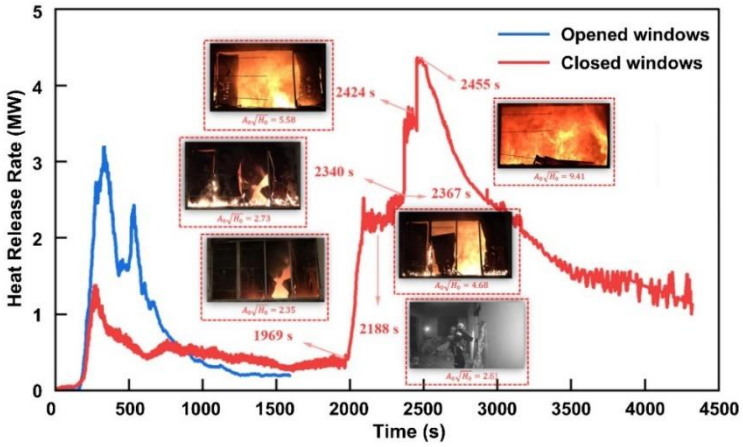

Fig. 1.14 Fire development in a residential building with windows and doors either opened or closed (adapted from Ref. [163]).

The test results vividly demonstrate that window glass not only serves as a building element experiencing breakage in fire but also actively influences the compartment fire dynamics through its fallout patterns. Specifically, the timing of glass failure directly affects ventilation conditions, oxygen supply, and consequently the heat release rate, temperature stratification, and smoke propagation within the compartment. Such interactions can dramatically alter the fire growth pattern in modern building compartments, especially when the fire field exhibits high non-uniformity. However, such fire-glass interaction is often ignored in current research, and initial openings were often adopted. Therefore, understanding and capturing the glass-fire interaction is essential to fire simulation and fire risk evaluation, which could potentially foster new fire design strategies for building fire safety.

1.2.3 Identified research gaps

The review of compartment fire research has suggested that localized fire flames in large open-plan compartments can reduce the likelihood of window glass fallout, especially at an early stage. On the other hand, glass windows are currently assumed as initial openings in experimental tests and numerical simulation, regardless of small compartment fires or large compartment fires. The late glass fallout would challenge this prevalent assumption of initial window opening and the provision of sufficient ventilation through glass windows, which was found as the key premise for travelling fire behavior.

While recognizing that the changed ventilation conditions owing to window glass fallout can significantly alter fire behavior patterns in large compartments, it is essential to integrate the interaction between window glass and fire in modern compartment fire research. For numerical models, a model to describe window glass fallout and ventilation changes should be integrated into CFD fire models. For experimental research, fire tests dedicated to large compartment fire behavior should potentially include glass windows.

Furthermore, significant uncertainties in glass strength are normally reported in glass fracture research, which can lead to variability in the timing of glass fallout. This variability could potentially lead to complex changes in ventilation conditions for compartment fires. Such uncertainties should be necessarily addressed in the studies of modern compartment fire development considering glass effect, which will further support the development of innovative solutions to mitigate fire development.

Lastly, the deviation of modern large compartments from the concept of compartmentation underlines the need for a re-assessment of fire safety practice and calls for innovative solutions to improve fire safety performance without compromising the modern design features.

1.3 Research objectives

This thesis aims to re-evaluate the role of window glass in the evolution of fires in modern large compartments and to explore innovative fire safety strategies adapted to contemporary architectural designs. The outcomes of this thesis are grounded in fire simulations of existing large open-plan compartment fires and our experimental investigations of medium-scale compartment fires. The objectives are briefly outlined as follows:

(1) To establish a modelling approach to simulate the interaction between glass fallout and fire development. The use of the proposed approach in modelling existing fire tests will provide a preliminary exploration of the glass effect on fire development in large open-plan compartments.

(2) To optimize the proposed modelling approach by incorporating the uncertainty in glass fallout. This optimization will provide more realistic ventilation boundary conditions for fire simulations and allow for a statistical analysis of the glass effects on fire behavior.

(3) To propose a new firefighting strategy to mitigate fire development based on the updated knowledge of open-plan compartment fires considering window glass effects.

(4) To demonstrate the feasibility of the proposed firefighting strategy under laboratory conditions. Medium-scale fire tests will be conducted to reveal the mitigation effects of the proposed strategy.

(5) To explore the performance of the proposed firefighting strategy in real building environments. Fire simulations of modern high-rise buildings will be performed to critically assess the pros and cons of the proposed strategy and clarify key considerations for its future application in engineering practices.

1.4 Outline of the thesis

This thesis contains seven chapters in total, which includes a chapter for introduction and literature review (this chapter), five core chapters reporting the research conducted by the author of this thesis, and a chapter for conclusion and further work plan.

Chapter 1 introduces the research background and motivation, including the history of compartment fire research and a literature review related to glass fracture. It highlights the importance of considering glass in modern fire research and the need for exploring interaction between glass and fire dynamics.

Chapter 2 proposes a 'criterion-controlled' strategy for simulating glass fallout behavior in CFD fire simulations. Specifically, window glass is divided into multiple sub-modules, and the existence of each sub-module is determined based on its surface temperature and incident heat flux to mimic the glass fallout. This model is initially applied to the simulation of existing large compartment experiments to explore window glass effects on fire behavior.

Chapter 3 incorporates the uncertainty of glass fallout conditions into the simulations. By summarizing glass fallout criteria from existing fire tests, a three-parameter Weibull distribution is derived to quantify the glass fallout probability with surface temperature. This probabilistic distribution is used to optimize the 'criterion-controlled' strategy outlined in Chapter 2 to provide more realistic simulations on interaction between glass and fire dynamics.

Chapter 4 explores an 'active opening' strategy that uses a preset activation temperature to open window glass upon detecting fires. This strategy is preliminarily implemented in CFD fire simulations and is found to effectively prevent rapid overheating within compartments, especially when windows are opened at lower activation temperatures and higher positions on the building facade.

Chapter 5 focuses on the experimental validation of the 'active opening' strategy. Two fire tests were conducted in a scaled open-plan compartment with real glass windows. The first test with regular window settings demonstrated a rapid fire spread, while the second test with 'active opening' strategy, effectively prevented a major fire. This mitigation effect is revealed by analyzing test data of heat release rates, smoke temperatures and floor heat fluxes.

Chapter 6 delves into the performance of the 'active opening' strategy in real building applications. It considers factors such as the locations of fire ignition, the methods of opening windows, and the non-uniform distribution of combustibles, while also assessing the risk of vertical fire spread induced by opening windows.

Chapter 7 summarizes key findings of the thesis and outlines potential avenues for future research.

Chapter 2: Simulation Framework for Modelling Dynamic Fire-glass Interaction

Summary

As reviewed in Chapter 1, previous studies on traditional small compartment fires typically simplified glass fallout by assuming initial openings at window locations. However, this 'no-glass' assumption becomes problematic when applied to modern open-plan compartments. In such scenarios, this assumption artificially provides sufficient ventilation at the early stage, facilitating the formation of slower 'travelling fire' with relatively lower fire intensities. Under this fire impact, window glass is less likely to fall out rapidly, leading to ventilation insufficiency that directly contradicts the 'no-glass' assumption. This contradiction highlights the necessity to reconsider the role of window glass when evaluating fire behavior in open-plan compartments. For this purpose, this chapter introduces a 'criterion-controlled' model to CFD fire models to simulate the interaction between glass fallout and fire behavior. The proposed modeling approach has demonstrated excellent agreement with experimental observations from the Shields Test, successfully predicting the cracking points and timeline of glass failure. By implementing the glass failure model in the large compartment fire models adapted from the Kirby Test and the Malveira Test models, significant insights into the impact of glass fallout on fire behavior were obtained. Specifically, in the adapted Kirby Test model with glass panes the presence of window glass led to markedly faster fire growth compared to scenarios with initially open windows of no glass. When considering the window glass failure in Malveira Test model, the slow 'travelling fire' behavior found in the full-scale test is changed to a fast spread fire and the window glass panels fail to provide the desired ventilation. These findings suggest the inadequacy of assuming complete openings at windows and emphasize the critical importance of considering window glass effects in modeling fire behavior in contemporary large open-plan compartments.

This chapter has been reported as a journal paper: 'T. Chu, L. Jiang, G. Zhu, A. Usmani (2024). Integrating glass breakage models into CFD simulation to investigate realistic compartment fire behavior, ***Journal of Building Engineering****, 82, 108314.'*

2.1 Introduction

As reviewed in Chapter 1, the early studies conducted by Kawagoe [35], Thomas et al. [15,37] and Harmathy [40,41] led to the widely used *Compartment Fire Framework*, which relates the fire burning rate with the 'opening factor' of compartment and categorizes them as ventilation-controlled or fuel-controlled fires. However, those fire scenarios, rapid glass fallout typically occurs during the early stages of fire due to the intense thermal exposure from accumulated hot smoke on glass panels. However, contemporary building designs frequently incorporate large open-plan floor areas with extensive glass windows. Under these conditions, the fire action applied on window glass in a large compartment may be much lower [164] if 'travelling fire' is observed [165]. Consequently, the traditional assumption of initial openings in large compartment fires becomes inconsistent with actual fire behavior. Therefore, it is essential to integrate criterion-based glass fallout behavior into CFD models of large compartment fires to understand the fire-glass interaction in the fire growth period and to accurately capture the realistic fire development characteristics.

This chapter begins with developing a simulation framework for modelling the fire-induced glass fallout in CFD models, which is then implemented in a model of real fire test (Shields Test [145,166]) to validate the fallout model as these tests were dedicated to studying the stepwise glass fallout in compartment fires. The glass model is thereafter implemented into large compartment fire models, which refer to the existing full-scale fire tests (Kirby Test [8] and Malveira Test [10]) in large compartments. With simulation results, it has been found that a fast-spread fire can occur if considering window glass in a long compartment with discrete fuel bed. For the large compartment with a continuous fuel bed, glass failure does not occur at the early stage as traditionally expected, which then changes the fire behavior from a travelling pattern when considering initially open windows to a faster-spread and a much larger fire when including glass in the CFD fire model. Based on the work of this chapter, it underlines the importance of integrating the glass failure model in CFD analyses and in the research related to large open-plan compartments of modern buildings.

2.2 Framework for modelling glass fallout in CFD fire simulation

Fig. 2.1 presents the detailed workflow of the proposed 'criterion-controlled' framework for modelling fire-induced glass fallout. The glass pane in the FDS model is equally discretized into multiple sub-module components. This discretization approach is based on the grid size used in the FDS model, ensuring each sub-module component dimension matches or exceeds the grid size for accurate identification within the simulation. Each sub-module is independently monitored by sensors installed on the fire-exposed surface, tracking critical indicators such as surface temperature and incident heat flux. The monitored data is then transferred to the AT_LEAST control logic, which places the glass sub-module into a pre-fallout state when the tracked indicators meet predefined glass fallout criteria. Additionally, one parameter (TIME_DELAY) of this logic is enabled, which allows the linked sub-module to be removed if the activation conditions last for more than one data output interval. This

setting can prevent the sensors from misfunctions due to the over-sensitivity to extreme situations (e.g., transient contact by flame).

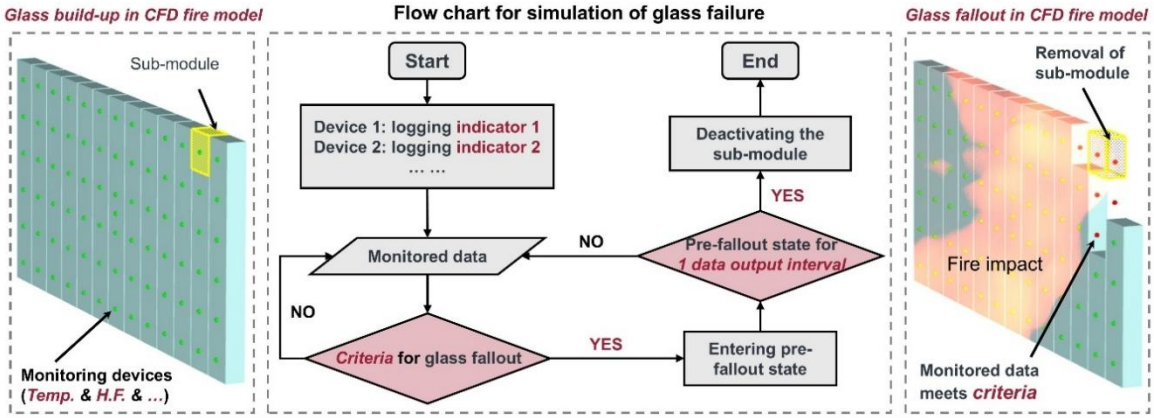

Fig. 2.1 Control flow for modelling glass failure in fire simulation.

For an initial attempt, this work adopts the glass fallout criteria derived by Shields et al. [145,166]. In their investigations on glass fallout, two series of experiments were conducted in an ISO-9705 standard room, testing the performance of the single-pane float glass exposed to corner fires and center fires, respectively. Their experiments revealed that vent creation due to glass fallout was a gradual rather than instantaneous process, with the glass typically breaking into smaller fragments that progressively fall away. Based on statistical analyses of these experimental results, two primary indicators for glass fallout were identified:

(a) the surface temperature of the glass pane exceeds 447 ^{o}C, or

(b) the heat flux received by the exposed surface of glazing reaches 35 kW/m^2.

It is worth noting that the proposed approach based on Shields' criteria estimates the fire induced progressive glass removal to change ventilation, whereas the glass fallout may be also affected by many other factors, such as the manufacturing technique, installation method of the window glass panes, and the non-uniformity of heating. Nonetheless, it is generally applicable to the similar configuration of window glass to the Shields Test.

2.3 CFD simulation of a small compartment fire considering glass fallout

2.3.1 Description of the CFD model for Shields Test

As mentioned before, the studies by Shields et al. [145,166] presented full-scale experiments on compartment fires with window glass failure. As shown in Fig. 2.2a, an ISO 9705 standard enclosure (3.6 m × 2.4 m × 2.4 m) with an opening (0.4 m × 2.0 m) was built using 100 mm thick concrete blockwork. A set of windows (including three 6 mm-thick float glass panels) was installed on one wall of the enclosure, and a square burner was placed in the center of the room to represent the fire source. According to the test description, an FDS model as shown in Fig. 2.2b for this test compartment is

established using concrete (density ρ of 2280 kg/m^3, specific heat c_p of 1.04 kJ/(kg·K), and thermal conductivity λ of 1.8 W/(K·m)) and float glass (density ρ of 2500 kg/m^3, specific heat c_p of 1.1 kJ/(kg·K), and thermal conductivity λ of 0.95 W/(K·m)). The fire over the 0.9 m × 0.9 m burner of mineralized methylated spirits is modelled as a burning surface with a defined time-dependent mass loss rate. The time-varying burning rates are extracted from the report and then set in this FDS model. The glass panels in the FDS model are built as several 0.05 m × 0.05 m (identical to grid size) square sub-modules with a thickness of 6 mm. The physical state of each glass sub-module is dominated by the control logic assigned to each sub-module following the 'criterion-controlled' modelling framework. The basic settings of CFD fire models are detailed in Appendix A, and the corresponding computational environment is provided in Appendix B.

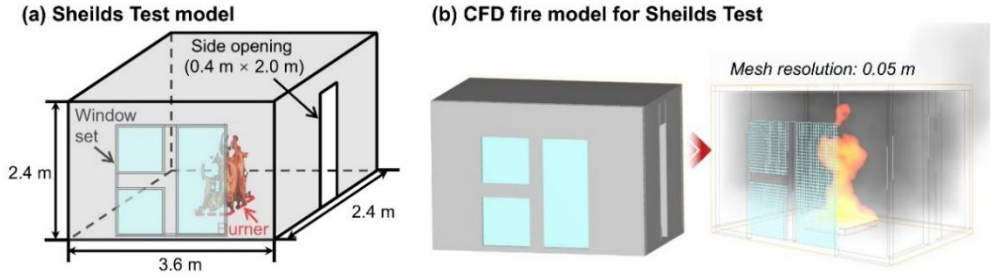

Fig. 2.2 Setup of experimental compartment and corresponding CFD fire model.

In the fire model of the Shields Test, six thermocouples and six radiometers are placed on the inner side of the front wall where the window set was installed, as shown in Fig. 2.3. The recorded temperatures by thermocouples A-F and heat fluxes by radiometers 1-6 are then used to validate the FDS model.

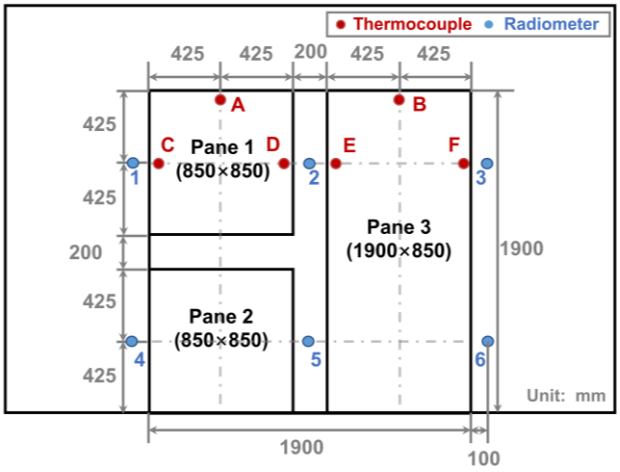

Fig. 2.3 Layout of thermocouples and radiometers in the Shields Test.

The comparison displayed in Fig. 2.4 indicates that the simulated gas-phase temperatures (solid lines) are close to the test data (dashed lines), despite relatively large deviations in the decay phase and a few fluctuations at the plateau. These discrepancies probably originate from the higher sensitivity of the numerical nodes compared to the real devices. Regarding the radiative heat flux, all radiometers in

the FDS model exhibit lower levels in the plateau phase than those in the Shields Test, while showing good performance in the remaining phases. The reason for the underestimation of the plateau phase can be twofold: (a) underestimation of the flame surface temperature in FDS model, i.e., the mesh size fails to perfectly resolve the flame surface so that the grids where the flame surface is located will also contain non-flame portions, and the presence of the non-flame portions can reduce the average temperature of those grids, thereby underestimating the radiant heat fluxes; (b) systematic errors of radiometers in the Shields Test, i.e., the filters of radiometers fail to block all the convective heat. In general, the FDS model produces acceptable results in comparison to the test data, whereas the heat fluxes in FDS are lower than the test data during the period of glass fallout.

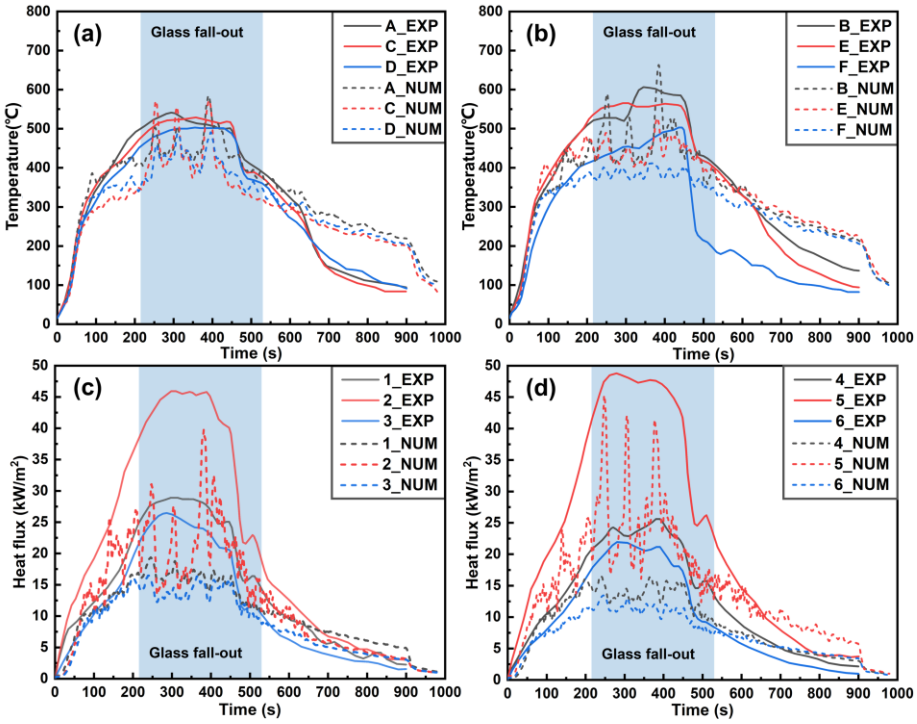

Fig. 2.4 Comparison of CFD simulation results with Shields Test data.

Several diagrams were presented in the technical notes of the Shields Test, describing the positions of glass failure points and their corresponding timings. The drawings were extracted from the test notes and then compared with the results of the FDS model, which is shown in Fig. 2.5. The left middle of Pane 3 was recorded as the first part undergoing glass fall-out at around 215 s, which is well replicated at 223 s in the FDS model, as shown in Fig. 2.5a. Most of Pane 3 then failed successively within 115 s, but this time span is underestimated as 93 s by the FDS model. Afterwards, Pane 1 suffered a failure in its upper right part at 510 s and then experienced a large area of fall-out within about 20 s. This procedure is closely modelled by the present model, as displayed in Fig. 2.5c and Fig. 2.5d, where Pane 1 initiates failure from its right edge and then fails almost completely within 30 s. Pane 2 shows no fallout in the FDS model (see Fig. 2.5e), and this result is consistent with the test records where Pane 2 only broke but remained on the window frame.

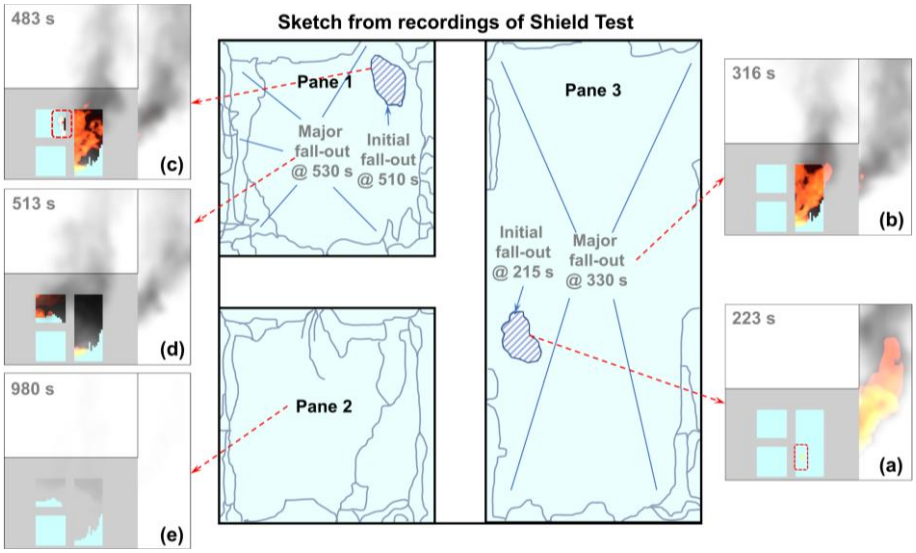

Fig. 2.5 Comparison of failure points of glass panes in FDS model with the Shields Test.

Fig. 2.6 further shows the variation in residual glass with time in the FDS model as well as the experimental recordings in the test report. It can be seen that the failure behavior of the window glazing could be captured in a relatively precise manner using the 'criterion-control' approach, although the fire damage to Pane 3 is underestimated by about 11% and overestimated by nearly 7% for Pane 1.

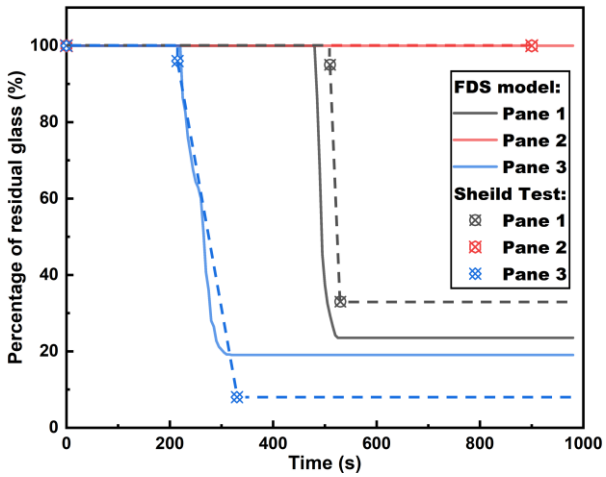

Fig. 2.6 Percentage of residual glass as a function of time.

Despite these deviations, it remains appropriate to use the glass failure model to simulate the ventilation change in FDS with respect to the whole fire development, since glass fallout itself is of considerable uncertainties and the slight inaccuracy of fallout time casts insignificant effect on a one-hour or even longer fire.

2.3.2 Effect of glass fallout to fire development in a small compartment

Based on the glass fallout integrated CFD simulation model, the effect of glass to the fire evolution in Shields Test can be further explored as a typical small compartment fire. Fig. 2.7a shows the variations of total HRR, internal HRR and external HRR of Shields Test in the FDS model, and the time steps when the window glass panes underwent fallout are shaded in light yellow. The time-varying

internal HRR shows that the fire grows rapidly within the first 90 s and then reaches a plateau of about 450 kW due to the limited ventilation, during which the excess fuel vapor is induced to exit through the side opening by the static pressure difference, forming external combustion. Thereafter, Pane 3 experiences a fallout, offering an increasing ventilation condition for the internal burning, and then the internal HRR gradually increases to its peak. As can be seen in Fig. 2.7b, the fallout of Pane 3 also causes a gradual shift of the external flame from the side opening to the window openings. With the formation of the vent at Pane 1 and the consumption of fuel inside, the fire is completely converted to internal combustion.

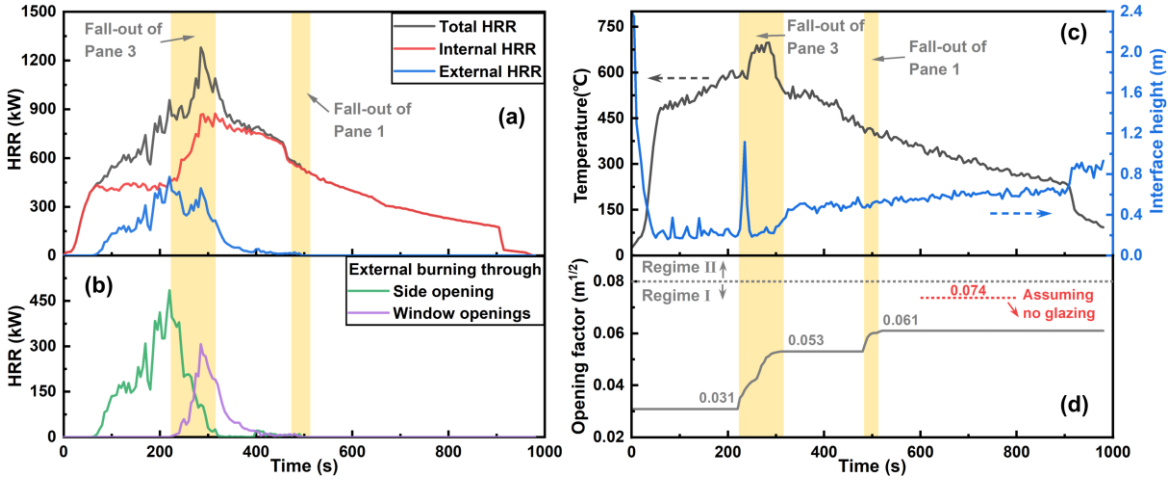

Fig. 2.7 The evolution of key parameters when considering the modelling of glass fallout.

The average temperature and height of the hot smoke layer are shown in Fig. 2.7c, and they both experience rapid changes in the first 90 s. During the progressive fallout of Pane 3, the temperature of the hot smoke layer is elevated due to the enhanced internal HRR. Meanwhile, due to the disruption of the pressure equilibrium, the hot smoke is suddenly released to reach a new steady state, causing a rapid growth in its height. The subsequent fallout of Pane 1 has a less significant impact on the hot smoke layer since the fire has already entered the decay stage. Notably, the fire-induced fallout of window glass can lead to substantial changes of the ventilation condition for fires, and the resulting stepwise increase in opening factor shown in Fig. 2.7d contrasts with traditional 'no-glass' assumption. These findings suggests the common simplification of neglecting window glass may not accurately reflect realistic fire scenarios, which was recently demonstrated in the full-scale Lai'an Fire Test [163].

2.4 Fire simulation of large open-plan compartments with/without window glass

2.4.1 A long compartment with discrete fuel bed: Kirby Test

Kirby et al. conducted the full-scale fire tests (denoted as Kirby Test) in a large compartment at Cardington in 1994 [8]. As shown in Fig. 2.8, the test compartment was 22.8 m long, 5.6 m wide and 2.8 m high, with one end kept open to allow ventilation. The sidewalls were made of 215 mm thick lightweight concrete slabs, while the ceiling was made of 200 mm thick reinforced concrete slabs. The

floor was filled with 125 mm deep liquid sand and the other inner surfaces of the compartment were lined with 50 mm thick ceramic fiber blankets. The thermal properties of the materials used in the FDS model are summarized in Table 2.1.

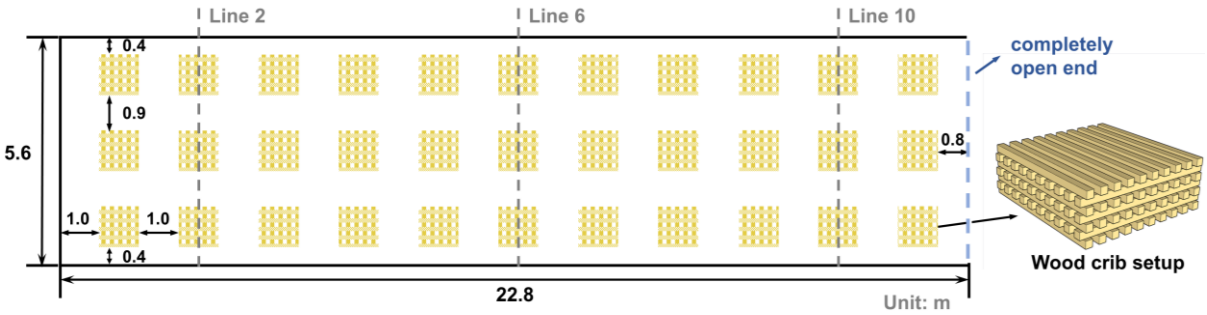

Fig. 2.8 Layout of the compartment and wood cribs.

Table 2.1 Thermal properties of construction materials used in FDS fire model of Kirby Test [8]

Properties	Unit	Lightweight concrete	Reinforced concrete	Fluid sand	Ceramic fiber
Density ρ	kg/m^3	1375	450	1750	128
Specific heat c_p	kJ/kg·K	0.75	1.05	0.80	1.13
Thermal conductivity λ	W/m·K	0.42	0.16	1.0	0.02
Emissivity e	-	0.9	0.9	0.8	0.9

There were 33 wood crib blocks evenly distributed on the compartment floor, forming a fuel bed matrix of 3 rows and 11 columns, with a spacing of 0.9 m between rows and 1 m between columns, as illustrated in Fig. 2.8. The configuration of wood cribs is also presented, while each block consisted of 7 layers wood sticks with 10 sticks per layer. Each stick was 1 m long, of a cross-section of 0.05 m × 0.05 m.

2.4.2 CFD model of Kirby Test

The FDS fire model of Kirby Test is built according to the test configurations described, which provides a simulation model of no window openings at the longitudinal wall. While modeling the original configuration of wood cribs (Fig. 2.9a) requires a finer mesh resolution as shown in Fig. 2.9b, resulting in prohibitively high computational costs. Herein, this work adopts an equivalent wood crib model proposed by Janardhan and Hostikka [167] to effectively reduce computational expenses.

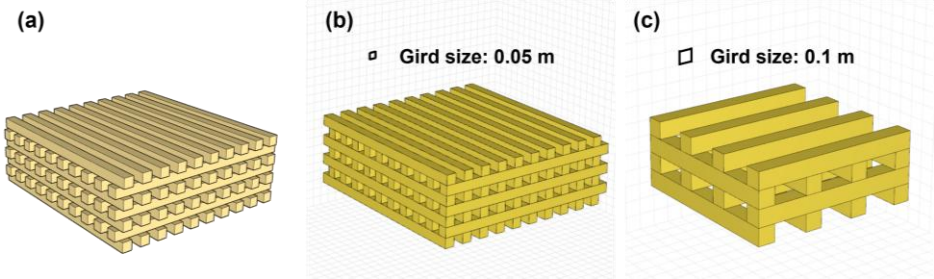

Fig. 2.9 Setup of wood crib block: (a) in Kirby Test, (b) in original fire model and (c) in equivalent fire model.

The equivalent setup of wood crib was modified to 4 layers with 4 wood sticks in each layer, where the cross-section of sticks was set as 0.1 × 0.1 m, as illustrated in Fig. 2.9c. This equivalent model will cause the decrease of exposed area of wood crib in the FDS model, which in turn reduces the mass loss rate of the burning wood sticks. To consider this effect, the parameter AREA_MULTIPLIER is applied, which is calculated as:

$$\mathrm{AM} = A_{real}/A_{FDS} \tag{2.1}$$

where A_{real} and A_{FDS} are the effective exposed areas of wood crib in real and FDS models, respectively. Moreover, the parameter BULK_DENSITY is correspondingly defined to ensure the designated fuel density. The choice of BULK_DENSITY [168] can be specified as:

$$BD = \frac{FLD \cdot A_{floor}}{V_{FDS} \cdot \Delta H_c \cdot (1 - y_{char}) \cdot (1 - y_{mois}) \cdot AM \cdot n_{crib}} \tag{2.2}$$

where FLD is the designed fuel load density of the compartment with floor area of A_{floor}, and V_{FDS} is the effective volume of wood per crib in the FDS model. ΔH_c denotes the heat of combustion of wood, which was reported as 19.5 MJ/kg [8]. y_{char} and y_{mois} are the char yield and moisture content of the wood stick, which are reported as 0.195 and 0.1, respectively. n_{crib} represents the number of wood cribs within the compartment. Thus, two essential parameters, AREA_MULTIPLIER and BULK_DENSITY were determined as 2.135 and 306.6, respectively.

The burning of wood cribs is resolved by a single-step pyrolysis model [168] that includes two parallel reactions, i.e., the pyrolysis of dry wood to produce fuel vapor and char, and the evaporation of the moisture content of the wood. For this purpose, the fuel surface in the FDS model is specified as two component layers according to the moisture content, i.e., dry wood layer and moisture layer, and the relevant thermal and chemical parameters are listed in Table 2.2.

Table 2.2 Thermal and chemical parameters used in the pyrolysis model [8,168,169].

Properties	Unit	Dry wood	Char	Moisture
Density ρ	kg/m^3	450	135	1000
Specific heat c_p	kJ/kg·K	1.35	1.08	4.18
Thermal conductivity λ	W/m·K	0.15	0.13	0.1
Pre-exponential factor A_a	s^{-1}	1.41×10^5	-	9.57×10^{22}
Activation energy E_a	kJ/mol	8.97×10^4	-	1.36×10^5
Order of reaction n	-	1.69	-	3.31
Heat of reaction ΔH_r	kJ/kg	250	-	2500

In the FDS model, the energy required to ignite the first crib column is provided by three 0.3 m^2 burners on the floor, and their HRR per unit area is set as a linear increase to 500 kW/m^2 within 60 s,

followed by a constant value of 500 kW/m^2 for 220 s, and then burns out as linear decrease to 0 at 300 s.

Three thermocouple lines are located above the crib columns 2, 6 and 10, which are indicated as Line 2, 6 and 10 in Fig. 2.8. Fifteen thermocouples are installed on each line was installed to record the horizontal temperature profiles across the width of the compartment. Their average temperature profiles are extracted for the validation of the FDS model for Kirby Test. The comparison between the simulated temperatures (dash line) against the reported average temperatures (solid line) is illustrated in Fig. 2.10.

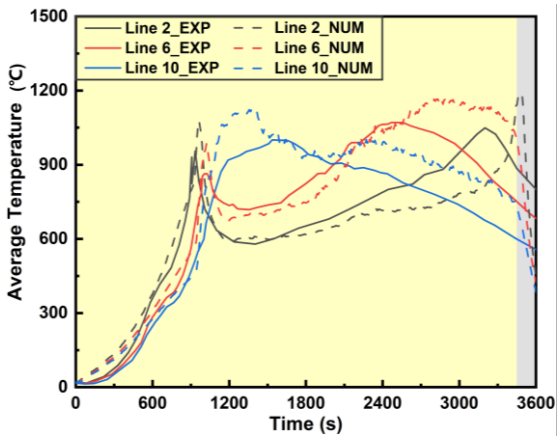

Fig. 2.10 Validation results against the experimental data of Kirby Test.

It is clearly observed that the current FDS model well predicts the temperature development in the first hour, whereas discrepancies are found in the decay stage (shaded in light grey). Nevertheless, the point of interest with regards to the glass fallout is cast on the fire development stage, where the fire model is credibly validated and can be used for further investigation. In addition, Fig. 2.11 compares the simulated outcomes with the photos of the field experiments extracted from Ref. [8].

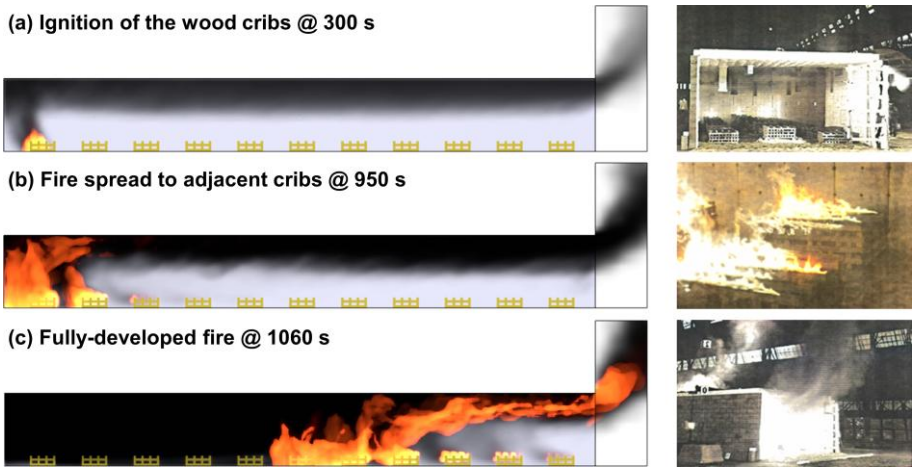

Fig. 2.11 Comparison of FDS modelling results with experimental observations [8].

The experimental observations are well reproduced in the FDS model. The first column of wood cribs is ignited, and its flame establishes locally at the early stage, as demonstrated in Fig. 2.11a. After

that, the flame remotely ignites the adjacent cribs (Fig. 2.11b) and then rapidly sweep across the floor, forming a spilled flame at the open end as shown in Fig. 2.11c.

2.4.3 A large compartment fire test with initial window openings: Malveira Test

The Malveira Test [10] was conducted in Portugal, which exhibited a slow 'travelling fire' behavior for more than 150 minutes in a large open-plan compartment with large area of windows without glass panels for sufficient ventilation. As illustrated in Fig. 2.12, the floor area of this long compartment was 21.1 m × 4.7 m, and its effective ceiling height was approximately 2.6 m. The enclosure was made of concrete with masonry block infill. Several concrete columns were attached to the two longitudinal walls as shown in Fig. 2.12a, and three concrete beams were present beneath the ceiling as shown in Fig. 2.12b. Five windows on the front wall were not glazed, and their dimensions are shown in Fig. 2.12c. In addition to these vents given by initial window openings, a door that is 0.8 m wide and 1.8 m high was opened by firefighters at about 148 minutes to enhance the air circulation.

The fuel used in this experiment was a continuous wood crib bed of 16.8 m in length and 2.4 m in width, as shown in Fig. 2.12a. The fuel bed was constructed using 1.2 m long wood sticks with a cross-section of 0.05 m × 0.05 m as a three-layer stack. The wood sticks in the top layer were spaced at 0.15 m and 0.05 m in the other two layers. The density of the wood sticks was estimated to be 510 kg/m^3, along with an average moisture content of 19% and a char yield of around 20%. The heat of combustion of the wood and the designed fuel load density were approximately18 MJ/kg and 420 MJ/m^2, respectively. In addition to the wood cribs as source of fuel, there was a 0.1 m thick cork layer as ceiling lining at the right-hand part of the compartment (Fig. 2.12b).

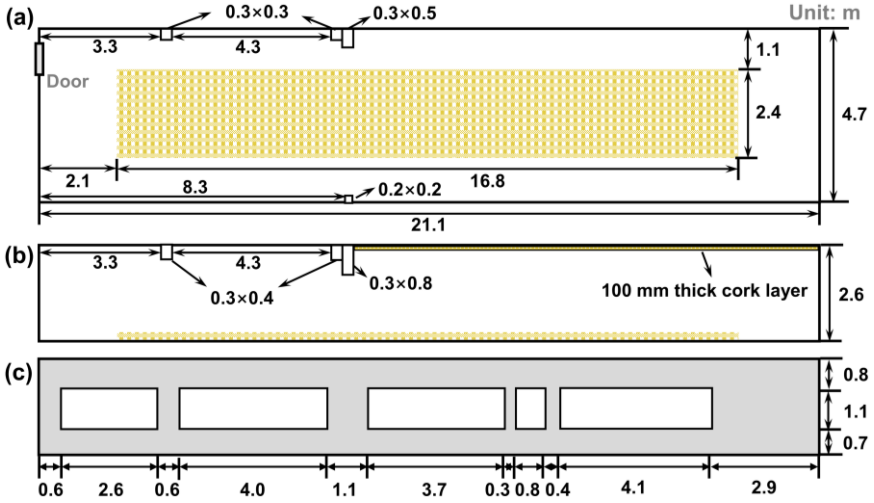

Fig. 2.12 Experimental setup of the Malveira Test: (a) floor plan, (b) longitudinal axis profile and (c) front view.

2.4.4 CFD model of Malveira Test

The CFD model of Malveira Test is built as an upper-bound case with respect to ventilation, as it comprises 5 initially open windows along the longitudinal wall. Similar to the fire model of Kirby Test, the equivalent wood crib model is employed to reduce the computational cost on modelling the stick-

by-stick burning of wood. The configuration of the wood crib in the FDS model (Fig. 2.13b) is modified to two layers of wood sticks with a stick spacing of 0.1 m and the cross section of each stick is set to 0.1 × 0.1 m. Moreover, the AREA_MULTIPLIER and BULK_DENSITY parameters are used to compensate for the burning surface area and fuel density, which are set as 3.205 and 311.1, respectively.

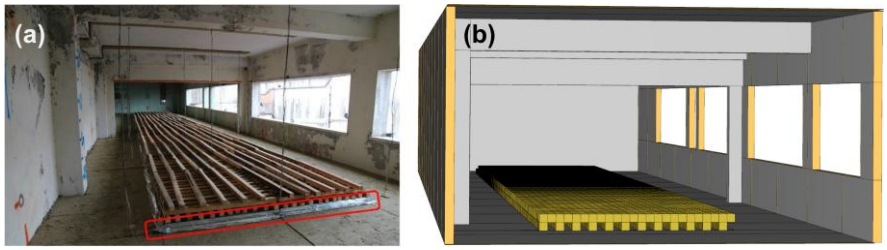

Fig. 2.13 Setting of wood cribs: (a) in the Malveira Test [10] and (b) in FDS model.

The aforementioned single-step pyrolysis model is used to resolve the burning of wood crib, while the cork layer is modelled using the ignition temperature model. In the model, the ignition temperature and HRR per unit area are set as 400 °C [10] and 160 kW/m^2 [170], respectively. The igniter of the wood cribs is given as a 2.4 m line burner with a peak HRR of 500 kW. The present FDS model well reproduces the characteristic fire behavior during the Malveira Test, including the localized burning, the travelling behavior, and the fast fire spread. During the fire test and simulation, the localized burning can be observed with a nearly constant flaming area that slowly moves forward, exhibiting a typical 'travelling fire' behavior as shown in Fig. 2.14a. Later, this steady burning behavior is interrupted by the additional combustion of the cork layer, which triggers a 'flashover' in the right-hand side of the compartment at around 237 min (or at about 13300 s in the FDS model), as shown in Fig. 2.14b.

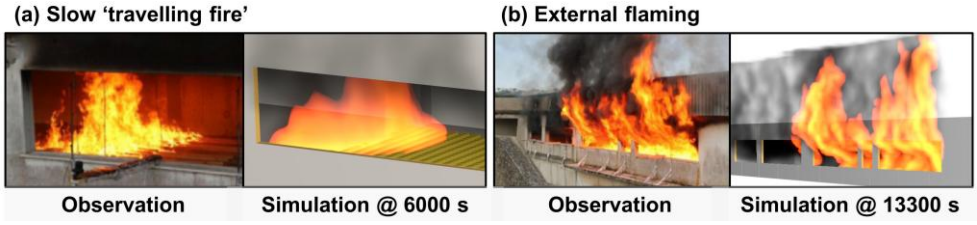

Fig. 2.14 Comparison of experimental observations [10] with the modelling results.

In addition to the agreement of experimental observations, the fire model also demonstrates its good performance on estimating the time-variant HRR as shown in Fig. 2.15. In general, the HRR curve given by the fire model is very close to that obtained from the test, especially in the travelling fire stage (shaded in yellow). Slight overestimation of the released heat is observed in the ignition phase (shaded in light grey), because it accounts for the total HRR including the igniting fuel, which was not presented quantitatively in Ref. [10]. Some discrepancies could be also found during the claimed 'growing fire' phase after the door being actively opened. Nevertheless, the CFD model provides acceptable performance for the later study on the effect of including glass in this large compartment.

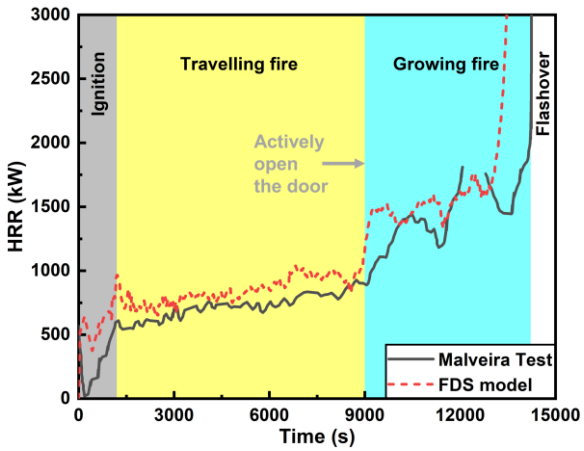

Fig. 2.15 HRR Comparison between the simulation and the data obtained in Malveira Test.

2.5 Effect of including glass behavior into idealized large compartment fire tests

2.5.1 Adding window glass into Kirby Test and Malveira Test

In the original setup of Kirby Test, the hot smoke layer was ineffectively ventilated (i.e., a lower bound) and forced to move to the only open end. It can be also treated as fully closed 'windows' at the long-edge wall, which caused fast spread of flames even on a discrete (or non-continuous) fuel bed. On the contrary, the Malveira Test setup perhaps assumed an upper bound of ventilation as it comprised a large area of windows without glass. In this chapter, the effect of window glass to the realistic fire behavior in large compartments is one main objective. For this purpose, the proposed glass modelling framework is applied to the FDS models of Kirby Test and the Malveira Test (Fig. 2.16), which serve as the intermediate ventilation conditions between the lower bound (Kirby Test) and the upper bound (Malveira Test).

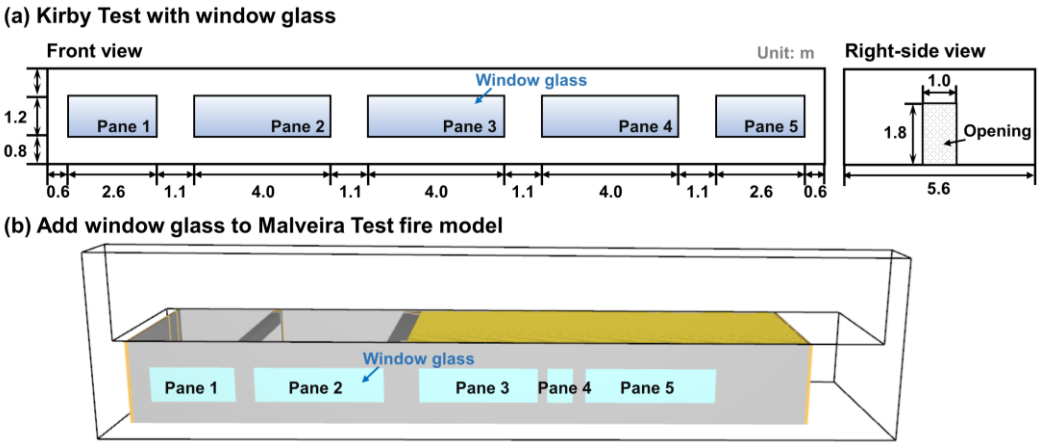

Fig. 2.16 Modifications of the FDS model for: (a) Kirby Test and (b) Malveira Test.

Since the Kirby Test model used solid walls on the long edges, the CFD model is now changed with windows and an end door similar to the Malveira Test compartment but with glass panels. As shown in Fig. 2.16a, the windows of a symmetrical distribution are added, and the dimensions of these windows are presented. Two models adapted from the Kirby Test model are analyzed in FDS, i.e., a

case with windows but without glass panels (similar to Malveira Test), and another case with glass panels. Similarly, five glass panels are added to the validated Malveira Test fire model (see Fig. 2.16b) in order to explore the effect of window glass on the 'travelling fire' behavior.

2.5.2 Effect of including glass windows to Kirby Test model with discrete fuel bed

The above mentioned two cases adapted from the Kirby Test model have been simulated in FDS. For the case with initially open windows, the hot smoke could be promptly expelled through the window openings, and the fast spread has been largely mitigated. After ignition, localized burning on the wood crib blocks can be observed, and the flame fails to jump to the adjacent wood crib, as shown in Fig. 2.17a. This significantly differs from the original test observations, in which the fast fire spread, and a 'flashover' behavior was found as a result of smoke accumulation and side opening induced flame spread.

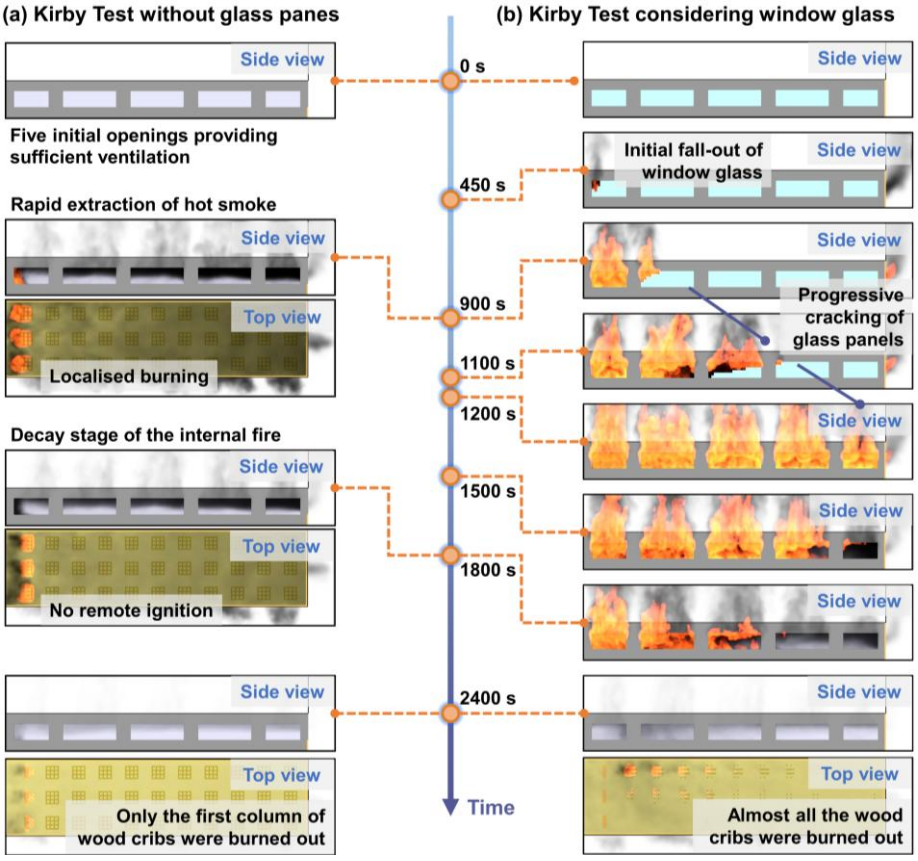

Fig. 2.17 Timelines of the extrapolated cases of Kirby Test.

The second case is a further adapted case of Kirby Test model, which implements the proposed glass fallout modelling approach to all the windows on the long-edge wall. As shown in Fig. 2.17b, the presence of glass hinders the extraction of hot smoke and allows heat to accumulate rapidly in the vicinity of initially ignited wood cribs. At about 450 s, the upper right part of Pane 1 began to fall off under the thermal impact from the localized fire. The complete fallout of Pane1 at around 900 s provides additional ventilation for the fire spread, while a portion of the fuel vapor is diverted to the window opening, forming flame ejection. In the next 300 s, the rest of glass panes fail sequentially as the fire

propagates across the discrete wood cribs. Eventually, the fire-induced glass fallout allows sufficient ventilation for the fire development, resulting in a catastrophically large fire where all the combustibles are ignited till the burnt-out.

The comparison of these timelines reveals the importance of the window glazing in modern compartment fires, where the long duration is a striking feature as indicated in Fig. 2.18. The fallout process from the initial cracking of Pane 1 to the removal of all panes is completed in nearly 12 minutes. This suggests that the fall-out of glass panes is a highly coupled interaction with the fire dynamics in a large compartment. The initial existence of glazing glass lessens the effective ventilation, which is more prone to the fire behavior in the original Kirby Test model. The increasing HRR along with accumulated hot smoke then leads to glass fallout, which reduces the smoke immediately. However, the ventilation remains much lower than the case with initially open windows.

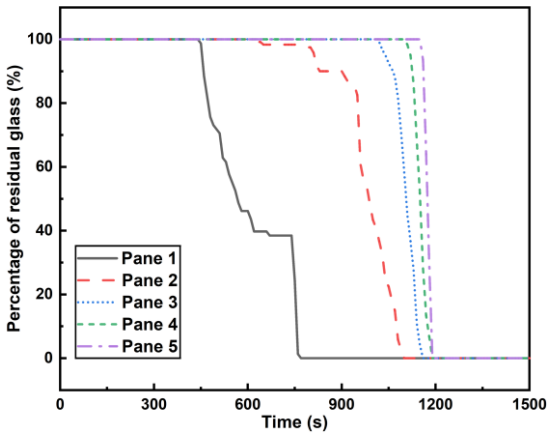

Fig. 2.18 Percentages of residual glass panes in Kirby model with glass windows.

Fig. 2.19a displays the feedback of fire-induced glass fallout to the fire development, and the timeslots corresponding to the fallout of glass panels as shaded in different colors. If comparing the internal HRR, adding glass panels caused slightly higher HRRs at the early stage of the fire, which indicates that the accumulated heat can allow additional wood cribs to be remotely ignited. After that, the developed fire exerts an enhanced thermal impact on the surroundings, triggering the gradual fallout of Pane 1. A portion of the fuel vapors are then vented through the windows and side openings and burned outside. This sudden change in ventilation induces the flame to the vicinity of the longitudinal wall with windows, which facilitates the destruction of Pane 2.

As Pane 2 approached complete fallout, the internal HRR experienced a dramatic surge, which in turn accelerated the subsequent glass fallout process. Moreover, the fire intensity continuously increases during the progressing fallout of the glass panes and peaks at around 23 MW when all panels fall out. The influence of the glass on the average gas-phase temperature (Fig. 2.19b) in the compartment is of a similar pattern to the HRR. A rapid rise in room temperature is seen in the first 400 s. The openings owing to the glass fallout allow for the enthalpy exchange and reduce the gas phase temperature, which is followed by a gradual increase resulting from the flame spread. The temperature eventually reaches

around 1400 °C after all the glass panes fail, which may cause severe damage to structural members. In contrast, a much lower peak temperature (around 500 °C) is seen in the case without glass panes, as the fire flames are localized to the initially ignited wood cribs.

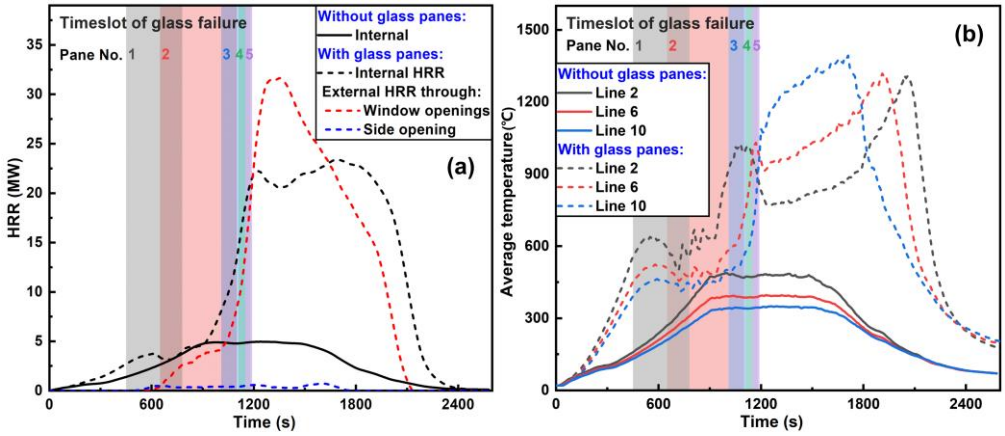

Fig. 2.19 Differences caused by window glass in: (a) HRRs and (b) averaged upper layer temperatures.

2.5.3 Effect of including window glass to Malveira Test model with continuous fuel bed

A slow travelling fire was observed in the Malveira Fire test and reproduced in the corresponding model while assuming initial opening at the windows. In the CFD model of Malveira Test compartment with the added window glass, different fire behavior as shown in Fig. 2.20 has been found. A localized fire is found after ignition, which cannot induce high enough thermal impact on glass panes to cause damage and fallout. This undermines the premise that all windows are initially open without window glass as it was believed to have glass fallout at a very early stage. Consequently, the existence of window glass would reduce the effective ventilation to the localized fire and cause the accumulation of hot smoke, which would change the fire behavior as shown in Fig. 2.20a. The movement of localized flames is much faster and it only takes 1200 s to reach the other end of the compartment. The glass pane is observed to undergo fallout at about 7600 s, which causes a backdraft behavior and fast spread of fire flames later. However, in the Malveira Test without glass panes, the small localized fire only travels a few meters after 9000 s (see in Fig. 2.20b).

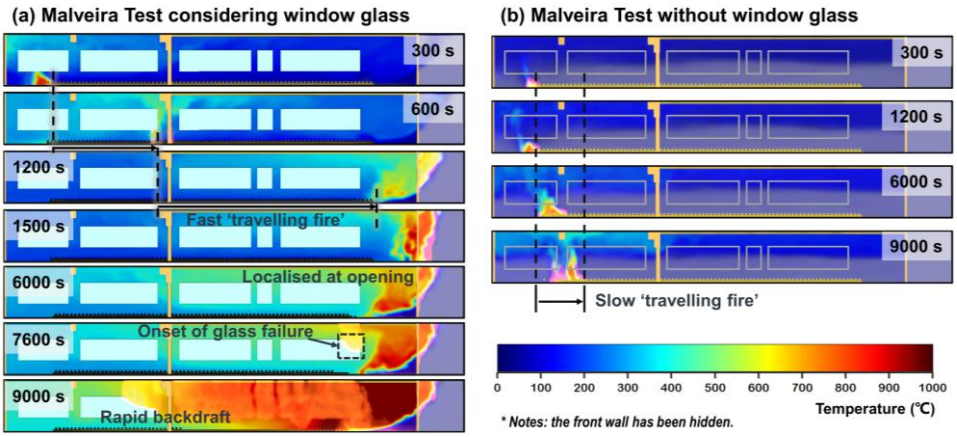

Fig. 2.20 Fire behavior in the Malveira Test models with and without glass panes.

If retrieving the HRR and recorded data from these fire models, the influence of window glass can be illustrated in Fig. 2.21. The interface height of smoke layer rapidly reaches about 0.5 m above the floor after ignition, which is followed by a much lower interface height (around 0.4 m) compared to the case without glass pane (original Malveira Test setup) as shown in Fig. 2.21a. The accumulation of smoke significantly raises the inner gas phase temperature, as shown in Fig. 2.21b. The localized fire near the window opening exhibits a significantly higher internal HRR, approximately five times that of the no-glass scenario. Initially, the fire grows gradually, causing a slight increase in room temperature. However, as the glass panes begin to fail, window openings are formed, allowing oxygen to enter and subsequently intensifying the fire, which in turn accelerates the fallout of the remaining glass panes.

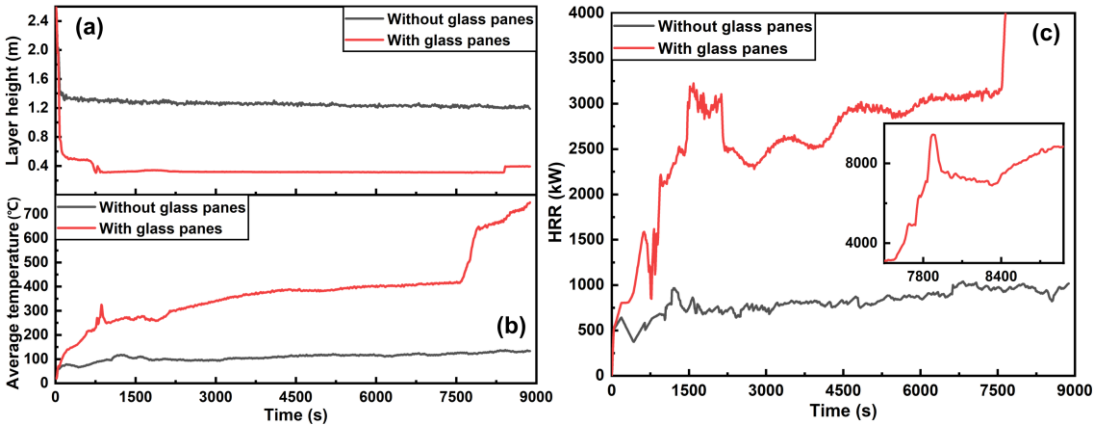

Fig. 2.21 The influence of glass panes on: (a) smoke layer height, (b) average temperature of smoke layer, and (c) internal HRR.

A comparative analysis of cases with and without window glass clearly demonstrates the necessity of accounting for ventilation changes induced by glass fallout. Fire behavior in large compartments is closely linked to the dynamic process of glass failure, and assuming idealized sufficient ventilation, as in the no-glass case, may lead to an underestimation of fire intensity.

2.6 Conclusions

This chapter proposes a 'criterion-controlled' framework for modelling the fire-induced glass fallout in CFD fire models. The Shields Test model with multiple window glass panels in a small compartment has been first employed for validation of the proposed glass fallout model. To investigate the effect of considering window glass to the fire behavior in large compartments, CFD models have been established and validated against the test data. The models were then adapted to include glass windows by using the proposed glass fallout model. Detailed discussion has been presented in this chapter upon these models, and the key points of conclusion can be drawn as follows:

(1) A 'criterion-controlled' framework comprising glass sub-modules, virtual monitoring devices, and the control logic to deactivate the obstruction has been established in the CFD fire models to simulate the progressive fallout of glass panes and the resulting ventilation changes during a fire.

(2) The Shields Test as a fire test in a small compartment with multiple glass panels is simulated

using the proposed FDS fire model integrating glass fallout. The fallout of Glass Pane 1 and 3 starting at 200 s and 500 s in the test have been well captured in the CFD model. The simulation model also shows good performance in predicting the time-variant temperatures and heat fluxes monitored in the test.

(3) The CFD models for large compartment fire tests have been built to lay down the simulation basis to the later investigations on glass behavior. The Kirby Test conducted in a long compartment without windows on long-edge walls and with discrete wood crib bed shows fast fire spread. The Malveira Test conducted in a long compartment with initially open windows and continuous wood crib bed presents travelling fire behavior. These two tests can mark the 'lower bound' and the 'upper bound' of window ventilation, whereas the compartments with window glass provide intermediate ventilation conditions.

(4) The validated fire models of Kirby Test and Malveira Test are then adapted to include the window glass for realistic fire scenarios. If providing sufficient ventilation through initially open windows to the Kirby Test model of discrete fuel bed, the localized fire sustains at the originally ignited wood crib. However, fast fire spread and a sweeping fire occurs at 1100 s in the case of Kirby Test fire model including window glass. On a continuous fuel bed, the fire spread becomes much faster in the case of Malveira Test fire model with glass, which does not cause glass fallout in the first 2 hours and shows a backdraft fire afterwards.

(5) The fire behavior in large compartments can be significantly altered when the effect of window glass fallout is explicitly considered in CFD models. Despite certain inherent limitations of the current fallout modeling approach, the findings clearly indicate that the traditional 'no-glass' assumption may be inadequate. The proposed modeling framework provides a foundation upon which future research can integrate refined glass fallout criteria. This facilitates a deeper understanding of fire-glass interactions in modern open-plan compartments.

Chapter 3: Considering Uncertainties of Glass Fallout on Changing Fire Behavior

Summary

Chapter 2 has established a 'criterion-controlled' framework for modelling the effects of glass fallout to fire development in large open-plan compartments. However, this framework relies on deterministic glass fallout criteria, whereas in reality, the conditions governing glass fallout exhibit inherent uncertainty. Building upon the proposed simulation framework in Chapter 2, this chapter investigates the impact of glass fallout uncertainty on fire dynamics. To quantify the stochastic nature of glass failure, a three-parameter Weibull distribution is introduced to model the variability in glass surface temperature as a triggering condition for glass fallout. A total of 200 fire simulations incorporating this probabilistic glass fallout model are conducted using a designed modern compartment fire model with three glass panels. The findings identify four distinct fire development patterns (P1-P4), categorized based on the timings of glass fallout and HRR histories. Among these, the earliest glass fallout as category P1 could effectively inhibit fire spread, whereas slightly delayed fallout in category P2 can cause accelerated fire progression. Although occurring with only 1% probability, the fire in P2 imposes severe long-lasting thermal impact on adjacent structural components, leading to the least favorable fire scenario. Category P3 is the most frequently observed fire scenario, accounting for 83% of all simulations. Additionally, category P4 experiences the most delayed fallout due to the enhanced fire performance of glass panels, substantially slowing down fire progression. These findings highlight the critical role of incorporating glass fallout uncertainty in fire risk assessments. Neglecting this variability may lead to oversimplified predictions and underestimated safety margins in fire safety design of modern open-plan compartments.

The work of this chapter has been reported in a journal paper: 'T. Chu, R. Van Coile, L. Jiang. Effects of uncertainty in glass fallout criteria on fire behavior (Submitted).'

3.1 Introduction

The ‘criterion-controlled’ modeling framework developed in Chapter 2 has effectively illustrated the influence of window glass fallout on fire development histories. The deterministic Shields’ criteria, adopted in this framework, describe the relationship between fire-induced thermal stress and glass strength, wherein glass fallout occurs when the thermal stress exerted by the fire exceeds the inherent strength of the glass. However, glass strength and fire induced glass stress are both of considerable uncertainties in real buildings, which vary with glass manufacturing processes and fire conditions. These variations inevitably result in the uncertainties of the timing and patterns of glass fallout during compartment fires. Such uncertainties were also found in experimental studies, in which different fallout criteria were proposed. For instance, unlike the Shields criteria, Manzello et al. [159] reported using glass surface temperatures exceeding 416 ºC or heat fluxes surpassing 50 kW/m² as indicators. Wang et al. [160,161] utilized the temperature difference between the glass surface and edge as their primary criterion. Apparently, adopting deterministic criteria may over-simplify glass breakage behavior in fires, which would directly impact the formed ventilation conditions through glass fallout and change the fire development paths, especially when the glass-fire interaction plays a critical role.

To address this concern, the current chapter extends the previous modeling framework established in Chapter 2 by explicitly incorporating the glass fallout uncertainty into the CFD simulation models. This integration involves a probabilistic analysis of existing fire test data based on principles derived from solid fracture mechanics. A three-parameter Weibull distribution is then derived to model the probability of glass fallout as a function of glass surface temperature, while the ‘size effect’ factor is incorporated to account for variations in glass failure temperatures due to differences in glass area. This uncertainty-based distribution is utilized to replace the Shields’ deterministic criteria, forming an updated simulation framework. Using this updated framework, a series of 200 independent CFD simulations are performed in a compartment fire model featuring three window glass panels. The simulations reveal four distinct fire development patterns, and statistical analyses are performed on key fire parameters, including HRR histories, timings of glass fallout, opening factors, and indoor temperatures. The findings underscore the critical impact of glass fallout uncertainty on fire behavior, providing valuable scientific insights for fire safety engineering. Moreover, these results offer practical guidance for developing innovative fire protection strategies and improving fire safety measures in modern building designs.

3.2 Comprehensive analysis of glass fallout uncertainty

3.2.1 Evidence of glass fallout uncertainty from existing fire test data

The earliest systematic criterion for glass fallout was summarized by Shields, who conducted extensive investigations into the fire performance of glass panels through 33 pool fire tests within a full-scale ISO 9750 standard compartment [144,145]. The window assembly tested comprised three glass

panels, each 6 mm in thickness, arranged as shown in Fig. 3.1a. Through statistical analysis of temperature and heat flux data recorded at the moment of glass fallout, Shields derived the first conservative criteria for predicting glass fallout, specifically:

(a) the fire-exposed glass surface temperature exceeds 447 °C, or

(b) the average incident heat flux to glass surface exceeds 35 kW/m^2.

Following this, Manzello et al. [159] conducted a full-scale fire test to investigate the fire response of single-pane and double-pane tempered glass with thickness of 6.35 mm, and the configuration of this window set is shown in Fig. 3.1b. Their findings yielded a distinct set of fallout criteria for single-pane glass:

(a) the fire-exposed glass surface temperature exceeds 416 °C, or

(b) the average incident heat flux to glass surface exceeds 50 kW/m^2.

For the laminated double-pane glass, the inner pane fell out at approximately 400 °C, while the outer pane remained intact.

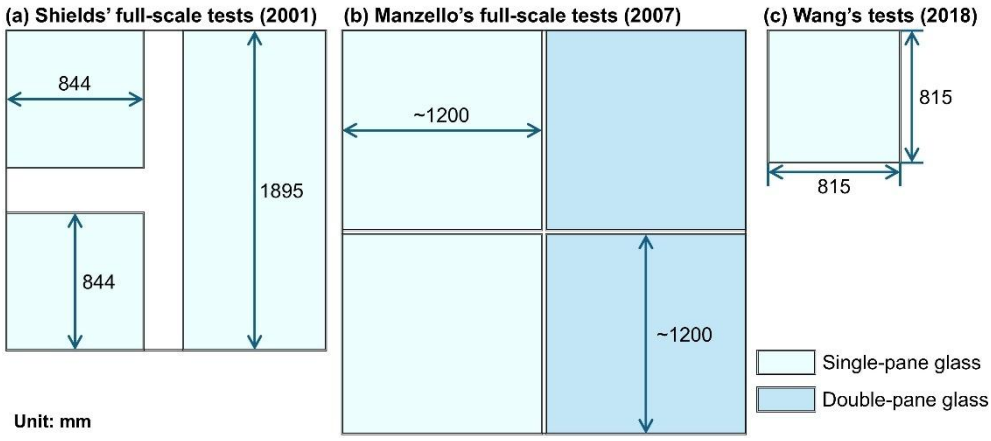

Fig. 3.1 Setups of window glass in fire tests recording the glass fallout [145,159,160].

In 2018, Wang et al. [160,161] conducted two series pool fire tests on 6 mm-thick tempered glass panels (Fig. 3.1c), utilizing the same compartment geometry but obtaining two different glass fallout criteria. Their first test series, involving 11 fire tests [160], identified the criteria as:

(a) the temperature difference between the glass surface and edge exceeds 301 °C or

(b) the average incident heat flux to glass surface exceeds 36 kW/m^2.

While their second test series consisting of 8 tests [161] yielded slightly different fallout criteria:

(a) the temperature difference between the glass surface and edge exceeds 340 °C or

(b) the average incident heat flux to glass surface exceeds 46 kW/m^2.

To address this glass fallout uncertainty highlighted in Wang's experiments, Xie et al. [162] performed statistical analyses using Wang's test data, including the temperatures of the fire-exposed glass surface and edges, along with their temperature differences, and incident heat fluxes. Their findings indicated that the fire-exposed surface temperature was the most reliable indicator for predicting glass fallout and then provided a best-fitted three-parameter Weibull distribution to model the glass fallout uncertainty in Wang's tests:

$$P_f(T) = 1 - \exp\left(-\left(\frac{T - 497.1}{48}\right)^{2.012}\right) \tag{3.1}$$

where P_f represents the cumulative probability of glass fallout under fire-exposed surface temperature T.

These studies demonstrate inherent uncertainty in glass fallout behavior under fire exposure, suggesting that deterministic criteria may not reliably capture realistic glass fallout scenarios. Therefore, it is crucial to incorporate glass fallout uncertainty into predictive models to characterize its effects on compartment fire dynamics.

3.2.2 Three-parameter Weibull distribution for modelling glass fallout uncertainty

The superior fitting performance of the three-parameter Weibull distribution identified by Xie et al. [162] can be traced back to the fundamental two-parameter Weibull distribution [121] for modeling glass strength mentioned in Section1.2.2. This initial relationship is expressed as:

$$P_f(\sigma) = 1 - \exp\left(-\left(\frac{\sigma}{\theta_c}\right)^{\beta}\right) \tag{3.2}$$

where P_f represents the cumulative probability of glass fallout under a tensile stress σ. θ_c is the scale parameter that determines the peak of the probability distribution curve, and β is the shape parameter governing the distribution range. In this expression, the parameter θ_c depends on glass surface conditions and can be expressed as:

$$\theta_c = \frac{\sigma_c(a_0)}{M^{1/\beta}} \tag{3.3}$$

where M denotes the total population of surface flaws in the glass pane, and σ_c the critical tensile stress required to propagate a surface flaw with an initial depth a_0. Due to practical difficulties in accurately measuring the parameters M and a_0, standard R400 tests [125] are typically conducted repeatedly to empirically estimate the Weibull parameters θ_c and β. For ordinary float glass, recommended reference values are typically adopted as θ_c= 74 MPa and β = 6 [123].

For tempered glass, which is widely used in modern buildings, an additional pre-stress σ_T is introduced during the tempering process to improve its tensile resistance. This pre-stress effectively shifts the Weibull distribution horizontally by a magnitude of σ_T, without altering its inherent scale and

shape parameters, as illustrated in Fig. 3.2. Consequently, equation (3.2) is modified into a three-parameter Weibull distribution to account explicitly for the pre-stress σ_T effect:

$$P_f(\sigma) = 1 - \exp\left(-\left(\frac{\sigma - \sigma_T}{\theta_c}\right)^{\beta}\right) \tag{3.4}$$

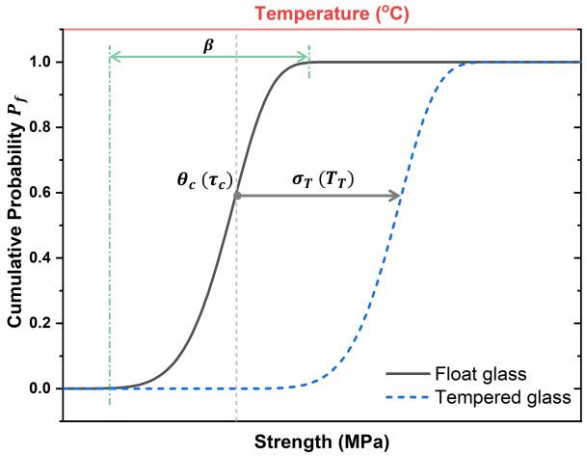

Fig. 3.2 Illustrations of parameters in equation (3.4) and their linear transformation from strength to temperature.

Glass fallout during a fire scenario is primarily attributed to the thermal stress resulting from constrained thermal expansion of glass when exposed to fire heating. Such thermal stress is typically assumed to vary linearly with temperature rise [131], expressed as $\sigma = E\alpha(T - T_0)$, where E and α represent the Young's modulus and thermal expansion coefficient, respectively. Thus, the cumulative probability distribution for glass fallout expressed as a function of the glass surface temperature can be derived as:

$$P_f(T) = 1 - \exp\left(-\left(\frac{T - T_T}{\tau_c}\right)^{\beta}\right) \tag{3.5}$$

where τ_c corresponds to a linear transformation of θ_c, which can be expressed as:

$$\tau_c \propto \theta_c = \frac{\sigma_c}{M^{1/\beta}} = \frac{E\alpha(T_c - T_0)}{M^{1/\beta}} \tag{3.6}$$

In this formulation, T, T_T and T_c represent the temperatures of the fire-exposed glass surface that result in thermal stresses of σ, σ_T and σ_c, respectively. The underlying relationship captured by equation (3.5) effectively explains the uncertainty in glass fallout temperatures observed under identical experimental conditions. This relationship underscores why the three-parameter Weibull distribution (the blue dash line in Fig. 3.3 reported by Xie et al. [162]) provided the best fit to the Wang's test. However, it is noteworthy that all three Weibull parameters in Xie's mathematical expression, including the shape parameter β, were empirically derived from experimental data. In fact, the shape parameter β should theoretically be an intrinsic property related to the glass material itself. This oversight has been addressed and corrected in the current study.

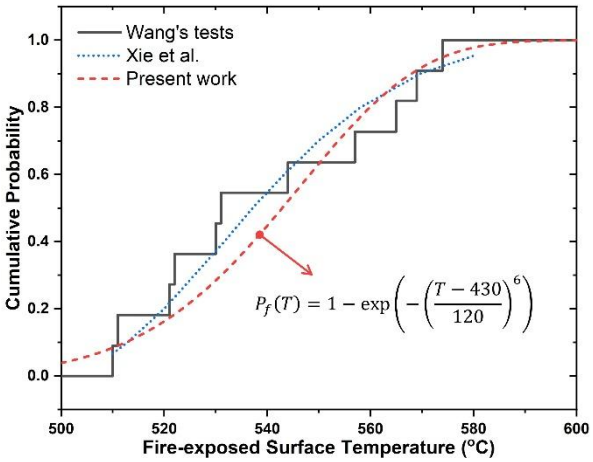

Fig. 3.3 Three parameters Weibull distribution fittings for Wang's tests.

Throughout the derivation from equation (3.2) to equation (3.5), the parameter β remains constant and retains its value of 6. Whereas the accurate determination of τ_c, similar to θ_c, remains challenging due to uncertainties in measuring M in equation (3.6). Thus, it requires empirical calibration through experimental data. By applying equation (3.5) to Wang's experimental test data and performing statistical fitting, a new three-parameter Weibull distribution is derived for modelling the glass fallout probability based on glass surface temperatures, as shown by the red dash line in Fig. 3.3. Nevertheless, minor deviations from test data still exist, possibly stemming from other complex factors such as slight variations in glass panel sizes and added pre-stress during tempering process, which will be discussed in the following sub-section.

3.2.3 Uncertainty associated with glass size and added pre-stress

The geometry of glass panes significantly influences their fallout behavior under fire conditions, an effect referred to as the 'size effect.' Evidence for this size effect on glass fallout can be drawn from these mentioned fire tests summarized in Fig. 3.1, particularly in the Shields' tests, where larger glass panes were always observed to fall out earlier than smaller ones under comparable fire exposures. According to the principles of fracture mechanics, this size effect is considered by correcting the strength σ using the following relationship [123]:

$$\frac{\sigma(A_1)}{\sigma(A_2)} = \left(\frac{A_2}{A_1}\right)^{1/\beta} \tag{3.7}$$

where $\sigma(A_1)$ and $\sigma(A_2)$ are the tensile strength of glass panes with surface areas of A_1 and A_2, and is β the shape parameter of the Weibull distributions as introduced earlier. Likewise, this size effect can be applied to the three-parameter Weibull distribution of glass fallout probability by adopting the linear transformation between thermal stress σ and glass surface temperature T, formulated as:

$$\frac{T(A_1) - T_0}{T(A_2) - T_0} = \left(\frac{A_2}{A_1}\right)^{1/\beta} \tag{3.8}$$

where $T(A_1)$ and $T(A_2)$ represent the critical glass fallout temperatures corresponding to areas A_1 and A_2, respectively. T_0 is the initial reference temperature.

In addition to glass geometry, variations in pre-stress introduced during the tempering process also contribute significantly to uncertainties in glass fallout behavior. Slight deviations in pre-stress σ_T are inevitably present [171], despite established quality control standards, such as ASTM C1048 [22], GB 15763 [172] and EN 12150 [173], have been proposed to regulate this process for quality control. These deviations may substantially influence glass fallout temperatures during fire exposure. Due to the limited availability of comprehensive datasets, accurately quantifying the precise effects of such deviations remains challenging. To address this limitation, this chapter employs an idealized approach by assuming that the added pre-stress follows a normal distribution with error tolerance range of 10% [172]. These considerations enable more accurate representation of glass conditions, allowing the exploration of fire development influenced by stochastic glass fallout events.

3.3 Integrating glass fallout uncertainty into CFD fire simulations

3.3.1 Updated modelling framework incorporating stochastic glass fallout behavior

To effectively address the inherent uncertainty in glass fallout during fires, the current work updates the previously established 'criterion-controlled' modelling framework [174] by replacing the deterministic Shields criteria with the uncertainty-based three-parameter Weibull distribution derived in Section 3.2. Specifically, the glass fallout temperature is stochastically sampled from the derived Weibull distribution and subsequently assigned to randomly selected glass sub-modules within the computational fire models. As illustrated in Fig. 3.4, the workflow of the updated modeling approach consists of three key procedures:

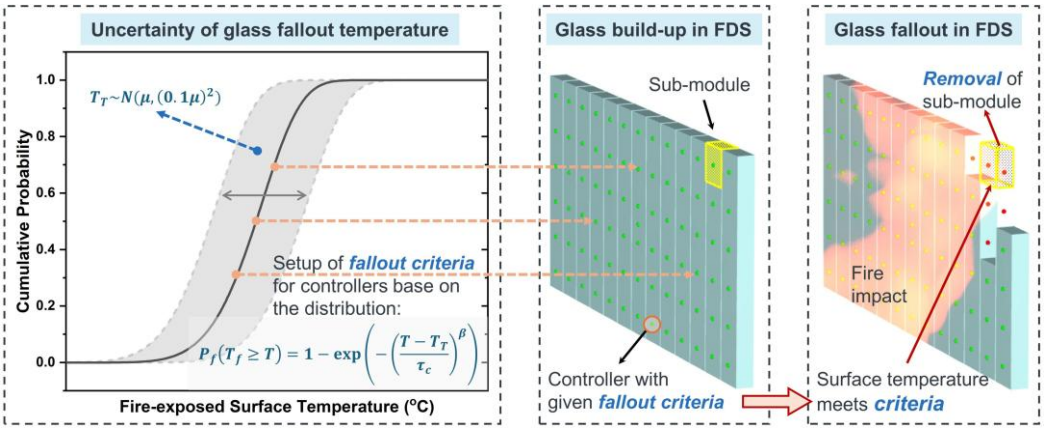

Fig. 3.4 Integration of uncertainty in glass fallout criterion into glass modules in FDS.

(a) Characterization of glass fallout uncertainty: The reference three-parameter Weibull distribution illustrated in Fig. 3.3 is adjusted using a 'size effect' factor, resulting in a tailored probabilistic description of glass fallout temperatures suited to the specific test configurations to be

investigated. Additionally, a normal distribution with error tolerance range of 10% [172] is used to account for the variability of pre-stress added to the glass panels.

(b) Configuration of glass sub-modules: The glass panels in the fire model are divided into several sub-modules. Each sub-module is independently assigned a specific fallout temperature threshold sampled from the adjusted Weibull distribution, thereby representing inherent uncertainty in glass fallout under fire conditions.

(c) Removal of glass sub-modules: When the monitored temperature of a glass sub-module exceeds its assigned stochastic fallout temperature, the respective sub-module is removed from the simulation domain in the subsequent computational step.

The improved uncertainty-based framework is expected to capture the realistic interactions between window glass fallout and fire dynamics, while its performance will be checked through our design CFD fire models.

3.3.2 Description of CFD fire models adopting updated simulation framework

To systematically investigate the effects of glass fallout uncertainty on fire dynamics, a prototype compartment model is developed with three window glass panels. As illustrated in Fig. 3.5, the internal dimensions of the compartment model are 3.95 m × 1.95 m × 1 m. he outer shell of the compartment is constructed from zinc-coated steel, while the interior surfaces of the walls and ceiling are lined with 2 cm thick cement fiberboard (density of 1150 kg/m^3, thermal conductivity of 0.31 W/m^2·K, and specific heat of 1.23 kJ/kg·K).

To represent longitudinal ventilation in modern large compartments, three windows are installed on the front wall, as depicted in Fig. 3.5a. Each window set measures 1.0 m in width and 0.5 m in height, with a vertical clearance of 0.1 m to the ceiling. The dimensions of each glass panel are approximately 0.9 m by 0.4 m when excluding the window frames. Additionally, the opening on the right-hand side wall is about 0.55 m high, following a semi-confined design approach [175], as shown in Fig. 3.5b.

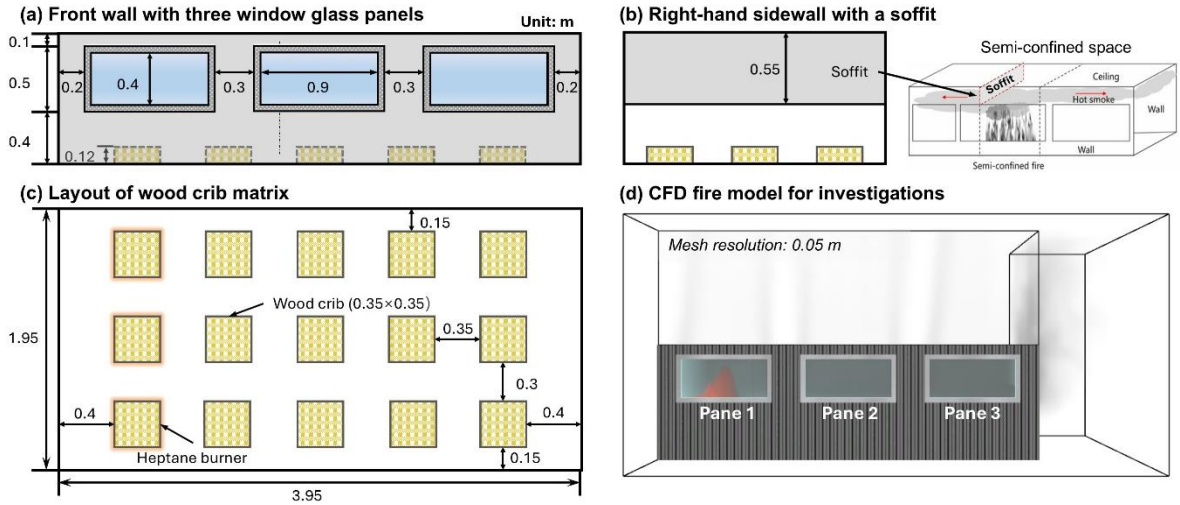

Fig. 3.5 Configuration of the reduced-scale compartment fire tests.

As shown in Fig. 3.5c, fifteen wood crib blocks are uniformly placed on the floor, allocated in a fuel bed matrix of 3 rows by 5 columns to represent the fuel load. The spacing between two adjacent rows is 0.3 m, and the spacing is 0.35 m among columns. Each wood crib block consists of 3 layers, with each layer composed of 4 wood sticks. Each wood stick measures 0.35 m in length, with a square cross-section of 0.05 m × 0.05 m. The moisture content and heat of combustion of wood materials are specified as 10.5% and 17.5 MJ/kg [176], respectively. The combustion process of wood cribs is modeled in three primary stages: moisture evaporation, thermal decomposition, and conversion of residual char to ash. The reaction kinetics parameters for each stage are determined through thermogravimetric (TG) analysis of real pine sticks, with details provided in Appendix C. Three heptane burners are simulated by incorporating heating surfaces beneath the first column of the wood crib matrix to replicate the ignition process. The heat release rate per unit area (HRRPUA) is set to linearly increase from 0 to 300 kW/m^2 within 30 s, maintaining this rate until 180 s, which is followed by a linear decay to 0 at 360 s.

Based on the above description of the compartment model, the CFD fire model is established for numerical investigations, as illustrated in Fig. 3.5d. The computational domain is expanded around the windows and side openings to ensure sufficient space for smoke movement and flame ejection. The entire domain is modelled with a uniform grid resolution of 0.05 m. To incorporate the stochastic nature of glass fallout, the updated modeling framework, which accounts for glass fallout uncertainty, is applied to the glass panels in the prototype fire model. A total of 200 independent fire simulations are conducted, with each simulation featuring unique glass fallout criteria sampled from the derived Weibull distribution. This extensive parametric study allows for a comprehensive assessment of the influence of glass fallout uncertainty on fire development.

3.4 The role of glass fallout uncertainty in fire development

3.4.1 Distinct fire development patterns due to glass fallout uncertainty

The evolution of fire behavior in the simulations conducted in this study exhibits substantial variability due to the uncertainty in window glass fallout. In all fire simulations, flames initially originate from the first column of wood cribs (Fig. 3.6a) before spreading toward the right-side opening. As the fire progresses and additional wood cribs become involved to enhance flame intensity, causing the flames to spill out through the right-side opening. This flame spillage highlights the strong dependency of fire growth on oxygen availability, thereby suggesting that any change in ventilation caused by glass fallout can significantly alter fire dynamics.

Fig. 3.6c illustrates the potential fire scenarios following glass fallout as observed in the simulations. It is found that the newly formed openings due to window glass fallout provided additional pathways for external flames, thereby altering the fire propagation direction and redirecting part of the

flames toward the fallen window glass area. This impact on fire development is reflected in the HRR histories that are obtained from the CFD fire models.

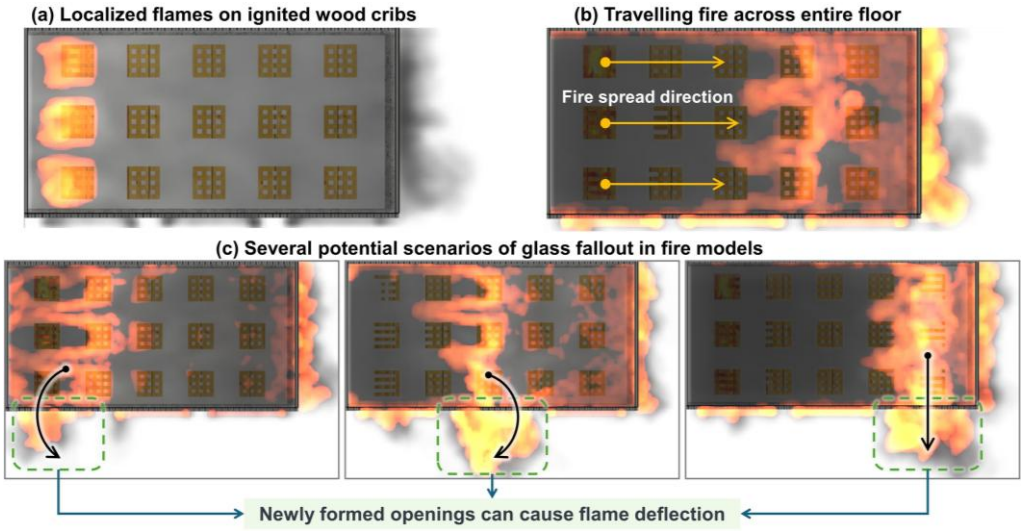

Fig. 3.6 Illustration of interactions between glass fallout and fire spread (top view of the compartment).

The HRR curves extracted from 200 fire simulations are presented in Fig. 3.7, clearly showing the variations in HRR evolution due to the uncertainty in glass fallout. These curves can be classified into four distinct patterns: P1, P2, P3, and P4, each represented by different colors in the figure. The P1 pattern represents the most favorable outcome where fire intensity does not get further enhanced, accounting for 10.5% of all simulations. The P2 pattern exhibits extremely rapid-fire growth and high-intensity flames but is the least common fire scenarios, occurring in only 1% of simulated cases. The P3 pattern, which is the most frequently observed, accounts for 83% of simulations and is characterized by a rapid fire development within approximately 15 minutes, with the HRR peaking at 1 MW. The P4 pattern exhibits a more moderate fire intensity growth, with a plateau phase in HRR significantly lower than those of P2 and P3, representing 5.5% of all cases. It is important to note that due to the simulation time constraint of 1500 s, the lower HRR observed in the P4 pattern may only be a transient phenomenon. If the fire duration were extended, this pattern might follow a trend similar to P3.

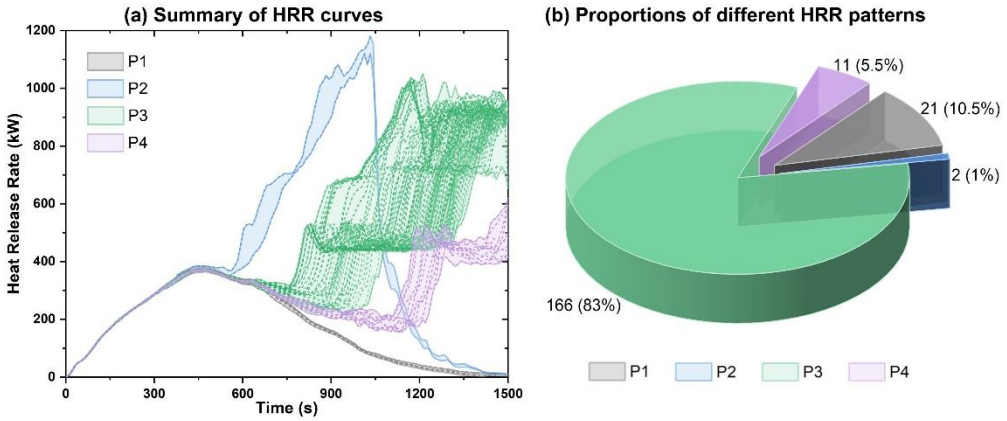

Fig. 3.7 Four HRR patterns identified from 200 simulations considering glass fallout uncertainty.

As illustrated in in Fig. 3.8, these four distinct HRR patterns are primarily dictated by the varying fallout sequences of the three window glass panels. For P1 and P2 patterns, glass fallout initiates at Pane 1 (left window). In the P1 scenario, approximately 11 glass submodules of Pane 1 fall out at an early stage while the flames remain localized. This passive opening ensures sufficient ventilation near the first column of wood cribs, which cools the indoor environment and prevents further fire spread, thereby inhibiting subsequent window glass fallout. Whereas, in the P2 scenario, Pane 1 does not experience significant fallout in the early stage, and glass fallout exactly begins after the fire spreads to adjacent combustibles. Thus, this delayed glass fallout results in an additional oxygen supply for the spreading fire, leading to sequential fallout from Pane 1 to Pane 3 (right window).

In the P3 category, glass pane 1 does not experience significant fallout, while extensive fallout is observed in Pane 2 (middle window) and Pane 3 as the localized fire travels toward the right-side opening. This pattern can be further subdivided into three subcategories: (a) P3a in which the Pane 2 falls out first, followed by the Pane 3; (b) P3b where there is fallout in Pane 2 and Pane 3 almost simultaneously; and (c) P3c where the fallout of Pane 2 starts later than Pane 3. Nonetheless, these subcategories do not exhibit significant differences in the HRR curves. In the P4 scenario, neither Pane 1 nor Pane 2 undergoes extensive fallout. Only Pane 3 falls out after the flames reach the right-side opening. These variations in the timing of glass fallout provide varied ventilation conditions for the developing fire, thereby leading to distinct fire consequences as observed in Fig. 3.7a.

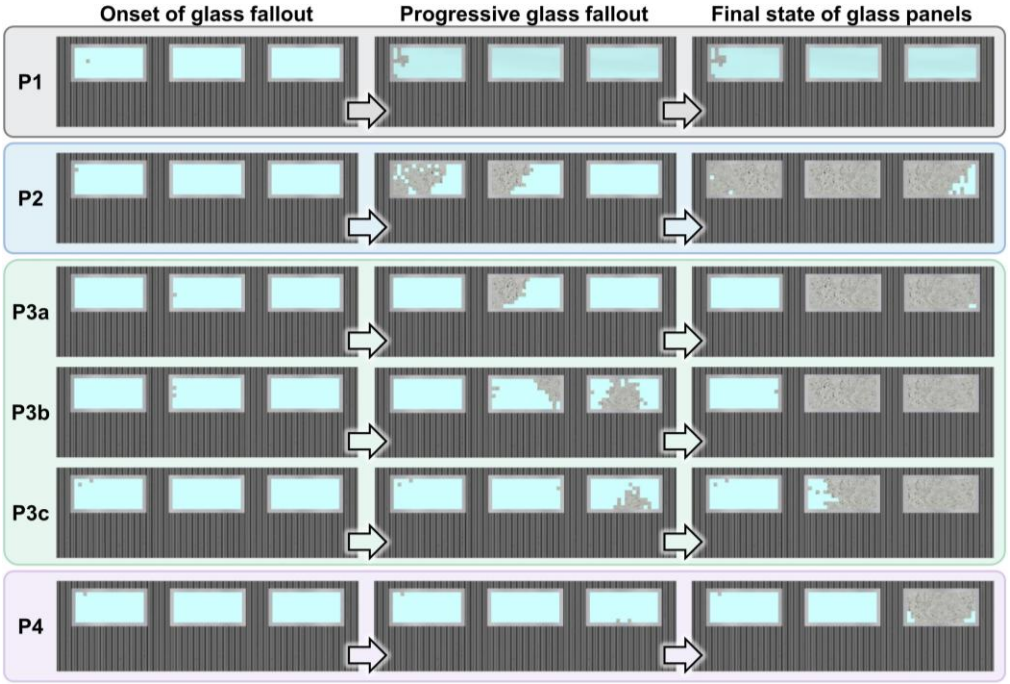

Fig. 3.8 Typical sequence of glass fallout in fire models associated with different HRR patterns.

3.4.2 Variations in ventilation conditions caused by glass fallout uncertainty

To analyze the variations in glass fallout timing, this study conducted a statistical assessment of the initial fallout time for the three window glass panes (denoted as Pane 1, Pane 2, and Pane 3) across

all simulations, as illustrated in Fig. 3.9. In this analysis, minor early-stage fallout events (i.e., involving no more than three glass submodules) were excluded from the initial fallout time calculation. For instance, the small-scale fallout of Pane 1 in P3c and P4 as shown in Fig. 3.8, since these events did not significantly enhance ventilation conditions. Additionally, glass panes that remained intact throughout the simulation were not included in the statistical evaluation.

The results presented in Fig. 3.9 reveal distinct distributions in the initial fallout times of the three window glass panes. These differences are not primarily attributed to the stochastic nature of the glass fallout criterion but are instead governed by fire dynamics, particularly the different phases of fire development. The fire progression can be broadly categorized into three stages: the localized fire stage, the transition stage, and the fire spread stage, and the typical fire behaviors during these stages are displayed in Fig. 3.9. It can be found that the initial fallout of Pane 1 predominantly occurs during the localized fire stage and the backward movement phase of flame spread stage, where intense thermal radiation is concentrated on Pane 1, leading to its large-scale fallout. Notably, in two exceptional cases, Pane 1 exhibited an initial fallout during the transition stage. In these cases, the enhanced ventilation from glass fallout promoted further fire spread, ultimately contributing to the rapid growth and high-intensity fire scenario observed in the P2 category.

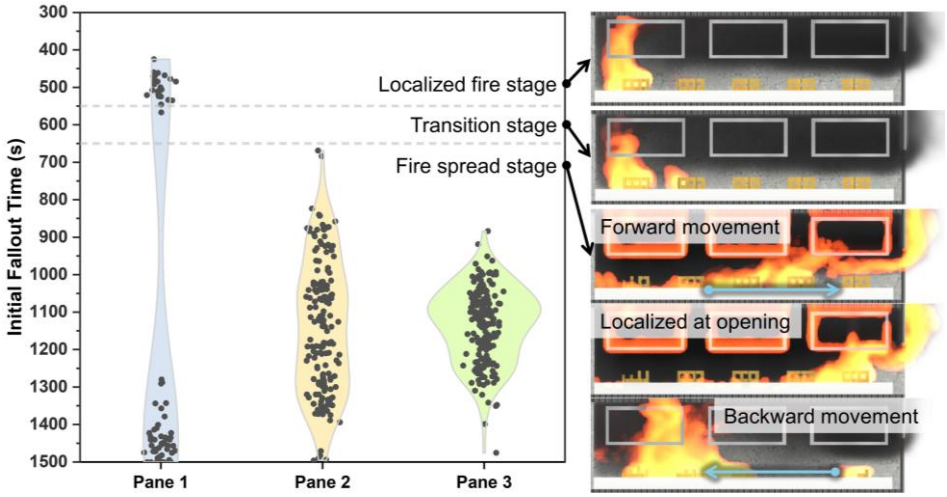

Fig. 3.9 Statistic analysis on timings of initial fallout of each glass pane.

For Pane 2, the initial fallout time is evenly distributed throughout the flame propagation stage, with two relatively minor peaks. These peaks correspond to large-scale fallout events caused by the core heating area of the flames moving forward and backward across Pane 2. The fallout times of Pane 3 are more concentrated than Pane 2 during the flame spread stage, primarily because the flames stay at the right-side opening for an extended period, causing sustained heating to Pane 3. Due to relatively stable heating conditions, the variation in the fallout time of Pane 3 is mainly due to the uncertainty in the glass fallout criteria, showing a concentrated time distribution with a single peak.

These mentioned distribution patterns of initial fallout timings are further illustrated in Fig. 3.10. The statistical findings show that the time difference between the initial fallout of Pane 2 and Pane 3 is typically less than 300 s, as indicated by the grey dash lines. In the P2 category, Pane 2 begins to fall out at approximately 650 s, followed by Pane 3 at around 900 s. In contrast, in the P3 category, the fallout times of Pane 2 and Pane 3 are generally later than in the P2 category. Furthermore, the occurrence of Pane 2 falling out before or after Pane 3 is nearly equal, displaying a symmetrical distribution along the diagonal axis. In the P4 category, the initial fallout times predominantly occur after 1250 s, slightly later than the average values in the P3 category. The fallout pattern in the P4 category closely resembles the specific conditions observed in the P3c subcategory, where most glass submodules exhibit a higher-than-average fallout temperature threshold.

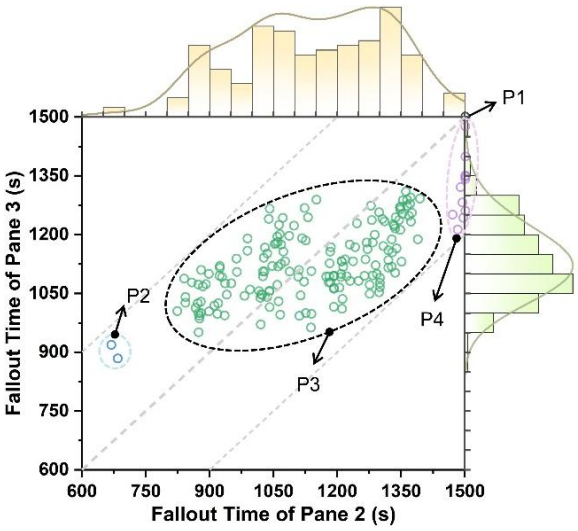

Fig. 3.10 Correlation analysis between fallout times of Pane 2 and Pane 3.

Fig. 3.11a illustrates the evolution of ventilation conditions across the four fire categories, quantified using the glass fallout ratio (i.e., the ratio of the fallen glass area to the total window area). In the P1 category, glass fallout typically occurs between 420 s and 520 s. The small-scale fallout (less than 4%) facilitates heat dissipation during the localized burning stage, thereby preventing further fire spread and suppressing subsequent glass fallout. In contrast, in the P2 category, the fallout timing coincides with the transition to flame spread stage, where early ventilation intensifies the fire severity.

Compared to the P2 category, the P3 category exhibits a later onset of ventilation changes with a slower development rate. The ventilation evolution in the P4 category follows a trajectory similar to that of the P3 category but occurs later, potentially exhibiting a trend analogous to P3 beyond the 1500 s simulation timeframe. Fig. 3.11b presents the final state of opening factors at the end of the simulations (1500 s). The results indicate that most of the fire simulations yield opening factors ranging from 0.072 to 0.082 $m^{1/2}$, rather than reaching the upper limit as assumed in traditional fire tests where all glass panes have already fallen out. Notably, in the highest probability distribution range, Pane 2 and Pane 3 have completely fallen out while Pane 1 remains nearly intact. This high-frequency occurrence may be

attributed to a thermal equilibrium between the heat released by internal combustion and the cooling effect of ventilation, which stabilizes the surface temperature of the remaining glass and reduces the likelihood of further fallout. For the P1 category, since the fire did not spread further, its data exhibits a distribution that is independent of the other categories.

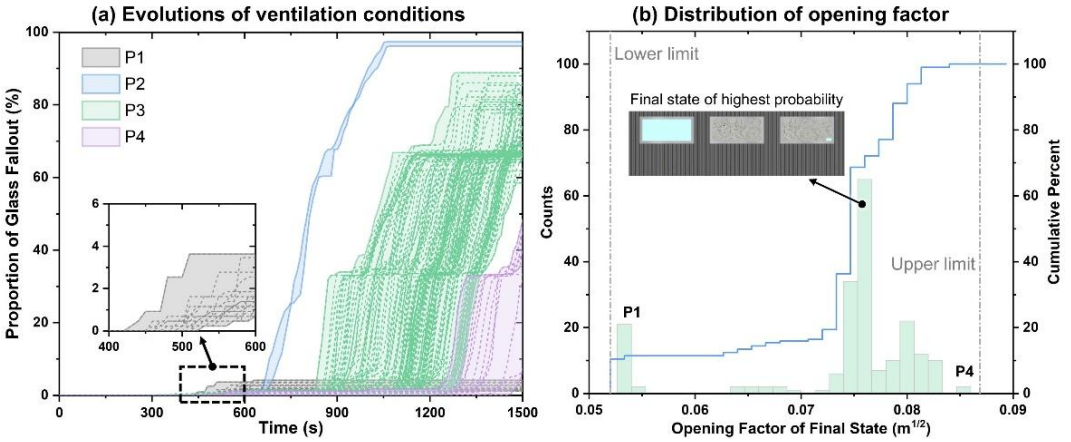

Fig. 3.11 Evolutions of ventilation conditions and resultant final opening factors.

3.4.3 Deviations in thermal exposure considering glass fallout uncertainty

The preceding subsection has analyzed the influence of glass fallout uncertainty on the ventilation factor, which directly affects the indoor fire dynamics and heat release characteristics. Building on this foundation, this subsection further investigates the specific effects of glass fallout uncertainty on thermal exposure to structures, with a particular focus on the evolution of indoor temperature. Fig. 3.12 presents the temporal variation of ceiling temperatures recorded by thermocouples.

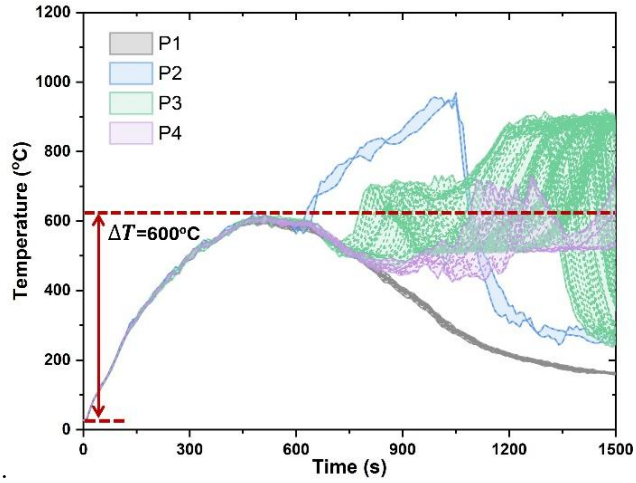

Fig. 3.12 Evolutions of gas phase temperatures of near-ceiling region.

At approximately 400 s, the localized flames in each simulation scenario have fully developed, leading to an initial peak temperature of around 600 °C, lasting for approximately 200 s. Subsequently, the temperature trajectories begin to diverge across different scenarios. In the P1 scenario, glass fallout occurs shortly after the temperature peak, effectively mitigating further temperature rise. In contrast, in the P2 scenario, glass fallout occurs slightly later, coinciding with the onset of flame propagation. This

delay allows a substantial influx of fresh air to fuel the flames, causing a rapid temperature to rise from approximately 600 s onward. This increase lasts for roughly 450 s, reaching a peak temperature close to 1000 ºC.

The temperature curves for the P3 and P4 scenarios exhibits partial overlap. In the P3 pattern, the temperature rise primarily occurs between 750 s and 1200 s, with peak temperatures typically reaching approximately 900 ºC after 1200 s. In the P4 scenario, the temperature rise is delayed by approximately 200 s relative to P3, and its peak temperature remains lower than that observed in P3. To facilitate a detailed quantitative analysis of these temperature variations, this study further examines the duration where temperature rise exceeds 600 ºC and the average temperature during this period. The corresponding results are illustrated in Fig. 3.13. The horizontal axis represents the heating duration, while the vertical axis indicates the average temperature rise. The heating duration of fire is primarily distributed between 200 s and 400 s, corresponding to an average temperature rise of 700 ºC to 760 ºC. Within this period, the correlation is observed between heating duration and average temperature can be observed, indicating that prolonged heating typically facilitates the accumulation of heat, thereby leading to an increased temperature. The P2 category, the most unfavorable fire scenario, exhibits a rapid temperature rise at the early stage and thus imposes a long-duration high-intensity thermal effect on surrounding structures. Notably, certain P3 cases exhibit longer heating durations than those in the P2 category. These cases share a common characteristic: a prolonged time gap between the initial fallout of their Pane 2 and Pane 3. During this time gap, the fallout of one pane will fuel the fire intensity while the other intact glass pane will constrain the ventilation, leading to prolonged combustion. These cases, as well as the fire pattern P2 should be given additional consideration to ensure sufficient safety margins for fire safety design.

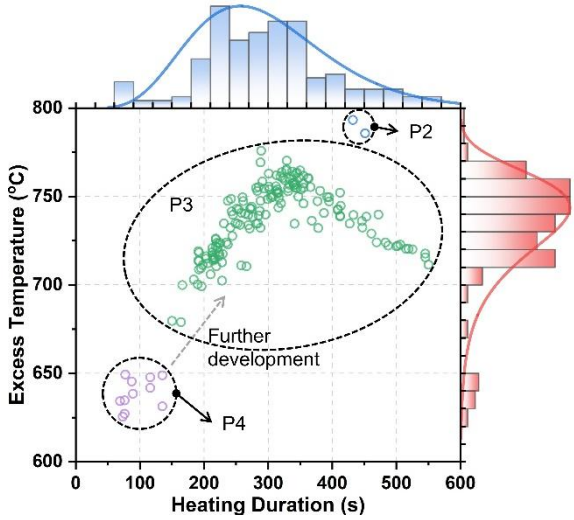

Fig. 3.13 Evolutions of gas phase temperatures of near-ceiling region.

In the P4 category, the slower fire progression results in a shorter heating duration within the 1500 s simulation time. This category generally exhibits incomplete temperature development and could

exhibit consequences similar to those of the P3 category if a further fallout of Pane 2 occurs. This slower progression of fire is primarily due to later initial glass fallout. This fact confirms that enhancing the fire resistance of glass to delay fallout is a conventional method to mitigate fire thermal impacts. Surprisingly, from the P1 scenario, it can be inferred that reducing the fire performance of glass to ensure its removal before the fire spreads further can also be an effective strategy to mitigate fire development.

The results of this study highlight the significant influence of glass fallout uncertainty on fire severity. This underscores the need for greater attention to the role of window glass in building fire development within fire safety design, to enable more precise predictions and informed mitigation strategies that prevent extreme fire conditions.

3.5 Conclusions

This chapter employs a three-parameter Weibull distribution to characterize the uncertainty in glass fallout. This uncertainty is quantified based on glass surface temperature and incorporated into the glass fallout modeling framework. A total of 200 CFD fire scenarios are simulated, each with distinct glass fallout conditions governed by the Weibull distribution. The influence of glass fallout uncertainty on fire development is statistically evaluated in terms of HRR histories, glass fallout timings and areas, opening factors, indoor temperature rises, and fire durations.

The simulation results indicate that variations in the fallout behavior of the three window glass panes lead to four distinct fire development patterns (P1–P4). These variations are primarily influenced by the stochastic nature of glass fallout and the evolving thermal boundary conditions throughout the fire development process. In the P1 category, Pane 1 falls out early during the localized fire stage, thereby avoiding further fire spread. Conversely, in the P2 category - the least favorable scenario - fire spreads rapidly after openings appear in the first pane while the localized fire is at its peak intensity, aided by increased influx of fresh air. Although the probability of this scenario occurring is relatively low (approximately 1%), its rapid and intense fire development warrants attention. The P3 category, observed in 83% of simulated cases, represents the most common fire development pattern, characterized by rapid fire growth within approximately 15 minutes, reaching an HRR peak of around 1 MW. The P4 category, on the other hand, is associated with higher fire resistance of window glass, leading to restricted oxygen supply and delayed fire development, ultimately maintaining a relatively controlled fire intensity. Notably, findings from the P1 category suggest that early glass fallout, despite being conventionally perceived as unfavorable, may function as a ‘passive opening’ mechanism that enhances heat dissipation and effectively mitigates fire growth. This mechanism may, in fact, offer greater fire control benefits than the restricted ventilation observed in the P4 category. This insight provides a novel perspective for fire safety design in modern large-space buildings.

The glass modeling approach proposed in this chapter not only provides new insights into the interaction between window glass integrity and fire dynamics but also underscores the importance of considering glass fallout uncertainty in fire risk assessment and design strategies. Further empirical studies are essential to refine this approach and promote its integration into performance-based fire safety design.

Chapter 4: A Novel 'Active Opening' Strategy to Mitigate Fire Development in Large Open-plan Compartment

Summary

Chapter 3 has demonstrated complex fire behaviors when considering glass fallout uncertainty, particularly emphasizing two slow-developing fire patterns that warrant further investigation. The first fire pattern P4 occurs when the high fire resistance of window glass delays its fallout, restricting oxygen supply and slowing fire growth. The second scenario, P1, represents the opposite condition, where glass panels with low fire resistance fall out earlier, creating 'passive openings' that provide sufficient ventilation and effectively mitigate fire growth. Nevertheless, with the increasing use of fire-resistant glass in modern buildings, relying on 'passive openings' as a fire mitigation strategy has become increasingly impractical. To address this challenge, this chapter explores an 'active opening' strategy, aiming to provide adequate ventilation in the early stages. The proposed strategy introduces an activation temperature as a control parameter for window openings, which has been implemented in CFD fire models. Two extreme cases are initially examined: one assuming windows are initially opened, and the other assuming windows remain closed throughout the fire. A striking contrast in fire behavior is observed that the former case leads to localized burning while the latter case results in flashover. Further investigations are conducted to assess the influence of activation temperature and window upper edge on the effectiveness of fire mitigation. The results indicate that a lower activation temperature facilitates the earlier removal of hot smoke, effectively preventing spontaneous ignition and reducing fire severity. Additionally, the study reveals that increasing window upper edge reduces the thickness of the hot smoke layer, thereby lowering thermal radiation to the floor and mitigating rapid fire spread. The proposed 'active opening' approach provides a scientifically grounded and practical strategy for improving fire mitigation measures in buildings with fire-resistant glazing systems.

The work of this chapter has been reported as a journal paper: 'T. Chu, L. Jiang, A. Usmani (2023). Introducing an active opening strategy to mitigate large open-plan compartment fire development. ***Fire Safety Journal****, 141, 103981.'*

4.1 Introduction

In Chapter 3, a total of 200 fire simulations incorporating the uncertainty-based glass fallout model have revealed four distinct fire development patterns (P1–P4). Among these different fire histories, Notably, the P1 category suggests that very early glass fallout, although very rare in reality, can enable 'passive opening' mechanism leading to slow fire spread and low fire intensity. As modern buildings increasingly adopt strengthened window glass of multi-layers and façade fire resistance, relying on the 'passive opening' strategy for the P1 scenario becomes impossible. Therefore, it is necessary to establish an 'active opening' strategy to form early ventilation conditions in the context of large compartment fires, which may be approximate to the initial opening setup in travelling fire tests. Ideally, a large compartment fire such as the Malveira fire test [10], can exhibit a slow 'travelling fire' behavior that maintained a low fire intensity around 1 MW for over 150 minutes after the ignition, which would be significantly beneficial to structural fire safety and firefighting.

Motivated by this counter-intuitive phenomenon in the P1 scenario and the premise of slow 'travelling fire', this chapter proposes an 'active opening' strategy, where glass panels are actively lifted upon fire detection. The objective is to regain the favorable ventilation conditions for 'travelling fire' at the early stage, thereby preventing rapid fire spread in large open-plan compartments (i.e., typically with one dimension exceeding 20 m). A series of case studies are conducted to demonstrate this strategy while introducing ceiling temperature-controlled flip of glass panels in CFD fire models. The results demonstrate that implementing 'active opening' leads to significantly slower fire spread and enhanced 'travelling fire' behavior. Moreover, the effect of activation temperatures and window upper edges are investigated, which suggests an appropriate triggering temperature and height of 'active opening' are needed to maximize the fire mitigation efficiency of the 'active opening strategy'.

4.2 Conceptual design of 'active opening' strategy for sufficient ventilation

As previously demonstrated in Chapter 2, the existence of window glass panels significantly alters ventilation conditions, thereby influencing fire behavior in open-plan compartments. As briefly illustrated in Fig. 4.1, in the absence of glass panels, fire development remains slow and localized from ignition up to 1800 s, showing a behavior consistent with observations from existing travelling fire tests.

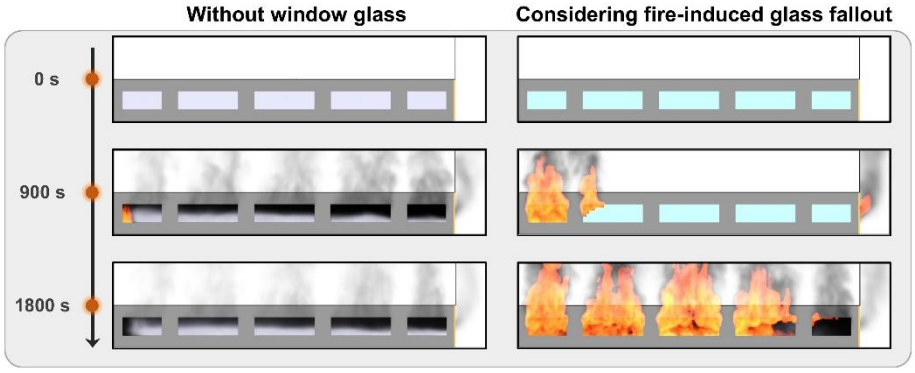

Fig. 4.1 Timeline of large compartment fire development with and without glass panes (front view).

However, when glass panels are present, the localized fire could develop into a fully developed fire in fire simulation incorporating glass fallout. Given that in modern buildings, window glass panels are typically kept closed for energy efficiency purposes, adequate ventilation may not be readily available in the event of a fire. This lack of ventilation can contribute to catastrophic fire growth, as seen in the latter scenario.

To mitigate such risks, this chapter explores an alternative fire control strategy that actively enhances ventilation through windows in large open-plan compartments. Rather than adhering to conventional fire mitigation approaches that restrict ventilation, this study proposes an 'active opening' strategy, which seeks to control fire development by providing timely and controlled ventilation.

The conceptual design of the 'active opening' strategy links the activation of window openings with a control logic based on ceiling gas phase temperature. As illustrated in Fig. 4.2, a virtual array of equally spaced temperature detectors is installed beneath the ceiling in the CFD fire model. These detectors continuously monitor gas-phase temperatures and trigger the movement of window glass panels from a closed position to an open state. The activation of opening windows occurs when the monitored temperatures of two detectors exceeding the specified threshold (activation temperature). In this model, the 'active opening' mechanism is realized through a flipping movement of the glass panels, where the panels rotate about their upper edge, functioning as a horizontal spandrel to redirect and deflect released hot smoke away from the compartment. By shifting the focus from restricting ventilation to actively managing airflow, this strategy presents a novel and promising approach to controlling fire dynamics in large compartments, offering new perspectives for fire safety design in modern buildings.

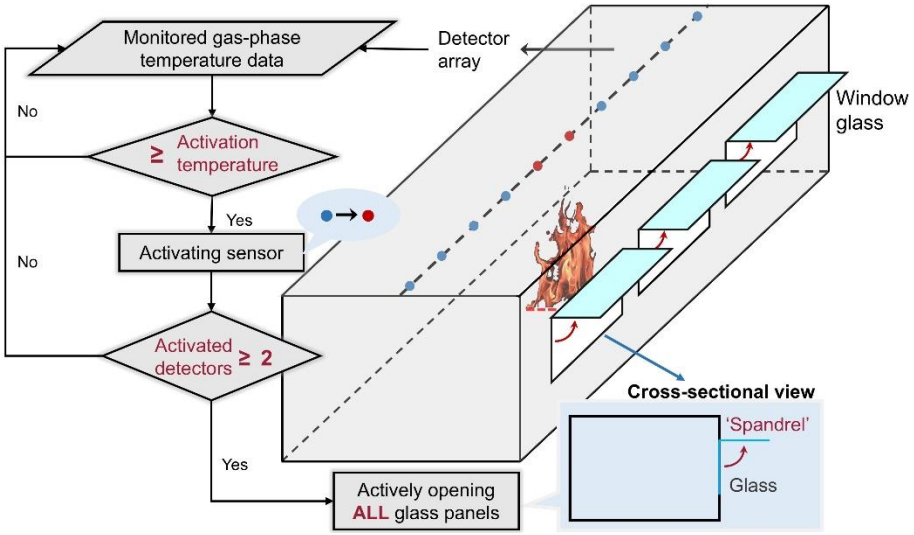

Fig. 4.2 Illustration of the control logic for opening windows mechanically.

It is important to clarify that this chapter serves as a preliminary exploration and demonstration of the 'active opening' concept. Future research will refine the control logic of window openings by investigating more advanced activation mechanisms, such as sequential opening of windows from the

nearest to the adjacent ones, stepwise opening configurations, and partial opening adjustments based on real-time fire conditions. Moreover, the heating impact on the external wall and the flipping window panels should be further studied to ensure the overall fire safety of implementing the 'active opening' strategy.

4.3 Numerical simulation for demonstrations of 'active opening' strategy

4.3.1 Description of prototype fire model

The prototype fire model used to demonstrate the 'active opening' strategy is based on the Kirby fire test [8], which was previously introduced in Chapter 2. A brief overview of the test configuration is provided in Fig. 4.3.

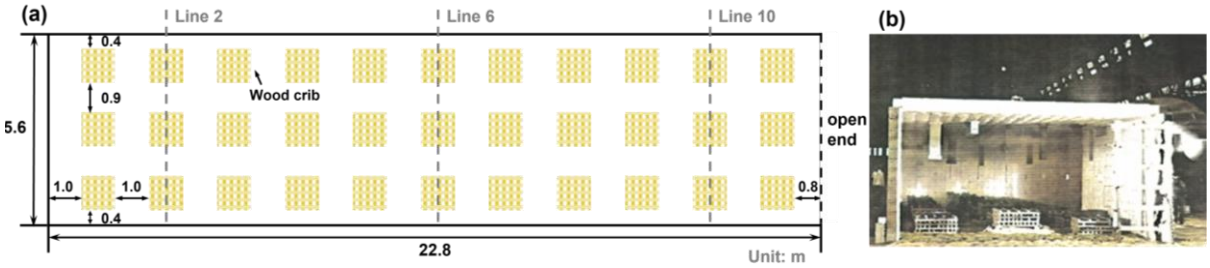

Fig. 4.3 Layout of the tested compartment.

The tested compartment measured 22.8 m in length, 5.6 m in width, and 2.8 m in height, with one end fully open to the external environment. The sidewalls along the longitudinal direction were constructed using 215 mm thick lightweight concrete, while the ceiling consisted of a 200 mm thick reinforced concrete slab. The floor was filled with 125 mm of sand, and the other interior surfaces of the compartment were lined with 50 mm thick ceramic fiber blankets. A total of 33 wood cribs were evenly spaced in the compartment, forming a matrix of 3 rows and 11 columns with 0.9 m row spacing and 1 m column spacing. Since this fire model has already been validated in Chapter 2, the same modeling parameters and boundary conditions will be adopted in this chapter for consistency. A detailed description of these parameters can be found in Section 2.4.2.

4.3.2 Implementation of 'active opening' strategy in prototype fire model

To enable the modelling of the 'active opening' strategy at window glass panels, virtual thermocouples with a spacing of 1.2 m are employed in the fire models to represent the detectors to monitor gas-phase temperature, as shown in Fig. 4.4a. The parameter SETPOINT is utilized to define the activation temperature for implementing 'active opening'. The bead diameter of the thermocouple was defined as 0.003 m, and its density and specific heat were set as 8655 kg/m³ and 0.44 kJ/kg·K, respectively. Each thermocouple is associated with a control device (denoted as AT_LEAST) that can be activated once its reading exceeds the prescribed temperature. In this chapter, the value of the control device AT_LEAST is set to 2, which indicates that it will trigger the opening action of glass modules when it receives at least two signals from these monitoring thermocouples.

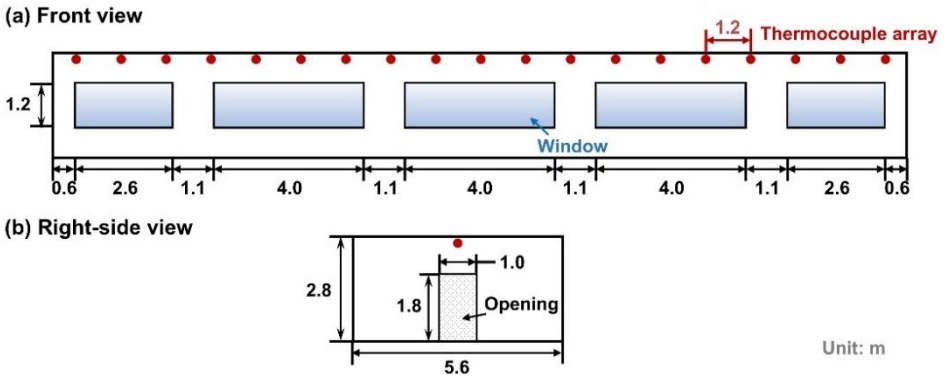

Fig. 4.4 Fire simulation model for case studies on 'active opening' strategy.

Based on the FDS model of the Kirby test, a collection of case studies is conducted to examine the feasibility of 'active opening' strategy and to investigate the opening control factors on fire development. As shown in Fig. 4.4a, five window panes were installed on the front wall of the validated model, similar to the setup of the Malveira Fire Test [10]. Besides, the fully open sidewall in Fig. 4.3 was replaced with a typical small opening as shown in Fig. 4.4b.

A total of 10 fire scenarios are divided into 3 groups, while the key difference is summarized in Table 4.1. The distance from window to ceiling is assumed as 0.8 m in Group A and Group B, and the two cases of A1 and A2 represent two special scenarios as lower bound and upper bound of activation temperatures, i.e., initially opened windows (Case A1) and windows of no 'active opening' (Case A2). In fire models of Group B, the critical temperature for 'active opening' is altered as 70 °C, 100 °C, 150 °C, 250 °C, which will reveal the sensitivity of activation temperature to the fire development while adopting 'active opening'.

Table 4.1 Summary of the setup of extrapolation cases.

Case No.	Distance from the top rim of windows to the ceiling H_w [m]	Activation temperature T_{act} [°C]
A1	0.8	20 (initial opening)
A2	0.8	- (no 'active opening')
B1	0.8	70
B2	0.8	100
B3	0.8	150
B4	0.8	250
C1	0.6	70
C2	0.6	100
C3	0.6	150
C4	0.6	250

Group C accounts for higher openings to allow for thinner smoke layers during the fires. The windows of Group C are placed at 0.6 m below the ceiling, whereas the activation temperature of each case is identical to that in Group B. The HRR of the fire, the smoke layer heights, the average smoke layer temperatures, and the heat fluxes received at the surface of each crib column are captured in these models, which are analyzed in the following sections.

4.4 Performance of 'active opening' strategy on mitigating large compartment fires

4.4.1 Lower and upper bounds of 'active opening'

When comparing the simulated fire behavior in Case A1 and A2, the smoke and flames accumulate rapidly in the compartment of A2, whereas a smaller fire is found in A1. The flame in Case A2 quickly spread over almost the entire wood cribs within 600 s, and a fully developed fire is observed. On the contrary, the smoke has been effectively ventilated in Case A1 through the initially opened windows and the fire development is much slower. As shown in Fig. 4.5, the flames remain localized at the initially ignited wood crib enabling a sustained small, localized fire. Besides, the opened glass panels can redirect the upward flow of hot smoke, and the smoke temperature is significantly reduced owing to a smaller fire.

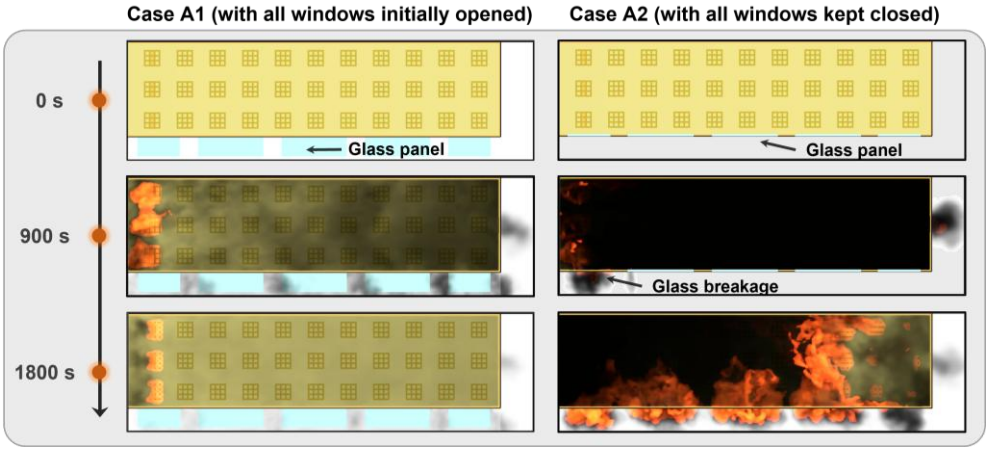

Fig. 4.5 Timeline of fire development for Case A1 and A2 (top view).

Fig. 4.6a demonstrates the different HRR histories while opening all windows at the initial stage (A1) and adopting no 'active opening' (A2). The upper section of Fig. 4.6a illustrates the variations of total HRR in both cases. With glass panels and no flip opening, the HRR of Case A2 is similar in the first 900 s to that in Case A1, which is followed by a higher fire intensity (peak HRR of over 50 MW) in A1 as more fuel surfaces are heated and ignited. As shown in the lower section of Fig. 4.6a, a large portion of gas burning occurs at the opening (EXT) of Case A2. The differences in smoke layer heights of the two cases are clearly observed in Fig. 4.6b. The height of the smoke layer in both cases decreased rapidly at the beginning. Due to the early opening in A1, most of the smoke is ventilated in time to maintain the smoke layer height at around 1.4 m instead of almost engulfing the wood cribs, as seen in Case A2.

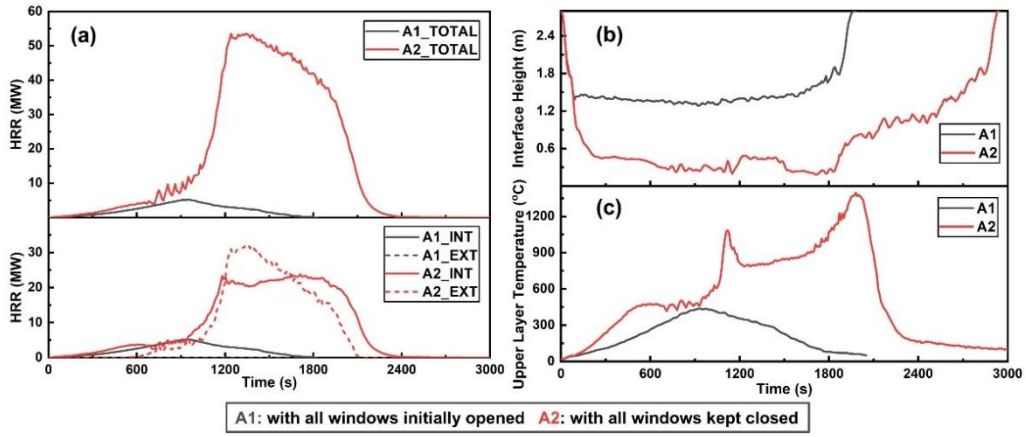

Fig. 4.6 Differences due to large opening strategy in: (a) HRRs, (b) interface height, and (c) upper layer temperature.

As indicated in Fig. 4.6c, the average temperature of the smoke layer of Case A2 developed faster than that of Case A1, reaching its peak of about 500 °C before 600 s. On the contrary, the peak average temperature of Case A1 was almost only 30% of that of Case A2, which was owing to the hot smoke accumulation being effectively inhibited. Furthermore, the duration of Case A2 was significantly greater than that of Case A1, leaving the structural elements exposed to elevated temperatures for a longer time.

4.4.2 Effects of activation temperature for 'active opening'

The setting of the activation temperature largely determines the sensitivity of the active window opening system. The simulated cases show various responses by using different activation temperatures. Case B1 (T_{act} =70 °C) successfully avoided fast fire propagation very similar to the initial opening as Case A1 (T_{act} =20 °C). However, as illustrated in Fig. 4.7, the activation of window openings in other cases of Group B failed to prevent fire spread, and a large fire was found as shown in Fig. 4.7a.

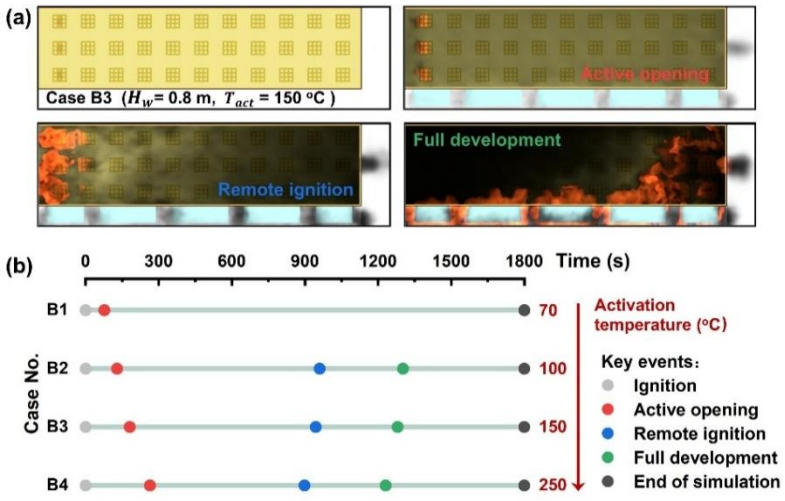

Fig. 4.7 Timelines of fire development after 'active opening': (a) representative fire development in Case B3 (top view) and (b) timelines of key events in Group B.

Fig. 4.7b compares the time points of key events in the fire evolution, including 'active opening' of windows, remote ignition of adjacent cribs, and full development of fire. Their timelines indicated

the delays in active window opening could shorten the onset of catastrophic fire, and even a delay of only about 50 s in opening windows between Case B1 and B2 would result in two distinct situations, as the initial conditions for the subsequent development might be significantly influenced.

In Fig. 4.8, the effects of activation temperature on the height and average temperature of the hot smoke layer as well as the average heat flux received by the adjacent wood cribs are illustrated. At the early stage, the smoke layer temperature histories are almost identical in all cases, which gradually increase as the fire develops. After triggering the action of opening windows in Case B1, its temperature rise rate dropped, showing a clearly different trend from the other cases, as shown in Fig. 4.8a. Similarly, as the windows were actively opened, the temperature rise curves of Case B2, B3 and B4 sequentially deviated from the extreme Case A2. This deviation indicated that the 'active opening' of windows can effectively mitigate the accumulation of heat within the compartment, as the smoke is rapidly evacuated from the window openings.

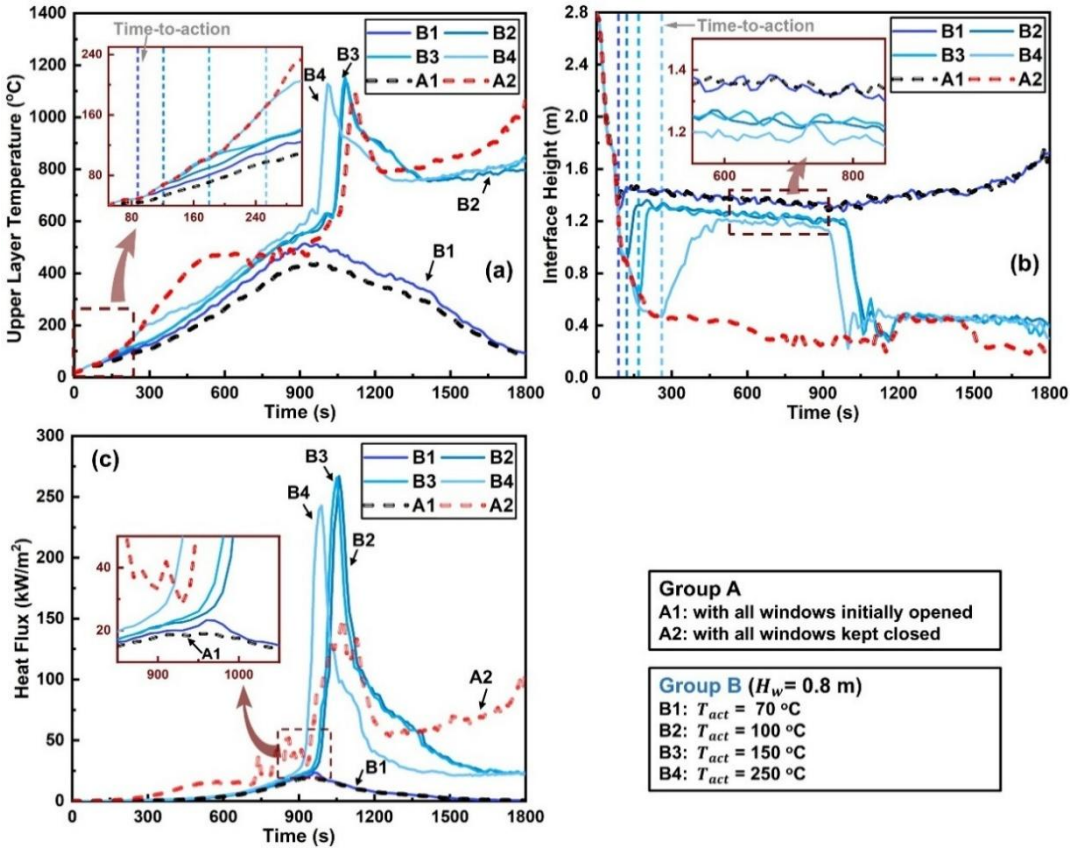

Fig. 4.8 Effects of activation temperature on: (a) upper layer temperature, (b) interface height, and (c) heat flux received by the second column of wood cribs.

Case B1 brought the smoke layer back up to a level comparable to extreme Case A2 within 20 s after the 'active opening' of windows. Moreover, the smoke layer temperatures in B2~B4 rise up to a level even higher than that of Case A2 without 'active opening', and then stabilized as shown in Fig. 4.8b. Nevertheless, their smoke layers were relatively thicker than that of the extreme Case A1 because of the late opening of the window, where Case B4 showed the largest deviation of around 0.2 m. Due

to this smallest distance to the floor as well as the highest temperature, Case B4 transferred the most heat to the wood crib surface below, which assisted the localized burning to induce the earliest remote ignition. Nevertheless, this measure of opening windows somewhat delayed the occurrence of remote ignition compared to Case A2, as indicated in Fig. 4.8c. Notably, Case B1 imposed a slightly enhanced heat flux at about 950 s in an attempt to ignite the wood surface below, but was promptly curbed by the favorable heat dissipation conditions. The levels of heat flux exerted on the adjacent wood surface by Case B2 and B3 were both comparable to that of Case B1, but their accumulation over a long period of time still triggered the remote ignition.

In general, the use of 'active opening' strategy can mitigate the progress of large open-plan compartment fires, mainly by raising the residual height of the smoke layer. However, the mitigation brought by an untimely response is temporary, which is likely to be followed by a catastrophic fire due to adequate oxygen supply. Therefore, a proper setting of the activation temperature needs to be found to meet the needs of performance-based design for this type of modern building.

4.4.3 Effects of window upper edge

The accumulation of the smoke layer dominates the fire development in large compartments, which has been presented in the cases of Group B. A thick smoke layer of high temperature can lead to higher floor radiation and faster flame spread. Group C was thus designed to counteract the accumulation of the hot smoke layer within the compartment by lifting the top edge of the windows. This alteration of the window arrangement proved to be effective in controlling the deposition of the hot layer compared to the Group B case, which is illustrated in Fig. 4.9. Raising the window upper edges effectively elevated the opening height at which smoke was released after the implementation of the active window opening strategy. This subtle change successfully resulted in Case C3 that prevented fire spread at a high activation temperature of 150 °C. Besides, the other cases in Group C by lifting the window upper edges all led to the effective mitigation of fire spread.

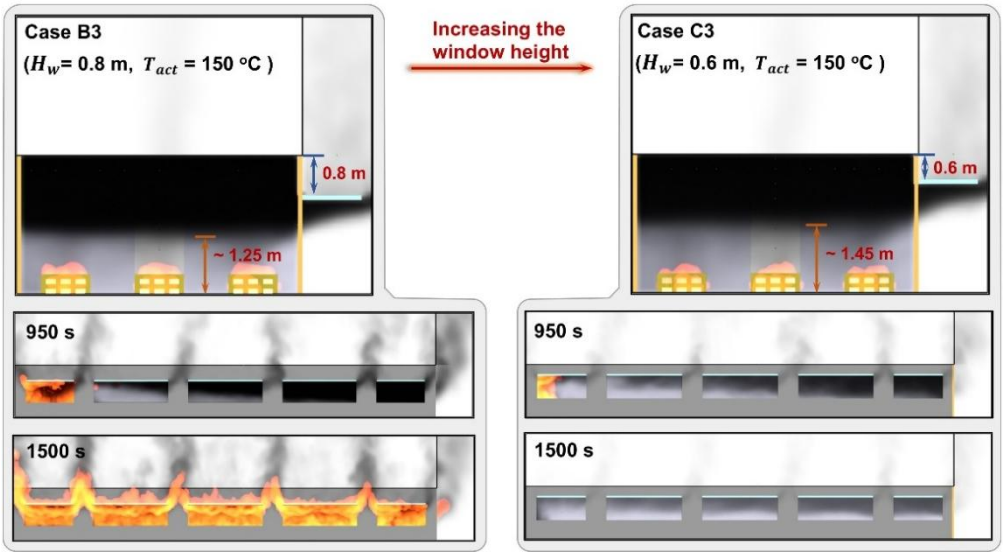

Fig. 4.9 Two distinct outcomes by elevating the window height.

Case B1 of the best performance in Group B is used to compare with the cases of Group C to demonstrate the effect of window height. As shown in Fig. 4.10a, the smoke in all cases both accumulated and sank rapidly in the compartments at the beginning of the fire. The smoke was released after the window opening action was triggered and then stabilized at variant heights. Similarly, the temperature of the smoke layer in each case developed slowly at the early stage, whereas the rate of temperature rise declined significantly as the windows were actively opened, as displayed in Fig. 4.10b. It can be seen that the earlier the 'active opening' was triggered, the higher the smoke layer height was shown and the lower the smoke layer temperature obtained at a steady state, which underlines the importance of the activation temperature setting for mitigating fire development. Moreover, the smoke layer heights of all cases in Group C were higher than that of Case B1, alongside lower smoke layer temperatures than B1 in all cases except Case C4, indicating that increasing the window height can improve the performance of smoke venting and heat removal, and thus enhance the effectiveness of the 'active opening' system. Notably, despite its thinner smoke layer, Case C4 with a slightly higher temperature transiently yielded a heat flux that exceeded that of Case B1 to the adjacent wood crib, which came close to a catastrophic fast spread fire, as presented in Fig. 4.10c. This observation implies that the 'active opening' strategy might become invalid if the activation temperature is raised too high, which highlights the need of early-stage activation similar to sprinkler systems.

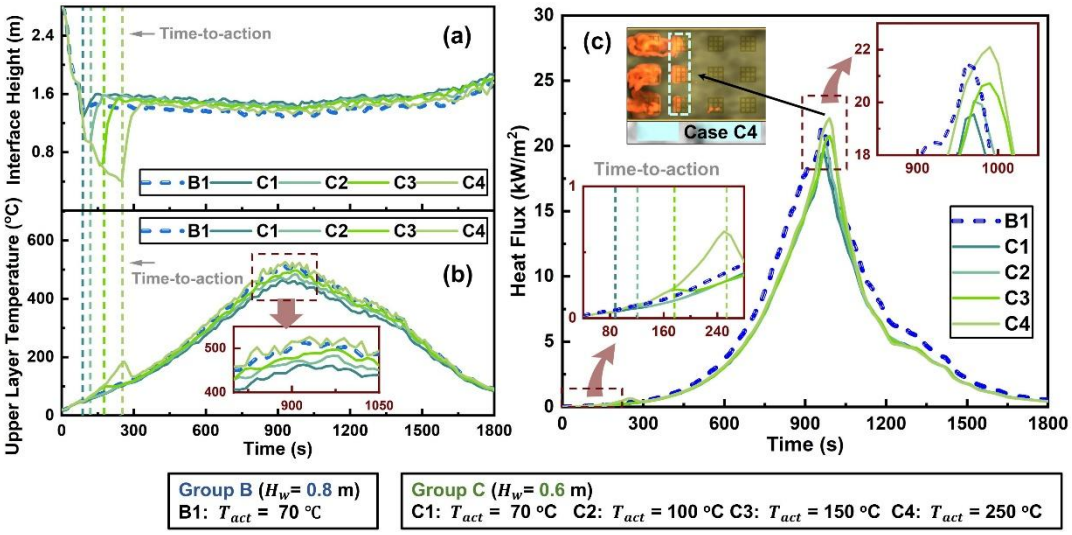

Fig. 4.10 Comparison of all the cases in Group C with Case B1 on: (a) interface height, (b) upper layer temperature, and (c) heat flux received by the second column of wood cribs.

In short, the demonstrations of Group C suggest that lifting the window upper edges at the architectural design level can be a wise solution to enhance the robustness of the 'active opening' strategy.

4.5 Brief discussions on 'active opening' mechanism

The work presented in this chapter provides preliminary numerical evidence supporting the effectiveness of this counter-intuitive concept in fire mitigation - the 'active opening' strategy. The

fundamental principle behind this strategy can be conceptually understood through an analogy with flood management. As illustrated in Fig. 4.11, flood control typically employs two principal approaches: containment and diversion. The containment strategy, such as dams, are effective for managing moderate water levels but may be overwhelmed under extreme conditions, leading to catastrophic failures. Conversely, the diversion strategy utilizes channels to guide excess water away, thereby mitigating the risk of overflow-induced damage.

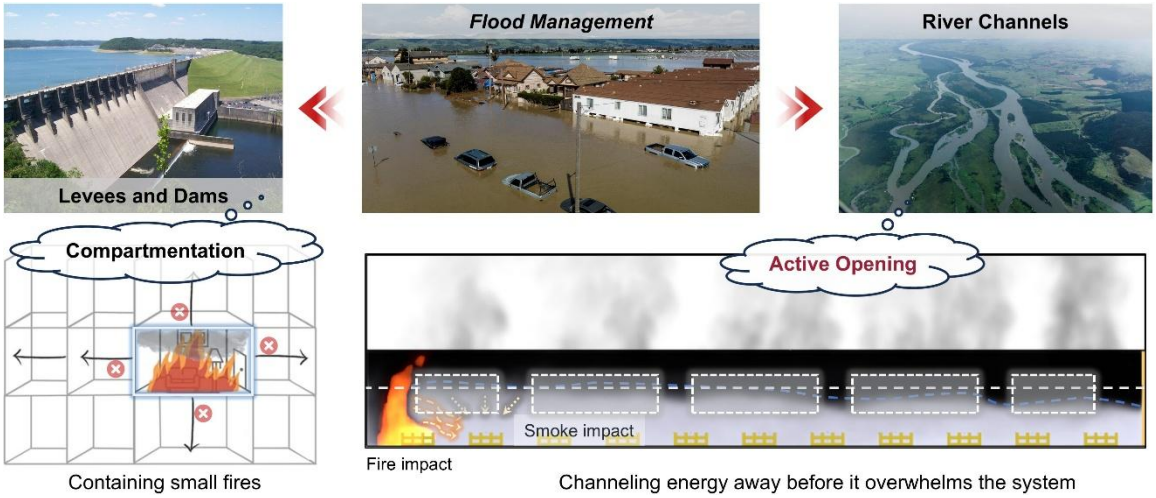

Fig. 4.11 An analogy between fire control strategies and flood management approaches.

In the context of fire protection, the traditional concept of compartmentation functions similarly to dams, confining fire and smoke within designated sections of a building. While effective for small-scale fires, this approach can be inadequate in large open-plan buildings, where extensive fuel loads contribute to rapid fire spread. Under severe fire conditions, the integrity of compartmentation may be compromised, potentially failing to control fire hazards. By contrast, the 'active opening' strategy proposed in this work aligns more closely with the concept of diversion. Rather than resisting the accumulation of heat and smoke, this approach facilitates controlled ventilation by strategically activating openings in response to fire dynamics. This mechanism allows excess heat to be vented before it overwhelms the compartment system. At present, our research has focused on preliminary simulations to evaluate the feasibility of this concept. Further investigations, including experimental validation and refined computational modeling, are necessary to confirm its robustness under diverse fire scenarios.

4.6 Conclusions

This chapter proposes an 'active opening' strategy on façade windows to mitigate the fire development in large open-plan compartments. This strategy monitors the ceiling sensor temperature to trigger the 'active opening', and the whole action flow has been implemented in the CFD fire models for pioneering investigations. Two extreme situations, i.e., initially opening the windows and no 'active opening', are simulated to showcase the effect of considering window glass. It is observed that the hot

smoke accumulated rapidly in the compartment with glass considered and exerted high levels of heat flux on the combustibles below, which will induce fast fire spread and even flashover in the compartment. On the other hand, the initial opening of the windows as assumed in the travelling fire research exhibits localized burning and maintains a relatively thinner smoke layer, which significantly reduces the heat release rate and benefits the potential firefighting.

This chapter then investigates the key parameters that affect the performance of the 'active opening' strategy. It is found that setting a lower activation temperature allows for the timely venting of hot smoke from the compartment, which can successfully avoid spontaneous ignition on remote items. While a higher activation temperature is in use, the 'active opening' becomes invalid in suppressing the fire development. The effect of window height is studied and discussed, which shows that the top rim of windows fundamentally controls the residual height of hot smoke after 'active opening', which can effectively reduce smoke and ensure valid mitigation even at high activation temperatures.

It should be admitted that there are several assumptions as well as limitations in the present work. This chapter considers no active fire suppression systems as the worst scenario of discussion, which is the same as the discussion of travelling fire research. In future applications, the sprinkler systems may be simultaneously triggered to further suppress the fire development. As mentioned before, this strategy may cause fire to spread to the upper floors of tall buildings or adjacent constructions. These side effects will be investigated in our upcoming work. Regarding the fuel arrangement, the simulated wood cribs are discrete and uniformly distributed, whereas a non-uniformly distributed fuel bed may cause other challenges to the 'active opening' approach. In addition, the density of sensors in the proposed control logic can also affect the response time of the system, which should be taken into further account. Nevertheless, the application of the 'active opening' strategy in modern buildings opens up new thinking of fire safety measures, which supplies ventilation through windows at the early stage rather than controlling ventilation. However, applying it in real buildings certainly requires more detailed research and experimental validations.

Chapter 5: Medium-scale Validation Tests of 'Active Opening' Strategy

Summary

Chapter 4 has presented a preliminary study on the feasibility of the novel 'active opening' strategy to regain travelling fire conditions and to mitigate fire spread. Chapter 4 primarily adopted CFD fire simulation to investigate the mitigation performance in comparison to fire behavior with window glass, whereas no experimental tests have been ever conducted to verify the findings and the effectiveness of the proposed 'active opening' solution. In this chapter, two scaled compartment fire tests have been conducted and reported, as the first ever experimental evidence pointing out the strikingly different fire development paths due to glass existence and active opening. The corresponding CFD fire models have been established with validation to provide more comprehensive information for understanding the interaction mechanisms between fire development and glass fallout. By analyzing the histories of heat release rates, smoke characteristics, and floor heat fluxes, it is found that the localized fire at an early stage could not create fall-off of the window glass to form ventilation, and the expected smoke venting does not occur until the fire flames rapidly spread. Through the analysis, it has been proved that actively opening windows could effectively reduce the smoke thickness and temperature, reducing the heat radiation to the adjacent floor fuel load. While not intensifying the growth of localized fire, the 'active opening' strategy could immediately reduce smoke accumulation, and successfully prevent fire spread. These would ultimately ensure the safety of people, reduce the damage to building structures, and facilitate firefighting.

The work of this chapter has been reported as a journal paper: 'T. Chu, W. Zeng, G. Wang, J. Wang, G. Zhang. D. Yuan, A. Usmani, L. Jiang. (2024) Explain why active opening of windows can mitigate fire spread in modern building compartments, ***Journal of Building Engineering,*** *99, 111615.'*

5.1 Introduction

Given that relying on window glass fallout at very early stage of fire ('passive opening') becomes unrealistic for modern glass windows, a conceptual strategy of 'active opening' [177] has been proposed in Chapter 4 as a new solution for regaining sufficient ventilation during the early localized fire period, thereby mitigating fast fire growth in large open-plan compartments. As depicted in Fig. 5.1, the proposed strategy involves fire detectors installed beneath the ceiling, which are linked to an automated window-opening module. Upon detecting fire at an early stage, these detectors would trigger the controlled opening of glass windows, effectively enhancing ventilation and modifying fire dynamics.

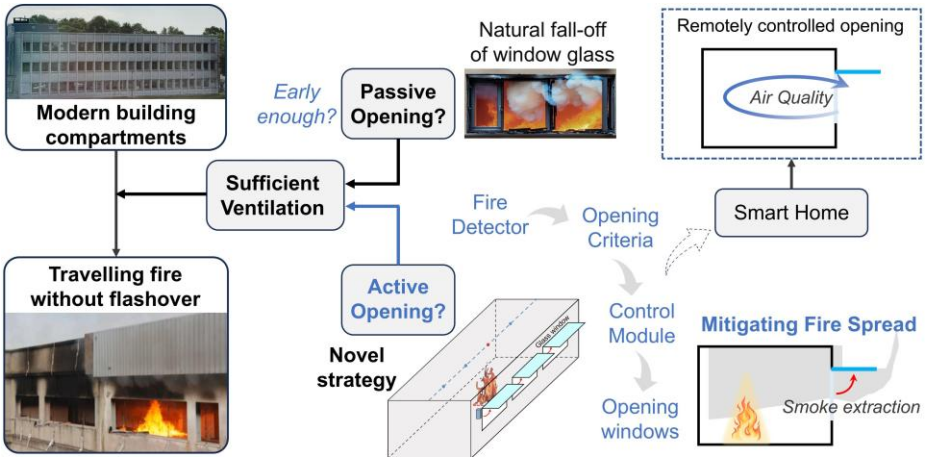

Fig. 5.1 A novel strategy of 'active opening' for mitigating fire spread

In the preliminary study conducted in Chapter 4, the fire simulation results have shown that the 'active opening' can substantially mitigate fire spread across the floor plan. Additionally, the flipping motion of the window frames about their upper edge creates a horizontal spandrel, which serves to deflect released hot smoke. Beyond fire mitigation, such a control module could potentially be integrated into smart home systems, enabling remote-controlled natural ventilation through façade windows to improve indoor air quality. Despite these promising findings, the 'active opening' strategy remains in an early research phase. There are no experimental tests being conducted to examine the adequacy of assuming early passive opening in a large compartment fire, nor to experimentally reveal the efficacy of 'active opening' in fire spread mitigation.

This chapter, for the first time, presents two fire tests to demonstrate the considerable benefits of the 'active opening' strategy and to investigate its underlying fire mitigation mechanisms. The two tests were conducted in a medium-scale long compartment setup, one experiment involving the early opening of glass windows, and the other maintaining closed windows without 'active opening'. The observed phenomena in these two tests have shown clear evidence of the faster fire development induced by window glass and the effectiveness of the 'active opening' strategy, neither of which has been demonstrated using real tests before. To further analyze these findings, additional investigations were conducted using CFD fire models, which offer greater data resolution and deeper insights into the fire behavior mechanisms compared to physical fire tests. It is found that the implementation of 'active

opening' effectively reduces the thickness of the smoke layer, thereby lowering radiation exposure to floor-level combustible. This mechanism routinely prevents rapid fire spread and plays a crucial role in mitigating the likelihood of global flashover. These findings establish 'active opening' as a viable fire mitigation strategy, warranting further investigation and integration into modern fire safety designs.

5.2 Medium-scale fire tests implementing novel 'active opening' strategy

5.2.1 Setup of medium-scale compartment fire tests

The two experimental fire tests were conducted in October 2023 at a large fire laboratory in Shenzhen, China, with identical configurations, except for the window opening setup. The test incorporating ordinary framed glass windows is referred to as 'Test A', while the test with identical configurations but implementing the 'active opening' strategy is referred to as 'Test B'. The design of tested compartment was developed as an improved version of the fire model introduced in Chapter 3. The scaled experimental compartments measured 4.16 × 2.15 × 1.32 m, representing a 1/3 scale model of a large open-plan compartment. A container-like structure was used as the main body to simulate a modern open-plan compartment with sufficient longitudinal ventilation. The outer shell of the compartments was made of zinc-coated steel, while the interior surfaces of the walls and ceiling were lined with 2 cm thick cement fiberboard density (density of 1150 kg/m^3, thermal conductivity of 0.31 W/m^2·K, and specific heat of 1.23 kJ/kg·K). In addition, a 2 cm thick rock wool layer (with density of 125 kg/m^3, thermal conductivity of 0.04 W/m^2·K, and specific heat of 0.75 kJ/kg·K) was bolted to the fiberboard to protect the structural integrity during the fire. A detailed illustration has been presented in Fig. 5.2.

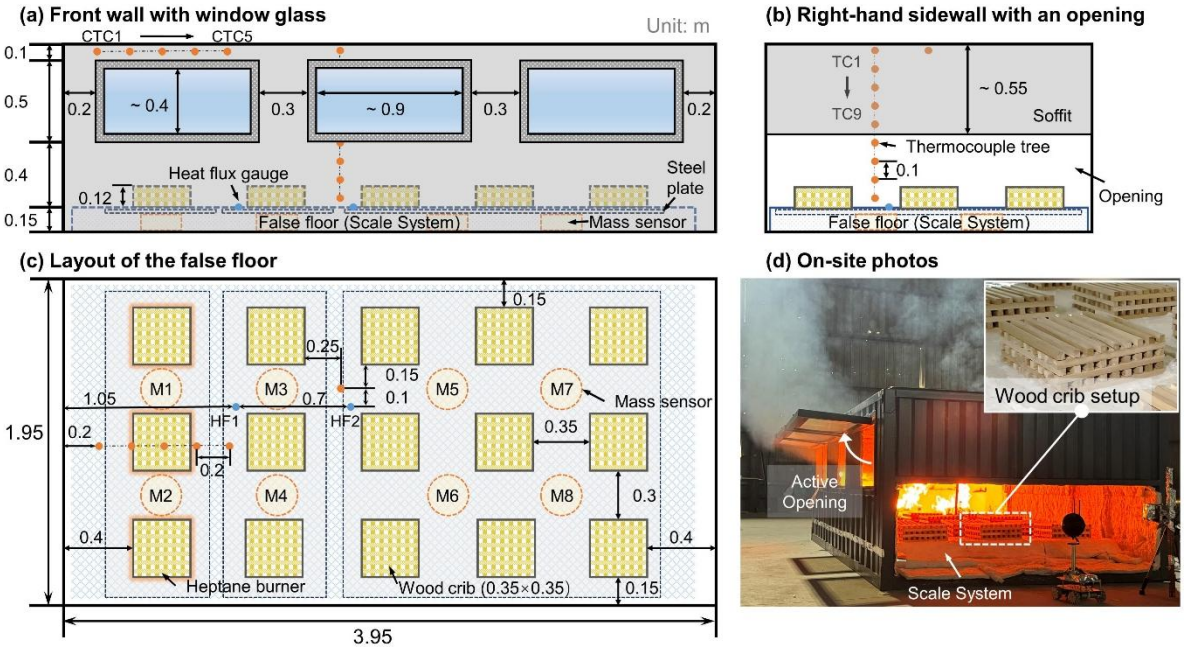

Fig. 5.2 Configuration of the reduced-scale compartment for experimentally investigating the effect of 'active opening'.

As shown in Fig. 5.2a, three windows were installed on the front longitudinal wall, each measuring 1.0 m in width and 0.5 m in height. The vertical distance between the upper edge of the windows and the ceiling was 0.1 m. Excluding the window frames, the dimensions of each glass panel were approximately 0.9 m × 0.4 m. As depicted in Fig. 5.2b, a 0.6 m high opening was included on the right-hand sidewall, following the semi-confined fire approach [175]. To enable accurate mass loss measurements of the wood crib fuel load, a 15 cm high false floor system was installed within the compartment. This system incorporated eight mass sensors with an accuracy of 0.5 g/s, supported by eight 4 cm-thick vermiculite boards, three 2 mm-thick stainless-steel plates, and a 2 cm-thick rock wool layer to ensure fire protection. The gaps between the false floor system and the compartment walls were filled with rock wool to enhance thermal insulation and protect the scale sensors throughout the fire tests. Additionally, heat flux gauges were embedded within the false floor system to provide thermal protection and enable accurate heat flux measurements.

Regarding the fuel load, there are 15 wood crib blocks evenly distributed on the false floor, forming a fuel bed matrix of 3 rows and 5 columns. The spacing between two adjacent rows is 0.3 m, and the spacing is 0.35 m in columns, as illustrated in Fig. 5.2c. Each wood crib block is stacked with wood sticks of 0.35 m long and of a cross-section of 0.02 m × 0.02 m. The average moisture content of wood sticks is around 10.5 % and the heat of combustion of wood is estimated between 15.5 and 19.5 MJ/kg. As depicted in Fig. 5.2d, one wood crib stack consists of 6 layers of wood sticks with 9 sticks per layer, and its average mass is approximately 2.75 kg. At the beginning of the fire test, the first column of wood cribs was ignited using three small burners, each containing approximately 150 ml of n-heptane. During each test, the scale system was configured to record the burning rate of all wood cribs at every second. In addition, a thermocouple tree of 9 thermocouples (TC1-TC9) at a vertical spacing of 0.1 m, was installed between the second and third columns of wood cribs to record room temperatures. These thermocouples with a bead diameter of 1.5 mm for up to 1200 ºC were used and their wire was wrapped in fireproof clay by foil tapes for additional protection. Two water-cooled Gardon-type heat flux gauges (HF1 and HF2) were clamped on the false floor near the second and third wood crib columns, oriented towards the ceiling, which monitored the received heat flux at the floor level. Two video cameras (1920 × 1080 pixels, 25 fps) were employed to document the testing observations from the front and right-hand side of the compartment, respectively. In the scenario with ‘active opening’, a thermocouple array comprising 5 thermocouples (CTC1-CTC5) at 0.2 m spacing is affixed to the ceiling above the initially ignited wood cribs to monitor ceiling temperature evolution. When the temperature readings of at least two of these thermocouples reached 70 ºC, all the glass panels were manually opened to implement the ‘active opening’ strategy, as illustrated in Fig. 5.2d.

5.2.2 Timelines of fire development with and without ‘active opening’

Significant differences were observed between the fire development histories when the fire tests were configured without and with the ‘active opening’ strategy (correspondingly Test A, B). The fire

development in the compartment with normal glass windows (Test A, i.e., without 'active opening') is presented in Fig. 5.3, which clearly shows the spontaneous ignition and full development after 10 minutes.

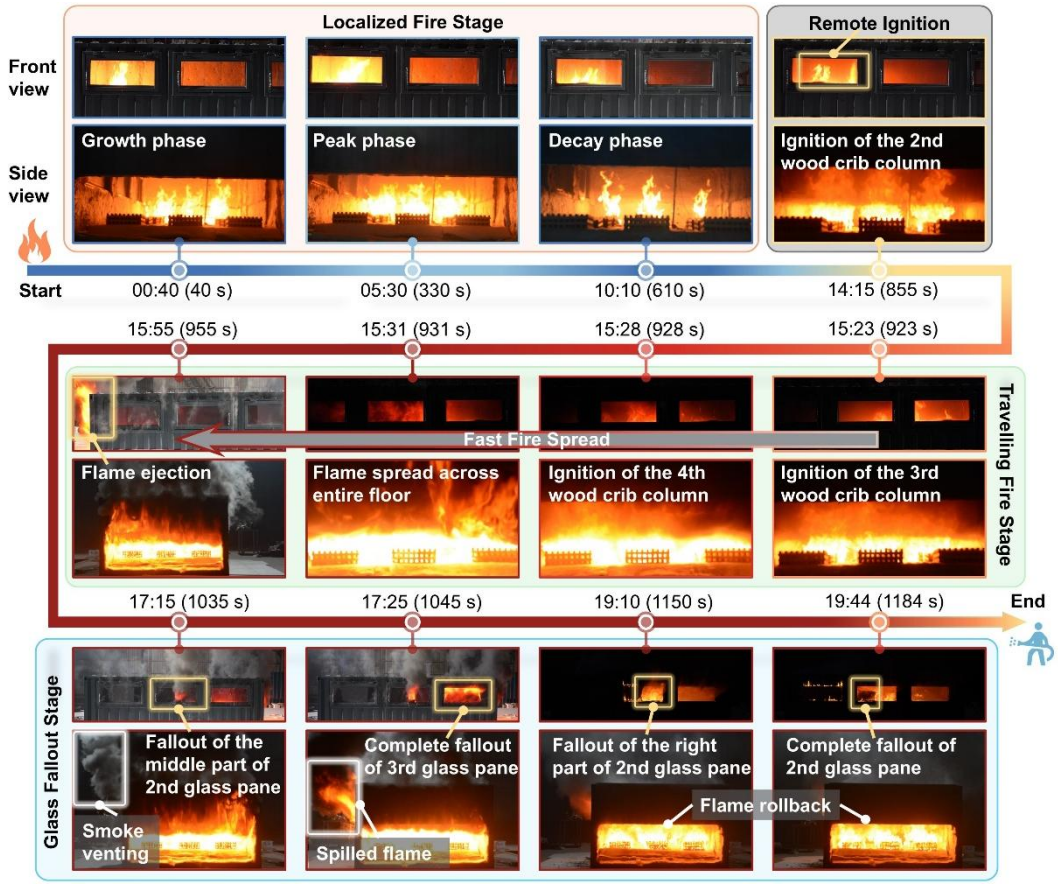

Fig. 5.3 Timeline of the Test A without 'active opening' strategy.

The localized flames were quickly growing after the first column of wood cribs was ignited by the heptane burners. At approximately 330 s, the localized fire reached its peak intensity. Heated by the growing localized fire and accumulated smoke, the first crack was found at the window glass pane near the ignited wood crib column (the first window) yet not leading to the fall-off of glass debris. At 610 s, the flames stepped into a local recession phase with a reduced fire size (flame height). Meanwhile, a dense smoke layer remained in the compartment due to the closed window (residing at the lower edge of the window assembly). The hot smoke continuously preheated the other wood cribs on the floor even before the flaming impinging on them. Resulting from the fire flames and hot smoke layer, the second wood crib column was ignited at approximately 855 s, followed by its surface flames rapidly developing and transitioning into fast fire spread mode. In a short period, the third column of wood cribs was ignited, and the flames rapidly swept across the entire floor within another 8 s. To this point, all the wood crib blocks were ignited, and the compartment fire entered the post-flashover stage, alongside fire flames ejecting from the side vent opposite to the ignition point.

An important finding with experimental verification is the considerable delay of fall-off of window glass panels in a compartment configured with longitudinal ventilation. In other words, the expected ventilation conditions as passive opening at the windows do not form at the early stage of a large compartment fire, even until the fire is developed for more than 10 minutes. Moreover, the relatively late fall-off of window glass has caused global flashover (i.e., simultaneous ignition of all combustible items), which was believed not to occur in such compartments. As observed in Test A, the first window near the ignition point did not experience fall-off at all. Instead, the second glass pane (middle window) of the tested compartment fell out at 1035 s, allowing a large volume of smoke to be expelled. This was soon followed by further growth of the fire and the complete detachment of the third glass pane, along with flames ejecting from the newly formed opening. Approximately 105 s later, the right half of the second pane fell out with the rollback of flames, and the second window glass was completely damaged at 1184 s. As the fire had entered the fully developed stage, the fire was manually extinguished at 1230 s. Till this point, the first glass pane remained firmly attached to the window frame, only with some visible cracks but not forming effective venting. It should be noted that the glass windows used in these two tests were made of single-layer float glass, supposed to easily fall off in a fire. If using laminated or insulated glass of multiple layers as adopted in modern windows, the fall-off of glass panes enabling effective ventilation would be even delayed. Therefore, unlike the rapid glass fallout induced by fast fire development in small compartments [49,178], the gradual interaction between window glass fallout and fire spread in a large open-plan compartment significantly affects the fire development behavior. With window glass, the previously observed localized burning alongside the 'travelling behavior' may not occur as the assumed sufficient ventilation conditions are considerably compromised by the delayed glass fall-off.

For Test B with the innovative 'active opening' strategy implemented at the windows, the framed glass panels were flipped upwards by 90°, which immediately formed openings at the triggering point (40 s after ignition), as shown in Fig. 5.4. During Test B, the flames remained localized at the first column of wood cribs, which did not proceed to the adjacent wood crib blocks. The localized fire reached its peak phase around 300 s, followed by the decay phase locally. Due to the 'active opening' of the windows at the early stage, the hot smoke produced by the localized fire is effectively vented through the façade windows.

It can be found that smoke was only trapped near the ceiling and above the window upper edge, as shown in Fig. 5.4. The height of the local flames further decreased at 600 s and the flames were barely observable at 840 s. Eventually, the fire entered self-extinguishment as a result of consumption of wood cribs around 1200 s, leaving only glowing embers on the floor. Throughout the whole fire test, the other columns of the wood crib were not ignited, which should be attributed to the reduced heating impact over them, owing to the small localized fire and the thin smoke layer. Benefiting from the reduced fire size and the cooler smoke layer, the smoke ventilated through the 'active opening' at the

windows is cooler, with no flames. Hence, the flipped window glass experienced no fire-induced damage, and the façade material was not damaged at all.

Fig. 5.4 Timeline of the Test B with 'active opening' strategy.

5.2.3 HRR histories in fire tests with/without 'active opening'

The scale serving as mass loss sensors (tagged as M1&2, M3&4, and M5-8 in Fig. 5.2c) are specifically allocated to record the mass changes of wood crib columns 1, 2, and 3-5, respectively. While Fig. 5.5a shows the mass loss rates (MLR) of Test A monitored by each scale set, the movement of flames at the wood crib bed can be clearly found in the fire scenario without 'active opening'. At about 200 s after the ignition, the MLR of the first wood crib column reached a plateau of around 13.8 g/s lasting for 300 s. During this period, the wood crib columns 2-5 underwent pyrolysis due to preheating by the localized fire flames. Notably, the MLR of the second wood crib column reached its first peak of about 2.8 g/s at around 600 s, and then it slowly declined as the wood cribs being consumed. Due to the continuous heating from adjacent fire flames and hot smoke layer, the second wood crib column was ignited at around 850 s, accompanied by a noticeable increase in its mass loss that eventually peaked at nearly 13.5 g/s. Shortly, the flames spread to wood crib columns 3-5 at about 910 s, where the MLR quickly escalated to 16.1 g/s and continued to increase to above 30 g/s after the glass fallout.

In Test B implementing the 'active opening' strategy, the MLR histories of wood crib columns were also measured by scale sensors and shown in Fig. 5.5b. For the first crib column, the variations of MLR exhibit a similar pattern to that obtained in the comparative test. The peak MLR (15.2 g/s) is only slightly higher than the peak value (14.6 g/s) in the test with no 'active opening'. An approximate plateau of MLR can be found in Fig. 5.5a, whereas no such plateau can be observed in Fig. 5.5b. This suggests that the burning rate of wood crib column 1 was maintained by the accumulated hot smoke

layer. The effect of the smoke layer can be clearly found in the MLR variations of wood crib Columns 2-5, as they were both ignited in the earlier test. However, because of 'active opening', the wood crib columns of 2-5 did not burn with flames, and the MLRs were at a very low level (up to 2.4 g/s). Along with the post-test observation, the wood crib columns 3-5 only underwent thermal-induced pyrolysis, leaving the charred surface of the second wood crib column as shown in Fig. 5.5b.

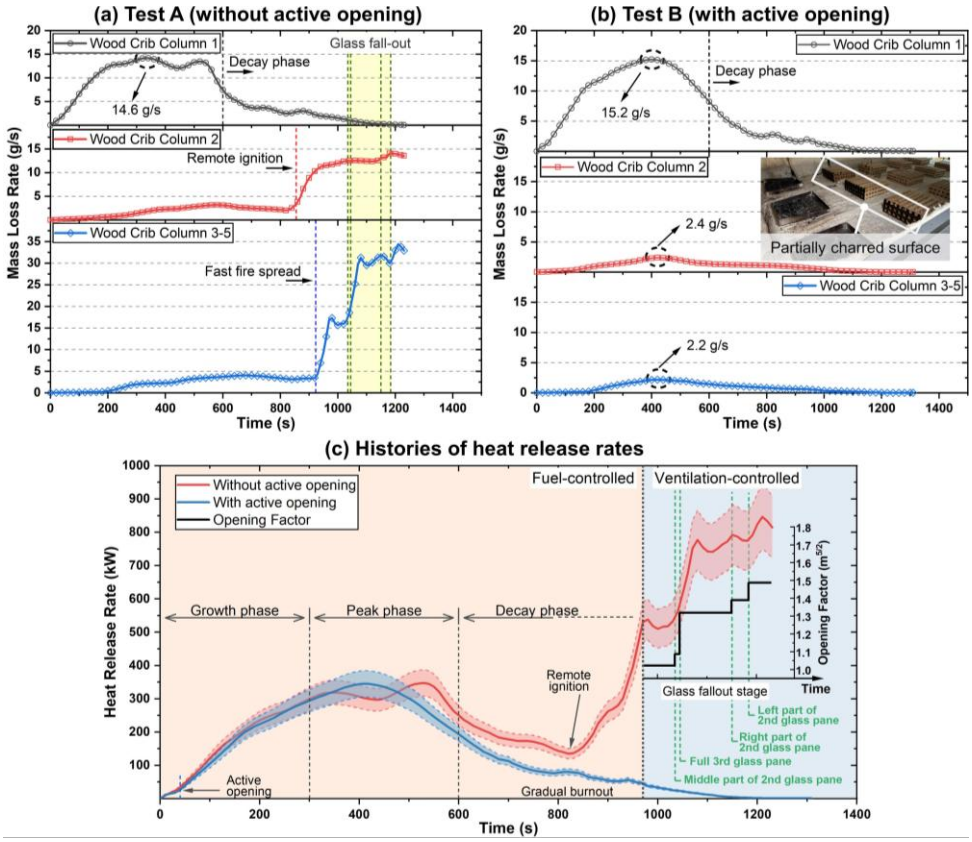

Fig. 5.5 Evolution of MLR of wood crib columns and HRR of two test scenarios.

With the measured data of MLRs, it is now possible to estimate the overall heat release rate (HRR) during the fire tests based on the heat of combustion of the wood crib. As this value for pine wood ranges from 15.5 to 19.5 MJ/kg [176]), the HRR histories can be estimated and illustrated as shown in Fig. 5.5c. At the early stage, the HRR variations in both fire tests (with/without 'active opening') are very close, which proves that the test setup is nearly identical other than the 'active opening' taking into action. Localized fires were formed on the first wood crib column, exhibiting a 'fuel-controlled' behavior. The differences in HRR histories in the peak phases are not significant, and the peak of Test A appeared slightly later than that in Test B. For the test with 'active opening', the localized fire gradually burnt out after entering its decay phase. Whereas in the test without 'active opening', the burning area expanded after a temporary decay stage. This is due to the remote ignition of wood cribs as they have been sufficiently preheated by the accumulated hot smoke layer. Restricted by the limited oxygen supply before the glass fall-off, the fire behavior gradually exhibits a 'ventilation-controlled' mode as a plateau of HRR development. When the fire intensity increases leading to the glass breakage

and fall-off. The HRR variation has shown stepwise growth, which is corresponding to the formation of new venting openings (i.e., the increase in opening factors $A_o\sqrt{H_o}$) induced by the glass failure. Through this test, the following observed phenomena are of considerable significance, but it should be admitted that the results are only based on the given experimental tests:

(i) The glass panels do not fall off at the early stage of a large compartment fire to form the expected openings;

(ii) The existence of glass panels has led to much higher HRRs as the fire enters the unexpected fast fire development stage.

(iii) The controversial strategy of actively opening windows can effectively mitigate the fire spread in a large compartment setup.

5.3 CFD fire modelling for numerical investigation

5.3.1 Configuration of fire simulation models

To understand the above-mentioned phenomena and the interaction mechanisms, it is necessary to retrieve more technical information in addition to the measured data in the real fire tests. Numerical modelling could certainly assist this investigation and enhance our understanding. Hence, the corresponding CFD fire models have been established in this chapter to grab more insights of the interaction mechanisms between glass fallout and fire development in large compartments, which could be also used in future simulation towards real-scale applications. In line with the descriptions in Section 5.2.1, the dimensions of the compartment, the parameters of the construction materials, and the layout of wood cribs are defined in the CFD fire model for high fidelity, as illustrated in Fig. 5.6. The computational domain of both models is expanded to include a sub-domain of 4 m × 1 m × 2 m near the windows and a sub-domain of 2 m × 3 m × 2 m at the right-side opening, to encompass the smoke flow area surrounding the compartment and the potential fire flames ejecting, as shown in Fig. 5.6a.

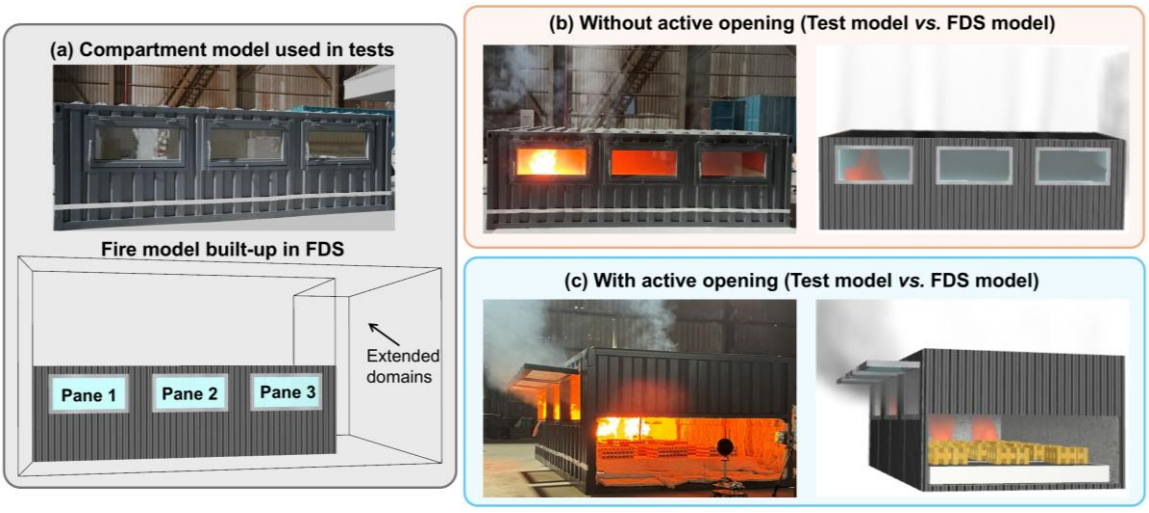

Fig. 5.6 Replication of fire tests using CFD fire models.

In the closed-window fire scenario (Test A), several interconnected HVAC nodes are employed to simulate the observed smoke leakage (Fig. 5.6b) through the edges of window frames in real tests (estimated to be about 2 mm wide in CFD models), as illustrated in Fig. 5.7. To model Test B with 'active opening', the activation of opening (Fig. 5.6c) is realized utilizing the control logic proposed in our previous work [177] with an activation temperature of 70 °C.

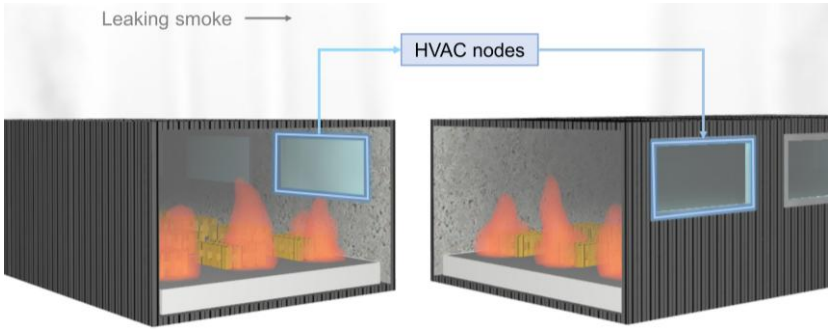

Fig. 5.7 Illustrations of simulation of leaking smoke from compartment

A uniform grid resolution of 0.05 m is used across the whole domain, which is based on the grid sensitivity check and previous modelling experience as a pilot study [167]. Notably this setup requires the use of the 'equivalent wood crib' method to adjust the wood sticks used in fire tests, which maintained the cross-sectional dimensions being smaller than the grid resolution. According to the 'equivalent wood crib' model [167], the parameter of AREA_MULTIPLIER of 1.728 is employed to compensate for differences in the effective surface area caused by the adjusted dimensions of wood crib model, while the parameter BULK_DENSITY is accordingly set at 259.85 to correct the total fuel mass. The adjusted wood cribs consist of three layers of wood sticks, with four sticks per layer and each stick is of a size of 0.35 m × 0.05 m × 0.05 m. Regarding the burning of wood sticks, the combustion reaction of wood is simplified with three main processes: the evaporation of moisture within the wood, the pyrolysis of the wood, and the further conversion of the residual char into ash. The reaction kinetics parameters for each process are determined through thermogravimetric (TG) analysis of the wood sticks used in the current fire test, which can be found in Appendix C. The heptane burners for ignition are simulated by positioning heating surfaces beneath the first column of the wood crib. The heat release rate per unit area (HRRPUA) is set to linearly increase from 0 to 300 kW/m^2 within 30 s, maintaining this rate until 180 s, which is followed by a linear decay to 0 at 360 s. This HRR-time curve is approximately derived based on pre-test measurements using the 150 ml heptane burner to ignite a single wood crib. In accordance with real test conditions, the ambient temperature and humidity in the simulation are set to 27.5 °C and 80% respectively, whilst no external wind influence is considered.

5.3.2 Validation of CFD fire models against fire tests

To validate the CFD fire models in simulating the above-presented fire tests, comparisons are made regarding the available data during each test. The comparisons of HRR histories are illustrated in Fig. 5.8.

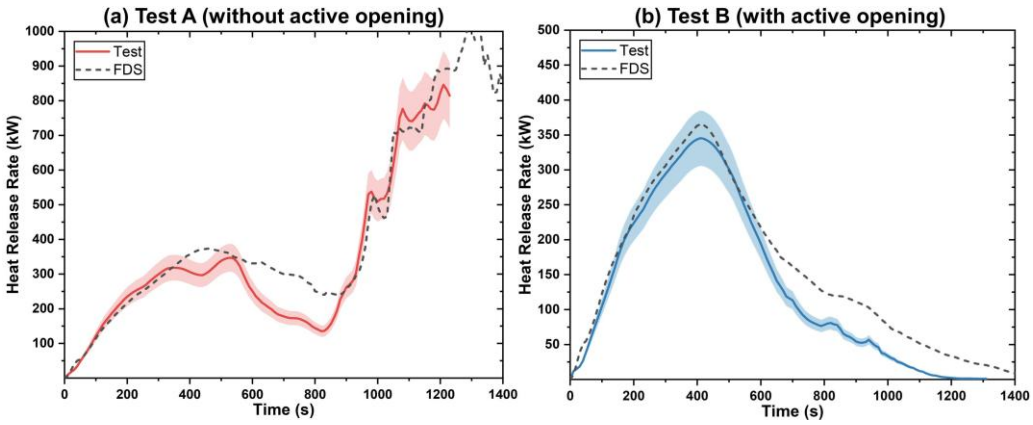

Fig. 5.8 Comparisons of the predicted HRR histories against test results.

The time-variant HRR in the scaled compartment without 'active opening' (i.e., Test A) is shown in Fig. 5.8a, and the HRR variations in the compartment with 'active opening' (i.e., Test B) is shown in Fig. 5.8b. The HRR histories obtained from the CFD fire models have presented very good agreement in terms of the early-stage growth, temporary decay, and the following fast development in Test A. When modelling Test B with 'active opening', the HRR variations agree well with the test data at the early growth stage, the peak, and the following decay stage. Notably, certain deviations can be found in the short decay stage of Test A and the decay stage of Test B, where the model predictions are slightly higher than the test data. This may be due to the incapability of the combustion model in capturing the decay of wood burning, as the stacks of wood sticks collapse after locally burning out. Besides, the temperature and heat flux data corresponding to the test measuring instrument are also compared in Fig. 5.9.

It can be seen in Fig. 5.9a that the CFD fire models are able to reproduce the gas-phase temperature results close to the experimental data at the corresponding measuring locations, regardless of the different setups at windows. Particularly, the temperature results agree well at high-temperature ranges, such as the thermocouples of TC1 to TC6. For the thermocouples of TC7-TC9 in the Test A setup, the gas-phase temperatures are below 100 ºC, whereas deviations exist between the test data and the simulated results. This might be caused by the thermocouple approximation in fire models compared to the real setup of thermocouples. General differences between model prediction and real data can be also found during the fast fire spread stage in Test A (from 900 s to 1200 s shown in Fig. 5.9a) and during the decay phase of Test B (from 1000 s to 1400 s in Fig. 5.9b), which are corresponding to the differences of HRR predictions. For the comparison of heat flux data at the locations of heat flux meters HF1 and HF2, the simulation data perfectly follows the varying trends of experimental measurements throughout the fire development. The floor heat fluxes monitored by HF1 in the test are slightly higher than those retrieved from the simulation model, but the maximum error is below 15%. Specifically, in Test A without 'active opening', the fire model accurately predicts the turning points of heat flux increases and the peaks of heat fluxes, despite the minor discrepancies that appeared in maintaining the peaks following the onset of fast fire spread (at 920 s).

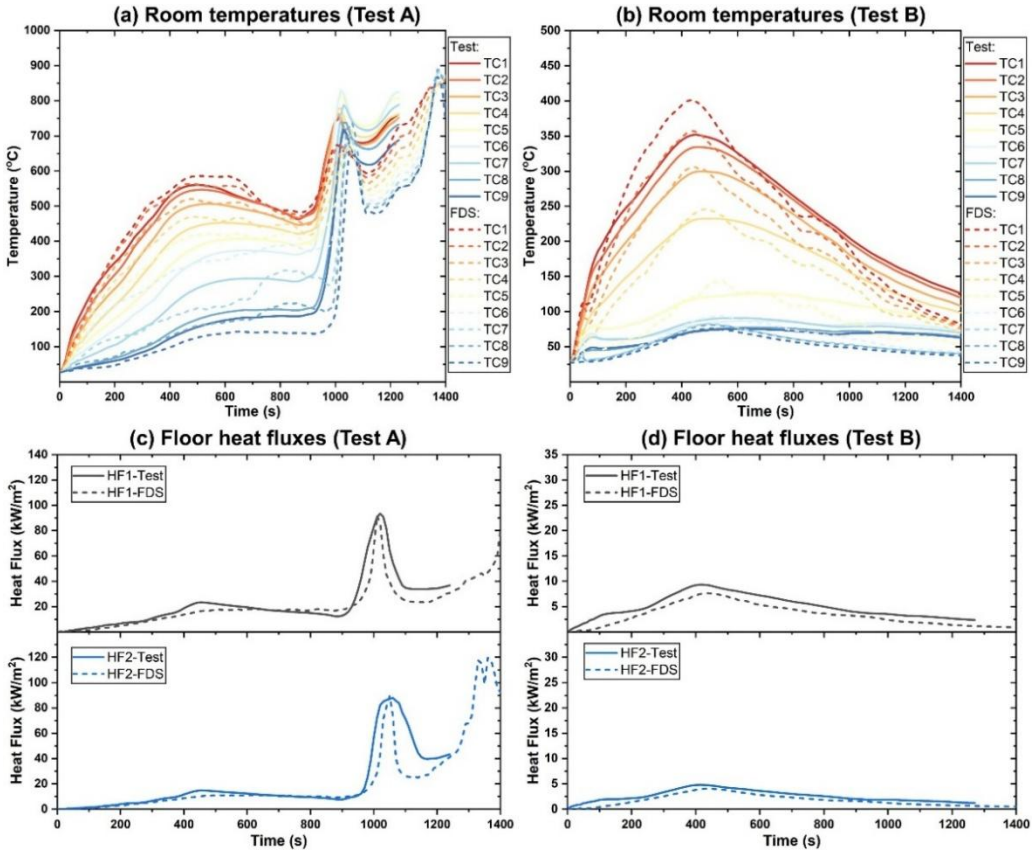

Fig. 5.9 Comparisons of the predicted room temperatures and floor heat fluxes in the simulation with experimental measurements.

5.3.3 Fire spread behavior shown in CFD fire models and fire tests

During the fire tests, the fire spread behavior was recorded by cameras, which provided a straightforward comparison to the predictions of the CFD fire models. The comparisons have been made for characteristic time steps (i.e., 300 s, 500 s, 1000 s, 1400 s), representing the typical fire development stages in each test, as shown in Fig. 5.10.

Compared with the test photos taken from the side opening, the CFD fire models have shown outstanding capabilities in reproducing flame shapes and the smoke layer. In the model of Test A (Fig. 5.10a), fire flames remain localized on the first column of the wood crib at 300 s and 500 s. Nevertheless, the accumulation of smoke in the scaled compartments is clearly shown in the CFD fire models. At 1000 s, a fast fire spread occurred, and all the wood crib blocks were ignited, accompanied by the ejecting fire flames from the openings as shown in the simulation illustration and test photos. Later, at 1400 s, the fire flames penetrating through the glass windows were found in the fire test due to the glass fall-off, which has been also successfully captured by the simulation model with glass fallout models included.

In Fig. 5.10b, the simulated fire behavior is compared against the test photos of Test B (with 'active opening'). In the fire model, it is clearly observed that smoke is ventilated through the actively opened windows (from 300 s to 1400 s) that is triggered by monitoring ceiling gas-phase temperatures. The

flame shapes on the first column of the wood crib are well predicted and remain localized on each stack throughout the whole fire test. Particularly, the height of the smoke layer is right below the longitudinal opening and even moved towards the ceiling at 1000 s, which is undoubtedly affected by the 'active opening' of glass windows.

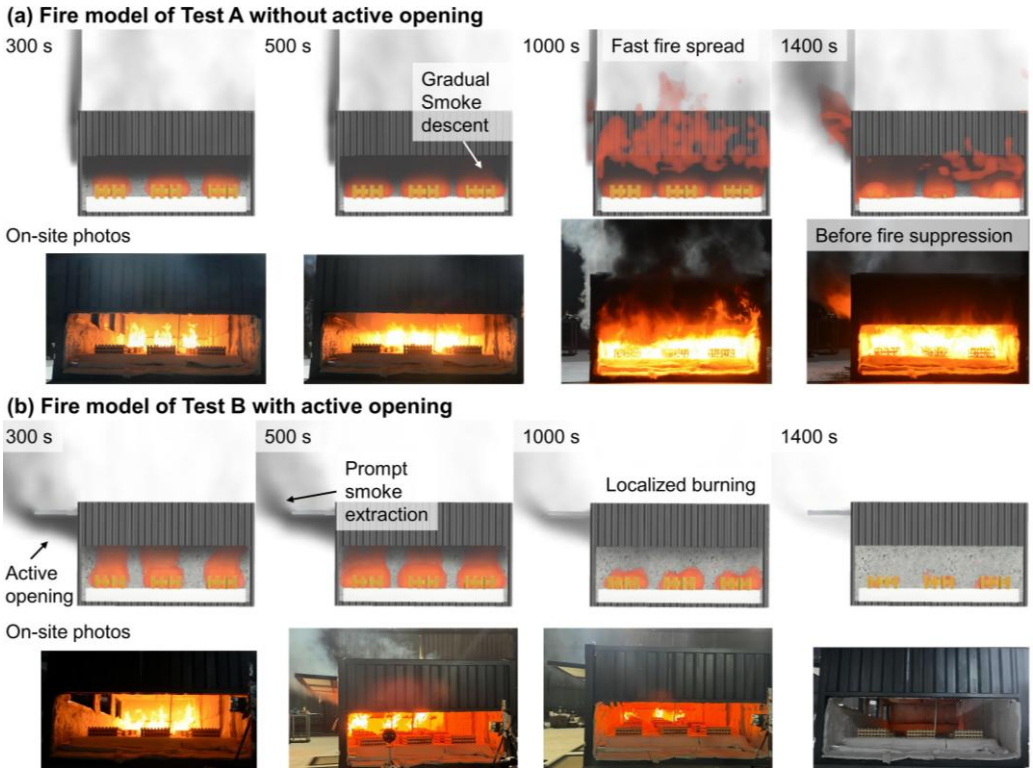

Fig. 5.10 Visual results from CFD fire models with and without 'active opening'.

Based on the above comparisons of HRRs, temperatures, heat fluxes, and flame shapes, the CFD fire models of different window opening setups have demonstrated their capabilities of reproducing the fire characteristics. With these two CFD fire models of high fidelity, it is now possible to retrieve more information to assist the understanding of the glass effect on fire development, which will be discussed in the following section.

5.4 Effects of glass existence and 'active opening' to fire development

In the previous sections, experimental tests on a scaled compartment with real glass panels and the other one with an 'active opening' have been presented, which are followed by the corresponding CFD fire models to provide supplementary data for further analyses. The fire spread in a long compartment has been found much faster while considering normal window glass being installed, which undermines the expectation of 'travelling fire' behavior represented by a slowly moving localized fire on the floor. While implementing the innovative strategy of actively opening windows at an early stage, a localized fire can be regained as the fire spread is substantially mitigated. With the data obtained from the tests and CFD models, the effects of glass existence on fire development in long compartments could be now analyzed and explained. Furthermore, the research question on how the novel 'active

opening' mitigates fast fire development in such compartments can be answered through data analysis, which is discussed in terms of internal energy conservation, heat losses, and heat generation.

5.4.1 Energy conservation within the large open-plan compartment

In a relatively large compartment (e.g., a long compartment of its length larger than 20 m), the smoke layer accumulates inside the compartment after ignition but does not fill the room rapidly. Instead, there exist two distinguished layers inside the compartment. This represented by a stratified temperature distribution can be visualized through the data recorded by the thermocouples TC1-TC9, as given in Fig. 5.9. Moreover, the energy conservation inside the open-plan compartments can be illustrated as Fig. 5.11, where the semi-confined concept is adopted to represent longitudinal ventilation.

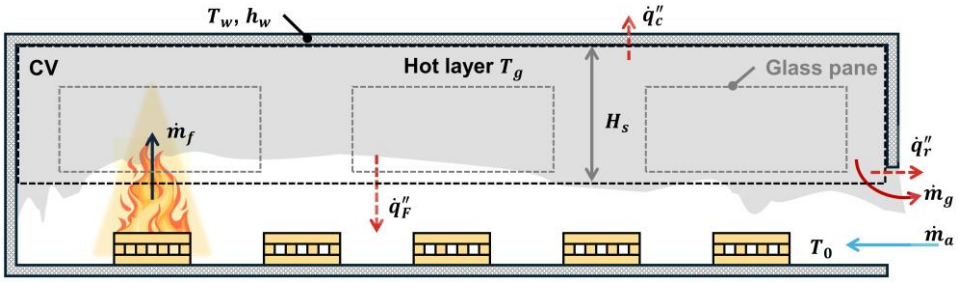

Fig. 5.11 Energy balance for the hot layer of localized fire in an open-plan compartment.

Hence, the temperature variations in the upper hot layer could be generally described using an idealized energy conservation [28], and this energy balance can be represented as follows:

$$c_{p,g}\frac{d(mT_g)}{dt} = G(T_g,t) - L(T_g,t) \tag{5.1}$$

where m is the mass of the gas in the hot layer, and $c_{p,g}$ is the specific heat capacity of the hot layer. Given the heterogeneity of temperature in open-plan space, T_g here refers to the average temperature of the hot layer. G and L denote the rates of energy gains and losses of the hot layer with time t, respectively. It is obvious that these two parameters governing the energy balance determine the evolution of temperature within the compartment. Hence, the success of the 'active opening' strategy lies in its ability to influence this balance and consequently slows down fire progression. Such influences in terms of the two variables, G and L, will be discussed separately in the following two subsections.

5.4.2 Heat losses due to 'active opening'

The energy loss term L consists of the following components: the energy loss due to mass transfer through openings, heat radiation to the floor, the heat loss through bounding walls and ceiling, and heat radiation losses through windows. Among these, the last component before glass fallout or 'active opening' is typically negligible, which was suggested to account for about 3% of the total losses in Harmathy's research [40]. Therefore, the expression of heat loss of the smoke layer L can be estimated as:

$$L = \dot{m}_g c_{p,g}\left(T_g - T_0\right) + \dot{q}_c'' A_s + \dot{q}_F'' A_F \tag{5.2}$$

where $\dot{m}_g$ is the mass rate of the discharged hot gases, and T_0 represents the temperature of the air. A_s is the area of the enclosure in contact with the smoke, while A_F is the floor area.

Obviously, the implementation of the 'active opening' strategy would directly enhance the first term (enthalpy exchange) representing the mass exchange induced heat loss. As depicted in Fig. 5.12, the opened windows effectively provide additional pathways for the expulsion of hot smoke, which facilitates the mass exchange $\dot{m}_g$ between the compartment and the outside environment. Meanwhile, the mass exchange of hot smoke through the window openings becomes more efficient if the lower surface of hot smoke is below the upper edges of windows.

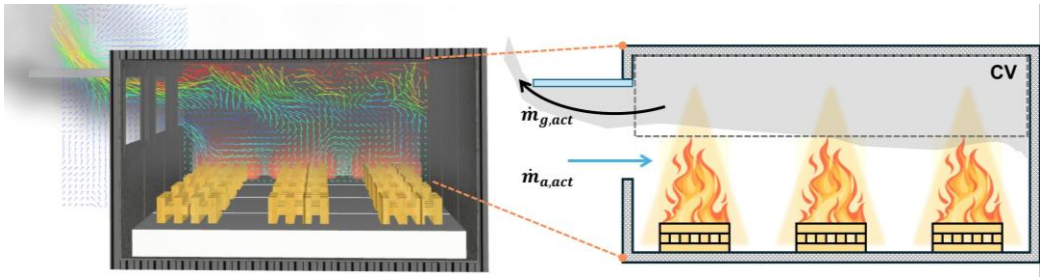

Fig. 5.12 Formation of new pathways for heat losses using 'active opening' strategy

Fig. 5.13 illustrates the mass exchange rate recorded at the window openings and side openings, which are extracted from the CFD fire model. In Test A with glass panels but no 'active opening', the mass exchange primarily occurs through the side opening representing semi-confined conditions. The ventilation capacity of this side opening is limited to only about 0.2 kg/s and even decreases to 0.15 kg/s before the glass fallout (i.e., 920 s to 1050 s), suggesting the hot smoke movement was held by the surrounded hot smoke and incoming fresh air. This tendency of flow field condition implies an increasing pressure inside the compartment, which typically triggers glass fallout as observed in Test A.

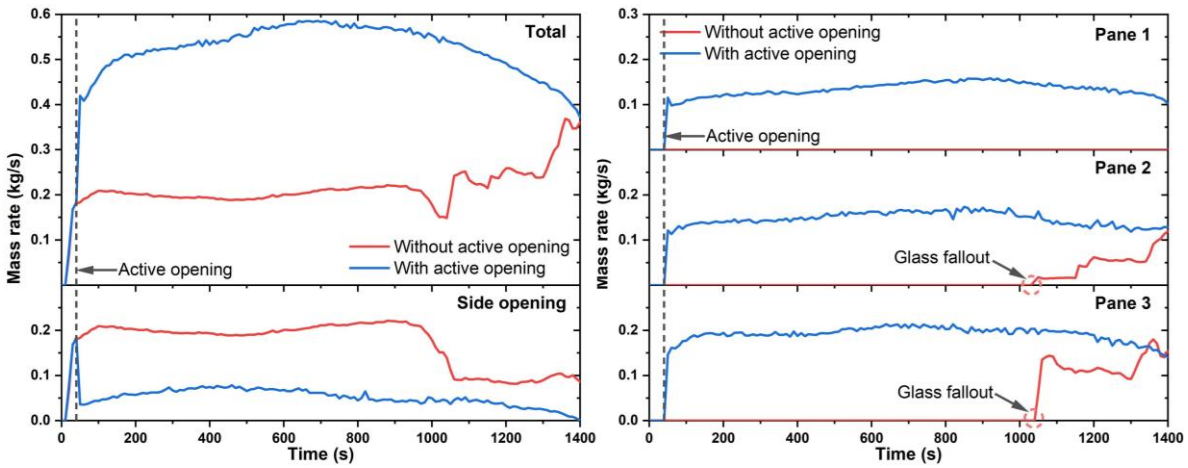

Fig. 5.13 Mass rates of expelled hot gas (total, through side opening, and through each window opening)

Once the glass fell off from the window frame, the fire flames have already spread to other wood cribs. At this point, the rapidly growing fire inside the compartment is able to break the glass panels to form new openings, where the ejecting flames at the windows can be found and the fire already enters the fast-spread stage. In contrast, for the fire scenario with 'active opening' (Test B), the triggered window openings at the early stage (about 40 s) immediately boost the total mass loss rate $\dot{m}_g$ from 0.2 kg/s to 0.4~0.6 kg/s. Notably, the opened windows alter the smoke movement pattern, where nearly 75% of the mass exchange through the side opening is diverted to the newly created window vents. This indicates that the 'active opening' strategy would be particularly useful for compartments of limited longitudinal ventilation, i.e., most of modern open-plan compartments.

5.4.3 Reduced floor heating from smoke layer

The main differences in mass and heat transfer are reflected by the variations of temperature and thickness of the smoke layer. With window glass installed and 'active opening', the floor heating conditions attributed to the smoke layer are changed. The temperature of the hot smoke layer T_g changing in accordance with time has been illustrated in Fig. 5.14a, which is calculated as the average smoke temperature at the locations above wood crib columns 2-5. Two distinct trajectories can be observed after 40 s, which is the activation time of 'active opening'. From then on, the smoke layer temperatures in Test B (with 'active opening') are significantly lower than the temperatures recorded in Test A model (without 'active opening'), where the smoke temperatures increase to 650 °C. Even before the fast fire spread, the smoke temperatures are around 400 °C. However, in Test A, the smoke temperature T_g peaks at only 300 °C, followed by a steady decay to 70 °C. This suggests that the smoke layer temperature could be well maintained below 300 °C after 'active opening', and the ventilated hot smoke of this temperature could not cause heating damage or ignition of façade materials.

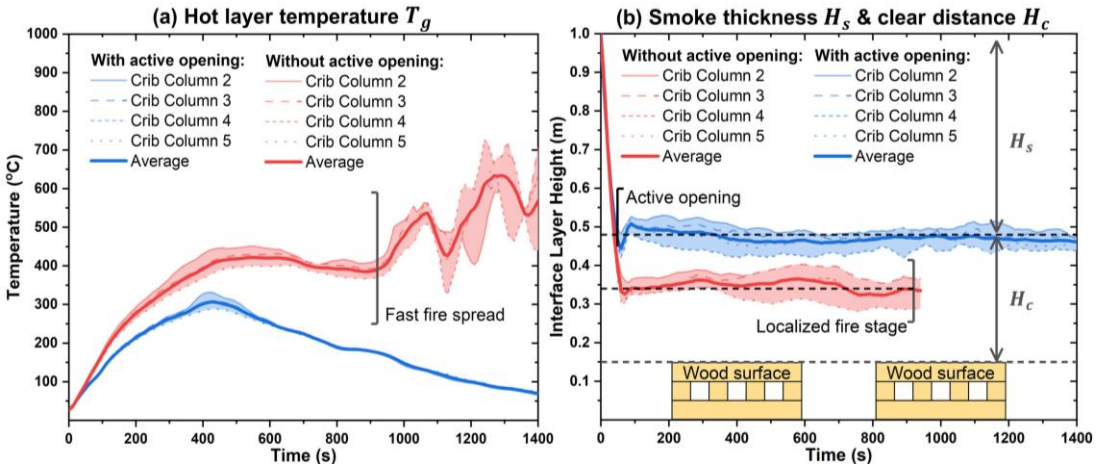

Fig. 5.14 Evolutions of temperature and thickness of residual smoke.

In addition to the smoke temperature differences, the 'active opening' of glass windows directly affects the smoke layer thickness H_s, as depicted in Fig. 5.14b. Before the 'active opening', the growth of smoke thickness due to the smoke accumulation from the initial localized fire experience the same

path. After the ‘active opening’, the smoke layer boundary undergoes a short fluctuation because of sudden outflow, it soon enters a plateau at 0.48 m from the floor. It effectively elevates the hot smoke boundary by 0.15 m (nearly 1/6 of the entire height of the scaled compartment) in the localized fire stage with reference to the smoke layer in Test A with no ‘active opening’. The results during the fast fire spread stage are not displayed, since the smoke layer has deviated from the idealized state shown in Fig. 5.11 due to the disturbance of flame movement. These differences in the temperature and position of the smoke layer can directly impact the heating effects on nearby combustible materials, which is crucial for the expansion of burning region as illustrated in Fig. 5.15.

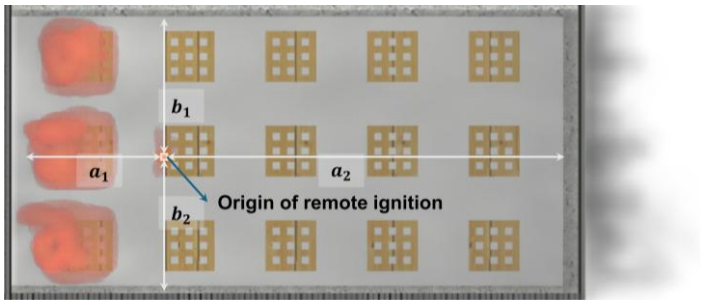

Fig. 5.15 Illustration of fire scenarios where the onset of remote ignition occurs.

During the fire, the thermal effect attributed to the radiation of hot smoke layer $\dot{q}_s''$ can be expressed by:

$$\dot{q}_s'' = F_{s\to o}\sigma\varepsilon_g\left(T_g^4 - T_0^4\right) \tag{5.3}$$

where $F_{s\to o}$ in Eq. (3) refers to the view factor. ε_g is the emissivity of the smoke layer, and σ is the Stefan–Boltzmann constant. While it is calculated regarding smoke radiation to the point of second wood crib column, the calculation is formed as below [179]:

$$F_{s\to o} = \frac{1}{2\pi}\sum_{j=1}^{2}\sum_{i=1}^{2}\left[\frac{a_i}{\sqrt{a_i^2+H_c^2}}\tan^{-1}\left(\frac{b_j}{\sqrt{a_i^2+H_c^2}}\right) + \frac{b_j}{\sqrt{b_j^2+H_c^2}}\tan^{-1}\left(\frac{a_i}{\sqrt{b_j^2+H_c^2}}\right)\right] \tag{5.4}$$

where a_i and b_i are the geometrical parameters of floor area that are labeled in Fig. 5.15. H_c represents the clear distance from fuel surfaces to the smoke layer, which can be obtained from Fig. 5.14b. The emissivity of the hot layer ε_g in Eq. (3) can be determined by:

$$\varepsilon_g = 1 - e^{-H_s\left(k_g + k_{soot}\right)} \tag{5.5}$$

where H_s is the thickness of the smoke layer, which is displayed in Fig. 5.14b. k_g and k_{soot} are the absorption coefficients for the hot layer and soot, respectively. k_{soot} is typically recommended as 1.9 m^{-1} [180] and k_g can be empirically estimated by [180]:

$$k_g = 0.3 + \frac{4.64\dot{m}_f}{\dot{m}_a + 0.6\dot{m}_f} \tag{5.6}$$

where $\dot{m}_a$ and $\dot{m}_f$ are the mass flow rate of fresh air and mass loss rate of wood cribs, which are extracted from the flow rate slices in fire models. The calculation results of view factor $F_{s\to o}$ and smoke emissivity ε_g are displayed in Fig. 5.16. As shown in Fig. 5.16a, a 30% reduction of the view factor is obtained through the implementation of the 'active opening' strategy.

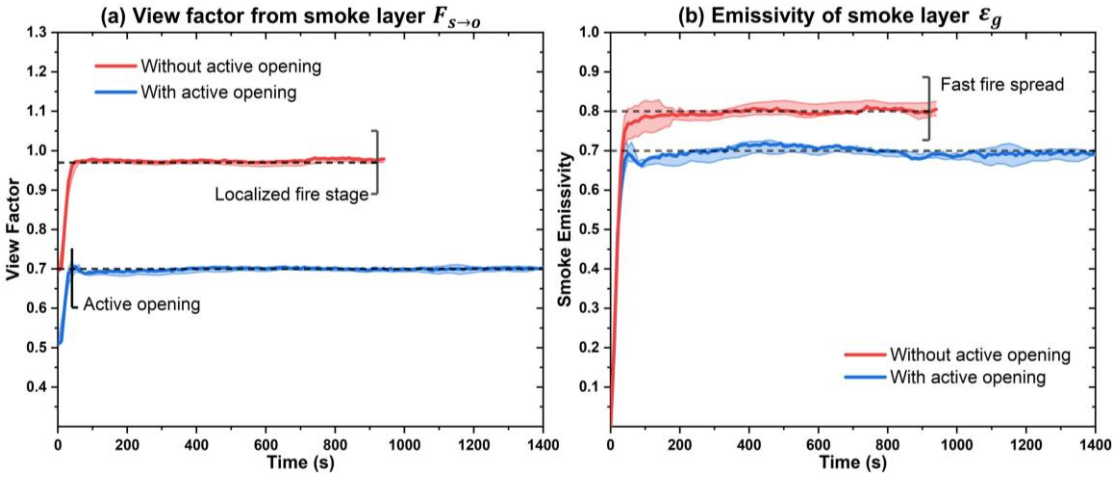

Fig. 5.16 Evolutions of view factor and emissivity of smoke layer.

Additionally, the emissivity of the smoke layer decreases by about 0.1 as displayed in Fig. 5.16b, further implying a weakened radiative capability of the smoke layer. Hence, the 'active opening' of window glass panels not only intuitively reduces the smoke layer thickness H_s and the smoke temperature T_g, but also leads to a lower view factor $F_{s\to o}$ and emissivity ε_g of the hot layer.

The aggregated effect of these factors thereafter results in a significant reduction in the heating impact of the smoke layer, from nearly 12 kW/m^2 in the normal glass window setup to a peak of 4 kW/m^2 in the 'active opening' case, as revealed in Fig. 5.17. This reduced heating impact from different smoke layer characteristics well addresses the positive effect of providing ventilation through windows at the early stage.

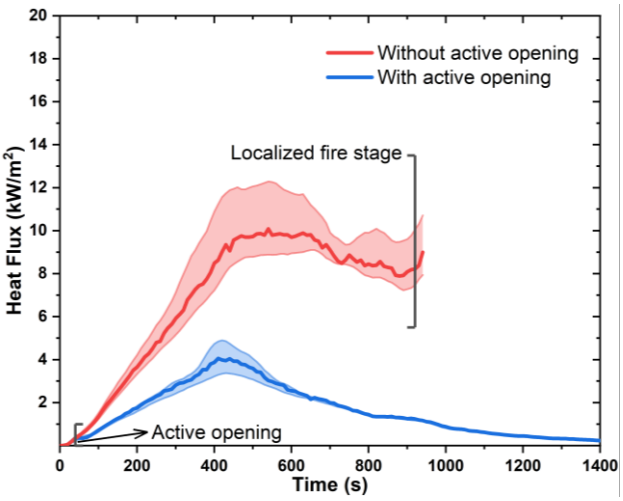

Fig. 5.17 Calculated heating impact of smoke layer $\dot{q}_s''$ using Eq. (3).

5.4.4 Active opening: providing fresh air or reducing hot smoke heating?

It should be admitted that the active opening of windows may incur negative effects, e.g., bringing fresh air to facilitate the growth of localized fire. This is the common knowledge base of not opening glass windows during the fire growth but may not remain valid in modern open-plan compartments. Fig. 5.18 illustrates the oxygen supply conditions when the second wood crib column gets ignited. At this stage, the upper hot smoke layer can only be vented through the right-side opening, while fresh air also enters near the origin of remote ignition through this same opening. This stratified flow field condition corresponds to the schematic shown in Fig. 5.11.

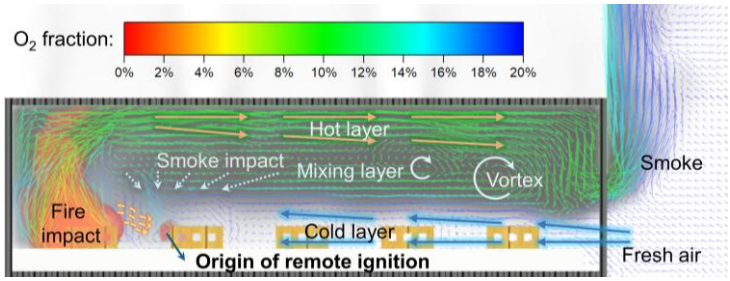

Fig. 5.18 The air flows during a localized fire in semi-confined compartment.

Recalling the heat balance during the localized fire stage, the energy generation term G is predominantly influenced by the rate of fuel supply to the fire, which can be estimated as follows:

$$G = \dot{m}_f \Delta h_c \tag{5.7}$$

where Δh_c represents the effective heat of combustion per unit mass of the fuel, and $\dot{m}_f$ is the mass flow rate of the fuel being consumed in the combustion. If with sufficient air supply, the mass flow rate is governed by the following equation [181]:

$$\dot{m}_f = \frac{A_f \dot{q}_e''}{\Delta h_L} \tag{5.8}$$

where Δh_L refers to the latent heat of pyrolysis, and A_f is the effective burning area. $\dot{q}_e''$ is the external heat flux imposed on the fuel surface, which can be decomposed as two main components: (i) heating impact from the localized fire plume $\dot{q}_f''$; and (ii) radiant heating from the hot smoke layer $\dot{q}_s''$.

The heat flux term of $\dot{q}_f''$ is correlated to the HRR of a localized fire, as commonly described in point-source [182] or line-source [183] models. As shown in Fig. 5.5, the HRR histories in both tests are almost identical at the early stage of fire. Hence, the heating action due to localized fire flames $\dot{q}_f''$ in both tests are quite close to each other from the ignition point to about 350 s. In other words, the heating contribution of $\dot{q}_s''$ is the dominant factor to the fire growth in a compartment with sufficient air for the combustion of localized fire.

In Fig. 5.19, the correlating variations between smoke heating action, floor heat fluxes, and HRR histories are presented. Here the floor heat fluxes were measured by the heat flux gauges HF1 and HF2.

It should be reminded that the HF1 gauge was located between the first and the second wood crib columns, whereas the HF2 gauge was between the second and the third columns. During the growth stage, HF1 received more heating from the fire flames compared to HF2, while HF2 should be closer to the radiant heating from the smoke layer. Noted the calculated heating action as discussed previously has been also illustrated in Fig. 5.19. The relationship between HF1, HF2, and smoke heating has shown an evident correlation during the fire, which further agrees well with the HRR development curves.

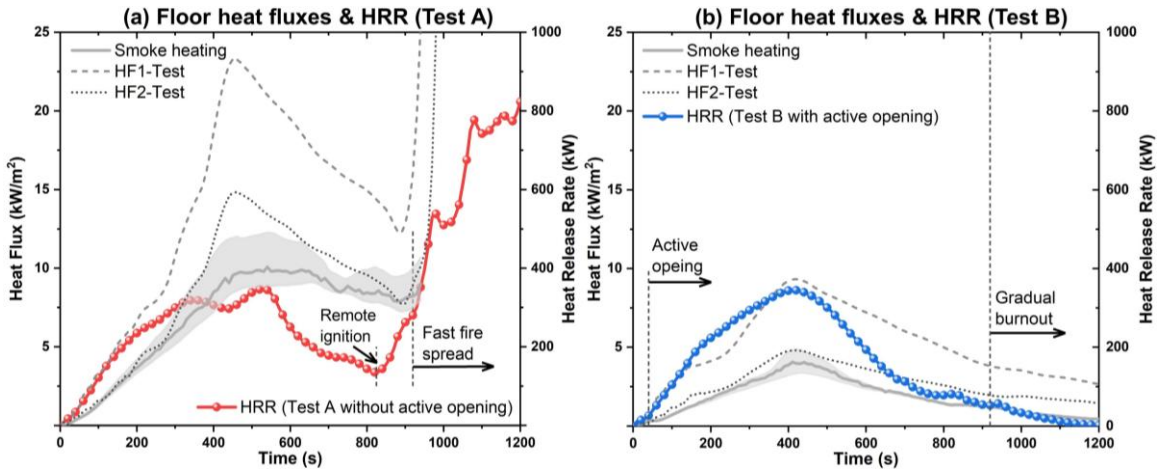

Fig. 5.19 Comparison of smoke heating with measured floor heat fluxes and resulting HRRs.

From Fig. 5.19a and Fig. 5.19b, it is clear that the difference between HF1 values and $\dot{q}_s''$ and the difference between HF2 data and $\dot{q}_s''$ are corresponding to the size of localized fire (i.e., HRR of localized fire). If comparing the two subfigures, the higher smoke heating due to the existence of window glass has caused much higher heating action on the floor wood crib. Because of a relative compartment setup, the oxygen needed for the early fire growth has not been hindered by the intact window glass panels. Therefore, the active opening of glass windows is effective to the mitigation of fire spread, as long as the oxygen supply to early fire growth is sufficient, which is generally common in modern building compartments of larger size and inner openings.

5.5 Conclusions

This chapter has conducted two scaled compartment fire tests alongside corresponding CFD fire simulations, marking the first-ever experimental demonstration of the critical role of glass-fire interaction in large open-plan compartments and the potential fire mitigation benefits of the 'active opening' strategy. According to the test results and analyses, several key findings are concluded as follows:

(1) From both the tests and simulation models, it has been observed that window glass experienced cracking but not immediately falloff to create openings for ventilation at early stage, and the actual window openings occurred during the fast spread of fire flames, which clearly showcases the initial opening assumption is invalid.

(2) The ‘active opening’ strategy significantly facilitates the heat and mass transfer of hot smoke layer, which limits the smoke temperatures to no more than 300 ^{o}C as well as raises up the smoke layer boundary by 0.15 m (1/6 of the entire height of the scaled compartment). Hence, the view factor between the smoke layer and the adjacent wood crib is reduced by 30%, and the heating impact in terms of heat fluxes from smoke radiation to floor wood crib is considerably reduced.

(3) The oxygen supplies to the early stage of fire are both sufficient in cases with/without active opening, which are reflected in the identical HRRs at early stage. The ventilated smoke at early stage (after fire detection) has led to weakened pre-heating of floor wood crib, which was governed by the radiation from localized fire and hot smoke layer. According to the monitored heat flux data and the calculated radiant heat flux from various smoke layers, it is found that active opening of windows does not intensify the localized fire, but it substantially reduces the smoke preheating on floor wood crib.

These findings emphasize the practical significance of providing early-stage ventilation in large open-plan compartments, reinforcing ‘active opening’ as a viable and innovative fire mitigation strategy. Given the promising results, further research is warranted, particularly practical challenges of implementing the ‘active opening’ strategy in real-world modern buildings. Future work will involve numerical simulations for realistic buildings, the outcomes of which will be detailed in Chapter 6.

Chapter 6: Realistic Applications of 'Active Opening' Strategy in Modern Buildings

Summary

Chapter 5 has experimentally validated the effectiveness of the 'active opening' strategy in mitigating fire spread and investigated the mitigation mechanisms. Note that the research was primarily based on reduced-scale models, and this chapter will extend the application to more realistic fire scenarios in a built environment. In this chapter, multiple aspects of realistic compartment configuration including fuel distribution, ignition locations, opening methods, and detector setups have been considered to evaluate the effectiveness of the 'active opening' strategy in mitigating fire spread. Results show the strategy significantly mitigates smoke accumulation and fuel bed preheating, especially at lower fuel load densities (400 MJ/m^2 and 600 MJ/m^2), where it inhibits flame propagation. At a fuel load density approaching 800 MJ/m^2, this strategy delays but does not entirely halt flame spread. Moreover, this strategy mitigates thermal impacts on façade walls, reducing the risk of external fire spread. It is found that the 'active opening' strategy performs well across a range of commonly used window configurations, underscoring its flexibility and adaptability. The exploration also reveals that the optimal fire mitigation does not require opening all windows. This suggests that a smart tiered opening strategy for 'active opening' can be further developed, which would dynamically adjust the number of opened windows in response to real-time fire progression dynamics. Through the present research, the window-integrated detector design is foreseen as a promising future of implementing 'active opening', which may only require minor changes on window setup but leading to effective mitigation on fire spread and smoke reduction.

The work of this chapter has been reported as a journal paper: 'T. Chu, W. Zeng, L. Jiang. Using 'active opening' of windows for fire safety of modern buildings considering more realistic setup (Submitted).'

6.1 Introduction

Chapter 4 and Chapter 5 of this thesis have demonstrated that the 'active opening' of glass windows can provide crucial ventilation conditions to mitigate fast fire spread in specific large open-plan compartments. Through CFD fire simulation and experimental tests, the presence of glass panels was found to aid the accumulation of hot smoke layer in compartments, whereas the early fire action was not able to cause glass fallout to form venting. The accumulated smoke layer results in much faster fire spread and eventually leads to flashover with a much higher thermal impact on building structures. To address the potential severity caused by delayed glass fallout, the 'active opening' strategy [177] was introduced in Chapter 4 and experimentally validated in Chapter 5. This strategy enables the 'active opening' of glass windows in open-plan compartments upon fire detection, to ensure the prompt acquisition of adequate ventilation. However, the application of the 'active opening' strategy has so far been limited to idealized fire scenarios without considering its potential impact on façade fire safety. The hot smoke released from actively opened windows may ignite or damage façade materials, thereby compromising the vertical compartmentation measures in tall buildings [184]. Furthermore, in real-world modern building designs, the fuel load distribution is often non-uniform and the fire starting point is uncertain [185], unlike the uniformly distributed fuel loads (e.g., wood crib blocks) commonly used in experimental fire tests [177].

To consider more realistic application scenarios, this chapter aims to implement the 'active opening' strategy in compartment fires of a more realistic setup, and to examine whether it remains effective in mitigating the rapid development of fire under practical conditions. To achieve this, this chapter develops a three-story open-plan building fire model using the FDS. Both uniform and non-uniform fuel load distributions are modeled to better reflect realistic fire scenarios while the effects of ignition locations are also incorporated. Additionally, the potential for façade fire spread is evaluated by simulating the pyrolysis and combustion of cladding materials on façade walls. The performance of the 'active opening' strategy on fire control is evaluated by comparing key indicators including fire HRRs, smoke layer heights and temperatures, façade wall temperatures, and incident heat fluxes on cladding materials. Furthermore, considerations related to window opening designs for 'active opening', the number of windows actively opened, and the detector designs for triggering 'active opening', are systematically examined. These findings provide critical data to support the practical implementation of the 'active opening' strategy in real-world building fire safety designs.

6.2 CFD fire models of modern buildings with 'active opening'

6.2.1 Description of prototype modern open-plan designed building model

The prototype building model of the present work is based on a three-story modern open-plan building. The single compartment on each floor measures nearly 22 m in length, 5.6 m in width, and 2.8 m in height. As shown in Fig. 6.1a, a base model for CFD fire analysis of this building has been

developed using FDS version 6.7.7, which will be utilized in various numerical simulation cases to investigate the application factors of ‘active opening’.

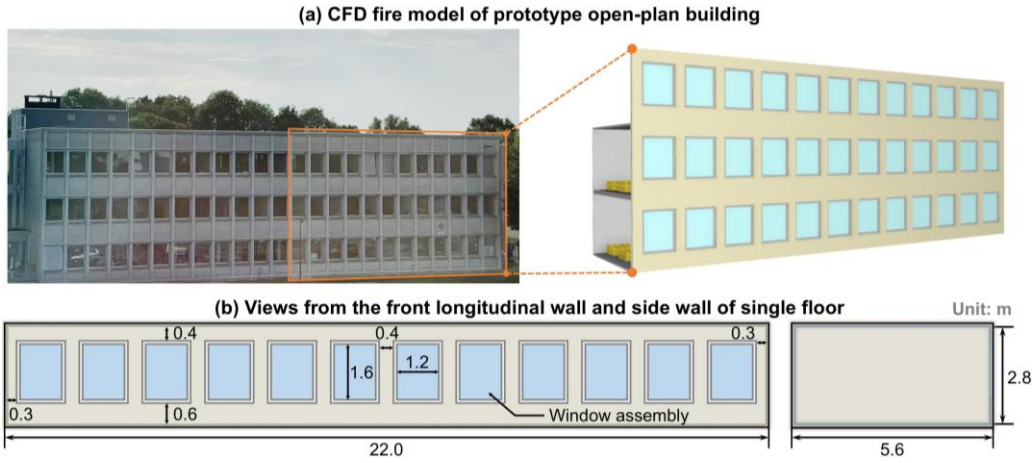

Fig. 6.1 Overview of CFD fire model based on a real-world building.

The first and second floors are identically configured in the model, including internal fuel load arrangements and façade designs, whereas the third floor is only constructed with the façade walls, identical to those on the lower floors, to focus on façade fire safety. The computational domain covers all floors and extends 2.5 m outward from the façade walls to capture outward smoke flow. Particularly, Fig. 6.1b provides details on the configuration of window assemblies. Each floor has twelve identical window sets uniformly installed on its façade wall, with a spacing of 0.4 m. Each window set is 1.2 m wide and 1.6 m high, and its upper edge is positioned 0.4 m below the ceiling.

6.2.2 Configuration of façade walls in fire models

Fire safety of external walls is essential for both maintaining compartmentation and preventing extensive fire spread. One major concern regarding potential façade fires, especially in the context of using the ‘active opening’ strategy, is the flammability of the external wall insulation system (EWIS) employed on building envelopes. The EWIS is widely used in new building construction and retrofitting existing structures due to its superior insulation performance, which enhances energy efficiency and improves occupant comfort [186]. As illustrated in Fig. 6.2, EWIS usually includes substrate wall, adhesive mortar, insulation board, finishing mortar, reinforcing mesh and decorative surface [187].

The substrate wall serves as the base layer of the entire insulation system, providing support and structural stability. The adhesive mortar is applied to firmly attach the insulation board to the substrate wall, ensuring the durability of the system. The insulation board, a major component of EWIS, reduces energy loss due to its low thermal conductivity. Over the insulation board, there exists a layer of finishing mortar, forming a solid base for the decorative surface and encapsulating the insulation board. Reinforcing mesh is embedded in the finishing mortar to enhance the integrity performance of the exterior layer, preventing cracking and detachment. The decorative surface is the outermost layer of the insulation system, enabling aesthetic appearance and durability protection.

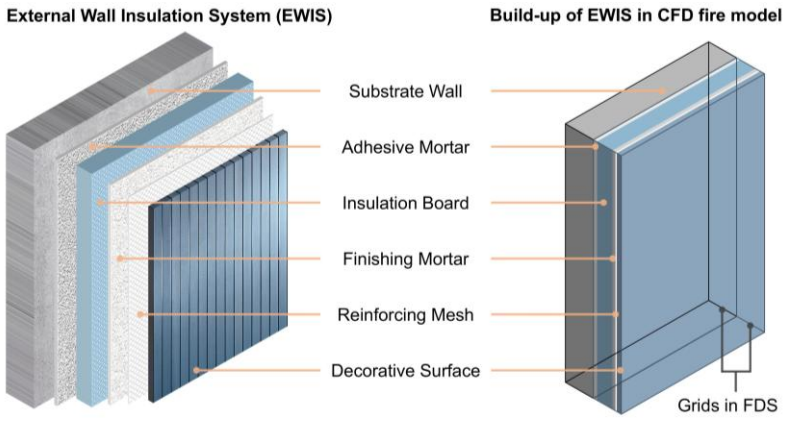

Fig. 6.2 Typical components of EWIS and their representation in fire models.

For current fire models, the involved material properties and layer thickness of each component of EWIS are listed in Table 6.1. Here, the EWIS is constructed in CFD fire models according to the layer thickness, and the model is illustrated in Fig. 6.2. Notably, the extruded polystyrene (XPS) board is selected as the insulation component, which is widely used in construction due to its excellent performance. The fire behavior of XPS is captured using a simple single-step pyrolysis model, with a pre-exponential factor A_a=3641 s^{-1}, an activation energy E_a=126 kJ/mol and a reaction of order n=2 [188].

Table 6.1 Parameters of each component layer of EWIS [189].

Component layer	Materials	Density [kg/m^3]	Specific heat [J/kg·K]	Thermal conductivity [W/m·K]	Thickness [m]
Substrate wall	Reinforced concrete	2450	960	1.4	0.3
Adhesive mortar	-	1550	880	0.61	0.01
Insulation board	XPS	34	1400	0.029	0.075
Finishing mortar	-	1650	900	0.32	0.01
Reinforcing mesh	Steel mesh	786	500	5.02	0.005
Decorative surface	Ceramic	2200	840	1.2	0.01

6.2.3 Settings of fuel loads and ignition points

In the concerned fire scenarios, wood crib blocks are placed on the floor to represent the room fuel load in the present open-plan compartment. This is in line with the widely adopted setup in experimental tests of compartment fire behavior [8,10,11,14,190,191], whereas real combustible items are of different materials which would be considered in future studies. In this chapter, the non-uniformity of the floor fuel load is considered as another major factor influencing realistic fire behavior. In Fig. 6.3a and Fig. 6.3b, , the uniformly distributed stacks are presented, whereas Fig. 6.3d and Fig. 6.3e depict wood crib stacks with varying heights and areas. For uniformly distributed stacks, three rows of wood crib stacks

are placed parallel to the longitudinal façade wall, with a spacing of 0.9 m. Each row consists of 11 wood crib stacks, spaced 1.0 m apart. Each individual wood crib stack consists of four layers of wood sticks, with each layer containing four 1 m-long sticks with a cross-section of 0.1 m × 0.1 m. The sticks at each layer intersect perpendicularly with those above or below, forming a lattice-like structure as illustrated in Fig. 6.3c.

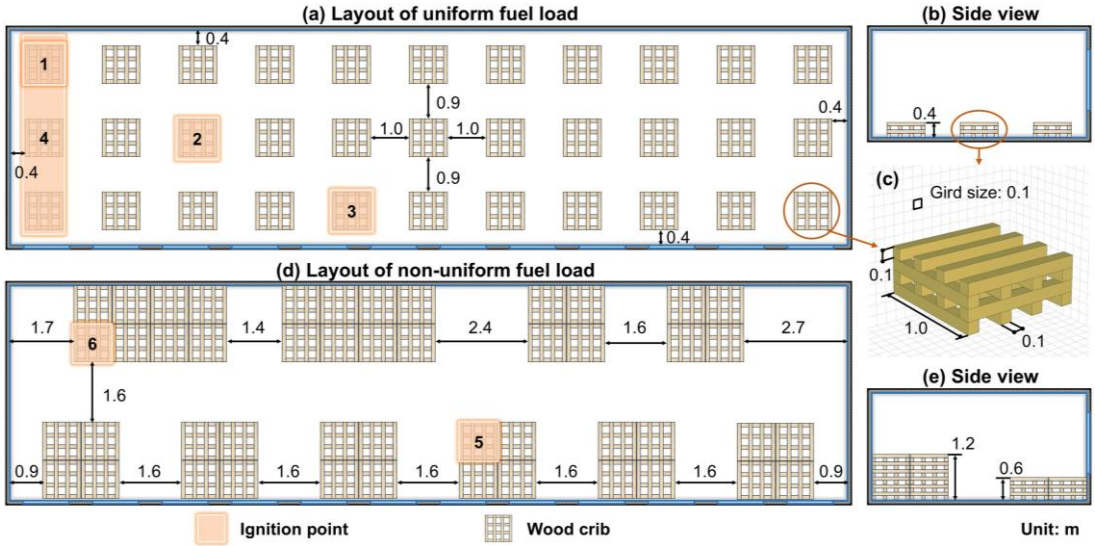

Fig. 6.3 Fuel load distributions and ignition points in fire models.

Furthermore, the non-uniformly distributed fuel load scenarios comprise two packages of 8 wood crib stacks (as depicted in the upper left of Fig. 6.3d) and eight packages of 4 wood cribs. Specifically, the 8-crib fuel packages reach a height of 1.2 m, comprising 12 layers of sticks, while the 4-crib fuel packages measure 0.6 m high, consisting of 6 layers of sticks, as illustrated in Fig. 6.3e. In this setup, the geometry of the wood sticks is primarily constrained by the grid resolution (0.1 m) of the CFD fire model. The current settings ensure the accurate capture of flame spread on wood cribs [167] while avoiding the substantial computational cost of finer meshes. The wood sticks used in fire models are made of pine, with an average moisture content of approximately 10% and a heat of combustion of 19.5 MJ/kg [176]. Following the wood crib modelling approach proposed by Janardhan and Hostikka [167], the designed fuel load density for the uniform fuel load is set as approximately 400 MJ/m², while varying densities (400, 600 and 800 MJ/m²) are specified for non-uniform fuel load scenarios. These fuel load densities are achieved by adjusting the BULK_DENSITY parameter of wood stick in fire models, without altering the structure of the wood cribs. All these settings are in accordance with the specifications of EN 1991-1-2 [25], which suggests a range of 400~800 MJ/m² for modern open-plan offices.

Four different ignition points (labelled as 1,2,3 and 4 in Fig. 6.3a) are designed for CFD fire models utilizing uniformly distributed fuel loads. The fires at ignition points 1, 2, and 3 start from a single wood crib, situated at a compartment corner, within the wood crib matrix, and near a window, respectively. Ignition point 4, however, ignites three wood cribs simultaneously at the left end of the floor. For the

fire model employing non-uniform fuel loads, two ignition points, labelled as 5 and 6 in Fig. 6.3d, are considered, with ignition point 6 specifically focusing on the impact of fuel load density (i.e., 400, 600 and 800 MJ/m²). Heating surfaces located at various ignition points enable the ignition process. The heat release rate per unit area (HRRPUA) of these surfaces is set to linearly increase from 0 to 500 kW/m^2 within 60 s, maintaining this level until 220 s, which is followed by a linear decay to 0 at 300 s. After the onset of ignition, the following reactions related to wood cribs are simplified to two concurrent processes: moisture evaporation and wood pyrolysis. The settings of parameters involved in these processes are listed in Table 6.2.

Table 6.2 Properties of materials involved in the wood combustion model [168,169].

Properties	Pine	Char	Moisture
Density ρ [kg/m^3]	450	135	1000
Specific heat c_p [kg/ kg·K]	1.35	1.08	4.18
Thermal conductivity λ [W/m·K]	0.15	0.13	0.1
Pre-exponential factor A_a [s^{-1}]	5.69×10^4	-	1.29×10^4
Activation energy E_a [kJ/mol]	9.01×10^4	-	4.12×10^4
Order of reaction n	1.69	2.0	1.0
Heat of reaction ΔH_r [kJ/kg]	-150	-	2500

6.2.4 Modelling 'active opening' and natural fallout of window glass panels

The 'active opening' strategy proposed in Chapter involves automatic opening of windows upon detection of fire signs to provide sufficient ventilation, thereby enabling a thinner smoke layer and mitigating rapid fire spread. In the present CFD fire models, a 15×3 array of temperature detectors, spaced 1.2 m apart, is used to trigger the 'active opening'. The fire detector arrangement, as illustrated in Fig. 6.4a and Fig. 6.4b, represents an idealized reference setup for early detection, whereas fewer detectors or alternative early fire detection methods could also be used to achieve early active opening. In the current models, the triggering condition is set such that the temperature of at least two detectors exceeds 70 °C, causing all window glass panels to lift around their top edge in a 'top-hung' style, as shown in Fig. 6.4c.

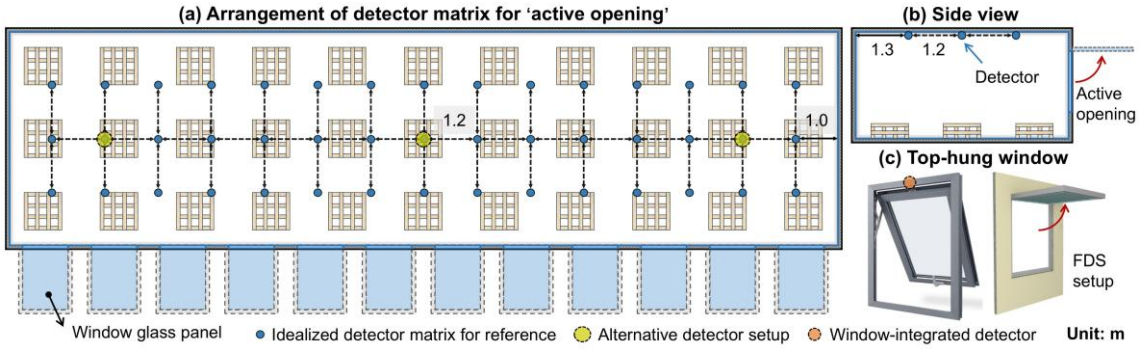

Fig. 6.4 Implementation of 'active opening' strategy in fire models.

In the comparative fire models without the 'active opening' strategy, the behavior of fire-induced glass fallout (passive opening) is considered. The simulation of glass fallout adopts a 'criterion-controlled' modelling approach proposed in Chapter 2, where each window glass is subdivided into glass sub-modules corresponding to the mesh dimensions of the fire models. These sub-modules will be removed to form ventilation openings when their surface temperature or received heat flux exceeds predetermined criteria. All cases mentioned in Section 6.2.3 are simulated both with and without the 'active opening' strategy, and the detailed settings are summarized in Table 6.3.

Table 6.3 Case configurations for CFD fire models.

Case No.	Fuel load distribution	Ignition point	Fuel load density	Action of window glass
1A	Uniform	1	400 MJ/m^2	Active opening
1B	Uniform	1	400 MJ/m^2	Glass fallout
2A	Uniform	2	400 MJ/m^2	Active opening
2B	Uniform	2	400 MJ/m^2	Glass fallout
3A	Uniform	3	400 MJ/m^2	Active opening
3B	Uniform	3	400 MJ/m^2	Glass fallout
4A	Uniform	4	400 MJ/m^2	Active opening
4B	Uniform	4	400 MJ/m^2	Glass fallout
5A	Non-uniform	5	400 MJ/m^2	Active opening
5B	Non-uniform	5	400 MJ/m^2	Glass fallout
6A	Non-uniform	6	400 MJ/m^2	Active opening
6B	Non-uniform	6	400 MJ/m^2	Glass fallout
7A	Non-uniform	6	600 MJ/m^2	Active opening
7B	Non-uniform	6	600 MJ/m^2	Glass fallout
8A	Non-uniform	6	800 MJ/m^2	Active opening
8B	Non-uniform	6	800 MJ/m^2	Glass fallout

6.3 3 Performance of 'active opening' strategy towards realistic fire conditions

6.3.1 Effect of ignition point location to a large compartment fire

Fig. 6.5a to Fig. 6.5d display snapshots of fire simulations at 660 s for four different ignition locations in fire scenarios with uniformly distributed fuel loads, comparing cases with and without the implementation of the 'active opening' strategy. The results clearly demonstrate that the implementation of the 'active opening' strategy substantially mitigates fire spread in the large open-plan compartment for all assumed ignition point locations. This mitigation effect is further evident in the HRR histories presented in Fig. 6.5e.

For the cases with the 'active opening' strategy, the HRR curves follow a typical growth pattern of a localized fire, with peak values remaining below 2.5 MW for fire scenarios where only one wood

crib is ignited. Comparatively, in cases where the 'active opening' strategy is not employed, the large size of open-plan compartments allows fires to develop more extensively due to relatively better oxygen availability. Once the thermal impact of the developing fire exceeds a critical heating threshold, the windows glass panels fall off, resulting in fire-induced 'passive openings'. Moreover, the ventilation through such openings can supply fresh air that further fuels the indoor fire, leading to a fully developed fire with a HRR peak of over 120 MW as shown in Fig. 6.5f. Meanwhile, the intense flames ejected from the well-developed indoor fire pose a significant threat to the safety of the façade walls and upper floors.

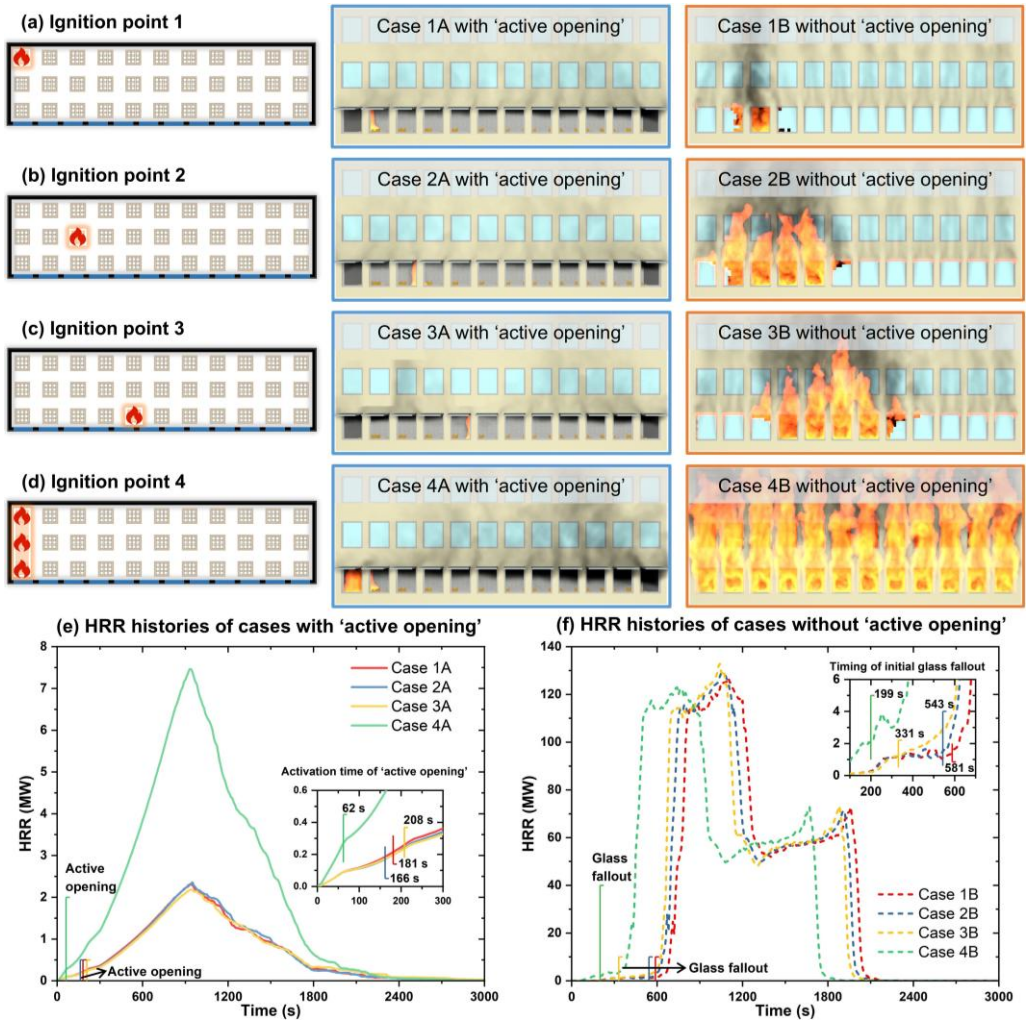

Fig. 6.5 Distinct fire development patterns with and without 'active opening' strategy.

Furthermore, the comparison of these four fire scenarios reveals that ignition point location significantly influences the timing of initial glass fallout. Specifically, cases where the ignition point is closer to the glass (i.e., ignition point 3) or involves a larger initial ignition area (i.e., ignition point 4) tend to experience earlier natural glass fallout. Notably, due to the larger initial burning area by simultaneously igniting 3 wood cribs, the fire in Case 4A develops more rapidly compared to other scenarios, advancing the onset of glass fallout to 199 s. While the 'active opening' system also responds

earlier at 62 s in this case, any delay or malfunction in fire detection could cause fire progression similar to that in Case 4B, potentially resulting in catastrophic fire growth.

Additionally, in Cases 1A, 2A, and 3A, where the initial burning areas are identical, each involving only one ignited wood crib, the differences in 'active opening' activation times appear minor and are likely influenced by the detector matrix layout. Under the current setup of detectors in Fig. 6.4a, Case 2A triggers the 'active opening' system more readily due to a higher detector density near ignition point 2. It is noteworthy that in this study, the spacing among detectors is designed to be 1.2 m, which is denser than current regulatory requirements [192–194]. Nevertheless, the primary objective here is to validate the feasibility of the 'active opening' strategy in practical applications, whereas the influence and further optimization of the detector matrix layout will be discussed independently in subsequent sections.

6.3.2 Performance of 'active opening' in indoor and façade temperature control

The 'active opening' strategy is observed to significantly improve indoor temperature conditions. Using the fire simulations at ignition point 2 as an example, Fig. 6.6 illustrates the temperature distribution along the longitudinal central axis of the compartment and the temperature slices at windows 2, 5, 8, and 11 at 1000 s. With 'active opening' providing sufficient ventilation, the heat generated by the initially ignited wood crib does not significantly affect the surrounding environment, resulting in a clear temperature stratification, as depicted in Fig. 6.6a. The temperature slices at the windows reveal that the influx of fresh air and the expulsion of hot smoke through window openings create effective air circulation, facilitating the cooling of the indoor environment. However, due to the limited air circulation capacity of these openings, a portion of the smoke is not directly expelled but instead moves longitudinally through the compartment, gradually settling along its path. Additionally, the second floor and façade wall are not significantly affected by the expelled hot smoke, mainly because each flipped glass panel acts as a 'flame deflector'. This structural arrangement diverts the upward trajectory of the hot smoke away from the façade, thereby reducing the risk of igniting the external insulation system and combustibles on the second floor. Nevertheless, the flipped glass panels situated closer to the fire source (e.g., window 2) are found to be exposed to gas temperatures of up to 450°C. Under these conditions, ordinary glass panels are more prone to fallout, potentially causing secondary hazards from falling debris. Adopting tempered or laminated glass panels can help mitigate this risk, thereby enhancing both safety and fire resistance.

In scenarios where the 'active opening' strategy is not employed, such as in Case 2B shown in Fig. 6.6b, flames quickly spread from the initially ignited wood crib to engulf the entire floor, resulting in a nearly uniform high temperature environment. The temperature slices at the windows demonstrate that the cold air entering through the windows is rapidly consumed by indoor combustion and thus fails to penetrate deeply enough to cool the inner regions, where the hot air currents form internal circulations. Due to intense combustion at the windows, upward flames affect the second floor and its façade, causing

the fallout of window glass panels on upper floors. The thermal effects of flames uniformly raise the indoor temperature of the second-floor compartment to about 600 °C, indicating that the combustibles on the second floor are on the verge of global flashover.

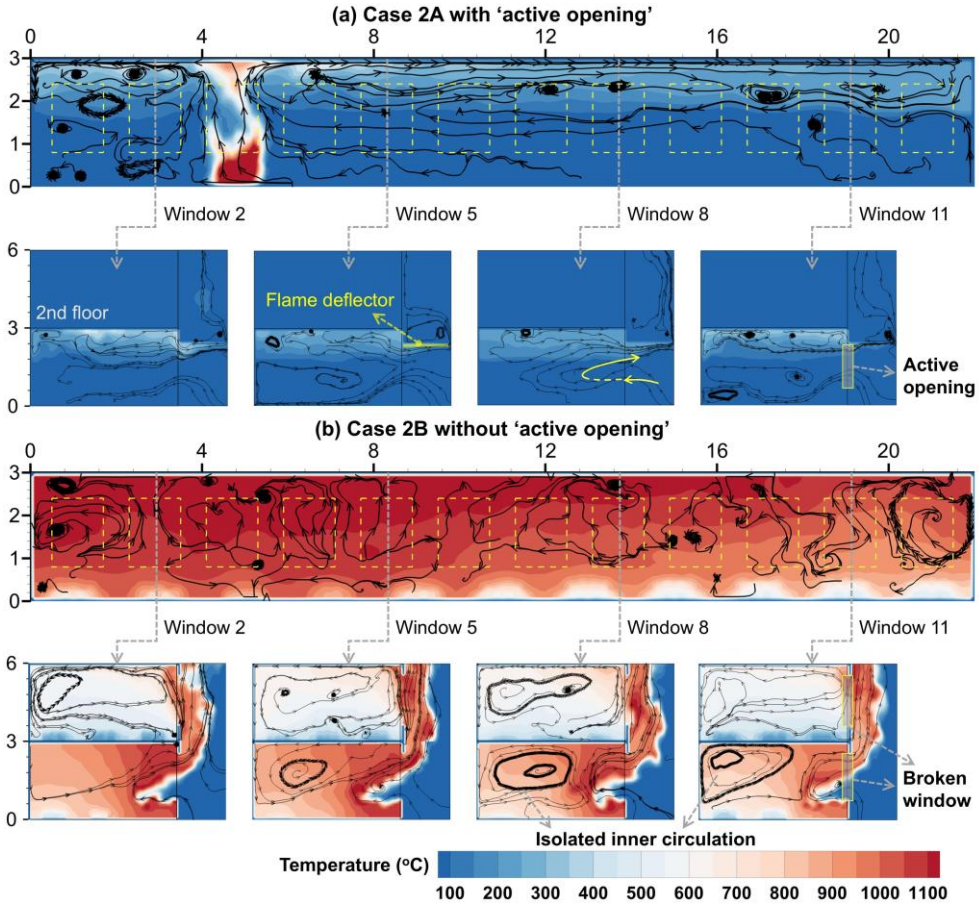

Fig. 6.6 Temperature profiles of Case 2A & 2B (time step: 1000 s).

The clear contrast shown in Fig. 6.6 is primarily attributed to the timely control over the smoke layer enabled by the 'active opening' strategy. Fig. 6.7 further presents the average temperatures and heights of residual smoke layer extracted from slices at windows 2,5,8 and 11 in Case 2A and 2B. It is evident in Fig. 6.7a that the downward trend of the smoke layer in Case 2A is promptly suppressed after implementing the 'active opening' strategy, showing a significant deviation from Case 2B, where the 'active opening' strategy is not used. As shown in Fig. 6.7b, the timely expulsion of hot smoke also mitigates the indoor temperature rise rate in Case 2A, while in Case 2B, the smoke layer temperature gradually climbs to nearly 450°C. Once window glass begins to fall out in Case 2B, the smoke layer briefly lifts before undergoing significant fluctuations due to flow disturbances from spreading flames, as seen in Fig. 6.7a. This progression results in a marked temperature rise, driven by the expanding burning area.

The variations in incident heat flux and temperature of the façade wall are presented in Fig. 6.7c and Fig. 6.7d. In Case 2A, the implementation of the 'active opening' strategy reduces the peak heat flux received at the exterior walls to less than 1 kW/m^2, substantially lower than the direct flame impact

of 150 kW/m^2 experienced in Case 2B. Similarly, the peak temperature of façade wall in Case 2A is only 87.6 °C, far lower than the 1000 °C recorded in Case 2B. Although the thermal impact on the façade wall is slightly intensified at the early stage following the implementation of the 'active opening' in Case 2A, the use of glass panels as 'flame deflectors' significantly reduces the direct impact of hot smoke on the façade wall, compared to Case 2B without 'active opening'. This strategy can further prevent the ignition of claddings observed in Case 2B, as shown in Fig. 6.7d. Similar situations are also observed in three other fire models with uniformly distributed fuel loads, but these details will not be elaborated upon here to avoid redundancy.

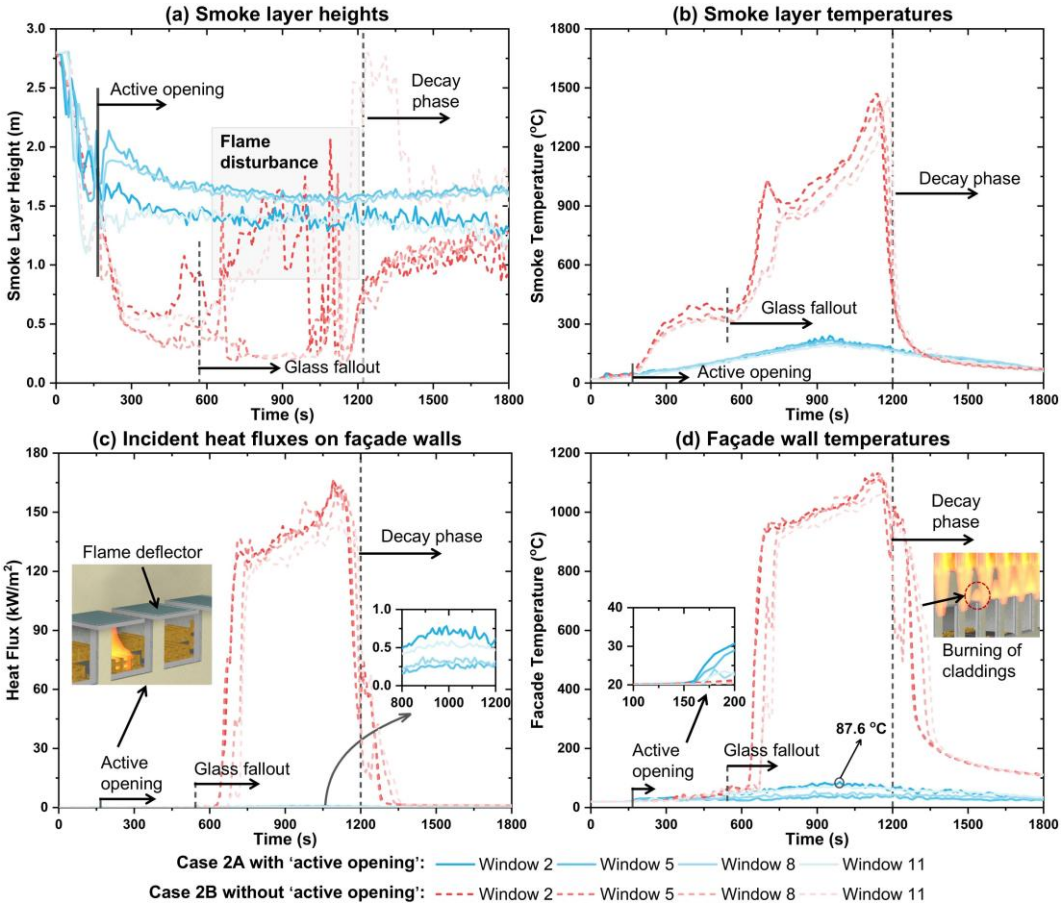

Fig. 6.7 Comparisons of smoke layer characteristics and façade thermal impacts between Case 2A and 2B.

6.3.3 Considerations of non-uniformly distributed fuel beds

Given that real fire scenarios rarely feature perfectly uniform fuel loads, and this non-uniformity can lead to varied fire development patterns. Consequently, examining the performance of the 'active opening' strategy under non-uniform fuel load conditions becomes particularly important. To facilitate this analysis, Cases 5 and 6 are introduced for comparison with Case 3 (ignition point near the window) and Case 1 (ignition point at the compartment corner), respectively. As detailed in Fig. 6.3d, the ignition point of Case 5 is set on a 4-crib fuel package, where the fuel load density is lower than the uniform condition, aiming to simulate an initial fire point of lower intensity. By contrast, the ignition point in

Case 6 is designed in a higher fuel load density area (i.e., an 8-crib fuel package in the compartment corner), corresponding to a higher-intensity initial fire point.

Fig. 6.8 presents the timeline of natural fire behavior in both non-uniform and uniform fuel load scenarios without the 'active opening' strategy. In both Case 5B with non-uniform fuel loads and Case 3B with uniform fuel loads, the windows near the ignition points begin to fall off due to the thermal effects of localized fires, as depicted in Fig. 6.8a. However, the lower fuel load density at the ignition point in Case 5B results in a notably slower fire development compared to Case 3B. At 900 s, the fire in Case 5B remains localized, impacting only the three nearest windows. In stark contrast, the fire in Case 3B rapidly spreads to adjacent wood cribs, leading to the failure of all windows and flame ejections. By 1200 s, the fire development in Case 5B has only reached a state similar to that of Case 3B at 900 s, whereas in Case 3B, the first-floor combustibles have been almost entirely consumed.

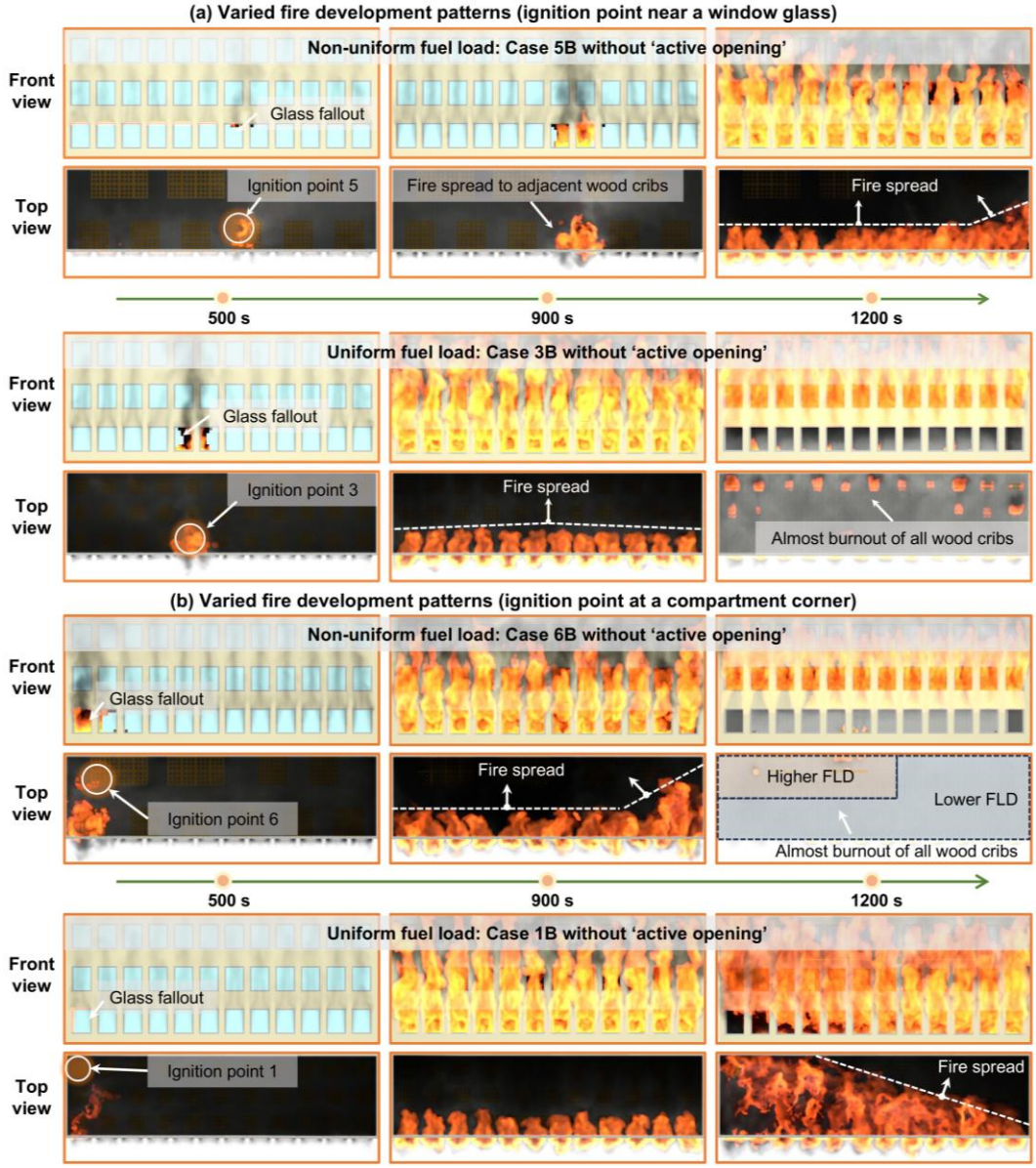

Fig. 6.8 Differences in natural fire behaviors under uniform and non-uniform fuel load distributions.

In Case 6B, where the ignition point occurs in a higher fuel load density area, the initial localized fire exerts a stronger thermal impact than in Case 1B, resulting in faster fire development. As shown in Fig. 6.8b, the intense fire heating causes the fallout of nearby window glass by 500 s, with flames concentrating near the newly formed window openings and gradually spreading to the surrounding area. By 900 s, the wood cribs in the lower fuel load area near the windows are ignited, and as these fuel packages burn out, the flames shift toward the higher fuel load areas. Nearly all combustibles are consumed by 1200 s. In contrast, in Case 1B with uniform fuel loads, only minor fallout occurs at the first glass panel by 500 s. Nevertheless, the fire becomes fully developed as the remaining glass panels gradually fall off. Notably, because of the uniform fuel load layout, the trajectory of fire spread shows a uniform progression along the diagonal from the first window, as illustrated in the top view of Case 1B at 1200 s in Fig. 6.8b. This pattern starkly contrasts with the non-uniform fuel load scenario, where fire progression typically transitions from areas of lower to higher fuel load density.

The comparative analysis of these four cases confirms that non-uniform fuel distributions strongly affect the timing of glass fallout. For instance, even though the ignition point in Case 6B is farther from the windows, its position in a higher fuel load density area results in a faster fire growth compared with Case 5. This indicates that the higher fuel load density at the ignition point correlates with earlier glass fallout and quicker fire propagation. Moreover, preliminary observations from current simulations suggest that fires generally progress from areas of low to high fuel load density, with the latter sustaining combustion for prolonged periods. Given the considerable randomness in fuel load distribution within real buildings, accurately pinpointing areas of high fuel load density poses a significant challenge, resulting in high unpredictability in fire progression. Nevertheless, current simulation results indicate that the ‘active opening’ has the potential to effectively simplify fire dynamics and mitigate the threat to overall building safety.

As illustrated in Fig. 6.9, the implementation of ‘active opening’ creates additional pathways for air exchanges, significantly reducing the accumulation of hot smoke. This active intervention in ventilation conditions effectively transforms a confined space fire into a more manageable localized fire in a relatively open space, as evidenced by Case 5A, successfully halting the fire spread to a broader area. Also, in Case 6A, where the ignition point is in a high fuel load density area, despite the greater impact of the localized fire, the ‘active opening’ strategy still effectively weakens its propagation capability. The fire can impact only a few adjacent wood cribs and eventually get self-extinguished under adequate ventilation conditions.

Compared to a fully enclosed space or a ‘passive opening’ scenario (i.e., natural glass fallout), the ‘active opening’ strategy proves more effective in lowering fire intensity. Nonetheless, the potential of the ‘active opening’ strategy in fire control warrants further in-depth research, particularly given that this study has not fully addressed the complexity of fuel loads in realistic fire scenarios, especially the varied combustion rates of diverse combustibles.

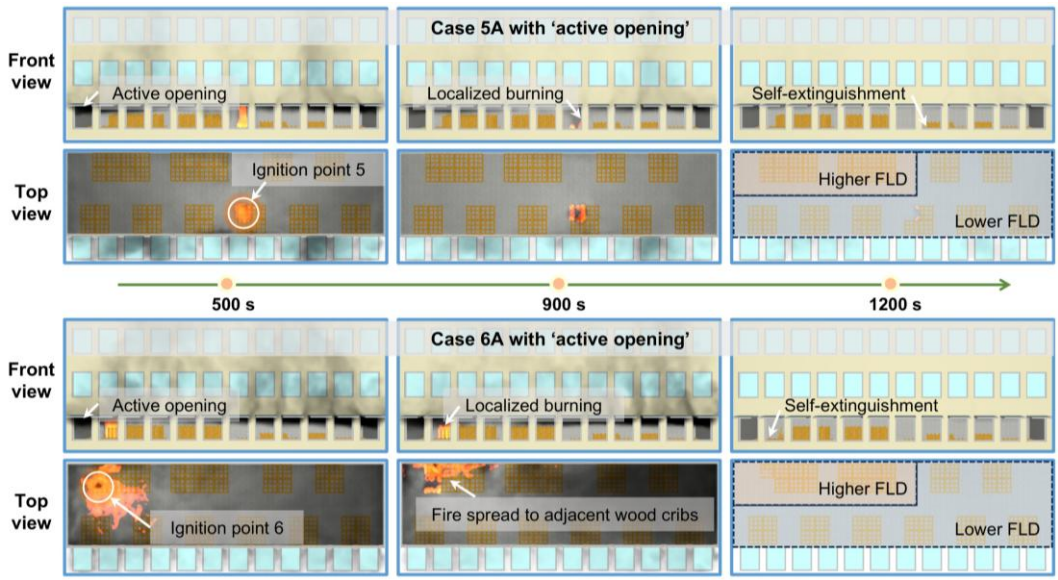

Fig. 6.9. Fire mitigation performance of the 'active opening' strategy in scenarios with non-uniform fuel loads.

6.3.4 Effect of fuel load density on mitigation performance of 'active opening' strategy

The aforementioned results from Case 5 and Case 6 not only confirm the applicability of the 'active opening' strategy in fire scenarios with non-uniform fuel loads but also indicate that the fuel load density may influence the mitigation performance. To further explore this aspect, the fire scenario in Case 6 is extrapolated to include Case 7 and Case 8, each characterized by higher average fuel load densities of 600 MJ/m^2 and 800 MJ/m^2, respectively. The results of these two extrapolated cases, along with Case 6, are presented in Fig. 6.10. Similar to Case 6A in Fig. 6.10a, the 'active opening' strategy effectively controls flame spread in Case 7A with a fuel load density of 600 MJ/m^2. Although the fire initially spreads to several adjacent wood cribs by 900 s, it transitions to a self-extinguished state at around 1200 s, as depicted in Fig. 6.10b. The occurrence of this self-extinguishment is primarily due to the lower fuel load densities where the burnout rate of the wood cribs exceeds the flame propagation rate [195], preventing the flames from sustaining themselves. In contrast, in scenarios without the 'active opening' strategy, partial window glass panels fall out due to fire-induced damage by 500 s, allowing fresh air to enter and facilitating more extensive burning. Consequently, the entire compartment is fully involved before 900 s.

For Case 8A with a fuel load density of 800 MJ/m^2, the implementation of the 'active opening' strategy successfully confines the flames to a localized area during the first 500 s, as illustrated in Fig. 6.10c. However, the higher fuel load density prolongs the combustion process, reducing the burnout rate and preventing complete self-extinction. As a result, wood cribs connected to the ignition point are ignited by 900 s, with flames spreading along the ceiling toward window 8. By 1200 s, the fire has extended to involve wood cribs on the left half of the compartment, fully engulfing the ceiling. In contrast, Case 8B without the 'active opening' strategy allows the intense heat to cause extensive glass fallout by 500 s, which increases oxygen intake and accelerates fire propagation. Consequently, the

flames reach the external walls of the second and third floors by 900 and 1200 s, respectively. Notably, although the 'active opening' strategy does not completely halt fire spread under the higher fuel load density of 800 MJ/m^2, it markedly slows down the fire development, avoiding the premature onset of the catastrophic fire scenario presented in Case 8B.

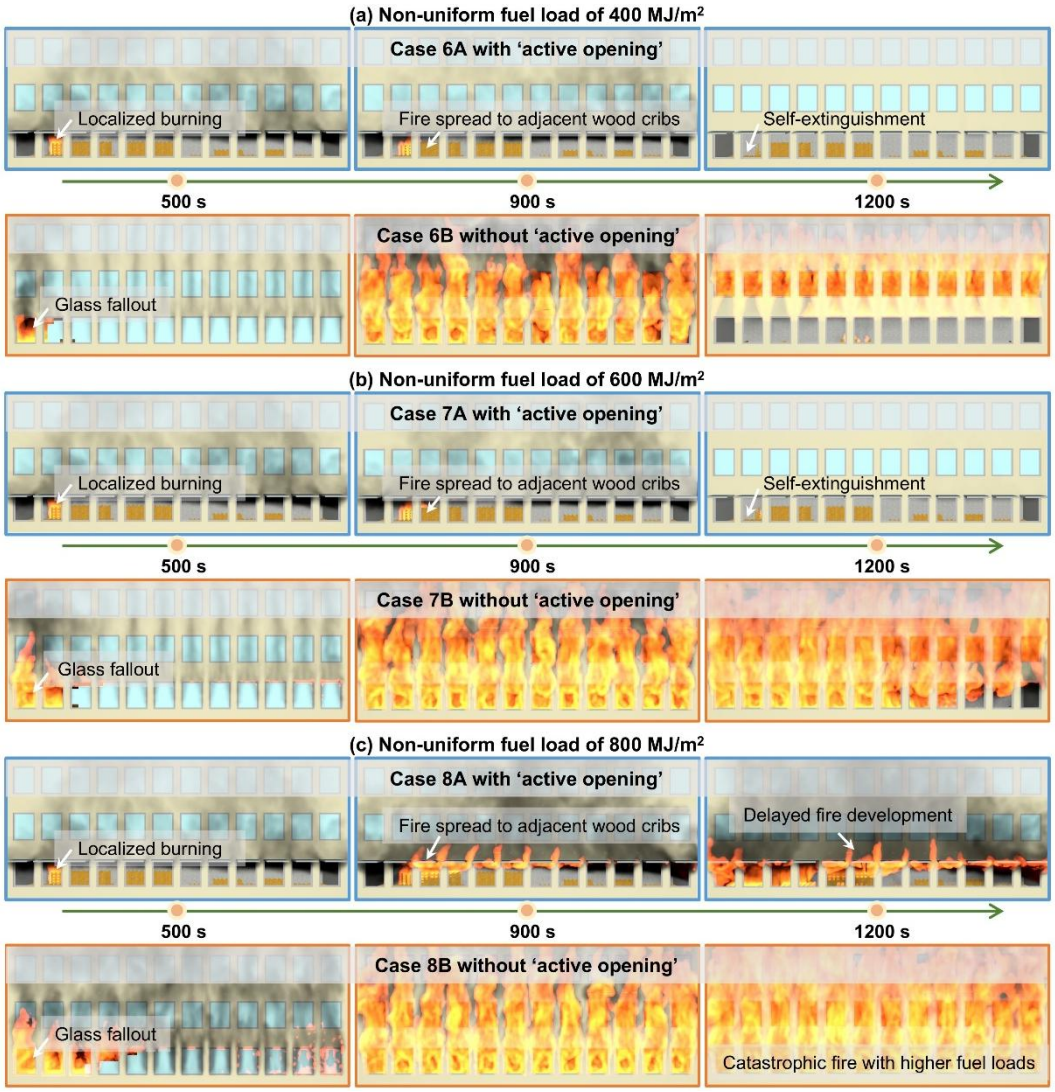

Fig. 6.10 Fire developments over non-uniform fuel loads with and without 'active opening' strategy.

Fig. 6.11a and Fig. 6.11b illustrate the effects of fuel load density on the indoor fire development and the smoke layer temperatures at window 2. It is evident that the fire scenarios with fuel load densities of 400 MJ/m^2 and 600 MJ/m^2 exhibit similar behaviors. In these scenarios, the 'active opening' strategy effectively maintains smoke temperatures below 470 °C by venting the hot smoke, thereby limiting fire spread to adjacent wood cribs and keeping the fire localized with a HRR of around 6 MW. In contrast, in Case 6B and Case 7B, where 'active opening' is not implemented, the lack of timely ventilation and smoke extraction leads to the accumulation of hot smoke within the compartment. This change in smoke characteristics causes the initial fallout of glass panels at around 360 s, and the sudden influx of fresh air further intensifies the fire to more than 100 MW. During this glass fallout process, the indoor smoke temperature rapidly rises to nearly 1200 °C, ultimately peaking at around 1400 °C.

For cases with a non-uniform fuel load of 800 MJ/m^2, the implementation of the 'active opening' strategy in Case 8A effectively controls the smoke layer temperature rise rate until 680 s, as shown in Fig. 6.11b. However, as the fire spreads further on the fuel beds in near-fire region, the smoke layer temperature significantly rises to more than 1000 °C, indicating a loss of control over the indoor fire. From these simulations across three different fuel load densities, it is evident that the fuel load density primarily affects the fire duration and HRR peaks, with a relatively minor impact on the early stage of fire development. For this reason, the timings of 'active opening' and glass fallout remain nearly consistent in all scenarios. Meanwhile, it is noteworthy that in cases of higher fuel load density, it is precisely the prolonged fire duration renders the 'active opening' strategy less effective, which underscores the importance of regulating fuel load density in comprehensive fire management strategies.

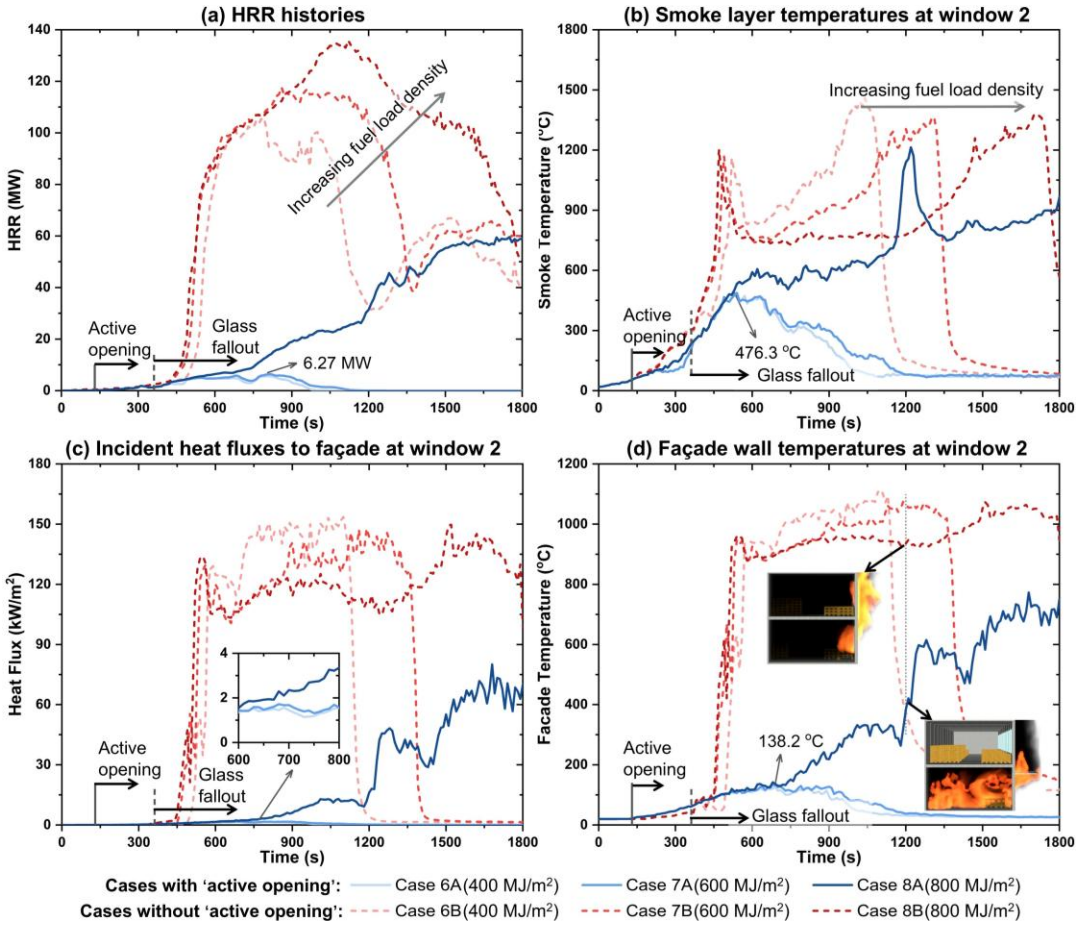

Fig. 6.11 Effects of fuel load density on indoor fire development and fire impact on façade walls.

Fig. 6.11c and Fig. 6.11d demonstrate the mitigation of thermal effects on the façade wall by implementing the 'active opening' strategy. Specifically, in scenarios without the 'active opening' strategy, the fallout of window glass allows the indoor fire to spill out, resulting in a more direct and intense thermal impact on façade walls. In these cases, the façade wall is exposed to a continuous heat flux of up to 120 kW/m² after 500 s, causing its temperature to rapidly rise above 900°C. This intense heating substantially increases the risk of the external cladding burning through and facilitates the ignition of the underlying insulation materials. Conversely, in Cases 6A and 7A, where the fuel load

density is relatively lower and the 'active opening' strategy is implemented, the peak heat flux received by the external walls remains below 2 kW/m^2, with the maximum external wall temperatures capped at 140°C. In Case 8A with higher fuel loads, despite more intense fire conditions, the 'active opening' strategy still successfully controls the heat flux reaching the façades to below 13 kW/m^2 until 1200 s. However, beyond this point, due to the loss of control over the indoor fire, the thermal impact on the façade wall becomes increasingly intense, exceeding 60 kW/m^2. Under these circumstances, the flipped window glass by 'active opening' could fall off, thus failing to act as a 'flame deflector' to block the thermal impact of spilled fires on upper floors. Additionally, falling debris from glass panels may cause unintended damage to the lower floors, and further research into window opening designs could potentially address this concern, which will be discussed in the following section.

6.4 Investigation of realistic opening designs for 'active opening' application

6.4.1 Consideration of different window opening designs

The 'active opening' strategy, when applied to 'top-hung' window assemblies, has been shown to effectively mitigate the development of indoor fires. However, it also introduces potential risks that require careful consideration. Specifically, the rising hot airflow exerts dynamic pressure, coupled with heating effects of up to 450 °C, on the glass surface. This impact may cause the flipped glass panels to fall off, potentially causing secondary damage to lower floors from falling debris. Additionally, since not all existing buildings utilize 'top-hung' windows, it is important to consider other commonly used window assemblies, such as 'casement' and 'tilt-and-turn' windows. Accordingly, this subsection conducts a preliminary investigation into the application of the 'active opening' strategy to these commonly used window types, employing the fire model from Case 4 as a basis for evaluation, as shown in Fig. 6.12.

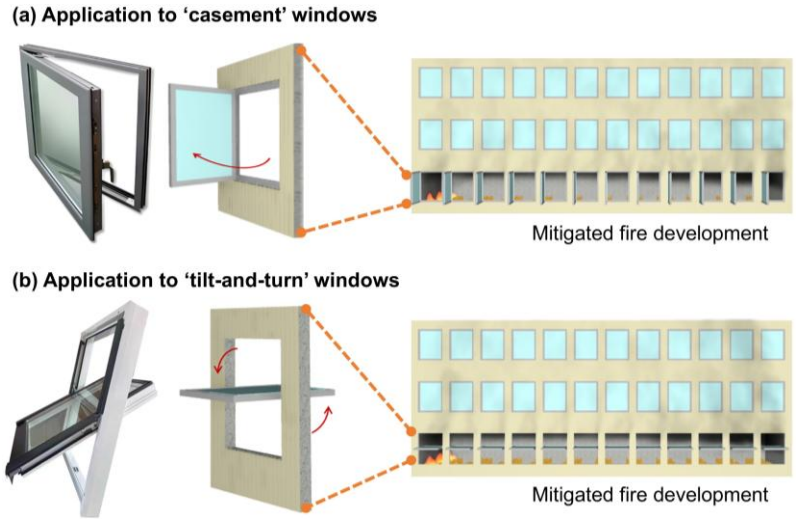

Fig. 6.12 Illustrations of 'casement' and 'tilt-and-turn' window and corresponding fire simulations.

The 'casement' window is designed to rotate outward around its the left edge until it is perpendicular to the façade wall, as depicted in Fig. 6.12a. In the 'tilt-and-turn' window configuration,

the window glass panel is opened by rotating 90° around the horizontal midline of the window frame, as shown in Fig. 6.12b. In fire simulations with 'casement' and 'tilt-and-turn' window configurations, the implementation of 'active opening' also significantly mitigates fire development, as illustrated in Fig. 6.12.

To elucidate the effects of different window configurations, Fig. 6.13 compares the smoke characteristics across the various 'active opening' scenarios. The 'active opening' strategy under the 'top-hung' window configuration shows a slightly less pronounced effect on smoke control, leaving a residual smoke layer approximately 0.05 m thicker as displayed in in Fig. 6.13a. Nevertheless, this difference is insufficient to impact the overall fire development trend. Across all three window configurations, the indoor temperature control achieved by the 'active opening' strategy remains consistent, as shown in Fig. 6.13b.

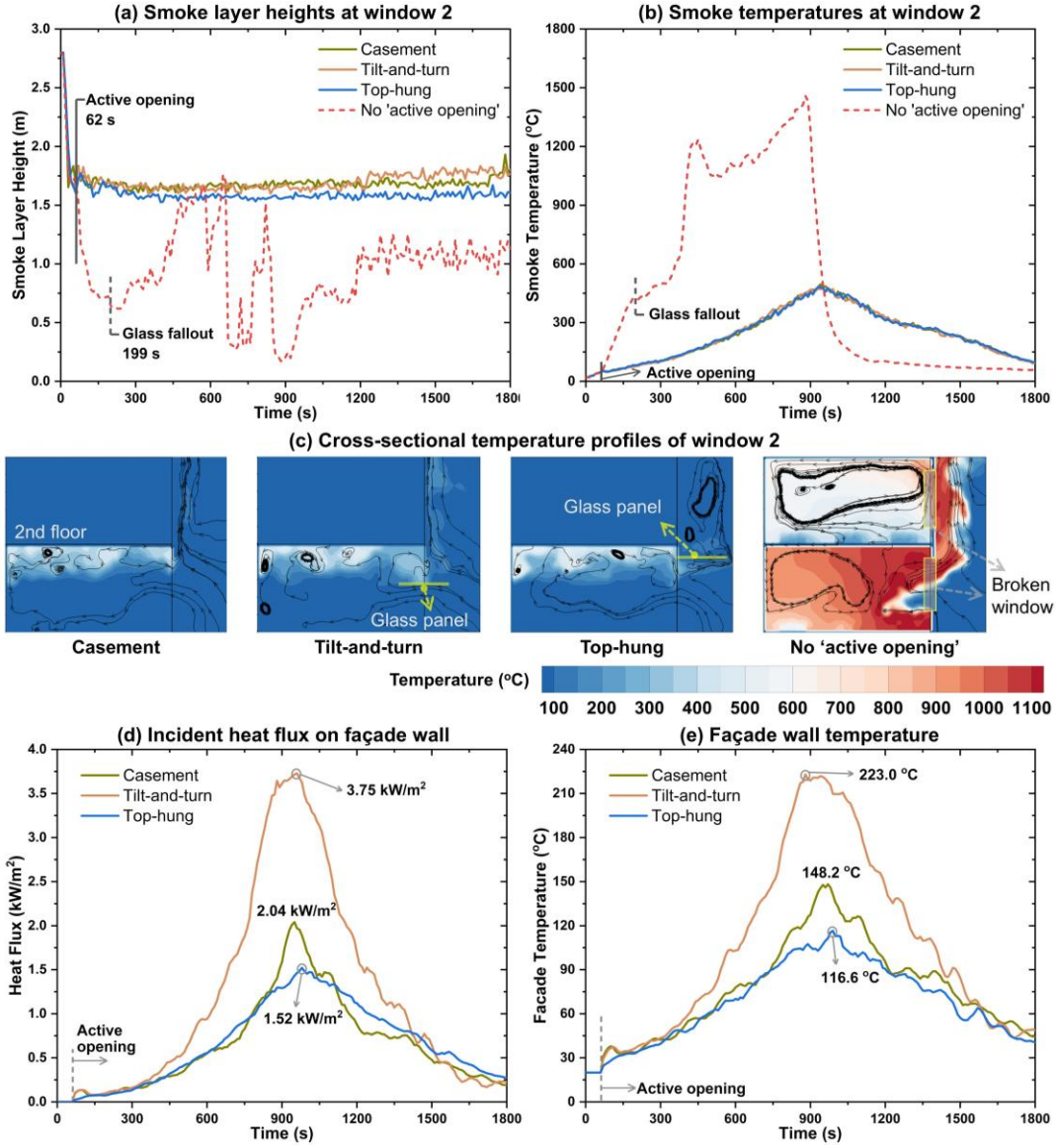

Fig. 6.13 Outflow mass rates of different window configurations and resulting smoke layer heights.

Notably, the different window configurations result in distinct flow patterns around the window openings, as illustrated in Fig. 6.13c. For the 'casement' window, the smoke vents directly through the window opening without obstruction by the glass panel. Whereas, in the 'tilt-and-turn' configuration, the flipped glass panel guides airflow via the Coanda effect [196]: cool air enters beneath the panel while hot smoke exits above, altering the neutral plane. Under the 'top-hung' scenario, the flipped glass panel forces the smoke to flow along the panel before rising, which reduces venting efficiency, explaining the thicker residual smoke layer observed in this scenario.

Further, the differences in flow patterns also affect thermal impact on the façade walls, as presented in Fig. 6.13d and Fig. 6.13e. In the 'top-hung' scenario, the glass panel acts as a 'flame deflector', shielding the façade wall from direct thermal exposure. As a result, the façade wall experiences the lowest heat flux of less than 1.5 kW/m^2 with a wall temperature capped at 116.6 ^oC. In contrast, the 'casement' and 'tilt-and-turn' configurations lack such deflection. Even worse, the flipped panel in 'tilt-and-turn' configuration directs hot smoke to exit from above, resulting in a notably higher thermal impact on the façade walls. Notably, the 'casement' configuration demonstrates similar mitigation performance on heating impacts on the façade walls compared to the 'top-hung' configuration, while offering the additional benefit of reduced glass panel fallout risk due to its smaller contact area with rising hot smoke. Additionally, the 'casement' window opens faster than the other two window configurations in practical use, making it more convenient for implementing the 'active opening' strategy. Overall, regardless of the window configuration, the 'active opening' strategy effectively slows fire progression. This suggests that retrofitting buildings with 'active opening' capabilities does not necessitate a specific window design.

6.4.2 Consideration of the number of windows opened for 'active opening'

In addition to window configurations, the number of actively opened windows is further explored. As displayed in Fig. 6.14, rather than the default strategy of opening all windows to achieve sufficient ventilation, the strategies that open only 6, 4, or 3 windows near the fire region are simulated based on the fire model setup in Case 4A.

The simulation results reveals that, in addition to the scenario where all windows are actively opened as in Case 4A, fire models with only 6 or 4 windows opened also effectively confine the flames to the ignition areas, demonstrating outstanding fire control performance. However, when the number of opened windows is reduced to just three, the 'active opening' strategy failed to prevent further flame spread. as shown in Fig. 6.14a.

As seen from the temporal variations in smoke layer heights and temperatures illustrated in Fig. 6.14b and Fig. 6.14c, the implementation of the 'active opening' strategy resulted in a significant lift of the smoke layer and a notable reduction in indoor temperature rise rate across in all fire scenarios. Nevertheless, in the case where only 3 windows are opened, the downward trend of the smoke layer is

not suppressed as rapidly as in the scenario where all windows are actively opened. Instead, the smoke layer continues to descend gradually towards the floor with the average indoor temperature exceeding 500 °C, eventually leading to the ignition of adjacent wood cribs. As the fire progresses, the hot smoke that is not fully expelled in time can worsen indoor fire conditions, eventually posing a threat to the façade and upper floors once other glass panels undergo their fallout.

These findings indicate that it is not strictly necessary to actively open all windows to achieve effective fire control. Opening a portion of windows can still significantly slow down the fire growth, highlighting the robustness of the 'active opening' strategy in real-world applications, especially in situations where certain windows may not be operable. Opening a subset of windows can still significantly slow fire growth, demonstrating the robustness of the 'active opening' strategy in real-world applications, especially in situations where certain windows may not be operable. This flexibility offers more practical options for fire response strategies in building fire safety designs.

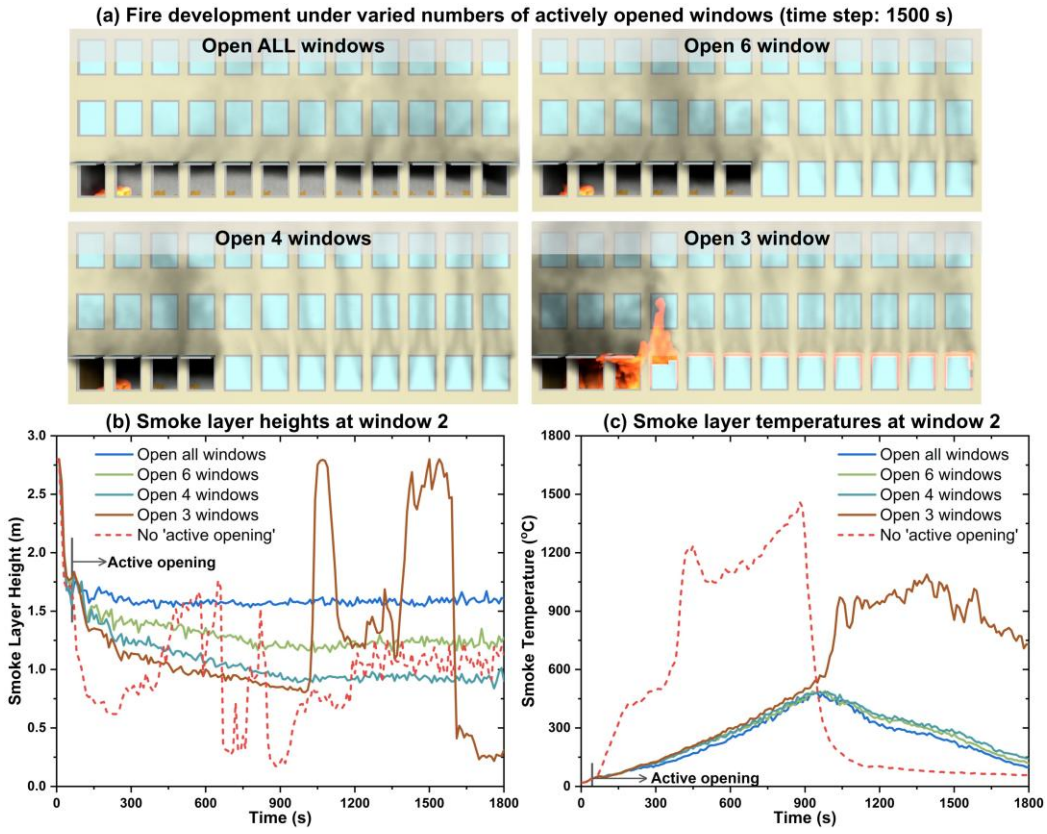

Fig. 6.14 Fire development patterns and smoke characteristics in scenarios with varied number of windows opened for 'active opening'.

6.4.3 Consideration of detector matrix designs to trigger 'active opening'

As previously noted, the reference detector matrix shown in Fig. 6.4a may exhibit an overly conservative performance in triggering the 'active opening' system due to its dense arrangement of 45 detectors. To address this, two alternative layouts are explored based on the fire alarm system design code GB 50116 [192]. As depicted in Fig. 6.15a, one configuration involves a 7-detector array with a

spacing of 3.3 m, while the other adopts a 3-detector array with a spacing of 6.6 m. Additionally, unlike the conventional detectors installed on ceilings, a novel approach is further explored in which in detectors are integrated directly into window components, such as window actuators. This unique design can facilitate easier installation and maintenance in real-world applications.

The exploration of detector matrix designs is conducted using the fire model setup from Case 4. Simulation results show that all three assumed detector designs effectively mitigate the indoor fire development, particularly in controlling the smoke layer as illustrated in Fig. 6.15b. It is can be seen that, for designs using ceiling-mounted detectors, the number of detectors significantly influences the activation timing of the 'active opening' strategy. Specifically, reducing the detector number from 45 to 7 causes the response time to double, while further reduction to 3 detectors prolongs the response time to 146 s. Despite this delay, these two detector configurations with fewer detectors still manage to lift the smoke layer to levels comparable to the 45-detector scenario by promptly venting the hot smoke. Therefore, as presented in Fig. 6.15c, similar fire control performance can be achieved even with fewer detectors, offering the benefit of lowering installation costs.

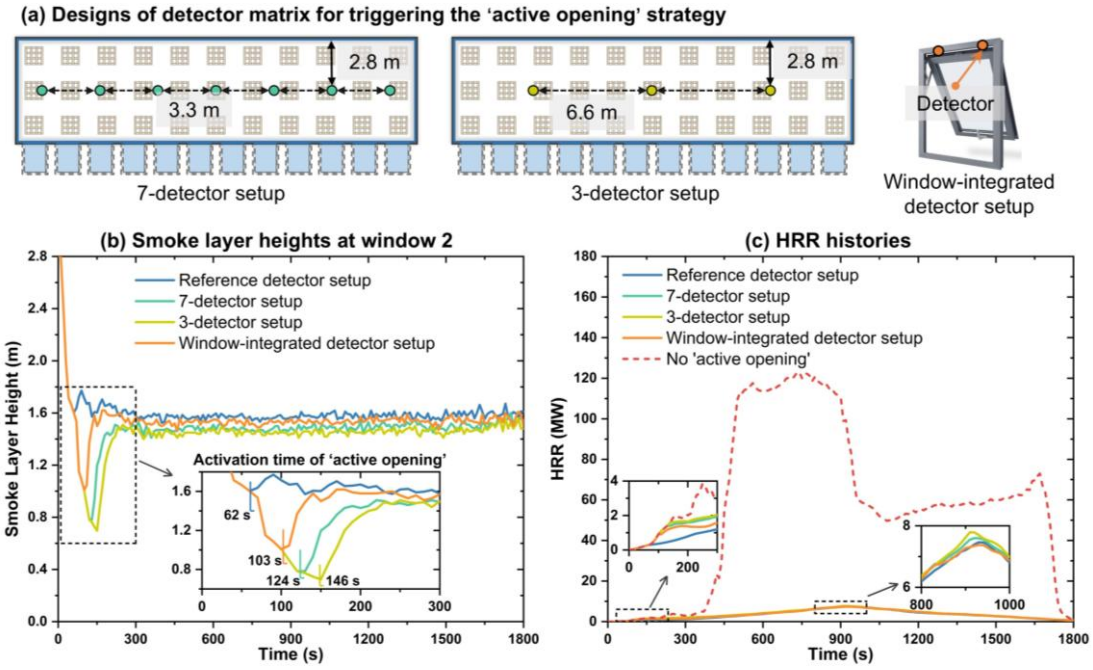

Fig. 6.15 Different detector matrix designs for 'active opening' and their performance in fire control.

It should be noted that when the number of detectors is reduced to 3, the response time of the 'active opening' strategy closely approaches the timing of initial glass fallout (199 s) observed in Case 4B, after which the fire becomes increasingly severe. Considering that fully opening the windows requires additional operational time, this delay may pose challenges for fire protection designs that rely exclusively on ceiling-mounted detectors. Interestingly, the design that integrated detectors into window assembly demonstrates superior response performance, triggering the 'active opening' at 103 s to counter fire progression. This successful integration presents a new approach for retrofitting existing

buildings with the ‘active opening’ function and offers valuable insights into optimizing detector configurations.

6.4.4 Future explorations on ‘active opening’ strategy

The present work provides important references for the future application and optimization of ‘active opening’ strategy in real buildings. The results demonstrate that the ‘active opening’ strategy exhibits high effectiveness in suppressing fire development under various window configurations. However, it is worth noting that in the current fire model, all window configurations are modeled with a flip angle of 90° whereas the maximum opening angle of real-world windows may not be designed to reach 90° [197]. A smaller window opening angle may significantly reduce the effective area for smoke venting, potentially rendering the ‘active opening’ strategy ineffective. This limitation and its potential implications merit further investigation to ensure the ‘active opening’ strategy can be effectively implemented across a broader range of practical conditions. Additionally, the compartment sizes [198], as well as external wind effects [199], may influence the effectiveness of ‘active opening’, and additional considerations should be given to these aspects.

The number of windows opened is a crucial factor influencing the capability to expel hot smoke, as more window openings can provide better ventilation pathways for rapid smoke discharge. Nevertheless, in practical applications, opening all windows immediately in an emergency situation may be too aggressive. The findings of this section indicate that even fewer actively opened windows can still achieve effective fire mitigation outcomes. This highlights that a performance-based fire safety design can be adopted to determine the optimal number of window openings based on compartment configurations, such as its size, available windows, and potential fuel load. This performance-based approach can evolve into an intelligent ‘active opening’ system. By deploying a network of sensors to continuously monitor key indicators such as smoke temperatures and smoke layer heights, the system can dynamically adjust window openings in real time. For instance, upon detecting a fire, windows closest to the fire source could be opened first. If the indoor temperature continues to rise, the system could then increase the number of open windows to enhance smoke removal. This dynamic adjustment can minimize unnecessary resource use while maintaining safety, resulting in a more efficient fire control solution.

Moreover, preliminary validation has shown that integrating detectors into window components is feasible, enabling seamless interaction with existing smart home devices such as window actuators. With this design, the ‘active opening’ function can be directly connected to an application (App), thereby allowing for flexible and intelligent ventilation management. Further practical trials will be conducted as follow-up work.

6.5 Conclusions

This chapter utilizes CFD fire simulations to explore the application of the 'active opening' strategy in mitigating fires in modern buildings. The investigation considers factors such as the flammability of façade materials, the randomness of ignition points and the non-uniform distribution of fuel loads. The outcomes of these simulations provide a systematic evaluation of the performance of the 'active opening' strategy, with the following main conclusions:

(1) The 'active opening' strategy demonstrates strong early-stage control of hot smoke under different fuel load conditions. For lower fuel load densities (i.e., 400 and 600 MJ/m^2), the strategy successfully suppresses further propagation of the flames. For higher fuel load densities of up to 800 MJ/m^2, although this strategy cannot entirely halt fire spread, it significantly delays fire development, thereby securing crucial time for firefighting operations.

(2) The 'active opening' strategy markedly reduced the thermal impact on exterior façade walls. At lower fuel load densities, the heat flux received by the façade wall is greatly reduced. This reduction effectively prevents the premature ignition of façade materials, enhancing the overall fire safety of the whole buildings.

(3) The ignition point of the fuel load affects the response time of the 'active opening' strategy, which is also closely linked to the detector matrix layout. Using fewer detectors may result in a delayed response or even the failure of the 'active opening' strategy, while overly dense detector placement increases costs. The detector-integrated window assembly proposed in this study offers a cost-effective alternative with strong potential for practical application.

(4) The implementation of the 'active opening' strategy effectively slows down fire progression across various commonly used window configurations. This finding suggests that adding the 'active opening' function to existing buildings does not require adherence to a specific window design, providing greater flexibility for retrofitting older buildings.

(5) Increasing the number of actively opened windows can improve smoke exhaust efficiency, but fully opening all windows is not the optimal solution. A smart tiered opening strategy that dynamically adjusts the number of opened windows based on fuel distribution and fire progression dynamics can ensure fire safety while minimizing unnecessary resource use. This approach, which aligns with intelligent building design principles, is indeed worth further in-depth investigation.

Chapter 7: Conclusions and Future Works

7.1 Summary of the current work

This thesis is dedicated to re-evaluating the role of window glass in the development of fires within modern large open-plan compartments and to innovating fire safety strategies suitable for contemporary architectural designs. **Chapter 1** sets the stage by delineating the research background and motivation. It reviews the interconnection between glass fracture research and compartment fire research, emphasizing the crucial need to integrate considerations of window glass into modern fire safety studies.

Chapter 2 proposes a 'criterion-controlled' approach to simulate glass fallout in CFD fire models. This approach aims to reflect the impact of ventilation changes due to glass fallout on realistic fire behaviors. In this method, glass panels are segmented into various glass sub-modules, with fallout criteria based on the Shields Tests determining the necessity for removing each sub-module. The effectiveness of the proposed approach is initially validated in fire simulations of the Shields Tests, where the timings and points of glass fallout are accurately captured, with a close match to the measured time-varying temperatures and heat fluxes. This 'criterion-controlled' modelling method is then applied to fire simulations of large open-plan compartments, with adaptations from the prototype Kirby Test and Malveira Test to include window glass. In the Kirby test model with window glass, the fire spread rapidly, sweeping across the entire floor. Similarly, in the adapted Malveira test with window glass, the fire spread more quickly, and a backdraft occurred following the glass fall-out. These behaviors contrast sharply with the slow 'traveling fire' observed in real fire tests without glass configurations, highlighting the necessity of considering window glass settings in experiments to explore real fire behaviors.

Chapter 3 refines the 'criterion-controlled' approach by incorporating the uncertainty associated with window glass fallout. This uncertainty is quantified using a three-parameter Weibull distribution, which models the probability of glass fallout as influenced by glass surface temperature. This probabilistic model replaces the simplistic and conservative criteria previously employed in **Chapter 2**. Utilizing this refined methodology, two hundred CFD fire models are identically configured in alignment with a medium-scale fire test. The analysis identifies four fire development patterns (P1-P4) resulting from the stochastic nature of glass fallout and changing thermal conditions. P1 shows early fallout of the first window glass can halt fire spread during the localized fire stage, while P2 experiences rapid fire spread facilitated by slightly delayed glass fallout at peak fire intensity, which occurs rarely (only 1% probability) but with severe long-term thermal impact on surrounding structures. P3 represents the most common situation (accounting for 83%), where the data and observations of medium-scale fire tests align closely with this pattern, validating the current modeling approach. P4 demonstrates delayed fire development due to superior glass resistance. The refined glass modeling method successfully unveils the complex interplay between window glass fallout behavior and fire dynamics. Importantly,

P1 demonstrates that, while seemingly disadvantageous, early glass fallout can actually promote better fire control, providing new perspectives for innovative fire safety strategies in large open-plan spaces.

Chapter 4 introduces an innovative strategy of early opening windows to mitigate fire growth, inspired by the findings from P1 scenario in **Chapter 3**. This strategy, termed 'active opening', leverages temperature readings from ceiling sensors to trigger window openings, and has been investigated in CFD fire models. The simulations demonstrate that in compartments with closed windows, thermal smoke rapidly builds up, directing intense heat flux towards floor-level combustibles, potentially leading to swift fire propagation and even flashover. Conversely, the implementation of 'active opening' constrains the fire to localized burning and maintains a thinner smoke layer, considerably aiding firefighting efforts. Preliminary explorations suggest that setting a lower activation temperature of 'active opening' facilitates a faster removal of hot smoke from the compartment, proving more effective in fire suppression. Additionally, simulations indicate that the top edge of the window fundamentally controls the residual height of the hot smoke after 'active opening', enhancing fire mitigation even at higher activation temperatures. The application of the 'active opening' strategy in modern architecture represents a forward-thinking shift in fire safety protocols, prioritizing early ventilation over controlled containment.

Chapter 5 experimentally demonstrates the mitigating effects of the 'active opening' strategy on fire development. Two experiments are conducted in a medium-size open-plan compartment with window glass, one implementing the 'active opening' strategy and the other without it. The observations confirm that limited ventilation with closed windows significantly worsens fire development, leading to elevated temperature peaks and catastrophic damage. In contrast, the 'active opening' strategy plays a crucial role in moderating fire intensity and spread rate. Data collected on smoke temperatures, floor heat fluxes, and burning rates helps reconstruct corresponding CFD fire models, and further analysis reveals the underlying mechanisms of the observed mitigating effects through energy conservation. Specifically, this strategy alters the airflow patterns within the compartment and changes the primary pathways of heat loss by introducing new ventilation openings. Additionally, it significantly lessens the thermal impact on adjacent materials by affecting not only the thickness and temperature of the hot smoke layer, but also its emissivity. All these changes contribute to a reduced likelihood of further expansion of the burning area.

Chapter 6 investigates the practical issues of the 'active opening' strategy in real-world modern buildings. Multiple aspects of realistic compartment configuration including fuel distribution, ignition locations, opening methods, and detector setups are considered to evaluate the effectiveness of the 'active opening' strategy in mitigating fire spread. The simulations affirm that at lower fuel load densities (400 MJ/m^2 and 600 MJ/m^2), the 'active opening' strategy successfully controls the early accumulation of hot smoke and suppresses further flame propagation. At a fuel load density approaching 800 MJ/m^2, this strategy delays but does not entirely halt flame spread. Moreover, this strategy mitigates

thermal impacts on façade walls, reducing the risk of external fire spread. It is found that the 'active opening' strategy performs well across a range of commonly used window configurations, underscoring its flexibility and adaptability. The exploration also reveals that the optimal fire mitigation does not require opening all windows. This suggests that a smart tiered opening strategy for 'active opening' can be further developed, which would dynamically adjust the number of opened windows in response to real-time fire progression dynamics. Through the present research, the window-integrated detector design is foreseen as a promising future of implementing 'active opening', which may only require minor changes on window setup but leading to effective mitigation on fire spread and smoke reduction.

7.1.1 Further improvement of glass fallout modeling in fire simulations

The glass fallout model proposed in this thesis, while yielding insightful preliminary results, remains constrained by several limitations. One notable limitation is the relatively small sample size of experimental data currently available. Consequently, the accuracy and generalizability of proposed modelling framework in predicting glass fallout under varied fire scenarios are restricted. Future studies should prioritize expanding experimental datasets through more comprehensive testing, incorporating a broader range of glass types, framing conditions, and compartment fire configurations. This enhanced dataset would significantly improve the robustness and predictive capability of glass fallout models, allowing more reliable fire safety design applications.

Furthermore, an important phenomenon that warrants further investigation is the influence of soot deposition on window glass surfaces during fires as illustrated in Fig. 7.1, and its subsequent impact on glass fallout behavior. Soot accumulation alters the radiative heat transfer characteristics of glass, potentially increasing its absorptivity and emissivity. This could lead to accelerated heating, enhanced thermal gradients, and consequently an increased likelihood of early glass failure.

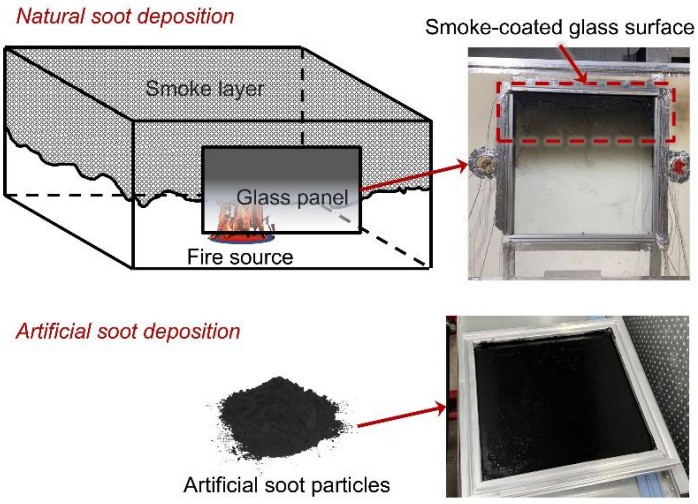

Fig. 7.1 Preliminary investigations on the effects of soot deposition on glass fallout.

Therefore, future studies should systematically explore soot deposition mechanisms through combined experimental and numerical approaches. Specifically, investigations should include measuring and modeling the optical and thermal properties of soot-coated glass surfaces, quantifying

their effects on thermal stress, and deriving updated fallout criteria. Clarifying how soot deposition affects glass failure could enhance the accuracy of current glass fallout prediction models. Currently, preliminary research is underway, in which we are simulating natural soot deposition by manually coating clean glass surfaces with artificial soot particles, as illustrated in Fig. 7.1. Experimental tests are being conducted to quantitatively evaluate the impact of soot deposition on glass fallout behavior, and these studies will provide valuable data to guide future numerical model improvements.

In addition to the proposed purely CFD-based simulation framework for fire-glass interaction, an alternative methodology, hybrid simulation, can be explored based on the coupling of CFD fire models and H-TRIS [198], as illustrated in Fig. 7.2. The general workflow is that the thermal impact received by glass modules in FDS simulations is obtained and transmitted in real-time to the control system (PLC) of H-TRIS. The PLC will then adjust the position of the radiation plate or the fuel/air mixture ratio to impose the same heating impact on the glass specimen in the real world. When the failure of the glass is recognized by means of the set-up sensors or computer vision tools, the FDS simulations will receive the signal to remove the glass modules via specific devices.

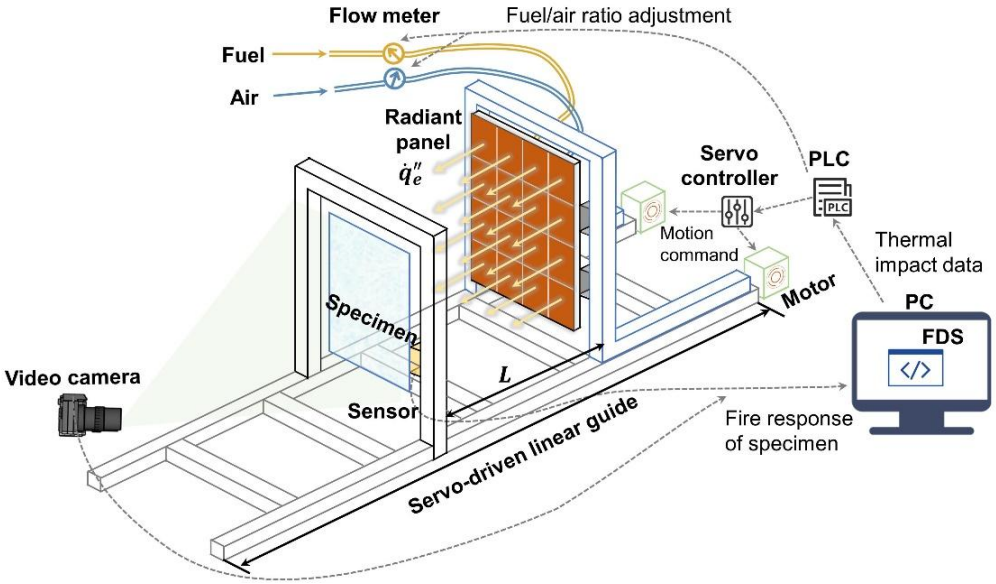

Fig. 7.2 Illustration of the hybrid simulation system for modelling glass fallout.

7.1.2 Development of windows designed for 'active opening' strategy

Future research could pivot towards crafting specialized window designs tailored for the 'active opening' strategy. These windows would need to be capable of responding dynamically to fire detection systems, with built-in mechanisms for automatic opening and closing based on real-time fire data. Engineering challenges include designing windows capable of withstanding extreme temperatures and pressures while maintaining reliable operation during fire incidents. The newly designed windows should be seamlessly integrated with advanced fire detection and control systems. This integration entails developing interoperable protocols that allow windows to communicate with fire alarms, smoke detectors, and building management systems.

Upon development and integration with fire safety systems, their efficacy and performance should be validated in real-fire scenarios. Conducting full-scale fire tests in modern tall buildings will be crucial. These experiments should aim to observe and analyze the behavior of these windows under various fire conditions, examining factors like fire control, smoke management, and structural integrity.

Following successful testing and validation, research should also explore how these innovative window designs can be incorporated into building codes and standards. This involves working with regulatory bodies to ensure the findings are translated into practice, potentially setting new benchmarks for fire safety in building design.

7.1.3 Integration of 'active opening' strategy into smart building framework

Future research could enhance the 'active opening' strategy by incorporating advanced detection networks. These systems would continuously monitor not only temperatures but also other crucial parameters such as gas concentrations. Such advancements could lead to more dynamic and adaptive fire safety systems that respond more accurately to the immediate conditions of a fire, potentially integrating IoT (Internet of Things) technology for smarter building management.

Artificial Intelligence (AI) stands to play a crucial role in processing the data collected by these advanced detection systems, enabling real-time decisions about window operations. Future investigations could focus on developing AI models that harness data from previous fire incidents and simulations to predict optimal window-opening strategies under varied conditions. This AI-driven approach aims to finely tune the balance between smoke ventilation and fire containment, significantly reducing damage and enhancing occupant safety.

For maximum efficacy, integrating the 'active opening' strategy into Building Management Systems (BMS) is essential. This integration would not only synchronize operation between the fire safety systems and other building controls, such as HVAC systems, but it could also enhance daily indoor air quality management. By enabling the 'active opening' strategy to function as both a fire safety mechanism and a regular feature of indoor climate control, buildings could maintain optimal air quality and comfort for occupants under all conditions. Research should also explore the development of communication protocols and interfaces that facilitate this comprehensive integration.

Appendix A

Basic settings of CFD fire models

All CFD fire simulations in this thesis were conducted using the FDS version 6.7.7 [70], a widely adopted computational tool for high-fidelity fire modeling. FDS numerically solves the Navier-Stokes equations for low-speed, thermally-driven flows on a rectilinear grid, making it particularly suitable for simulating fire-driven phenomena [199].

To identify a computationally efficient yet accurate turbulence modeling approach suitable for current research, three turbulence models, i.e., Large Eddy Simulation (LES), Very Large Eddy Simulation (VLES), and Simple Very Large Eddy Simulation (SVLES), have been comprehensively evaluated using the Shenzhen Fire Test model. The performance of each model was primarily assessed through comparisons of four critical parameters closely related to glass fallout events: (a) mass flow rates through openings; (b) heat fluxes to fuel surfaces; (c) gas-phase temperatures near the ceiling; (d) glass surface temperatures. As shown in Fig. A.1, the VLES model can produce results remarkably similar to those obtained from the LES model, maintaining comparable accuracy across all four parameters investigated.

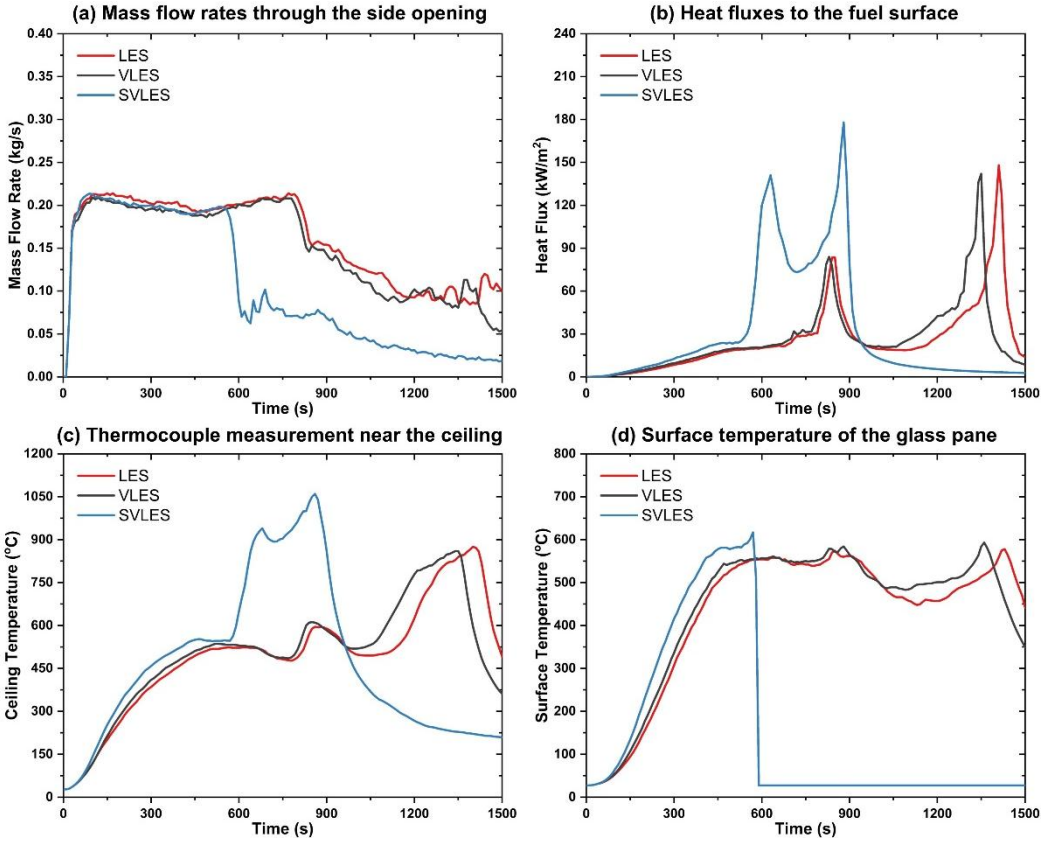

Fig. A.1 Comparative analysis of key parameters using different turbulence models.

Importantly, the computational cost, measured as the clock-wall simulation time, for the VLES was approximately only one-third that of the LES, highlighting its considerable computational advantage. Based on these results, the VLES model emerges as an optimal compromise, achieving accuracy close to LES while significantly reducing computational overhead. Thus, the VLES method is adopted in all models presented with near-wall regions treated using the Smagorinsky model combined with the Van Driest damping function [200].To account for radiative heat transfer, the grey-gas radiation model was used, with 200 solid angles configured to ensure adequate directional resolution.

A suitable grid resolution is essential for balancing simulation accuracy with computational efficiency. For simulations involving buoyancy-driven flames, a widely accepted guideline [199] from the National Institute of Standards and Technology (NIST) recommends that the ratio of the cubic grid cell size δ_x to the characteristic diameter of the fire source D^* should lie between 4 and 16. Herein, D^* is defined as:

$$D^* = \left(\frac{\dot{Q}}{\rho_\infty c_P T_\infty \sqrt{g}}\right)^{2/5} \tag{A.1}$$

where $\dot{Q}$ is the heat release rate of the fire source (kW), and ρ_∞, c_P, T_∞ and g represent the ambient density (kg/m^3), specific heat of air (kJ/(kg·K)), ambient temperature (K) and gravitational acceleration (m/s^2).

Additionally, accurate prediction of air mass flow through openings becomes crucial in under-ventilated fire conditions, as it governs the combustion extent both inside and outside the enclosure. To evaluate whether the grid resolution is sufficient for capturing ventilation-driven flow, Zhao et al. [201] proposed two length scales ratios. The first criterion ℓ_1^* considers the ratio of the ventilation factor to the grid cell size:

$$\ell_1^* = \frac{\left(A\sqrt{H}\right)^{2/5}}{\delta_x} \tag{A.2}$$

where A is the opening area (m^2) and H is the opening height (m). The second parameter ℓ_2^* considers the ratio of the hydraulic diameter D_h of the opening to the grid cell size:

$$\ell_2^* = \frac{D_h}{\delta_x} = \frac{2WH/W + H}{\delta_x} \tag{A.3}$$

where W is the opening width (m). It is recommended that a length scale ratio of ℓ_1^* or ℓ_2^* exceed a value of 10 is sufficient to ensure adequate resolution of vent flows in compartment fires. Based on these three criteria (i.e., fire diameter ratio, ventilation factor ratio, and hydraulic diameter ratio), the grid resolutions adopted for each fire model are summarized in Table A.1, which includes the estimated grid sizes and justification for the selected mesh schemes.

Table A.1 Grid settings of each fire model.

Name of fire models	Opening geometry [m]		Estimated grid size by different criteria [m]			Grid size used [m]
	Width	Height	D^* criterion	ℓ_1^* criterion	ℓ_2^* criterion	
Shields Fire Test	0.850	0.850	⩽0.236	⩽0.085	⩽0.085	0.050
	0.850	1.900		⩽0.138	⩽0.117	
	0.400	2.000		⩽0.105	⩽0.667	
Kirby Fire Test	2.600	1.200	⩽1.146	⩽0.163	⩽0.164	0.100
	4.000	1.200		⩽0.194	⩽0.184	
	1.000	1.800		⩽0.142	⩽0.128	
Malveira Fire Test	2.600	1.100	⩽0.810	⩽0.155	⩽0.155	0.100
	4.000	1.100		⩽0.184	⩽0.173	
	3.700	1.100		⩽0.179	⩽0.170	
	0.800	1.100		⩽0.097	⩽0.093	
	4.100	1.100		⩽0.186	⩽0.173	
	1.000	1.800		⩽0.142	⩽0.129	
Shenzhen Fire Test	0.900	0.400	⩽0.240	⩽0.055	⩽0.055	0.500
	1.950	0.650		⩽0.101	⩽0.098	
Three-story Building Fire	1.200	1.600	⩽1.512	⩽0.143	⩽0.137	0.100

Appendix B

Operating environment for CFD fire models

All fire simulations were conducted using a dedicated computational server configured with two 32-core Hygon 7285 processors and equipped with 256 GB RAM. Additionally, simulations were executed under the Linux operating system (Ubuntu 20.04 LTS). To provide insight into the computational performance of the CFD fire simulations presented throughout this thesis, the clock-wall times of each fire model from different chapters have been systematically recorded in Table B.1.

Table B.1 Summary of clock times for each fire model

	Description of fire models	Simulation time	Clock-wall time
Chapter 2	Shields Fire Test	980 s	5 d 13 h 20 min 0 s
	Kirby Fire Test	2400 s	2 d 2 h 16 min 0 s
	Kirby Fire Test with windows	2400 s	8 d 3 h 10 min 0 s
	Malveira Fire Test	14500 s	20 d 2 h 53 min 20 s
	Malveira Fire Test with windows	9000 s	12 d 6 h 36 min 40 s
Chapter 3	Shenzhen Fire Test (fire pattern P1)	1500 s	~ 15 h
	Shenzhen Fire Test (fire pattern P2)		~ 1 d 9 h
	Shenzhen Fire Test (fire pattern P3)		~ 1 d 2 h
	Shenzhen Fire Test (fire pattern P4)		~ 22 h
Chapter 4	Case A1	1800 s	1 d 2 h 22 min 0 s
	Case A2		4 d 21 h 10 min 20 s
	Case B1		1 d 11 h 27 min 0 s
	Case B2		4 d 20 h 36 min 0 s
	Case B3		5 d 4 h 13 min 20 s
	Case B4		4 d 23 h 48 min 0 s
	Case C1		1 d 10 h 52 min 40 s
	Case C2		1 d 13 h 14 min 0 s
	Case C3		1 d 14 h 8 min 0 s
	Case C4		1 d 16 h 44 min 0 s
Chapter 5	Shenzhen Fire Test	1500 s	1 d 4 h 53 min 20 s
	Shenzhen Fire Test (active opening)		7 h 5 min 0 s
Chapter 6	Case 1A	3600 s	1 d 23 h 30 min 0 s
	Case 1B		4 d 11 h 32 min 0 s
	Case 2A		1 d 21 h 50 min 0 s
	Case 2B		4 d 12 h 3 min 20 s
	Case 3A		1 d 23 h 46 min 40 s
	Case 3B		4 d 14 h 50 min 0 s

Description of fire models	Simulation time	Clock-wall time
Case 4A		2 d 5 h 53 min 20 s
Case 4A (3 windows)		4 d 12 h 36 min 40 s
Case 4A (4 windows)		2 d 7h 0 min 0 s
Case 4A (6 windows)		2 d 3 h 40 min 0 s
Case 4A (casement window)		2 d 8 h 23 min 20 s
Case 4A (tilt-and-turn window)		2 d 9 h 30 min 0 s
Case 4A (window-integrated detectors)		1 d 17 h 23 min 20 s
Case 4A (3 detectors)		2 d 4 h 46 min 40 s
Case 4A (7 detectors)		1 d 18 h 46 min 40 s
Case 4B		6 d 8 h 13 min 20 s
Case 5A		1 d 13 h 13 min 20 s
Case 5B		4 d 19 h 36 min 40 s
Case 6A		1 d 14 h 3 min 20 s
Case 6B		5 d 0 h 50 min 0 s
Case 7A		1 d 18 h 13 min 20 s
Case 7B		6 d 22 h 56 min 40 s
Case 8A		1 d 16 h 50 min 0 s
Case 8B		8 d 22 h 23 min 20 s

Appendix C

Thermogravimetric test for obtaining pyrolysis parameters

The thermogravimetric (TG) test is a technique used in materials science to evaluate the thermal stability and composition of a sample by measuring its mass changes during heating [202]. This method can identify different components within the material and assess thermal decomposition temperatures. The PerkinElmer STA6000 analyzer was used to conduct TG tests in an air atmosphere, utilizing approximately 4 mg of wood chips extracted from wood sticks used in the current medium-scale fire tests. The experimental conditions were set to heat from 30 ºC to 800 ºC at a rate of 30 ºC /min, and the tests were repeated three times. The average of these three tests was used to calibrate the reaction parameters in the FDS. A detailed comparison between TG simulations in FDS and actual TG tests is presented in Fig. C.1. The initial stage of mass loss observed around 100 ºC in Fig. C.1(a) is primarily attributed to the evaporation of moisture, accounting for approximately 10.5% of the total mass loss. Furthermore, two significant peaks of rapid mass loss were recorded in Fig. C.1(b): the first peak occurs around 310 ºC which indicates the pyrolysis process of wood, and the second peak represents the oxidation of residual char at about 450 ºC.

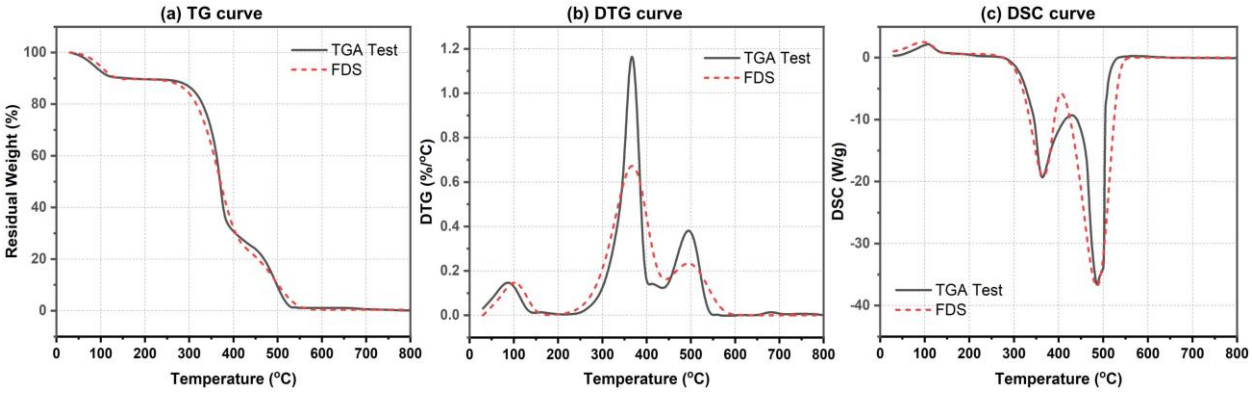

Fig. C.1 Comparison between TG simulations in FDS and real TG tests.

The Differential Scanning Calorimetry (DSC) curve shown in Fig. C.1(c) further aids in analyzing the endothermic or exothermic nature of the evaporation, pyrolysis, and oxidation stages. The thermal properties of the species involved in combustion, as well as the kinetic parameters identified through TGA tests, are listed in Table C.1.**错误!未找到引用源。**

Table C.1 Thermal properties [8,167,168] and kinetic parameters used in the combustion model.

Properties	Unit	Dry wood	Char	Ash	Moisture
Density ρ	kg/m^3	450	135	67	1000
Specific heat c_p	kJ/kg·K	1.35	1.08	2.0	4.18
Thermal conductivity λ	W/m·K	0.15	0.13	0.1	0.1
Pre-exponential factor A_a	s^{-1}	5.69×10^4	1.44×10^5	-	1.29×10^4

Properties	Unit	Dry wood	Char	Ash	Moisture
Activation energy E_a	kJ/mol	9.01×10^4	1.03×10^5	-	4.12×10^4
Order of reaction n	-	1.69	2.0	-	1.0
Heat of reaction ΔH_r	kJ/kg	-150	-3110	-	2500

References

[1] D. Alfirevic, S. Simonovic-Alfirevic, Open-plan in housing architecture: Origin, development and design approaches for spatial integration, Architecture and Urbanism (2016) 45–60. https://doi.org/10.5937/a-u0-11551.

[2] T. McAllister, W.G. Corley, World Trade Center building performance study: Data collection, preliminary observations, and recommendations, Federal Emergency Management Agency, Federal Insurance and Mitigation Administration ; FEMA Region II, Washington, D.C., New York, 2002.

[3] J. Gordon Routley, Charles Jennings, Mark Chubb, High-rise office building fire: One Meridian Plaza, Federal Emergency Management Agency, 1991.

[4] Shanghai fire, (2010). https://en.wikipedia.org/wiki/2010_Shanghai_fire.

[5] M.T. Ahmadi, A.A. Aghakouchak, R. Mirghaderi, S. Tahouni, S. Garivani, A. Shahmari, S. Epackachi, Collapse of the 16-story Plasco Building in Tehran due to fire, Fire Technology 56 (2020) 769–799. https://doi.org/10.1007/s10694-019-00903-y.

[6] Bank of Lisbon fire: Critical failures by government departments and emergency services uncovered in investigation report five years later, (2019). https://www.iol.co.za/news/bank-of-lisbon-fire-critical-failures-by-government-departments-and-emergency-services-uncovered-in-investigation-report-five-years-later-a8b087c0-fda0-422f-8cf4-6df08ea51845.

[7] Milan fire: Firefighters tackle blaze as flames engulf high-rise block of flats, (2021). https://news.sky.com/story/milan-fire-firefighters-tackle-blaze-as-flames-engulf-high-rise-block-of-flats-12394856.

[8] B.R. Kirby, D.E. Wainman, L.N. Tomlinson, T.R. Kay, B.N. Peacock, Natural fires in large scale compartments, British Steel Technical and Fire Research Station, 1994.

[9] J.P. Hidalgo, A. Cowlard, C. Abecassis-Empis, C. Maluk, A.H. Majdalani, S. Kahrmann, R. Hilditch, M. Krajcovic, J.L. Torero, An experimental study of full-scale open floor plan enclosure fires, Fire Safety Journal 89 (2017) 22–40. https://doi.org/10.1016/j.firesaf.2017.02.002.

[10] J.P. Hidalgo, T. Goode, V. Gupta, A. Cowlard, C. Abecassis-Empis, J. Maclean, A.I. Bartlett, C. Maluk, J.M. Montalvá, A.F. Osorio, J.L. Torero, The Malveira fire test: Full-scale demonstration of fire modes in open-plan compartments, Fire Safety Journal 108 (2019) 102827. https://doi.org/10.1016/j.firesaf.2019.102827.

[11] M. Heidari, E. Rackauskaite, M. Bonner, E. Christensen, S. Morat, H. Mitchell, P. Kotsovinos, P. Turkowski, W. Wegrzynski, P. Tofilo, G. Rein, Fire experiments inside a very large and open-plan compartment: x-TWO, in: Proceedings of the 11th International Conference on Structures in Fire (SiF2020), The University of Queensland, 2020. https://doi.org/10.14264/b666dc1.

[12] D. Rush, X. Dai, D. Lange, Tisova Fire Test – Fire behaviours and lessons learnt, Fire Safety Journal 121 (2021) 103261. https://doi.org/10.1016/j.firesaf.2020.103261.

[13] E. Rackauskaite, M. Bonner, F. Restuccia, N. Fernandez Anez, E.G. Christensen, N. Roenner, W. Wegrzynski, P. Turkowski, P. Tofilo, M. Heidari, P. Kotsovinos, I. Vermesi, F. Richter, Y. Hu, C. Jeanneret, R. Wadhwani, G. Rein, Fire experiment inside a very large and open-plan compartment: X-ONE, Fire Technology (2021). https://doi.org/10.1007/s10694-021-01162-6.

[14] A. Nadjai, A. Naveed, M. Charlier, O. Vassart, S. Welch, A. Glorieux, J. Sjostrom, Large scale fire test: The development of a travelling fire in open ventilation conditions and its influence on the surrounding steel structure, Fire Safety Journal 130 (2022) 103575. https://doi.org/10.1016/j.firesaf.2022.103575.

[15] P.H. Thomas, A.J.M. Heselden, Fully-developed fires in single compartments, Fire Research Notes No. 923 (1972).

[16] T.Z. Harmathy, Ventilation of fully-developed compartment fires, Combustion and Flame 37 (1980) 25–39. https://doi.org/10.1016/0010-2180(80)90069-3.

[17] P.H. Thomas, Fire modeling and fire behavior in rooms, Symposium (International) on Combustion 18 (1981) 503–518. https://doi.org/10.1016/S0082-0784(81)80056-2.

[18] J.G. Quintiere, A perspective on compartment fire growth, Combustion Science and Technology 39 (1984) 11–54. https://doi.org/10.1080/00102208408923782.

[19] P.H. Thomas, Modelling of compartment fires, Fire Safety Journal 5 (1983) 181–190. https://doi.org/10.1016/0379-7112(83)90016-4.

[20] N.R.M. Sakiyama, J.C. Carlo, J. Frick, H. Garrecht, Perspectives of naturally ventilated buildings: A review, Renewable and Sustainable Energy Reviews 130 (2020) 109933. https://doi.org/10.1016/j.rser.2020.109933.

[21] Ingberg, S. H., Tests of the severity of building fires, NFPA Quarterly 22 (1928) 43–61.

[22] BS 476-20: Fire resistance test to building material, (1987).

[23] ASTM E119: Standard test methods for fire tests of building construction and materials, (2000).

[24] ISO 834-1:2014 Fire-resistance tests - Elements of building construction - Part 1: General requirements, (2014).

[25] EN 1991-1-2: Eurocode 1: Actions on structures - Part 1-2: General actions - Actions on structures exposed to fire, (2002).

[26] T.E. Waterman, Room flashover: Criteria and synthesis, Fire Technology 4 (1968) 25–31. https://doi.org/10.1007/BF02588603.

[27] V. Babrauskas, Estimating room flashover potential, Fire Technology 16 (1980) 94–103.

[28] P.H. Thomas, M.L. Bullen, J.G. Quintiere, B.J. McCaffrey, Flashover and instabilities in fire behavior, Combustion and Flame 38 (1980) 159–171. https://doi.org/10.1016/0010-2180(80)90048-6.

[29] B.J. McCaffrey, J.G. Quintiere, M.F. Harkleroad, Estimating room temperatures and the likelihood of flashover using fire test data correlations, Fire Technology 17 (1981) 98–119. https://doi.org/10.1007/BF02479583.

[30] S.R. Bishop, D.D. Drysdale, Fires in compartments: The phenomenon of flashover, Philosophical Transactions of the Royal Society of London. Series A: Mathematical, Physical and Engineering Sciences 356 (1998) 2855–2872. https://doi.org/10.1098/rsta.1998.0301.

[31] R.D. Peacock, P.A. Reneke, R.W. Bukowski, V. Babrauskas, Defining flashover for fire hazard calculations, Fire Safety Journal 32 (1999) 331–345. https://doi.org/10.1016/S0379-7112(98)00048-4.

[32] T. Zhang, Z. Wang, H.Y. Wong, W.C. Tam, X. Huang, F. Xiao, Real-time forecast of compartment fire and flashover based on deep learning, Fire Safety Journal 130 (2022). https://doi.org/10.1016/j.firesaf.2022.103579.

[33] W. Weng, W. Fan, Critical condition of backdraft in compartment fires: a reduced-scale experimental study, Journal of Loss Prevention in the Process Industries 16 (2003) 19–26. https://doi.org/10.1016/S0950-4230(02)00088-8.

[34] C. Fleischmann, P. Pagni, R. Williamson, Quantitative backdraft experiments, Fire Safety Science 4 (1994) 337–348. https://doi.org/10.3801/IAFSS.FSS.4-337.

[35] K. Kawagoe, Fire behaviour in rooms, BRI Report No. 27 (1958).

[36] K. Kawagoe, Estimation of fire temperature-time curve in rooms, Transactions of the Architectural Institute of Japan 140 (1967). https://api.semanticscholar.org/CorpusID:113688124.

[37] P.H. Thomas, L. Nilsson, Fully developed compartment fires: New correlations of burning rates, Fire Research Notes No. 979 (1973).

[38] P.H. Thomas, Old and new looks at compartment fires, Fire Technology 11 (1975) 42–47. https://doi.org/10.1007/BF02590001.

[39] P.H. Thomas, Modelling of compartment fires, Fire Safety Journal 5 (1983) 181–190. https://doi.org/10.1016/0379-7112(83)90016-4.

[40] T.Z. Harmathy, A new look at compartment fires: Part I, Fire Technology 8 (1972) 196–217. https://doi.org/10.1007/BF02590544.

[41] T.Z. Harmathy, A new look at compartment fires: Part II, Fire Technology 8 (1972) 326–351. https://doi.org/10.1007/BF02590537.

[42] T.Z. Harmathy, Mechanism of burning of fully-developed compartment fires, Combustion and Flame 31 (1978) 265–273. https://doi.org/10.1016/0010-2180(78)90139-6.

[43] V. Babrauskas, R.B. Williamson, Post-flashover compartment fires: Basis of a theoretical model, Fire and Materials 2 (1978) 39–53. https://doi.org/10.1002/fam.810020202.

[44] V. Babrauskas, R.B. Williamson, Post-flashover compartment fires: Application of a theoretical model, Fire and Materials 3 (1979) 1–7. https://doi.org/10.1002/fam.810030102.

[45] J.L. Torero, A. Majdalani, C. Abecassis-Empis, A. Cowlard, Revisiting the compartment fire, Fire Safety Science 11 (2014) 28–45. https://doi.org/10.3801/IAFSS.FSS.11-28.

[46] T.Z. Harmathy, Design of buildings for fire safety: Part I, Fire Technology 12 (1976) 95–108. https://doi.org/10.1007/BF02629478.

[47] T.Z. Harmathy, Design of buildings for life safety: Part II, Fire Technology 12 (1976) 219–236. https://doi.org/10.1007/BF02624797.

[48] L. Margaret Law, A relationship between fire grading and building design and contents, Fire Research Notes No. 877 (1971).

[49] J. Prahl, H.W. Emmons, Fire induced flow through an opening, Combustion and Flame 25 (1975) 369–385. https://doi.org/10.1016/0010-2180(75)90109-1.

[50] Howard W. Emmons, The prediction of fires in buildings, Symposium (International) on Combustion 17 (1979) 1101–1111. https://doi.org/10.1016/S0082-0784(79)80105-8.

[51] H.W. Emmons, The calculation of a fire in a large building, Journal of Heat Transfer 105 (1983) 151–158. https://doi.org/10.1115/1.3245534.

[52] J.G. Quintiere, Growth of fire in building compartments, in: Fire Standards and Safety, ASTM International, 1976. https://doi.org/10.1520/STP37206S.

[53] J.G. Quintiere, B.J. McCaffrey, K.D. Braven, Experimental and theoretical analysis of quasi-steady small-scale enclosure fires, Symposium (International) on Combustion 17 (1979) 1125–1137. https://doi.org/10.1016/S0082-0784(79)80107-1.

[54] O. Sugawa, K. Kawagoe, Y. Oka, Burning behavior in a poor-ventilation compartment fire - ghosting fire, Nuclear Engineering and Design 125 (1991) 347–352. https://doi.org/10.1016/0029-5493(91)90341-E.

[55] L. Kerrison, E. Galea, M. Patel, A two-dimensional numerical investigation of the oscillatory flow behaviour in rectangular fire compartments with a single horizontal ceiling vent, Fire Safety Journal 30 (1998) 357–382. https://doi.org/10.1016/S0379-7112(97)00042-8.

[56] K. Himoto, T. Tsuchihashi, Y. Tanaka, T. Tanaka, Modeling thermal behaviors of window flame ejected from a fire compartment, Fire Safety Journal 44 (2009) 230–240. https://doi.org/10.1016/j.firesaf.2008.06.005.

[57] S. Vilfayeau, N. Ren, Y. Wang, A. Trouve, Numerical simulation of under-ventilated liquid-fueled compartment fires with flame extinction and thermally-driven fuel evaporation, Proceedings of the Combustion Institute 35 (2015) 2563–2571. https://doi.org/10.1016/j.proci.2014.05.072.

[58] F. Ren, L. Hu, X. Zhang, X. Sun, J. Zhang, M. Delichatsios, Experimental study of transitional behavior of fully developed under-ventilated compartment fire and associated facade flame height evolution, Combustion and Flame 208 (2019) 235–245. https://doi.org/10.1016/j.combustflame.2019.07.003.

[59] X. Sun, L. Hu, X. Zhang, F. Ren, Y. Yang, X. Fang, Experimental study on flame pulsation behavior of external venting facade fire ejected from opening of a compartment, Proceedings of the Combustion Institute 38 (2021) 4485–4493. https://doi.org/10.1016/j.proci.2020.06.181.

[60] S. Yokoi, Temperature distribution of hot air current issued form a window of a fire resistive construction in fire, (1958). https://doi.org/10.11196/kasai.7.2_41.

[61] Y.-P. Lee, M.A. Delichatsios, Y. Ohmiya, K. Wakatsuki, A. Yanagisawa, D. Goto, Heat fluxes on opposite building wall by flames emerging from an enclosure, Proceedings of the Combustion Institute 32 (2009) 2551–2558. https://doi.org/10.1016/j.proci.2008.06.130.

[62] Y.P. Lee, M.A. Delichatsios, Y. Ohmiya, The physics of the outflow from the opening of an enclosure fire and re-examination of Yokoi's correlation, Fire Safety Journal 49 (2012) 82–88. https://doi.org/10.1016/j.firesaf.2012.01.001.

[63] M.A. Delichatsios, Creeping flame spread: Energy balance and application to practical materials, Symposium (International) on Combustion 26 (1996) 1495–1503. https://doi.org/10.1016/S0082-0784(96)80371-7.

[64] M. Delichatsios, Enclosure and facade fires: Physics and applications, Fire Safety Science 11 (2014) 3–27. https://doi.org/10.3801/IAFSS.FSS.11-3.

[65] W.K. Chow, Numerical studies on the transient behaviour of a fire plume and ceiling jet, Mathematical and Computer Modelling 17 (1993) 71–79. https://doi.org/10.1016/0895-7177(93)90017-S.

[66] W.K. Chow, E. Cui, CFD Simulations on Balcony Spill Plume, Journal of Fire Sciences 16 (1998) 468–485. https://doi.org/10.1177/073490419801600606.

[67] L.H. Hu, K.H. Lu, F. Tang, M. Delichatsios, L.H. He, A global non-dimensional factor characterizing side wall constraint effect on facade flame entrainment and flame height from opening of compartment fires, International Journal of Heat and Mass Transfer 75 (2014) 122–129. https://doi.org/10.1016/j.ijheatmasstransfer.2014.03.059.

[68] L. Hu, K. Hu, F. Ren, X. Sun, Facade flame height ejected from an opening of fire compartment under external wind, Fire Safety Journal 92 (2017) 151–158. https://doi.org/10.1016/j.firesaf.2017.06.008.

[69] X. Sun, F. Tang, K. Lu, F. Ren, C. Shi, B. Merci, L. Hu, Fundamentals of window-ejected fire plumes from under-ventilated compartment fires: Recent progresses and perspectives, Progress in Energy and Combustion Science 94 (2023) 101039. https://doi.org/10.1016/j.pecs.2022.101039.

[70] Fire Dynamics Simulator, (2021). https://github.com/firemodels/fds/releases/tag/FDS6.7.7.

[71] F. Jia, E. Galea, M. Patel, The numerical simulation of the noncharring pyrolysis process and fire development within a compartment, Applied Mathematical Modelling 23 (1999) 587–607. https://doi.org/10.1016/S0307-904X(99)00003-7.

[72] A. Snegirev, G. Makhviladze, J. Roberts, Smoke coagulation in compartment fire modelling, Combustion Science and Technology 159 (2000) 315–349. https://doi.org/10.1080/00102200008935789.

[73] Z.M. Fu, G. Hadjisophocleous, A two-zone fire growth and smoke movement model for multi-compartment buildings, Fire Safety Journal 34 (2000) 257–285. https://doi.org/10.1016/S0379-7112(99)00045-4.

[74] R. Hasib, R. Kumar, Shashi, S. Kumar, Simulation of an experimental compartment fire by CFD, Building and Environment 42 (2007) 3149–3160. https://doi.org/10.1016/j.buildenv.2006.08.002.

[75] C. Luo, B. Dlugogorski, B. Moghtaderi, E. Kennedy, Computational study on toxic gases released from compartment fires suppressed with halogenated agents, Cybernetics and Systems 35 (2004) 607–625. https://doi.org/10.1080/01969720490499362.

[76] Z. Hu, Y. Utiskul, J.G. Quintiere, A. Trouve, Towards large eddy simulations of flame extinction and carbon monoxide emission in compartment fires, Proceedings of the Combustion Institute 31 (2007) 2537–2545. https://doi.org/10.1016/j.proci.2006.08.053.

[77] V. Novozhilov, Computational fluid dynamics modeling of compartment fires, Progress in Energy and Combustion Science 27 (2001) 611–666. https://doi.org/10.1016/S0360-1285(01)00005-3.

[78] T. Fry, A new design philosophy: An introduction to defuturing, UNSW Press, Sydney, 1999.

[79] S. Shyam-Sunder, R.G. Gann, W. Grosshandler, H.S. Lew, R.W. Bukowski, F.H. Sadek, F.W. Gayle, J.L. Gross, T.P. McAllister, J.D. Averill, J.R. Lawson, H.E. Nelson, S.A. Cauffman, Final report on the collapse of World Trade Center Building 7: Federal building and fire safety investigation of the World Trade Center disaster, National Institute of Standards and Technology, Gaithersburg, MD, 2008. https://doi.org/10.6028/NIST.NCSTAR.1A.

[80] Jennie Rhodes, 12 February 2005: Madrid's Windsor Tower goes up in flames, (2005). https://www.surinenglish.com/lifestyle/202102/12/february-2005madrid-windsor-tower-20210212102322-v.html.

[81] M.D. Engelhardt, B. Meacham, V. Kodur, A. Kirk, H. Park, Ij. Van Straalen, J. Maljaars, K. Van Weeren, R. De Feijter, K. Both, Observations from the fire and collapse of the Faculty of Architecture Building, Delft University of Technology, in: Structures Congress 2013, American Society of Civil Engineers, Pittsburgh, Pennsylvania, United States, 2013: pp. 1138–1149. https://doi.org/10.1061/9780784412848.101.

[82] G. Rein, X. Zhang, P. Williams, B. Hume, A. Heise, A. Jowsey, B. Lane, J.L. Torero, Multi-storey fire analysis for high-rise buildings, in: Proceedings of the 11th International Interflam Conference, London, UK, 2007: pp. 605–616.

[83] J. Stern-Gottfried, G. Rein, L.A. Bisby, J.L. Torero, Experimental review of the homogeneous temperature assumption in post-flashover compartment fires, Fire Safety Journal 45 (2010) 249–261. https://doi.org/10.1016/j.firesaf.2010.03.007.

[84] M.A. O'Connor, D.M. Martin, Behaviour of a multi-storey steel framed building subjected to fire attack, Journal of Constructional Steel Research 46 (1998) 295. https://doi.org/10.1016/S0143-974X(98)00122-9.

[85] T. Lennon, D. Moore, The natural fire safety concept - full-scale tests at Cardington, Fire Safety Journal 38 (2003) 623–643. https://doi.org/10.1016/S0379-7112(03)00028-6.

[86] P.J. Moss, G. Charles Clifton, Modelling of the Cardington LBTF steel frame building fire tests, Fire and Materials 28 (2004) 177–198. https://doi.org/10.1002/fam.868.

[87] I. Thomas, K. Moinuddin, I. Bennetts, Fire development in a deep enclosure, Fire Safety Science 8 (2005) 1277–1288. https://doi.org/10.3801/IAFSS.FSS.8-1277.

[88] C. G. Clifton, Fire models for large fire cells, 1996.

[89] J. Stern-Gottfried, G. Rein, Travelling fires for structural design-Part II: Design methodology, Fire Safety Journal 54 (2012) 96–112. https://doi.org/10.1016/j.firesaf.2012.06.011.

[90] R.L. Alpert, Turbulent ceiling-jet induced by large-scale fires, Combustion Science and Technology 11 (1975) 197–213. https://doi.org/10.1080/00102207508946699.

[91] K. Horová, T. Jána, F. Wald, Temperature heterogeneity during travelling fire on experimental building, Advances in Engineering Software 62–63 (2013) 119–130. https://doi.org/10.1016/j.advengsoft.2013.05.001.

[92] J. Degler, A. Eliasson, J. Anderson, D. Lange, D. Rush, A-priori modelling of the Tisova fire test as input to the experimental work, in: The First International Conference on Structural Safety under Fire & Blast, Glasgow, Scotland, UK, 2015.

[93] X. Dai, S. Welch, O. Vassart, K. Cábová, L. Jiang, J. Maclean, G.C. Clifton, A. Usmani, An extended travelling fire method framework for performance-based structural design, Fire and Materials 44 (2020) 437–457. https://doi.org/10.1002/fam.2810.

[94] E. Rackauskaite, C. Hamel, A. Law, G. Rein, Improved formulation of travelling fires and application to concrete and steel structures, Structures 3 (2015) 250–260. https://doi.org/10.1016/j.istruc.2015.06.001.

[95] M. Heidari, P. Kotsovinos, G. Rein, Flame extension and the near field under the ceiling for travelling fires inside large compartments, FIRE AND MATERIALS 44 (2020) 423–436. https://doi.org/10.1002/fam.2773.

[96] L. Jiang, Y. Jiang, Z. Zhang, A. Usmani, Thermal analysis infrastructure in opensees for fire and its smart application interface towards natural fire modelling, Fire Technology 57 (2021) 2955–2980. https://doi.org/10.1007/s10694-020-01071-0.

[97] A. Usmani, J. Zhang, J. Jiang, Y. Jiang, I. May, Using Opensees for structures in fire, Journal of Structural Fire Engineering 3 (2012) 57–70. https://doi.org/10.1260/2040-2317.3.1.57.

[98] The University of Edinburgh, Fire safety of modern timber infrastructure, (2016).

[99] CERIB Fire Testing Centre, Épernon fire tests programme, (2016).

[100] G. Rein, J.L. Torero, W. Jahn, J. Stern-Gottfried, N.L. Ryder, S. Desanghere, M. Lázaro, F. Mowrer, A. Coles, D. Joyeux, D. Alvear, J.A. Capote, A. Jowsey, C. Abecassis-Empis, P. Reszka, Round-robin study of a priori modelling predictions of the Dalmarnock Fire Test One, Fire Saf. J. 44 (2009) 590–602. https://doi.org/10.1016/j.firesaf.2008.12.008.

[101] A. Nadjai, N. Alam, M. Charlier, O. Vassart, X. Dai, J.-M. Franssen, J. Sjostrom, Travelling fire in full scale experimental building subjected to open ventilation conditions, Journal of Structural Fire Engineering (2022). https://doi.org/10.1108/JSFE-06-2021-0037.

[102] M. Charlier, J.-M. Franssen, F. Dumont, A. Nadjai, O. Vassart, Development of an analytical model to determine the heat fluxes to a structural element due to a travelling fire, Applied Sciences 11 (2021) 9263. https://doi.org/10.3390/app11199263.

[103] P. Kotsovinos, E. Rackauskaite, E. Christensen, A. Glew, E. O'Loughlin, H. Mitchell, R. Amin, F. Robert, M. Heidari, D. Barber, G. Rein, J. Schulz, Fire dynamics inside a large and open-plan compartment with exposed timber ceiling and columns: CodeRed #01, Fire and Materials 47 (2023) 542–568. https://doi.org/10.1002/fam.3049.

[104] P. Kotsovinos, E.G. Christensen, E. Rackauskaite, A. Glew, E. O'Loughlin, H. Mitchell, R. Amin, F. Robert, M. Heidari, D. Barber, G. Rein, J. Schulz, Impact of ventilation on the fire dynamics of an open-plan compartment with exposed timber ceiling and columns: CodeRed #02, Fire and Materials 47 (2023) 569–596. https://doi.org/10.1002/fam.3082.

[105] P. Kotsovinos, E.G. Christensen, A. Glew, E. O'Loughlin, H. Mitchell, R. Amin, F. Robert, M. Heidari, D. Barber, G. Rein, J. Schulz, Impact of partial encapsulation on the fire dynamics of an open-plan compartment with exposed timber ceiling and columns: CodeRed #04, Fire and Materials 47 (2023) 597–626. https://doi.org/10.1002/fam.3112.

[106] C. Chen, T. Chu, G. Rein, A. Usmani, L. Jiang, Fire development in large compartments with mixed-timber-section ceiling, in: 13th International Conference on Structures in Fire, Coimbra, Portugal, 2024.

[107] H. Mitchell, R. Amin, M. Heidari, P. Kotsovinos, G. Rein, Structural hazards of smouldering fires in timber buildings, Fire Safety Journal 140 (2023) 103861. https://doi.org/10.1016/j.firesaf.2023.103861.

[108] T. Engel, N. Werther, Impact of mass timber compartment fires on facade fire exposure, FIRE TECHNOLOGY 59 (2023) 517–558. https://doi.org/10.1007/s10694-022-01346-8.

[109] H. Emmons, The needed fire science, Fire Safety Science 1 (1986) 1–33. https://doi.org/10.3801/IAFSS.FSS.1-33.

[110] A.A. Griffith, The phenomena of rupture and flow in solids, Philosophical Transactions of the Royal Society of London. Series A, Containing Papers of a Mathematical or Physical Character 22 (1921) 163–198.

[111] J.E. Shelby, Introduction to glass science and technology, Royal society of chemistry, Cambridge, 1997.

[112] T.L. Anderson, Fracture mechanics: Fundamentals and applications, 3rd Edition, Taylor & Francis, Boca Raton, FL, 2005. https://doi.org/10.1201/9781315370293.

[113] G.R. Irwin, Analysis of Stresses and Strains Near the End of a Crack Traversing a Plate, Journal of Applied Mechanics 24 (1957) 361–364. https://doi.org/10.1115/1.4011547.

[114] B. Lawn, Fracture of brittle solids, 2nd Edition, Cambridge University Press, 1993. https://doi.org/10.1017/CBO9780511623127.

[115] M. Porter, Aspects of structural design with glass, PhD Thesis, University of Oxford, 2001.

[116] C. Brokmann, S. Kolling, J. Schneider, Subcritical crack growth parameters in glass as a function of environmental conditions, Glass Structures & Engineering 6 (2021) 89–101. https://doi.org/10.1007/s40940-020-00134-6.

[117] S.M. Wiederhorn, Influence of water vapor on crack propagation in soda-lime glass, Journal of the American Ceramic Society 50 (1967) 407–414. https://doi.org/10.1111/j.1151-2916.1967.tb15145.x.

[118] A.G. Atkins, Y.W. Mai, Elastic and plastic fracture: Metals, polymers, ceramics, composites, biological materials, Halsted Press, New York, 1985.

[119] E. Gehrke, C. Ullner, M. Hähnert, Effect of corrosive media on crack growth of model glasses and commercial silicate glasses, 1990.

[120] Jaroslav Menčík, Strength and fracture of glass and ceramics, 1992.

[121] W. Weibull, A statistical theory of the strength of materials, Proceedings of the American Mathematical Society 151 (1939) 1–45.

[122] Pareto distribution, (2002). https://en.wikipedia.org/wiki/Pareto_distribution.

[123] EN 572-1: Glass in building – Basic soda lime silicate glass products – Part 1: Definitions and general physical and mechanical properties, (2016).

[124] K. Blank, Thickness design of quadric-laterally supported rectangular glass panes under uniform surface load, Institute for Constructive Glass Construction, Gelsenkirchen, 1993.

[125] EN 1288-2:2000: Glass in building – Determination of the bending strength of glass – Part 2: Coaxial double ring test on flat specimens with large test surface areas, (2000).

[126] F.A. Veer, P.C. Louter, F.P. Bos, The strength of annealed, heat-strengthened and fully tempered float glass, Fatigue & Fracture of Engineering Materials & Structures 32 (2009) 18–25. https://doi.org/10.1111/j.1460-2695.2008.01308.x.

[127] I. Nurhuda, N.T.K. Lam, E.F. Gad, I. Calderone, Estimation of strengths in large annealed glass panels, International Journal of Solids and Structures 47 (2010) 2591–2599. https://doi.org/10.1016/j.ijsolstr.2010.05.015.

[128] D.Z. Yankelevsky, Strength prediction of annealed glass plates – A new model, Engineering Structures 79 (2014) 244–255. https://doi.org/10.1016/j.engstruct.2014.08.017.

[129] E. Symoens, R. Van Coile, B. Jovanović, J. Belis, Probability density function models for float glass under mechanical loading with varying parameters, Materials 16 (2023) 2067. https://doi.org/10.3390/ma16052067.

[130] A. Petzold, H. Marusch, B. Schramm, Glass as a building material: Fundamentals, properties, products, glass construction eements, applications, 3rd Edition, Publishing House for Construction, Schorndorf, Berlin, 1990.

[131] O. Keski-Rahkonen, Breaking of window glass close to fire, Fire and Materials 12 (1988) 61–69. https://doi.org/10.1002/fam.810120204.

[132] P. Pagni, A. Joshi, Glass breaking in fires, Fire Safety Science 3 (1991) 791–802. https://doi.org/10.3801/IAFSS.FSS.3-791.

[133] A.A. Joshi, P.J. Pagni, Fire-induced thermal fields in window glass: I Theory, Fire Safety Journal (1994) 19.

[134] M.J. Skelly, R.J. Roby, C.L. Beyler, An experimental investigation of glass breakage in compartment fires, Journal of Fire Protection Engineering 3 (1991) 25–34. https://doi.org/10.1177/104239159100300103.

[135] H. Chen, Y. Wang, Y. Zhang, Q. Wang, H. Zhao, G. Shao, Y. Su, J. Sun, L. He, Crack evolution process of window glass under radiant heating, Fire and Materials 41 (2017) 1016–1026. https://doi.org/10.1002/fam.2447.

[136] J.D. Jørgensen, Thermal resistance of framed windows: Experimental study on the influence of frame shading width, Safety Science (2022) 12.

[137] Y. Wang, Y. Zhang, Q. Wang, Y. Yang, J. Sun, The effect of glass panel dimension on the fire response of glass façades, Construction and Building Materials 181 (2018) 588–597. https://doi.org/10.1016/j.conbuildmat.2018.06.088.

[138] Q. Xie, H. Zhang, Y. Wan, Q. Zhang, X. Cheng, Full-scale experimental study on crack and fallout of toughened glass with different thicknesses, Fire and Materials 32 (2008) 293–306. https://doi.org/10.1002/fam.968.

[139] L. Li, Q. Xie, X. Cheng, H. Zhang, Cracking behavior of glazings with different thicknesses by radiant exposure, Fire and Materials 36 (2012) 264–276. https://doi.org/10.1002/fam.1108.

[140] Y. Yang, C.L. Chow, Transient temperature fields and thermal stress fields in glazing of different thicknesses exposed to heat radiation, Construction and Building Materials 193 (2018) 589–603. https://doi.org/10.1016/j.conbuildmat.2018.10.106.

[141] Y. Wang, X. Li, L. Bisby, Comparative study of thermal breakage of annealed and tempered glazing with different thicknesses under uniform radiation conditions, Fire Safety Journal 140 (2023) 103867. https://doi.org/10.1016/j.firesaf.2023.103867.

[142] S. Dembele, R.A.F. Rosario, J.X. Wen, Thermal breakage of window glass in room fires conditions – Analysis of some important parameters, Building and Environment 54 (2012) 61–70. https://doi.org/10.1016/j.buildenv.2012.01.009.

[143] F.W. Mowrer, Window breakage induced by exterior fires, National Institute of Standards and Technology, 1998.

[144] T.J. Shields, G.W.H. Silcock, M. Flood, Performance of a single glazing assembly exposed to a fire in the centre of an enclosure, Fire and Materials 26 (2002) 51–75. https://doi.org/10.1002/fam.783.

[145] T.J. Shields, G.W.H. Silcock, M.F. Flood, Performance of a single glazing assembly exposed to enclosure corner fires of increasing severity, Fire and Materials 25 (2001) 123–152. https://doi.org/10.1002/fam.764.

[146] J. Shields, G.W.H. Silcock, F. Flood, Behaviour of double glazing in corner fires, Fire Technology 41 (2005) 37–65. https://doi.org/10.1007/s10694-005-4629-3.

[147] Y. Wang, Q. Wang, J. Sun, L. He, K.M. Liew, Influence of fire location on the thermal performance of glass façades, Applied Thermal Engineering 106 (2016) 438–442. https://doi.org/10.1016/j.applthermaleng.2016.06.057.

[148] Y.K. Choi, J.T. Kim, M.G. Jeong, S.W. Cho, H.S. Ryou, The influence of fire size on breakage time for double glazed curtain wall system in enclosure fire, Journal of Mechanical Science and Technology 32 (2018) 977–983. https://doi.org/10.1007/s12206-018-0148-7.

[149] Y. Wang, Q. Wang, Y. Su, J. Sun, L. He, K.M. Liew, Fracture behavior of framing coated glass curtain walls under fire conditions, Fire Safety Journal 75 (2015) 45–58. https://doi.org/10.1016/j.firesaf.2015.05.002.

[150] Y. Wang, Investigation of thermal breakage and heat transfer in single, insulated and laminated glazing under fire conditions, Applied Thermal Engineering (2017) 11.

[151] Y. Wang, J. Hu, Performance of laminated glazing under fire conditions, Composite Structures 223 (2019) 110903. https://doi.org/10.1016/j.compstruct.2019.110903.

[152] Z. Ni, S. Lu, L. Peng, Experimental study on fire performance of double-skin glass facades, Journal of Fire Sciences 30 (2012) 457–472. https://doi.org/10.1177/0734904112447179.

[153] M.K. Hassan, M.R. Hasnat, K.P. Loh, M.D. Hossain, P. Rahnamayiezekavat, G. Douglas, S. Saha, Effect of interlayer materials on fire performance of laminated glass used in high-rise building: Cone calorimeter testing, Fire 6 (2023) 84. https://doi.org/10.3390/fire6030084.

[154] F. Binte Mohd Faudzi, J. Schulz, G. Dodd, Qualitative assessment of fire hazard posed by laminated glass balcony balustrades on fire spread, Fire Technology 57 (2021) 1951–1967. https://doi.org/10.1007/s10694-020-01085-8.

[155] Y. Wang, Q. Wang, J. Sun, L. He, K.M. Liew, Thermal performance of exposed framing glass façades in fire, Materials and Structures 49 (2016) 2961–2970. https://doi.org/10.1617/s11527-015-0698-z.

[156] Y. Wang, Q. Wang, Y. Su, J. Sun, L. He, K.M. Liew, Experimental study on fire response of double glazed panels in curtain walls, Fire Safety Journal 92 (2017) 53–63. https://doi.org/10.1016/j.firesaf.2017.05.016.

[157] Y. Wang, Q. Xie, Y. Zhang, Q. Wang, J. Sun, Sensitivity analysis of influencing factors on glass facade breakage in fire, Fire Safety Journal 98 (2018) 38–47. https://doi.org/10.1016/j.firesaf.2018.04.002.

[158] K. Harada, A. Enomoto, K. Uede, T. Wakamatsu, An experimental study on glass cracking and fallout by radiant heat exposure, Fire Safety Science 6 (2000) 1063–1074. https://doi.org/10.3801/IAFSS.FSS.6-1063.

[159] S.L. Manzello, R.G. Gann, S.R. Kukuck, K.R. Prasad, W.W. Jones, An experimental determination of a real fire performance of a non-load bearing glass wall assembly, Fire Technology 43 (2007) 77–89. https://doi.org/10.1007/s10694-006-0001-5.

[160] Y. Wang, Determination of critical fallout condition of tempered glass in an enclosure fire, Fire Safety Journal (2018) 7. https://doi.org/10.1016/j.firesaf.2018.08.010.

[161] Y. Wang, J. Sun, L. He, Q. Wang, D. Rush, Experimental study on fallout behaviour of tempered glass façades with different frame insulation conditions in an enclosure fire, Proceedings of the Combustion Institute 37 (2019) 3889–3898. https://doi.org/10.1016/j.proci.2018.07.111.

[162] Q. Xie, T. Wang, S. Guo, C. Ma, A comparative study of statistical methods for critical parameters at tempered glass fallout in an enclosure fire, Construction and Building Materials 266 (2021) 121033. https://doi.org/10.1016/j.conbuildmat.2020.121033.

[163] Y. Wang, T. Xia, M. Xu, Z. Fang, M. Zhang, H. Ruan, Lai'an fire tests: Influence of opening condition on the fire dynamics of real urban village dwellings, Fire Technology (2023). https://doi.org/10.1007/s10694-023-01377-9.

[164] L.S. da Silva, A. Santiago, F. Lopes, T. Heistermann, M. Veljkovic, N. Iqbal, F. Wald, T. Jána, B. Davisons, I. Burgess, S.-S. Huang, G. Dong, Y. Wang, P. Mandals, M. Jafarian, M. Skorepa, P. Velda, G. Koutlas, Design of composite joints for improved fire robustness (Compfire) : final report, Publications Office of the European Union, Luxembourg, 2014. https://doi.org/10.2777/76889.

[165] J. Stern-Gottfried, G. Rein, Travelling fires for structural design-Part I: Literature review, Fire Safety Journal 54 (2012) 74–85. https://doi.org/10.1016/j.firesaf.2012.06.003.

[166] T.J. Shields, G.W.H. Silcock, M. Flood, Performance of a single glazing assembly exposed to a fire in the centre of an enclosure, Fire and Materials 26 (2002) 51–75. https://doi.org/10.1002/fam.783.

[167] R. Kallada Janardhan, S. Hostikka, Predictive computational fluid dynamics simulation of fire spread on wood cribs, Fire Technology 55 (2019) 2245–2268. https://doi.org/10.1007/s10694-019-00855-3.

[168] R.K. Janardhan, S. Hostikka, When is the fire spreading and when it travels? – Numerical simulations of compartments with wood crib fire loads, Fire Safety Journal 126 (2021) 103485. https://doi.org/10.1016/j.firesaf.2021.103485.

[169] C. Chen, L. Jiang, J. Qiu, M.A. Orabi, W.S. Chan, A. Usmani, OPENSEES development for modelling timber structural members subjected to realistic fire impact, Fire and Materials (2022) fam.3115. https://doi.org/10.1002/fam.3115.

[170] M.J. Hurley, D. Gottuk, J.R. Hall, K. Harada, E. Kuligowski, M. Puchovsky, J. Torero, J.M. Watts, C. Wieczorek, eds., SFPE Handbook of Fire Protection Engineering, Springer New York, New York, NY, 2016. https://doi.org/10.1007/978-1-4939-2565-0.

[171] FA Veer, Variations in pre-stress in annealed, heat strengthened and fully tempered glass, in: Tampere, Finland, 2015: pp. 395--399.

[172] GB 15763.2-2005: Safety glazing materials in building-Part2: Tempered glass, (2005).

[173] EN 12150-1: Glass in building. Thermally toughened soda lime silicate safety glass Definition and description, (2015).

[174] T. Chu, L. Jiang, G. Zhu, A. Usmani, Integrating glass breakage models into CFD simulation to investigate realistic compartment fire behaviour, Journal of Building Engineering 82 (2024) 108314. https://doi.org/10.1016/j.jobe.2023.108314.

[175] A.A. Khan, Z. Nan, L. Jiang, V. Gupta, S. Chen, M.A. Khan, J. Hidalgo, A. Usmani, Model characterisation of localised burning impact from localised fire tests to travelling fire scenarios, Journal of Building Engineering 54 (2022) 104601. https://doi.org/10.1016/j.jobe.2022.104601.

[176] M.J. Hurley, D. Gottuk, J.R. Hall, K. Harada, E. Kuligowski, M. Puchovsky, J. Torero, J.M. Watts, C. Wieczorek, eds., SFPE Handbook of Fire Protection Engineering, Springer New York, New York, NY, 2016. https://doi.org/10.1007/978-1-4939-2565-0.

[177] T. Chu, L. Jiang, A. Usmani, Introducing an active opening strategy to mitigate large open-plan compartment fire development, Fire Safety Journal 141 (2023) 103981. https://doi.org/10.1016/j.firesaf.2023.103981.

[178] T.Z. Harmathy, Some overlooked aspects of the severity of compartment fires, Fire Safety Journal 3 (1981) 261–271. https://doi.org/10.1016/0379-7112(81)90048-5.

[179] M.F. Modest, Radiative heat transfer, Third Edition, Academic Press, New York, 2013.

[180] J.G. Quintiere, B.J. McCaffrey, K.D. Braven, Experimental and theoretical analysis of quasi-steady small-scale enclosure fires, Symposium (International) on Combustion 17 (1979) 1125–1137. https://doi.org/10.1016/S0082-0784(79)80107-1.

[181] X. Sun, X. Zhang, J. Lv, X. Chen, X. Fang, J. Yi, L. Hu, Experimental study on the heat losses of the fuel combustion inside the compartment, International Journal of Heat and Mass Transfer 216 (2023) 124565. https://doi.org/10.1016/j.ijheatmasstransfer.2023.124565.

[182] N. Tondini, J.-M. Franssen, Analysis of experimental hydrocarbon localised fires with and without engulfed steel members, Fire Safety Journal 92 (2017) 9–22. https://doi.org/10.1016/j.firesaf.2017.05.011.

[183] T. Chu, L. Jiang, G. Zhu, A. Usmani, Fire impact on vertical components subjected to a localised fire estimated using a line source model, Fire Technology 59 (2023) 2299–2331. https://doi.org/10.1007/s10694-023-01429-0.

[184] J.L. Torero, The building envelope: Failing to understand complexity in tall building design, in: Rethinking Building Skins, Elsevier, 2022: pp. 341–357. https://doi.org/10.1016/B978-0-12-822477-9.00001-2.

[185] C. Weinschenk, Analysis of search and rescue tactics in single-story single-family homes - Part I: Bedroom fires, UL‘s Fire Safety Research Institute, 2022.

[186] P.L. Simona, P. Spiru, I.V. Ion, Increasing the energy efficiency of buildings by thermal insulation, Energy Procedia 128 (2017) 393–399. https://doi.org/10.1016/j.egypro.2017.09.044.

[187] M. Pedroso, I. Flores-Colen, J.D. Silvestre, M.G. Gomes, L. Silva, P. Sequeira, J. De Brito, Characterisation of a multilayer external wall thermal insulation system. Application in a Mediterranean climate, Journal of Building Engineering 30 (2020) 101265. https://doi.org/10.1016/j.jobe.2020.101265.

[188] Y. Cui, M. Li, J. Wang, D. Chu, Study on decomposition characteristics and kinetics of extruded polystyrene foam, Science Technology and Engineering 17 (2017) 1671–1815.

[189] ASHRAE, ASHRAE handbook: Fundamentals, 2021st ed., American Society of Heating, Refrigerating and Air-Conditioning Engineers, Atlanta, GA, 2021.

[190] E. Rackauskaite, M. Bonner, F. Restuccia, N. Fernandez Anez, E.G. Christensen, N. Roenner, W. Wegrzynski, P. Turkowski, P. Tofilo, M. Heidari, P. Kotsovinos, I. Vermesi, F. Richter, Y. Hu, C. Jeanneret, R. Wadhwani, G. Rein, Fire experiment inside a very large and open-plan compartment: X-ONE, Fire Technology 58 (2022) 905–939. https://doi.org/10.1007/s10694-021-01162-6.

[191] T. Chu, W. Zeng, G. Wang, C. Chen, G. Zhang, D. Yuan, J. Wang, A. Usmani, L. Jiang, Explain why active opening of windows can mitigate fire spread in modern building compartments, Journal of Building Engineering 99 (2025) 111615. https://doi.org/10.1016/j.jobe.2024.111615.

[192] Ministry of Housing and Urban-Rural Development of the People’s Republic of China, GB 50116: Fire alarm system design code, (2013).

[193] European Committee for Standardization (CEN), EN 54: Fire detection and fire alarm systems - Part 1, (2021).

[194] National Fire Protection Association (NFPA), NFPA 72: National fire alarm and signaling code, (2022).

[195] V. Gupta, A.F. Osorio, J.L. Torero, J.P. Hidalgo, Mechanisms of flame spread and burnout in large enclosure fires, Proceedings of the Combustion Institute 38 (2021) 4525–4533. https://doi.org/10.1016/j.proci.2020.07.074.

[196] H. Coanda, Device for deflecting a stream of elastic fluid projected into an elastic fluid, (1936). https://patents.google.com/patent/US2052869A/en.

[197] X. Zhang, Y. Yang, X. Sun, F. Ren, X. Fang, L. Hu, A reduced-scale experimental investigation of facade flame behavior ejected from a top-hung window of fire compartment, Proceedings of the Combustion Institute 39 (2023) 3673–3681. https://doi.org/10.1016/j.proci.2022.07.210.

[198] C. Maluk, L. Bisby, M. Krajcovic, J.L. Torero, A Heat-Transfer Rate Inducing System (H-TRIS) Test Method, Fire Safety Journal 105 (2019) 307–319. https://doi.org/10.1016/j.firesaf.2016.05.001.

[199] K.B. McGrattan, G.P. Forney, J.E. Floyd, S. Hostikka, Fire dynamics simulator technical reference guide: User's guide, National Institute of Standards and Technology, Gaithersburg, MD, 2014. https://doi.org/10.6028/NIST.IR.6784.

[200] D.C. Wilcox, Turbulence Modeling for CFD, 3rd edition, DCW Industries, 2006.

[201] G. Zhao, T. Beji, B. Merci, Application of FDS to under-ventilated enclosure fires with external flaming, Fire Technol 52 (2016) 2117–2142. https://doi.org/10.1007/s10694-015-0552-4.

[202] A.W. Coats, J.P. Redfern, Thermogravimetric analysis: A review, Analyst 88 (1963) 906. https://doi.org/10.1039/an9638800906.